Bulletin of

The Geological Society of Finland

Number 67, Part 1b **1995**

HELSINKI

Pekka Tapio Salonsaari
May 10, 1964 - August 19, 1995

Pekka Salonsaari died of a heart attack on August 19, 1995, four weeks before the defence of his Doctoral Dissertation, at the age of 31 years.

Pekka Salonsaari was born in Oulu. After matriculation in 1983, he studied at the University of Oulu geology and mineralogy being his major subject and received his Master of Science degree in 1990. In 1991 - 1994 he was a Project Researcher at the Department of Geology, University of Helsinki, studying the bimodal Jaala-Iitti rapakivi granite complex. His Doctoral thesis "Hybridization in the subvolcanic Jaala-Iitti complex and its petrogenetic relation to rapakivi granites and associated rocks of southeastern Finland" was accepted for publication by the Faculty of Science of the University of Helsinki on June 1, 1995. In October 1994, Pekka Salonsaari was appointed as a mineralogist in the Geoanalytical Laboratory of Outokumpu Research Oy. In 1992 - 1993 he was Secretary of the Geological Society of Finland.

Pekka Salonsaari was outstandingly effective in both his work and research. His co-workers and fellow students knew him as a modest, kind and always helpful colleague. His untimely death was a shock for his parents and relatives, and all who knew and worked with him. Professor Bernard Bonin, who was appointed as Pekka Salonsaari's Official Opponent, stated in his letter to the Faculty: "Finland has certainly lost one of her most promising geologists."

Publications by Pekka Salonsaari

P. Salonsaari: Vanttauskosken alueen kallioperän deformaatio. Res Terrae, Ser. B, No: 15, 61 p. (1991)

P. T. Salonsaari: Deformation of the bedrock in the Vanttauskoski area in the eastern part of the Peräpohja schist area, northern Finland. In: P. Tuisku and K. Laajoki (eds.) Metamorphism, Deformation and Structure of the Crust. Res Terrae, Ser. A, 6, 72-75 (1991).

P. T. Salonsaari and I. Haapala: The Jaala-Iitti rapakivi complex; an example of bimodal magmatism and hybridization in the Wiborg rapakivi batholith, Finland. In: I. Haapala and O. T. Rämö (eds.) Symposium on Rapakivi Granites and Related Rocks, Abstract Volume. Geological Survey of Finland, Opas-Guide 34, p. 45 (1991).

I. Haapala, O. T. Rämö and P. T. Salonsaari (eds.): Salmi batholith and Pitkäranta ore field in Soviet Karelia. Symposium Rapakivi Granites and Relates Rocks. Excursion Guide. With contributions by Yu. Amelin, A. Beljajev, A. Larin, L. Neymark and K. Stepanov. Geological Survey of Finland, Opas-Guide 33, 57 p. 1991).

I. Haapala, L. Hyvärinen ja P. Salonsaari (eds.): Malminetsinnän menetelmät. Yliopistopaino, 256 p. (1993).

P. T. Salonsaari: Disintegration and recrystallization of magmatic mafic enclaves in rapakivi granites of southeastern Finland. Geological Society of America, Abstracts with Programs 25(3), p. 77 (1993).

P. Salonsaari and I. Haapala: The Jaala-Iitti Rapakivi Complex. An Example of Bimodal Magmatism and Hybridization in the Wiborg Rapakivi Batholith, Southeastern Finland. Mineralogy and Petrology 50, 21-34 (1994).

P. T. Salonsaari and J. M. Lintala: Ocellar, micrographic, and rapakivi textures in rapaivi granites in southeastern Finland. Abstracts, International Mineralogical Association 16th General Meeting, 4-9 September, Pisa, Italy, p. 363 (1994).

T. Rämö, I. Haapala and P. Salonsaari: Rapakivi Granite Magmatism: Implications for Lithospheric Evolution. In: M. Pajunen (ed.) High temperature - low pressure magmatism and deep crustal processes. Geological Survey of Finland, Guide 37, 61-68 (1994).

P. T. Salonsaari: Hybridizarion on the subvolcanic Jaala-Iitti complex and its petrogenetic relation to rapakivi granites and associated mafic rocks of southeastern Finland. Bulletin of the Geological Society of Finland 67, Part 1b, 104 p. (1995).

The publication of this monograph is financed by Outokumpu Oy Foundation and the Geological Society of Finland.

Bulletin of

The Geological Society of Finland

Number 67, Part 1b,
1995

Editor
JUHA PEKKA LUNKKA
University of Helsinki
Department of Geology
P.O. Box 11
FIN-00014 University of Helsinki, Finland

HYBRIDIZATION IN THE SUBVOLCANIC JAALA-IITTI COMPLEX AND ITS PETROGENETIC RELATION TO RAPAKIVI GRANITES AND ASSOCIATED MAFIC ROCKS OF SOUTHEASTERN FINLAND

PEKKA T. SALONSAARI

SALONSAARI, PEKKA T. 1995. Hybridization in the subvolcanic Jaala-Iitti complex and its petrogenetic relation to rapakivi granites and associated mafic rocks of southeastern Finland. *Bulletin of the Geological of Finland 67, Part 1b, 104 pages, 56 figures, 7 tables, and 2 appendices.*

The 1630 Ma Jaala-Iitti complex is an example of bimodal rapakivi granite magmatism in which the interaction of granite and diabase magmas have led locally to hybridization. The dyke-like complex is situated at the northwestern margin of the Wiborg rapakivi batholith in southeastern Finland, cutting both the Proterozoic Svecofennian metamorphic crust and the Wiborg batholith. The complex consists mainly of non-hybridized compositionally homogeneous granites, i.e., hornblende granite and hornblende-quartz-feldspar porphyry which represent the felsic end-member (ca. 68 wt% SiO_2) of the complex. The mafic end-member (ca. 51 wt% SiO_2) is present as globules of disaggregated Fe-rich tholeiitic magma forming magmatic mafic enclaves (MMEs) and composite MMEs. Commonly MMEs and large (up to 2 metres in diameter) pillow-like MMEs show magma mixing and mingling characteristics.

Hybrid rocks in the complex are monzogranitic and are characterized by (a) quartz grains and quartz aggregates (partially melted xenoliths) mantled by amphibole rims (ocellar texture) with occasional augite, (b) alkali feldspar megacrysts mantled by a micrographic plagioclase–quartz intergrowth, and (c) alkali feldspar megacrysts mantled by a plagioclase shell with occasional amphibole inclusions. These textures are also found in hybrid MMEs and especially in pillow-like MMEs. Alkali feldspar and quartz megacrysts in hybrid rocks are derived from partially crystallized felsic magma and from disaggregated rapakivi granite and granitoid xenoliths whereas in the MMEs the xenocrysts are solely derived from partially crystallized felsic magma.

Disaggregation of the mafic magma to form MMEs and equilibration with the host have produced micro-enclaves and recrystallized borders of MMEs. Disaggregation of the mafic magma has also produced needle-like apatite crystals

incorporated from the mafic magma into the hybrid magma; acicular apatite is typical in MMEs and pillow-like MMEs and is indicative of rapid crystallization.

The mass-fraction of mafic magma (X_m) in the hybrid rock is up to 0.3. The X_m in hybrid MMEs and pillow-like MMEs varies from 0.4 to 0.9. The temperature difference between the two magmas probably caused convection that spread the disaggregated mafic magma throughout the postulated layered magma chamber. The injected mafic magma simultaneously mingled and mixed with the felsic magma which was superheated, assisting the chemical exchange. The interaction of hybrid MME magma with the hybrid magmas was possibly made more effective by diffusion of fluorine from the felsic magma into the mafic magma.

The composition of minerals indicates intensive interaction of the mafic magma and the felsic host, with the temperature of equilibrium being in the range of 900° to 750°C. The crystallization of granites of the complex occurred between 850–650°C, with an oxygen fugacity parallel or slightly below the QFM buffer. Besides geochemical evidence, a hybrid origin for the rocks is also shown by the composition of Fe–Mg silicates. Pyroxenes, however, from the hybrid rocks and MMEs show disequilibrium having crystallized at various stages of the hybridization event. Mantling of the alkali feldspar megacrysts by micrographic plagioclase–quartz intergrowth and plagioclase shells has taken place at a temperature of 850° to 750°C at a pressure under 2 kbar.

In the main part of the Wiborg batholith, any indication of large-scale hybridization between rapakivi and diabase magmas are lacking. A possible high velocity underplate beneath the batholith may have been a heat source for the partially crystallized rapakivi granite magma to produce corroded partially melted alkali feldspar megacrysts and the rapakivi texture without intensive magma mixing.

Key words: granites, diabase, rapakivi, textures, mineral chemistry, geochemistry, genesis, magmas, mixing, crystallization, hybridization, rheology, Proterozoic, Jaala, Iitti, Finland.

Pekka T. Salonsaari, Department of Geology, P.O. Box 11 (Snellmaninkatu 3), FIN-00014 University of Helsinki, Finland

Present address: Outokumpu Research, Geoanalytical Laboratory, P.O. Box 74, FIN-83501 Outokumpu, Finland

CONTENTS

INTRODUCTION

Magma mixing

Since Bunsen (1851), the idea of mixing mafic and felsic magmas to form intermediate magmas has been found to be an important process for the evolution of the magmas in plutonic and volcanic environments. The interaction of mafic and felsic magmas has been widely recognized during the last few decades.

The mafic end-member of a bimodal association is frequently visible as mafic enclaves that represent globules of the mafic magma in a more felsic host; this is a feature reflecting magma mingling and mixing (Reid *et al.* 1983, Bacon 1986, Eberz & Nicholls 1988, Pesquera & Pons 1989, Zorpi *et al.* 1989, Castro *et al.* 1990a, 1990b, 1991a, Dorais *et al.* 1990, Lorenc 1990, Stimac *et al.* 1990, Poli & Tommasini 1991, Wiebe 1991, Bateman *et al.* 1992; see also Didier 1973 and Didier & Barbarin 1991a). In volcanic suites especially, magma mixing is visible as lava flows of an intermediate hybrid magma (Sakuyama 1981, Gerlach & Grove 1982, Bloomfield & Arculus 1989). Hybridization is also found on a smaller scale in composite dykes (Chapman 1962, Vogel & Wilband 1978, McSween *et al.* 1979, Taylor *et al.* 1980, Cook 1988) where the interacting magmas use the same conduit. The mafic magma is usually basaltic to andesitic in composition whereas the felsic end-member is commonly rhyolitic, or in some cases syenitic (Dorais & Floss 1992).

Textures in mafic enclaves (Reid *et al.* 1983, Vernon 1983, 1990, 1991, Vernon *et al.* 1988) and textures reflecting hybridization (Hibbard 1981, 1991, Vernon 1990, 1991) have helped in the identification of rocks generated by magma mixing. Mineral chemistry (Allen 1991, Debon 1991, Dorais & Floss 1992) and isotopic studies (Halliday *et al.* 1980, Gray 1984, Briot 1990, Lesher 1990, Allen 1991) of mafic enclaves and their host rocks indicate various degrees of equilibration between enclaves and host rocks, and cognate mineral chemistry and isotopic data show that chemical and thermal exchange took place between the magmas. It has also been shown that the megacrysts (quartz, feldspars) in mafic enclaves have often been derived from a partially crystallized felsic magma (e.g., Barbarin 1990, Gourgaud 1991).

Experimental and theoretical studies of magma mixing in a conduit (Koyaguchi 1985, Blake & Campbell 1986, Carrigan & Eichelberger 1990) or in a magma chamber (Huppert *et al.* 1982, Kouchi & Sunagawa 1983, 1985, Campbell & Turner 1985, 1986, Turner & Campbell 1986, Koyaguchi & Blake 1991, van der Laan & Wyllie 1993) with turbulent fountains have been carried out to evaluate whether two magmas with different viscosities, temperatures, and crystallinities can mix or not (Marsh 1981, Sparks & Marshall 1986, Frost & Mahood 1987, Frost & Lindsay 1988, Russell 1990, Blake & Koyaguchi 1991, Fernandez & Barbarin 1991, Fernandez & Gasquet 1994, Grasset & Albarède 1994). As magma mixing also seems to play an important role in granitoid evolution, the category of H-type (hybrid) granitoids has been proposed (Castro *et al.* 1991b) for granitoid rocks of unequivocal hybrid origin.

Rapakivi granites of Finland

Rapakivi granites, "A-type granites characterized by the presence, at least in the larger batholith, of granite varieties showing the rapakivi texture" as recently redefined by Haapala and Rämö (1992), show a wordwide distribution and numerous occurrences have been reported from all continents. The age of the rapakivi granites varies from Tertiary to Late Archean but most of the rapakivi granites are Proterozoic (1.0–1.7 Ga) (Rämö & Haapala 1995).

The rapakivi granites of the southeastern Fennoscandia form perhaps the best known rapakivi granite occurrence in the world. Active research on rapakivi granites in southeastern Fennoscandia has continued over a century starting from the work by Sederholm (1891), and continued by Wahl (1925, 1938, 1947), Eskola (1928, 1930, 1949), Hackman (1934), Sahama (1945, 1947), and Savolahti (1956, 1962) who introduced to the world the general petrographic and geochemical characteristics of the rapakivi granites. Vorma (1975, 1976), Haapala

(1977a), Nurmi and Haapala (1986), Haapala and Rämö (1990), Rämö (1991), and Rämö and Haapala (1990) have continued the characterization of the rapakivi granites. Detailed mineralogical (Simonen 1961, Haapala & Ojanperä 1969, 1972a, Simonen & Vorma 1969, Vorma 1971, 1972, Vorma & Paasivirta 1979), isotope geochemical (Vaasjoki 1977, Suominen 1987, 1991, Rämö 1991, Vaasjoki *et al.* 1991), and geophysical (e.g., Luosto 1990, Luosto *et al.* 1990, Elo & Korja 1993) works have focused on the origin and evolution of the 1.65–1.54 Ga rapakivi granites in southeastern Fennoscandia. Recent summaries of the metallogeny of rapakivi granites can be found in Haapala and Ojanperä (1972b), Haapala (1977a, 1977b, 1988, 1993, 1995), and Edén (1991); typical are greisen-, vein-, and skarn-type Sn(–W–Be–Zn–Cu–Pb) and Fe-oxide–Cu(–U–Au–Ag) deposits.

In southeastern Fennoscandia, rapakivi granites occur as several batholiths and/or stocks (Fig. 1a): Wiborg, Suomenniemi, Ahvenisto, Onas, Bodom, Obbnäs, Reposaari, Eurajoki, Kokemäki, Laitila, Vehmaa, Kökärsfjärden, Fjällskär, and Åland in Finland and Salmi and Sotjärvi (or Uljalegi) in the Russian Karelia. The classic Wiborg batholith (Fig. 1b) consists of several distinct rock types (see Vorma 1971, 1976, for detailed summaries).

Wiborgite and dark-coloured wiborgite show typical rapakivi texture (alkali feldspar ovoids mantled by plagioclase), and constitute about 80 % of the Wiborg batholith. Rapakivi texture (*sensu stricto*), is characterized by Vorma (1976, p. 5; see also Rämö *et al.* 1994) as having: ovoidal shape of alkali feldspar megacrysts; commonly mantling of ovoids by oligoclase–andesine shells and the ubiquitous occurrence of two generations of alkali feldspar and quartz, the latter having an idiomorphic older generation which crystallized as high quartz. When rapakivi granites have alkali feldspar ovoids which do not have a plagioclase mantle (or only in minor amounts) they are called pyterlites and the main difference relative to a porphyritic rapakivi granite is that the latter contains alkali feldspar megacrysts that are more euhedral. Even-grained rapakivi granites are medium- or coarse-grained, usually biotite-bearing granites but they may contain variable amounts of hornblende±fayalite ("tirilite") and occasionally alkali feldspar ovoids. Porphyry aplite is a rare rapakivi granite with (mantled or unmantled) alkali feldspar megacrysts in a fine-grained aplite-granite matrix (Vorma 1976).

Related Subjotnian tholeiitic diabases (Laitakari 1969, 1987, Boyd 1972, Ehlers & Ehlers 1978, Laitakari & Leino 1989, Lindberg *et al.* 1991, Rämö 1991) form dykes and dyke swarms running in a NE–SW or NW–SE direction (see Fig. 1a) with an age range of 1665 to 1635 Ma (Laitakari 1987, Siivola 1987, Suominen 1987, 1991, Vaasjoki & Sakko 1989, Rämö 1991, Vaasjoki *et al.* 1991) in southeastern Fennoscandia. In association with rapakivi granites, gabbroic and anorthositic rocks have been found at the Ahvenisto complex (Savolahti 1956, Johanson 1984, 1989, Vaasjoki *et al.* 1993) and minor gabbroic and anorthositic bodies occur in the Åland batholith area (Bergman 1979, Suominen 1987, 1991, Eklund *et al.* 1994). Large fragments of gabbroic and anorthositic rocks also occur within the Wiborg batholith at the Ylämaa and Simola districts (Simonen 1979a, 1979b; see also Fig. 1b).

The coeval occurrence of rapakivi granites and related mafic rocks reflects the bimodal characteristics of rapakivi granite magmatism (Haapala 1989, Johanson 1989, Lindberg & Eklund 1989, 1992, Rämö 1989, 1991, Vaasjoki & Rämö 1989, Andersson & Eklund 1991, Boyd & Rämö 1991, Eklund *et al.* 1991, 1994, Andersson 1992, Eklund 1993, Lowell & Young 1993, Salonsaari & Haapala 1994). Magma mixing has been proposed as an important factor in the evolution of the rapakivi granites (Wahl 1925, von Wolff 1932, Eklund *et al.* 1991, 1994, Eklund 1993) as well as forming rapakivi texture itself (e.g., Hibbard 1981, 1991). Magma mixing and (mainly) mingling occurrences reported from rapakivi areas are, however, small and there is no convincing evidence of a large-scale hybridization between the mafic and felsic magmas.

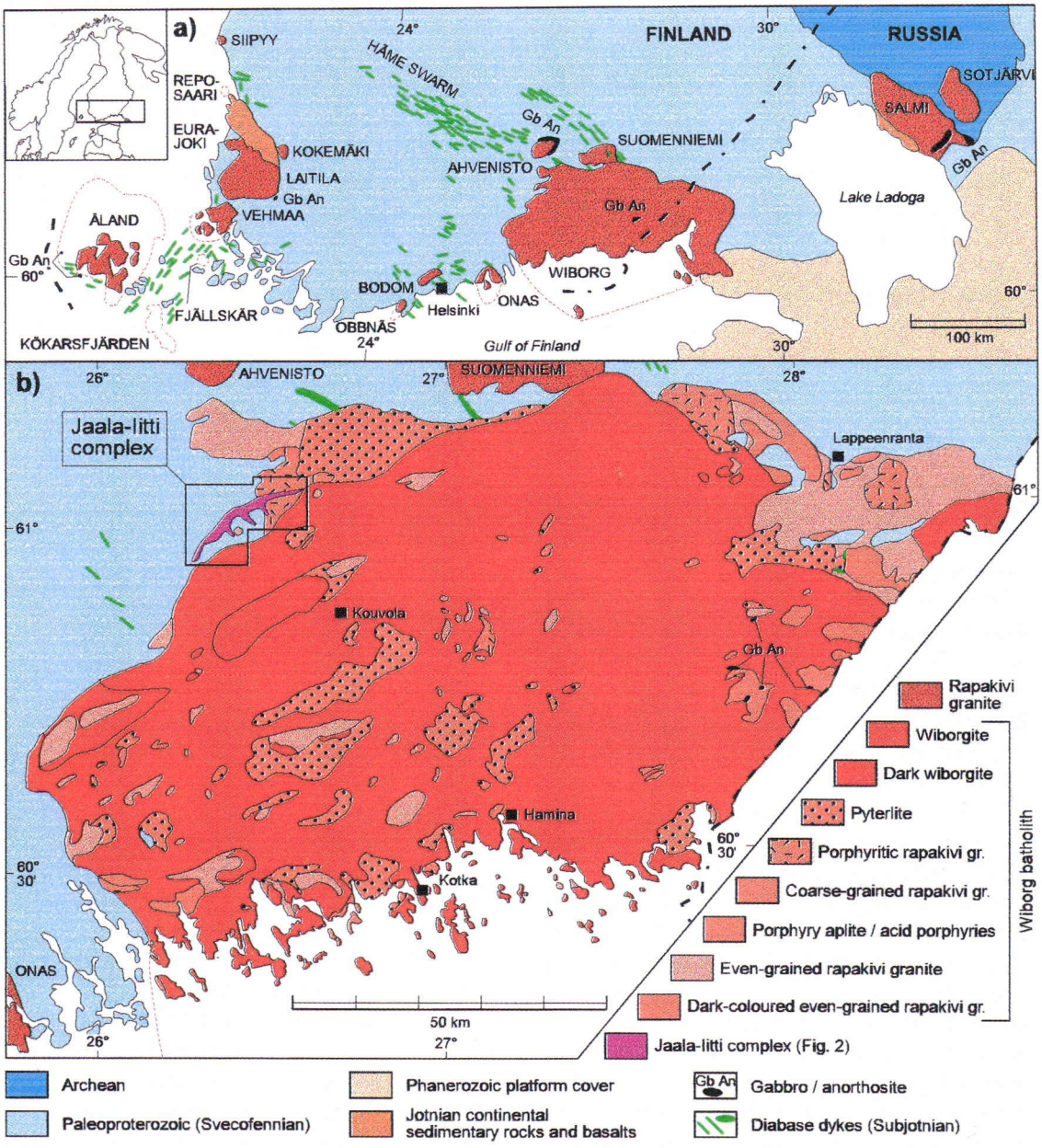

Fig. 1. a) 1.65 to 1.54 Ga rapakivi granite batholiths and associated gabbroic and anorthositic bodies and mafic dykes of southern Finland and Russian Karelia. Modified after Rämö (1991). b) Simplified map of the Finnish part of the Wiborg rapakivi granite batholith. Compiled after Härme (1980), Laitakari and Simonen (1962), Lehijärvi and Tyrväinen (1969), Meriläinen (1966), Rämö (1991), Simonen (1965, 1973, 1975, 1979a, 1979b), Simonen and Laitala (1970, 1972), Simonen and Lehijärvi (1963), Simonen and Tyrväinen (1965), and Vorma (1964).

Terminology on magma mixing

In this work, *mixing of magmas* results in a homogeneous liquid phase; the phenocrysts derived from the end-members may, however, either retain their original compositions or they may have partially re-equilibrated (Sparks & Marshall 1986). In some cases the evidence of magma mixing is thought to be given only by mineral disequilibria (Briot 1990). *Magma mingling* (or commingling) retains the identities of the original magmas through mechanical exchange (Wiebe 1979, Sparks & Marshall 1986) without pervasive mixing of the melts (Vernon 1983). Many interaction processes are, however, intermediate between these extremes (Barbarin 1988). When a significant proportion of intermediate rock (magma) is present, and both mixing and mingling processes have been operative, the term *hybridization* (producing a *hybrid rock*) is used.

Products of magma mingling are commonly present as *magmatic mafic enclaves (MMEs)* which represent pieces of the disaggregated mafic magma in felsic magma and *intermingling* of individual mineral grains from the one magma into another. The term enclave (Didier & Barbarin 1991b) describes a fragment of rock enclosed in another rock. The term magmatic refers to the igneous origin of the enclave, and the term mafic indicates that the enclave has a greater proportion of dark minerals than the host rock. Commonly used terms such as microgranular or microgranitoid instead of magmatic are used to describe the textures typical of MMEs. MMEs may also form *composite enclaves* (or double enclaves) in which one or several MMEs are enclosed in a host MME (Barbarin 1991, Bussy 1991, Didier & Barbarin 1991b).

In some instances, xenoliths are also included in the group of composite enclaves, but in this study allochthonous material is described simply as *xenoliths* or *xenocrysts*. The term *inclusion* is reserved for mineral grains, liquid, or gas enclosed in single crystals as noted by Didier and Barbarin (1991b).

The recent study

Starting in 1990, a project "Conditions of crystallization of rapakivi granites and rapakivi texture" has been undertaken at the University of Helsinki, Department of Geology, under the leadership of Professor Ilmari Haapala and with researchers Mrs. Jaana Lintala, M.Sc. and Dr Walter W. Boyd. After the first half of 1991, the author joined the project as a full-time researcher concentrating on the Jaala-Iitti complex. Preliminary mapping of the complex was done in the summer of 1990 and detailed mapping was completed in 1991.

The reason for choosing the Jaala-Iitti complex to study in detail was that, in the light of earlier studies (Lonka 1957, 1960, Lehijärvi & Lonka 1964) and preliminary investigations, it appears to offer valuable information on the interaction of diabase and rapakivi granite magmas. The complex was assumed to have been placed as a subvolcanic complex and hence registering features that could not be observed from rapidly crystallized volcanic rocks or from fractionated and chemically equilibrated plutonic rocks. It was also thought that the observed hybridization features could provide a means to assess the significance of magma mixing in the petrogenesis of rapakivi granite magmas.

Objectives of this work were to describe in detail hybridization of contemporaneous felsic and mafic magmas and the overall petrogenesis of the rocks in the Jaala-Iitti complex by concentrating on: 1) hybridization event(s) between the felsic and mafic magmas, 2) textures reflecting magma mixing and mingling, 3) petrographical, mineral chemical, and geochemical evidence of magma mixing or fractional crystallization, 4) the role of xenolith and xenocryst assimilation during evolution of the rocks, and 5) to compare rocks from the Jaala-Iitti complex with rapakivi granites and associated mafic rocks of southern Finland to evaluate the possible significance of hybridization in the overall evolution of rapakivi granites, especially the origin of rapakivi texture.

Geochemical comparison of the Jaala-Iitti complex is mainly done with rocks of the Wiborg batholith, the Häme diabase dyke swarm, and the

Suomenniemi complex. The Suomenniemi complex is frequently referred to throughout this study because abundant geochemical data are available for the complex (e.g., Rämö 1991), and because the rock types of the Suomenniemi complex are comparable to the rocks of the Jaala-Iitti complex. Preliminary results of this work have been reported in three IGCP 315 symposiums: Helsinki, Finland (Salonsaari & Haapala 1991), Rolla, Missouri, U.S.A. (Salonsaari 1993), and Pisa, Italy (Salonsaari & Lintala 1994). A brief description of the complex can be found in Salonsaari & Haapala (1994).

GEOLOGIC SETTING

The Jaala-Iitti complex is situated at the northwestern margin of the Wiborg rapakivi batholith in southeastern Finland (Fig. 1b). The complex (Fig. 2) is about 22 km long and 0.1 to 1.5 km wide. It forms a curved dyke with features similar to a ring-dyke. The central part of the complex has three SE-directed offsets that are mainly unexposed. Because of this, and lack of suitable geophysical data, contacts for the offsets in Figure 2 are speculative; they are based on a few observed field contacts and orientation of fragments in the rock. The western part of the complex cuts with sharp vertical contacts the Proterozoic Svecofennian (1.8–1.9 Ga) metamorphic crust that here consists of garnet-bearing granites and minor mica gneisses and amphibolites. In the east the complex is hosted by a porphyritic (Verla) rapakivi granite with a U–Pb zircon age of 1639±2 Ma (Vaasjoki *et al.* 1991). The U–Pb zircon age for the hornblende granite of the Jaala-Iitti complex is 1630±5 Ma (Vaasjoki *et al.* 1991) so it is only slightly younger than the surrounding rapakivi granite.

The lithology of the Jaala-Iitti complex was probably first mentioned by Moberg (1885) who described the rocks of the complex as quartz- and feldspar porphyries. Later Lonka (1957, 1960) and Lehijärvi and Lonka (1964) described its petrography and discussed its petrogenesis.

Three main rock groups are found in the bimodal Jaala-Iitti complex: 1) granites (hornblende granite and hornblende-quartz-feldspar porphyry), 2) diabase forming magmatic mafic enclaves (MMEs), and 3) hybrid rocks. All three are cut by pegmatite and aplite dykes, and xenoliths are found throughout the complex. Contacts between the two rapakivi granite types and the hybrid rocks are gradual; no sharp contacts indicative of several pulses of felsic magmas have been recognised. In terms of mineralogical and geochemical characteristics, the hybrid rocks and hornblende granites grade into each other, and therefore exact contacts between these types can not be shown.

The bulk of the complex consists of a homogeneous hornblende granite that shows little trace of magma mixing and mingling. Only the hornblende-quartz-feldspar porphyry lacks signs of hybridization; it occurs as lens-like bodies in contact with the surrounding country rocks. In the eastern part of the complex, at Ilvesvuori quarry (samples 91381 and 91382 in Fig. 2), a gradual change of hornblende granite to hornblende- quartz-feldspar porphyry occurs. Salonsaari and Haapala (1994) also included in the complex a topaz-bearing quartz-feldspar porphyry that occurs in the eastern part of the complex (southwest of Ilvesvuori). Areas exposed subsequently in the Ilvesvuori quarry show, however, that the topaz-bearing quartz-feldspar porphyry does not belong to the complex.

Mafic end-members of the complex generally occur in three different modes, sizes, and composition: 1) magmatic mafic enclaves, MMEs (term used in analogy with Didier & Barbarin 1991b) without quartz and feldspar xenocrysts, 2) MMEs which show hybrid features such as quartz and feldspar xenocrysts, and 3) large (up to 2 meters in diameter) pillow-like MMEs which are only found in relatively small areas of the southwestern part of the complex, north of Lake Kirkkojärvi. Pillow-like MMEs show intensive mixing and mingling. MMEs occur throughout the complex, but their occurrence is marked in Figure 2 only if the average proportion of MME is higher than one MME per square meter. Pillow-like MMEs are distinguished from the common MMEs with a larger symbol pattern in Figure 2. The amount of MMEs seems to

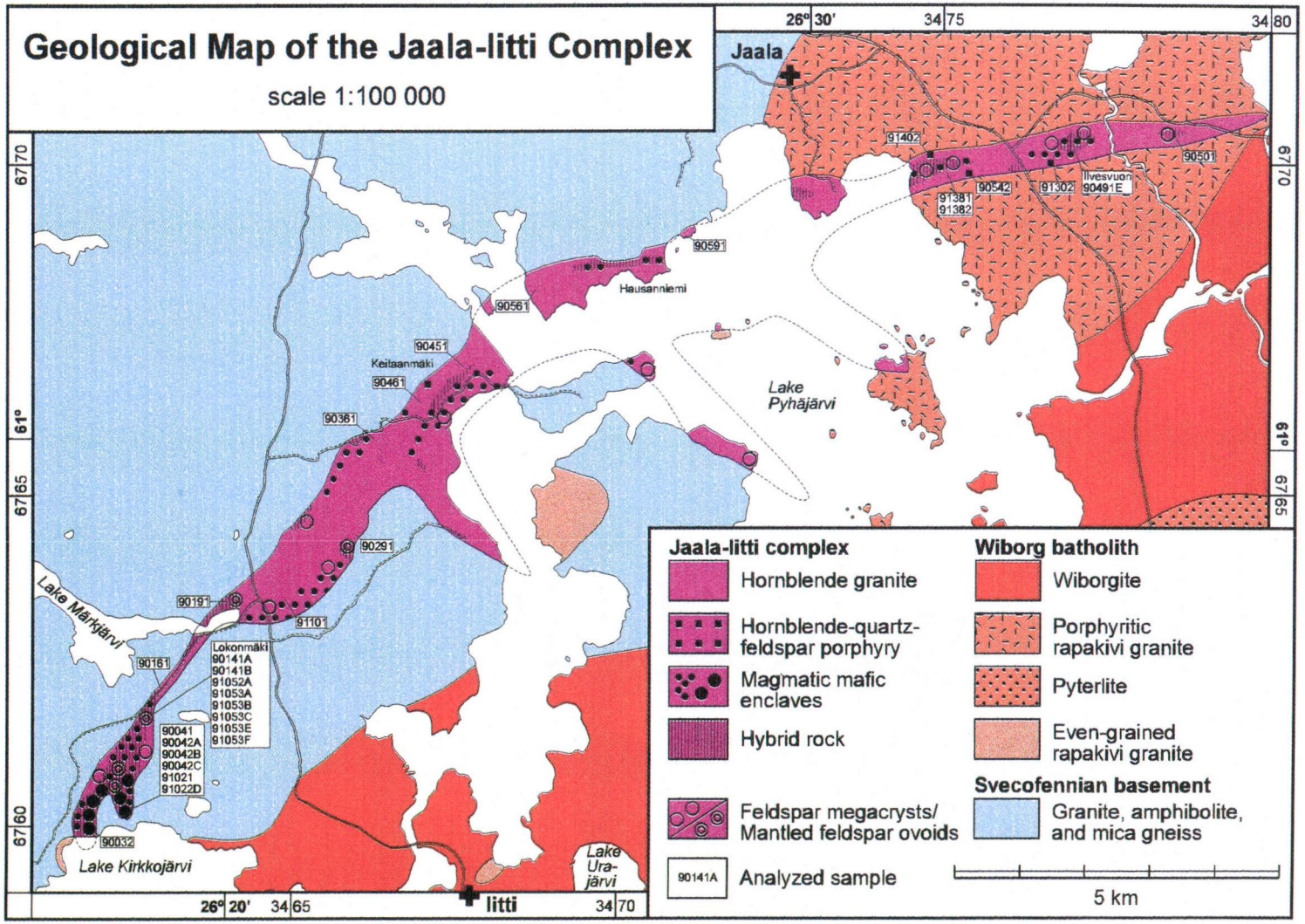

Fig. 2. Geological map of the Jaala-Iitti complex. Data for the Wiborg batholith and the Svecofennian basement are from Lehijärvi and Tyrväinen (1969) and Simonen and Lehijärvi (1963).

be lowest in the hornblende-quartz-feldspar porphyry, and highest in hybrid rocks.

Typical hybrid rocks occur for instance at the Lokonmäki (Fig. 2, samples 90141A through 91053F) in the southwestern part of the complex. These represent the most thoroughly mixed hybrid granite discovered in the complex. Criteria for separating hybrid rocks from granites is the occurrence of quartz grains surrounded by amphibole coronas, and the occurrence of textures such as micrographic plagioclase–quartz rims around alkali feldspar megacrysts as well as the common occurrence of MMEs. These criteria are used in the case of the Jaala-Iitti complex because granites resulting from magma mixing contain ocellar quartz, whereas in pure hornblende granites this texture is usually lacking even though they may contain quartz xenocrysts and xenoliths. The lack of outcrops as well as the fact that almost half of the complex is underwater makes it difficult to evaluate the exact proportion of hybrid rocks in the complex. Hybrid rocks dominate the southwestern part of the complex, whereas elsewhere hornblende granite is predominant.

Rocks of the complex locally contain varying amounts of country rock xenoliths, measuring up to several metres in diameter. In the southwestern and central parts of the complex, the xenoliths are mainly Svecofennian granitoids and gneisses and, to a lesser extent, rapakivi granites (porphyritic rapakivi granite and pyterlite). In the east, xenoliths are mainly rapakivi granite. Locally xenoliths may be partially disintegrated and they are assumed to be one source of xenocrysts for the different rock types of the complex.

PETROGRAPHY OF THE JAALA-IITTI COMPLEX

The modal composition of the granites, magmatic mafic enclaves, and hybrid rocks of the Jaala-Iitti complex are plotted in a quartz–alkali feldspar–plagioclase (QAP) diagram (Streckeisen 1973, 1976) in Figure 3.

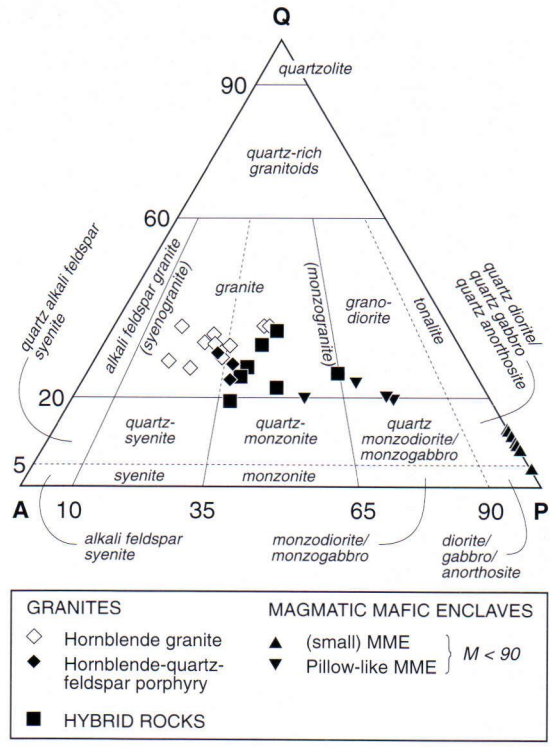

Fig. 3. Modal compositions of hornblende granites, hornblende-quartz-feldspar porphyries, MMEs, pillow-like MMEs, and hybrid rocks of the Jaala-Iitti complex presented in a QAP-diagram after Streckeisen (1973, 1976).

Granites

The granites forming the Jaala-Iitti complex are predominantly hornblende granite with minor amounts of hornblende-quartz-feldspar porphyry. Both types have their own petrographical characteristics, and their petrography as well as mineral chemistry and geochemistry are described separately. There is no indication that hornblende granite and hornblende-quartz-feldspar porphyry resulted from distinct intrusive episodes. The hornblende-quartz-feldspar porphyry probably represents a hornblende granite that crystallized rapidly. This is based on the observation that the rock usually exists in the vicinity of contact of the complex and that geochemically it is similar to the hornblende granite. The lack of outcrops through-

out the complex precludes knowing whether the rock represents the contact facies everywhere.

Hornblende granite

The hornblende granite is generally a dark red equigranular homogeneous rock. Locally, however, it shows mineralogical variations ranging from an equigranular hornblende granite to a porphyritic hornblende-quartz-feldspar porphyry. The occurrence of MMEs is lower here than in the hybrid rocks; usually less than one per square meter. The hornblende granite shows porphyritic features with phenocrysts of plagioclase, non-mantled alkali feldspar, and quartz in a hypidiomorphic-granular matrix. Rarely, thin and discontinuous amphibole mantles surrounding quartz may be present near Svecofennian granitoid xenoliths. The size of the alkali feldspar and plagioclase phenocrysts is commonly under 5 cm and 3 cm in diameter, respectively. The grain size of plagioclase, hornblende, and quartz in the matrix varies from 1 to 4 mm.

Plagioclase (An_{34}) phenocrysts may show synneusis twins, and usually are only slightly sericitized. Inclusions of amphibole, quartz, and sometimes fayalite, rimmed by amphibole, occur.

Corroded calcic plagioclase with more sodic rims (compositionally similar to the matrix) in granitoids have been described as a restite component (e.g., Presnall & Bateman 1973, White & Chappell 1977, Chappell 1978, Chen *et al.* 1990). Similar plagioclases were also found in the hornblende granites of the Jaala-Iitti complex where altered, more calcic (An_{50-53}) plagioclase is surrounded by an oligoclase (An_{20-35}) rim that is compositionally similar to matrix plagioclases. Corroded grains are usually altered to sericite and their diameter is under 2 mm. In case of the Jaala-Iitti complex, such grains could be restites but are more likely to be xenocrysts derived from an earlier gabbroic or anorthositic magma.

Alkali feldspar phenocrysts often contain inclusions, especially in the outer part of the phenocrysts: quartz, amphibole, plagioclase, biotite, and apatite. Plagioclase and amphibole inclusions are usually subhedral. Quartz inclusions are usually concave and occasionally euhedral. The occasional euhedral quartz inclusions in alkali feldspar phenocrysts indicate relatively early crystallization of quartz. Plagioclase inclusions in the outer part of the alkali feldspar phenocrysts have a thin shell of albite, but thin rims of quartz are also present. Perthitic alkali feldspar phenocrysts may contain zonally arranged round quartz inclusions, most of them with a similar optical orientation. Micrographic texture, typical of the hybrid rocks of the Jaala-Iitti complex is lacking in both alkali feldspar megacrysts and matrix. Granophyric quartz intergrowth in alkali feldspar is occasionally visible. Plagioclase mantles surrounding alkali feldspar megacrysts and rock fragments occur in hornblende granites of the complex. In Figure 4, a porphyritic rock fragment surrounded by plagioclase is shown; plagioclase in the mantle is almost completely seritized.

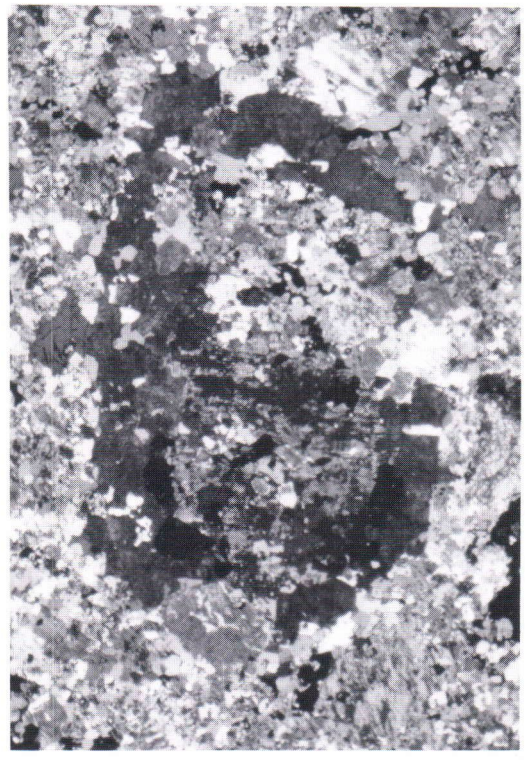

Fig. 4. Photomicrograph of alkali feldspar megacryst and rock fragment with a strongly seritized plagioclase mantle. Sample 9046. Width of the picture corresponds to 11.5 mm.

Amphibole occurs as large grains with occasional remnants of pyroxene and fayalite. Large amphibole grains (Ø = 2–3 cm) are usually subhedral whereas smaller grains in the matrix are anhedral and 0.5 to 1.0 cm in diameter. The fact that amphibole occurs both as phenocrysts and inclusions in other minerals suggests that amphibole crystallization continued throughout the crystallization of the rock. Amphibole also occurs in irregular aggregates with quartz and minor feldspars. The size of the aggregates is up to 1 cm in diameter; inclusions are common, being mainly apatite, Fe–Ti oxide, and quartz. Commonly anhedral amphibole has both magnetite and ilmenite inclusions whereas the matrix of the hornblende granite contains lamellar magnetite–ilmenite intergrowths. Pyrite inclusions also occur as well as apatite inclusions which are usually zoned; this is not the case with individual grains in the matrix. The crystallization history of Fe–Mg silicates has started with fayalite which is always rimmed by amphibole. At later stages amphibole has crystallized simultaneously with plagioclase with biotite occurring in the interstices.

Hornblende-quartz-feldspar porphyry

In contact with the basement rocks are a few occurrences of a dark, nearly black porphyritic rapakivi granite that Lehijärvi and Lonka (1964) called tirilite. This rock forms lens-like bodies (usually under 50 m in diameter) that grade into hornblende granite. The rock has occasional some xenocryst-free MMEs with a diameter less than 10 cm. On a weathered surface the rock is lighter with distinctive dark amphibole (±fayalite) spots (Fig. 5). The contact between the hornblende-quartz-feldspar porphyry and the topaz-bearing quartz-feldspar porphyry that forms the country rock of the complex at Ilvesvuori (Fig. 2) is strongly sheared.

The hornblende-quartz-feldspar porphyry has alkali feldspar, plagioclase, quartz, and amphibole phenocrysts varying from 1 to 3 mm in diameter in a fine-grained (ca. 0.1 mm) matrix (Fig. 6). Plagioclase (An_{32-37}) phenocrysts are commonly subhedral–euhedral and corroded. They occasionally have inclusions of euhedral quartz, but more often amphibole inclusions with a fayalite core. Some quartz phenocrysts show an euhedral bipyramid shape. Plagioclase phenocrysts commonly are aggregates (synneusis). Alkali feldspar phenocrysts in the hornblende-quartz-feldspar porphyry are rounded and usually strongly corroded. They do not contain perthitic albite and inclusions are relatively rare, but if present, they are mainly quartz, but amphibole (±fayalite) and plagioclase are also found. Inclusions are commonly situated in the outer part of the alkali feldspar phenocrysts where they form a regular rim of amphibole (±apatite). The grain size of plagioclase inclusions is usually under 0.3 mm in diameter, but occasionally inclusions reach a size of 0.8 mm in diameter. Amphibole

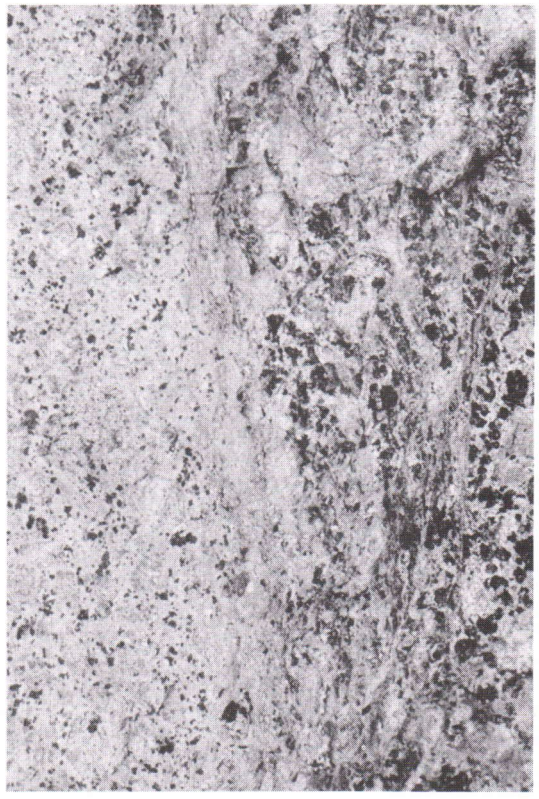

Fig. 5. Hornblende-quartz-feldspar porphyry (left) in (E–W trending) contact with topaz-bearing quartz-feldspar porphyry in Ilvesvuori. The dark spots in the hornblende-quartz-feldspar porphyry are fayalite phenocrysts rimmed by amphibole. Width of the picture corresponds to 17 cm.

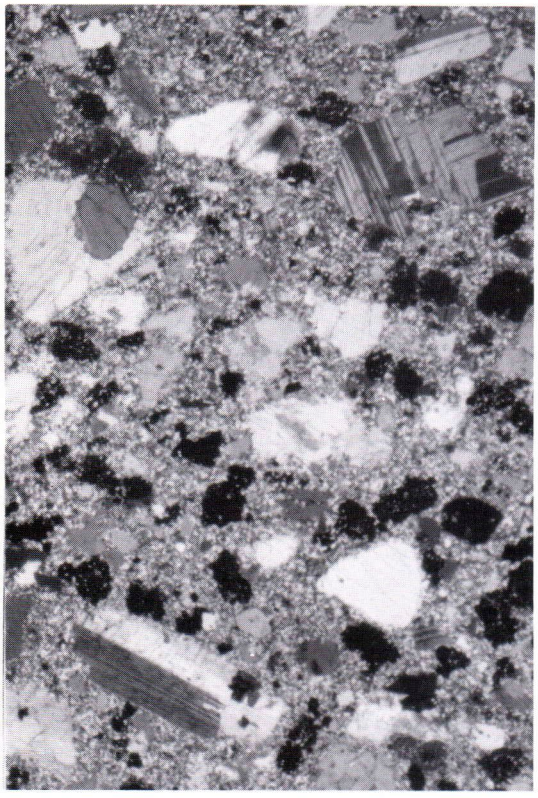

Fig. 6. Photomicrograph of hornblende-quartz-feldspar porphyry (sample 91302) at Ilvesvuori. The matrix consists of quartz, alkali feldspar, and plagioclase. Width of the picture corresponds to 11.5 mm.

occurs as ragged phenocrysts with remnants of fayalite (Fo_{3-5}) as inclusions. The grain size of the fayalite can be up to 1 mm in diameter. Granophyric quartz intergrowths are visible only adjacent to the alkali feldspar (and sometimes the plagioclases).

The matrix (grain size 0.05 to 0.1 mm) of the hornblende-quartz-feldspar porphyry consists of plagioclase, alkali feldspar, quartz, apatite, Fe–Ti oxide, and zircon. Some fluorite is also found. Ilmenomagnetite is more common in the hornblende-quartz-feldspar porphyry than in the other rock types of the complex. Amphibole and biotite are minor phases in the matrix.

The mineralogy and the mode of occurrence suggest that the hornblende-quartz-feldspar porphyry represents a contact facies of the hornblende granite. It shows little trace of magma mingling, more of mixing, and it is therefore used as a felsic end-member in the calculation of magma mixing relations.

Magmatic mafic enclaves

Small MMEs and pillow-like MMEs

MMEs in the Jaala-Iitti complex represent disaggregated mafic magma that has been intruded into a felsic magma; they represent the mafic end-member of the complex. MMEs occur as fragments of varying size, usually less than 50 centimetres in diameter (Fig. 7). They exist commonly throughout the complex but they are more common in hybrid rocks. No large separate mafic bodies or related dykes were discovered within or in the vicinity of the complex.

Fig. 7. MMEs in a hybrid rock from the Lokonmäki quarry (sample 90141). The smallest MMEs are under 1 cm in diameter. Width of the picture corresponds to 19 cm.

MMEs in the Jaala-Iitti complex are separated into two groups based on their size. Those mafic enclaves referred as MMEs represent the main mafic end-member throughout the complex; they have varying amounts of feldspar and quartz xenocrysts. MMEs without xenocrysts also occur and they are assumed to represent the initial (diabase) composition. In the southwestern part of the complex, north of lake Kirkkojärvi, MMEs occur in tight clusters composing more than 50 vol% of the rock. Their diameter ranges from a few centimetres up to two metres in diameter and they are separated from other MMEs of the complex by using the term "pillow-like" which is commonly adopted to describe relatively large MMEs with voluminous occurrence (see e.g., Didier & Barbarin 1991b). Their relative amount in the more felsic (hybrid) host is distinctly higher than in other parts of the complex. Pillow-like MMEs compared to other MMEs shows a more intensive intermingling of feldspar and quartz xenocrysts (Fig. 8) from granite.

There appears to be no correspondence of the abundance and occurrence of MMEs in relation to the contacts; they occur, in approximately equal frequency, both in the central part of the complex and near the contacts. Note that even though MMEs can be found throughout the complex, they are marked on the geological map only if their proportion is over one MME per square meter.

Figure 9 shows the size and orientation of MMEs and pillow-like MMEs from the Jaala-Iitti complex. Usually MMEs in hybrid rocks (Lokonmäki), hornblende granites (Keitaanmäki, Hausanniemi), and hornblende-quartz-feldspar porphyry (Ilvesvuori; a transition zone between hornblende granite and hornblende-quartz-feldspar porphyry) are under 50 cm in diameter, with an average of about 10 cm. The shape of the MMEs is commonly ovoidal with a length-width ratio less than 3, and only rarely with a ratio from 5 to 7. It is probable that the orientation (Fig. 9) and shape of the MME is controlled mainly by the flow of the host magma. The orientation of MMEs is parallel to the contacts of the complex in the Kirkkojärvi, Lokonmäki, and Keitaanmäki areas. In the Keitaanmäki and Hausanniemi locations (Fig. 9) the orientations of MMEs may be related to the SE-trending offsets of the complex. It should be noted that measurements of the orientation are from horizontal sections in outcrops.

Fig. 8. Part of a pillow-like MME with alkali feldspar, quartz, and plagioclase xenocrysts. Note also a composite hybrid enclave and an alkali feldspar megacryst partially enclosed in the MME. North of lake Kirkkojärvi, western part of the complex. The diameter of the coin is 2.4 cm.

The contact of the MMEs against the host rock is usually sharp and crenulated (Fig. 7). Indications of rapid crystallization of the mafic magma against the felsic magma such as chilled contacts, are rare; these chilled margins may contain some feldspar and quartz xenocrysts. More often a gradational change is visible as the grain size is larger in the margin than the central part of the MME. MMEs are occasionally surrounded by a thin (less than one cm) felsic zone unusually of the hybrid rock.

Some, especially pillow-like MMEs, show textures suggesting the flow of a mafic magma in a more viscous felsic magma. Field observations of

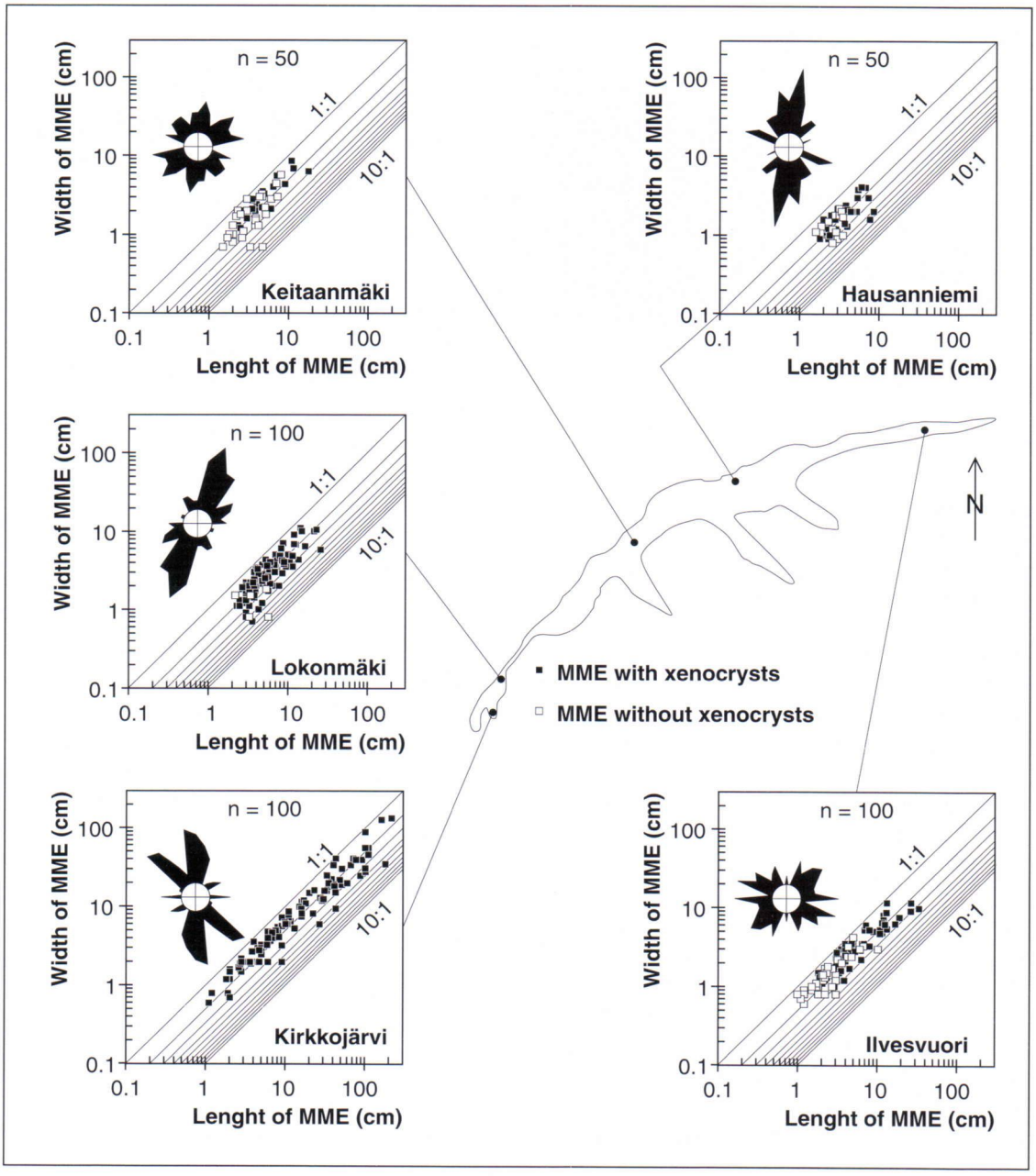

Fig. 9. Figure showing length, width, and orientation of MMEs from the hybrid rock (Kirkkojärvi, Lokonmäki) and hornblende granite (Keitaanmäki, Hausanniemi, Ilvesvuori). MMEs with and without xenocrysts are separated. Lines within figures represent length-width ratios of MMEs. See text for discussion.

several MMEs show that the direction and possible rotation of mafic magma (MME) can be evaluated on the basis of the four diagnostic features as shown in Figure 10. A tip of the MME separated parts of the mafic magma that have and have not been under the influence of erosion caused by movement of the

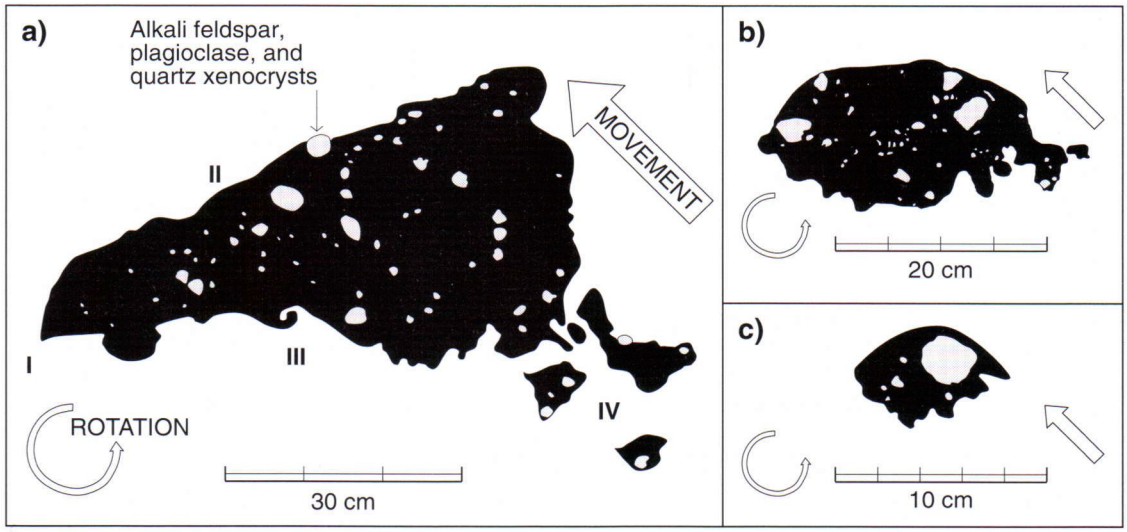

Fig. 10. Drawings based on horizontal sections of pillow-like MMEs of various sizes from north of lake Kirkkojärvi, western part of the complex. Arrows indicate components direction of movement and rotation at: (I) a tip of the MME, (II) curved part of the MME, (III) sheltered part of a MME with limited disintegration and small-scale convection of the mafic magma, and (IV) a tail of the MME showing disintegration of the mafic magma into smaller patches. See text for discussion.

mafic magma from those parts which have been sheltered. Active mechanical erosion of the mafic magma is visible as a smooth curved part of the MME. The typical shape of the sheltered part of the MME is a strongly crenulated margin, and it possibly shows small scale convection that indicates flow and rotation direction of the mafic magma. Viscosity contrast and movement also cause disintegration of the mafic magma into smaller magma globules forming a tail. These features tell about two phenomena. Firstly, mafic magma has moved within the felsic magma in a liquid stage, and it is presumed that this movement is caused by injection of mafic magma into a felsic magma. The possibility that a felsic magma was injected into mafic magma in not a probable explanation for generating the structures described above. This hypothesis is also supported by the existence of alkali feldspar, plagioclase, and quartz xenocrysts in the MMEs; these having been captured from the partially crystallized felsic magma surrounding the mafic magma. Secondly, structures indicating movement and rotation are found mainly in pillow-like MME which are larger than MMEs in other parts of the complex. The pillow-like MMEs probably represent less disintegrated globules of the injected mafic magma, and that MMEs in the other parts of the complex result from a higher rate of disintegration of the mafic magma generating ovoidal MMEs which have disintegrated into smaller enclaves and have become rounded during movement in the felsic magma.

Mode of occurrence of MME's and pillow-like MME's xenocrysts

Composite MMEs are found especially in the hybrid rock and pillow-like MMEs. They usually show a similar modal composition to the host MME in the latter occurrence, but the grain size is smaller. Commonly composite MMEs are xenocryst-free, but not invariably (Fig. 8). Mineral compositions and geochemistry show that these MMEs are similar to the least evolved MMEs of the complex. The occurrence of composite enclaves indicates that at least two mafic magma pulses (with similar composition) have been intruded into the felsic magma.

One criteria for subdividing MMEs in the Jaala-Iitti complex is the occurrence of alkali feldspar and quartz xenocrysts, occasionally also plagioclase. MMEs without xenocrysts occur more commonly in hornblende granites and hornblende-quartz-feldspar porphyries (see Fig. 9: Keitaanmäki, Hausanniemi, Ilvesvuori) with size of ca. 5 cm in diameter. Alkali feldspar, quartz, and especially plagioclase xenocrysts in MMEs are usually strongly corroded and they appear to be aggregates of several crystals (synneusis). Sometimes these xenocrysts are located partially within the MME and partially in the felsic rock. This is in accordance with the assumption that the xenocrysts were entrained by the mafic magma from a surrounding partially crystallized felsic magma (Fig. 8).

The diameter of the alkali feldspar, plagioclase, and quartz xenocrysts in MMEs are usually under 3 cm; commonly between 0.5 and 1 cm. Alkali feldspar xenocrysts usually contain concave quartz and are perthitic. All xenocrysts are strongly corroded and seritization of plagioclase especially is ubiquitous. Quartz xenocrysts may be rimmed by a fine-grained amphibole (ocellar texture), which is also typical for hybrid rocks of the complex. Alkali feldspar xenocrysts show inclusions such as plagioclase and quartz, and inclusion rim of amphibole often occurs in the margins of alkali feldspar and plagioclase xenocrysts. Some anhedral quartz may also be present.

Mantling of alkali feldspar xenocrysts by plagioclase can be generated by magma mixing (c.f., Hibbard 1981, 1991) and is occasionally found in some pillow-like MMEs. The occurrence of this texture seems to be correlated with the degree of the hybridization; in general, alkali feldspar xenocrysts in MMEs are not mantled but those in pillow-like MMEs are often surrounded by plagioclase and micrographic quartz(±plagioclase) mantles (Fig. 11). The alkali feldspar megacrysts are sometimes pigmented; in these instances the pigment also occurs in the plagioclase and micrographic rims. Between the micrographic and plagioclase rims in Figure 11 is a zone of apatite crystals. Their shape is stubbier than that of those in the matrix of the pillow-like MMEs. They probable do not represent entrained apatite from the mafic magma but represent a diffusion front of Ca, F, and P formed at relatively high temperatures in the first stages of hybridization.

Minerals in the matrix of MMEs are usually compositionally identical to those in the host rocks but their relative abundance and grain size differs. Modal composition of the MMEs differs with the degree of hybridization, but commonly the main minerals are hornblende and plagioclase with Fe–Ti oxides. Augite is frequently found in MMEs, but it is lacking in pillow-like MMEs. Occasional phenocrysts of pigeonite and enstatite also occur in xenocryst-free MMEs with altered rims indicating disequilibrium with the host rock; they probably

Fig. 11. Photomicrograph of an alkali feldspar xenocryst with a plagioclase mantle (plm) and micrographic texture (mct) in a pillow-like MME from north of lake Kirkkojärvi, western part of the complex. The width of the picture corresponds to 0.8 mm.

represent phases stable in the magma before hybridization.

Typical accessory minerals in pillow-like MMEs are biotite, magnetite, and apatite. No olivine has been found; interstitial quartz is usually present in small amounts. Plagioclase in the matrix of the MMEs forms 0.1–0.2 mm long laths, but larger (0.5 mm) plagioclase crystals occur. Green–yellowish green amphibole occasionally forms a spherulitic-like texture with ilmenite. Biotite content is high only in the pillow-like MMEs, where biotite with varying degrees of chloritization as well as amphibole may occur as phenocrysts up to two millimetres in diameter. Biotite may occur as chloritized grains but also as elongated grains termed blade biotite by Hibbard (1991). Pillow-like MMEs show a microgranular texture whereas spherulites and subophitic textures typical of other MMEs are rare.

Hybrid rocks

Hybrid rocks of the Jaala-Iitti complex usually occur as relatively small units in hornblende granites and are characterized by a greater abundance of MMEs (see Fig. 7) compared to the hornblende granites. In the hybrid rocks, the quartz grains are rimmed by amphibole±augite (ocellar texture; Fig. 12) and alkali feldspar megacrysts are mantled by plagioclase–quartz intergrowths (micrographic texture; Fig. 13). When megacrysts are lacking in the hybrid rocks, the micrographic texture occurs in the matrix (Fig. 14). Compared to the hornblende granites, hybrid rocks are greyer on nonweathered surfaces. Higher modal plagioclase content (22–40 vol%) in the hybrid rocks compared to the granite (10–25 vol%) varieties of the Jaala-Iitti complex leads to a monzogranitic composition (Fig. 3) for the hybrid rocks. The hybrid rocks also have a greater abundance of needle-like apatite crystals compared to the granites of the complex. Hybrid rocks are usually rather homogeneous but local variations are found mainly in the amounts of alkali feldspar, plagioclase, and quartz megacrysts as well as grain size, and the presence or mantling textures.

Locally, there are large amounts of xenoliths (Svecofennian granitoid rocks and rapakivi granites) and these are accompanied by a large number of megacrysts. This suggests that not all megacrysts in the hybrid rocks are from the hornblende granite or the hornblende-quartz-feldspar porphyry. Some of them are from disaggregated xenoliths. This is the probable explanation for the larger (over 10 cm in diameter) alkali feldspar megacrysts in the hybrid rock. In the granites of the complex, alkali feldspar phenocrysts rarely reach five centimetres in diameter.

The matrix of the hybrid rocks is fine- to medium-grained and is mainly alkali feldspar, plagioclase ($An_{25–40}$), quartz, and amphibole. Minor amounts of augite, biotite, Fe–Ti oxide (mainly ilmenite), needle-like apatite, fayalite, and chlorite occur. Zircon content in the hybrid rocks is low compared to that of granites in the complex.

Fig. 12. Hybrid rock from the Lokonmäki quarry with an alkali feldspar ovoid composed of several sectorially intergrown crystals. Note also quartz mantled by amphibole and alkali feldspar megacrysts with micrographic rim. Width of the picture corresponds to 16 cm.

Fig. 13. Hybrid rock from the Lokonmäki quarry with a alkali feldspar ovoid mantled by micrographic intergrowth of feldspar and quartz. Width of the picture corresponds to 14 cm.

Fig. 14. Photomicrograph of the matrix of the hybrid rock with widespread micrographic texture and two quartz ocelli at the top-left and top-right corners. Width of the picture corresponds to 2.1 mm.

Pyroxene and fayalite are found only as corroded remnants surrounded by amphibole or as irregular masses with amphibole, Fe–Ti oxide, and apatite. Amphibole with pyroxene and olivine occasionally forms aggregates including secondary biotite. This suggests that pyroxene and olivine were not in equilibrium with the main minerals of the matrix, i.e., plagioclase, alkali feldspar, and quartz, perhaps also amphibole.

The amount of biotite is variable but usually small. Biotite commonly occurs interstitially, but may form larger grains up to one millimetre across. Biotite is altered to chlorite and only rarely contains inclusions of apatite, zircon, or amphibole.

Amphibole usually forms anhedral grains and occasionally elongated crystals, but may also form euhedral grains up to 0.5 mm in diameter. Amphibole is also found rimming quartz crystals and quartz aggregates but some plagioclase megacrysts have been found rimmed by amphibole also with occasional augite inclusions. Amphibole surrounding quartz forms anhedral grains but when surrounding plagioclase it may show a more elongated shape where the long dimension of amphibole is perpendicular to the plagioclase. This is contrary to orientation of amphiboles surrounding quartz (ocellar texture) where the long dimension of the amphibole is usually parallel to the grain boundary.

Plagioclase megacrysts are commonly subhedral but may show euhedral grain boundaries especially with biotite. Seritization is usually pervasive throughout the megacrysts but may only be visible in the outer part of the plagioclase. Some plagioclase megacrysts may show amphibole inclusions throughout the grain along with euhedral apatite. In these cases more antiperthite is visible. Antiperthitic zones also occur in the outer part of the plagioclase megacrysts, again with amphibole inclusions and some apatite. In the matrix of the hybrid rock, plagioclase forms laths up to 0.5 mm in diameter.

Alkali feldspar megacrysts and mineral aggregates are up to 10 cm in diameter, and they sometimes consist of several sectorially intergrown units (Fig. 12). Alkali feldspar megacrysts are usually rimmed by a micrographic plagioclase–quartz intergrowth but also by a (alkali feldspar–quartz) granophyric intergrowth on the outer part of the megacrysts. Micrographic texture in the matrix is closely related to the presence of alkali feldspar grains where quartz forms sets of elongated crystals in the outer part of the grain oriented perpendicular to the matrix and especially toward plagioclase and quartz, but randomly toward amphibole or biotite. Occasionally the whole grain contains graphic quartz. This graphic texture may replace whole small alkali feldspar grains now recognized only by grain boundary remnants. This graphic texture is also present when occurring on the outer part of the grain surrounding the euhedral core of an alkali feldspar.

Rims around alkali feldspar megacryst are usually composed of micrographic plagioclase–quartz intergrowths. Some plagioclase intergrowths have also been identified from the rocks of the complex occurring in two different modes. Plagioclase intergrowths are also present in hornblende granites where there is a rim of usually thin seritized plagioclase (Fig. 4). A second type observed in intergrowths contains numerous inclusions of amphibole and in this case the plagioclase is less seritized (Fig. 15). The composition of plagioclase is similar to that of the matrix (An_{28-37}) but small remnants of more calcic plagioclase (An_{52}) may occur as a core for the rim plagioclase. It is possible that in the first case the texture represents a plagioclase intergrowth formed mainly before hybridization or that it represents a disequilibrium type of crystallization after a hybridization event. The latter type of plagioclase intergrowth is more likely to have formed just after the hybridization event before chemical equilibrium was reached and a more calcic plagioclase began to precipitate.

Fig. 15. Photomicrograph of plagioclase intergrowth in a hybrid rock. Note the amphibole inclusions in plagioclase and fringed quartz between the plagioclase and alkali feldspar megacryst. Width of the picture corresponds to 6.1 mm.

PETROGRAPHICAL EVIDENCE OF HYBRIDIZATION

Hibbard (1991; see also Hibbard 1981) lists twelve textures reflecting possible magma mixing: 1) rapakivi texture, 2) antirapakivi texture, 3) poikilitic texture in quartz or K-feldspar, 4) sphene with ocellar texture, 5) quartz–hornblende in ocellar tex-

ture, 6) hornblende/biotite zones in K-feldspar phenocrysts, 7) blade biotite, 8) acicular apatite, 9) small plagioclase laths, 10) spike zones in plagioclase, 11) boxy cellular plagioclase, and 12) spongy cellular plagioclase. Most of the textures described above and attributed to magma mixing systems are also found in the MMEs, pillow-like MMEs, and hybrid rocks of the Jaala-Iitti complex. Those that were not recognized are sphene ocellar texture, antirapakivi texture, and poikilitic alkali feldspar. Poikilitic quartz, however, occurs commonly in micro-enclaves. Plagioclase forms a common xenocryst in pillow-like MMEs, and disequilibrium and dissolution textures in Hibbard's categories 10–12 are present in the plagioclase megacrysts of the MMEs and hybrid rocks. Small lath-shaped plagioclase is also common in hybrid rocks and the MMEs of the complex. Blade-shaped biotite is found especially in pillow-like MMEs, but also in MMEs where it forms elongated grains and occurs interstitially (Hibbard 1991). Hornblende (±plagioclase±apatite) zones are common in alkali feldspar and plagioclase megacrysts, usually in the outer part of the grains, and were formed in the early stages of hybridization in a similar way to quartz rimmed by amphibole (Hibbard 1991). Thus, whilst this texture is common in hybrid rocks, it is also commonly found in non-hybrid rocks, i.e., hornblende granite and hornblende-quartz-feldspar porphyry of the complex. So, despite the disequilibrium between feldspar megacrysts and their host magmas, the texture also results from heterogeneous crystallization or changes in crystallization order. Three of the remaining textures indicating magma mixing, rapakivi texture, micrographic texture, quartz–hornblende ocellar texture, and acicular apatite are commonly visible in the hybrid rocks, MMEs, and pillow-like MMEs of the Jaala-Iitti complex.

Mantled alkali feldspar ovoids

Two different modes of mantled alkali feldspar megacrysts occur in the rocks of the Jaala-Iitti complex. Mantling of alkali feldspar by plagioclase is found in hornblende granites (Fig. 4), pillow-like MMEs (Fig. 11), and hybrid rocks (Fig. 15). Alkali feldspar megacrysts in the hybrid rocks, MMEs, and pillow-like MMEs are more commonly mantled by a rim of micrographic plagioclase–quartz intergrowth (Fig. 12). Some similarities between micrographic texture and plagioclase mantles may be noted, but whether these textures are formed by similar mechanisms is questionable. Petrographic similarities supporting their close relationship and origin are: 1) alkali feldspar forming ovoids is occasionally replaced by both plagioclase and micrographic texture (Fig. 11), 2) both intergrowths (Fig. 13) have also been observed surrounding disaggregated granitoid xenoliths, 3) intergrowths may exist together in the same alkali feldspar xenocryst in pillow-like MMEs (Fig. 11), both probably formed after capture of the xenocryst by a mafic magma, 4) alkali feldspars show exsolution of albite (and possible some quartz) and they contain usually numerous inclusions, 5) both textures usually contain varying amounts of amphibole, Fe–Ti oxide, and occasionally apatite (inclusions), and 6) both textures are found in hybrid rocks of the complex. Some plagioclase in micrographic texture also shows a larger grain size with more rapakivi texture-like appearance. The plagioclase mantles in the rocks of the Jaala-Iitti complex, however, contain only small amounts of quartz when compared with that of micrographic texture. Plagioclase forming complete rims is usually strongly seritized; only some discontinuous unaltered plagioclase mantles in pillow-like MMEs are found. Plagioclase mantles on alkali feldspar megacrysts also occur to some extent in hornblende granites where a micrographic texture is lacking. Because micrographic texture seems to be correlated with hybrid rocks, this chapter will concentrate mainly on its origin. The term micrographic texture is used here for that plagioclase–quartz intergrowth which is mantling alkali feldspar megacrysts (Fig. 16), whereas granophyric intergrowth (Fig. 17) describes a quartz-alkali feldspar symplectite within the alkali feldspar megacryst or as radiating fringes of quartz on the borders of alkali feldspar as defined by Smith (1974).

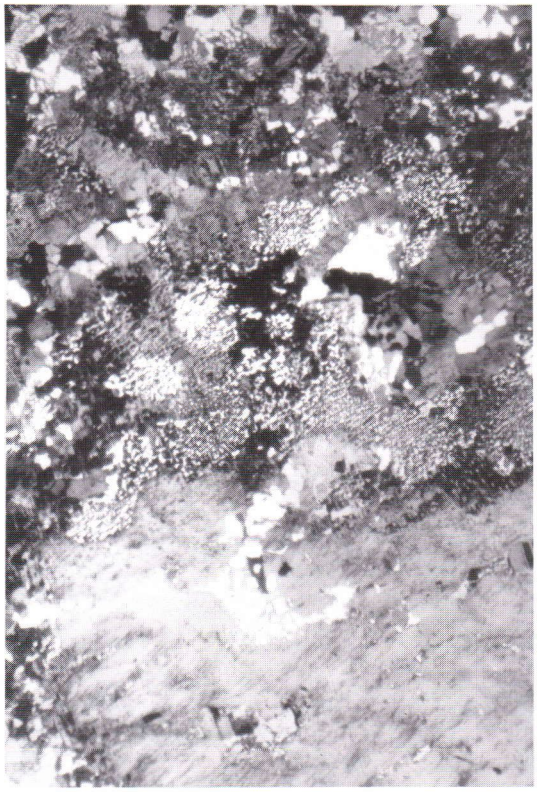

Fig. 16. Photomicrograph of micrographic texture surrounding an alkali feldspar megacryst in a hybrid rock of the Jaala-Iitti complex. Width of the picture corresponds to 8.0 mm.

Fig. 17. Photomicrograph of granophyric intergrowth in alkali feldspar megacryst (af) occurring in contact with quartz (qz) in a rapakivi granite xenolith from the hybrid rock of the Jaala-Iitti complex. Note also a swapped albite rim (arrow) between the alkali feldspars. Width of the picture corresponds to 0.8 mm.

The micrographic rim (Fig. 16) is usually less than one millimetre thick, but may occasionally be up to one centimetre thick. Usually large alkali feldspar megacrysts tend to be aggregates of alkali feldspar with quartz and plagioclase. Micrographic texture is also found mantling large granitoid xenoliths. Individual alkali feldspar grains mantled by micrographic texture are anhedral and corroded and contain numerous inclusions of quartz and plagioclase (An_{28-30}). Plagioclase inclusions are rimmed by quartz and occasionally by albite. Plagioclase inclusions are commonly euhedral and form grains of 0.5 mm in diameter. Quartz is also usually present within alkali feldspar megacrysts and occurs as a rim on plagioclase, as individual drop quartz grains, and quartz grains which are concave towards the matrix and form granophyric intergrowths. Granophyric intergrowths occur in the outer part of the large alkali feldspar megacrysts (Fig. 17) but are also common in the matrix of the hybrid rocks replacing alkali feldspar grains. Quartz grains also occur between the alkali feldspar grains implying a xenolith origin for the mantled aggregates. Quartz is also found between the alkali feldspar ovoid and plagioclase mantle with fringed shape (Fig. 15).

The contact between the micrographic rims and the alkali feldspar megacrysts are usually sharp and granular with alkali feldspar replaced by the micrographic plagioclase–quartz intergrowth (Fig. 18a; see also Figs. 11 and 16). Usually alkali feldspar megacrysts contain perthitic albite as in Figure 18b (compare to Fig. 18c). Near the outermost part

of the alkali feldspar megacryst there is occasionally a zone of anhedral apatite inclusions. This feature is also found in some mantled alkali feldspar xenocrysts in pillow-like MMEs, and they probably result from slow diffusion and enrichment of Ca, P, F, and H_2O at the border between the alkali feldspar and the host magma. The average size of the plagioclase grains in a micrographic rim is 0.1 to 0.5 mm. They appear as individual grains separated by quartz, but they may also form larger grains up to 4 mm in diameter. Elongated anhedral quartz in the micrographic rim is usually oriented toward the matrix of the host rock (Figs. 18d and 18e). The average grain size of quartz in the micrographic texture is 0.2 mm. Usually the micrographic rims lack alkali feldspar (Fig. 18f).

At least three different models for the origin of the alkali feldspar megacrysts with micrographic rims can be postulated. They may represent: (1) phenocrysts that crystallized from the magma that formed the host rock, (2) megacrysts captured from the felsic end-member of the complex during hybridization, or (3) xenocrysts derived from disaggregated country rock xenoliths. Derivation of the alkali feldspar megacrysts from the granite varieties (hornblende granite, hornblende-quartz-feldspar porphyry) of the complex is a reasonable possibility but does not explain all alkali feldspar megacrysts, as granites of the complex do not contain such large alkali feldspar phenocrysts (> 10 cm) as some of the megacrysts are. In pillow-like MMEs and MMEs, the diameter of the alkali feldspar megacrysts rarely reaches 3 cm and it is, therefore, presumed that most of the alkali feldspar xenocrysts are derived from the partially crystallized felsic or hybrid members of the complex.

Disintegration of porphyritic rapakivi granite xenoliths has locally produced large alkali feldspar and quartz xenocrysts in the hybrid rocks (Fig. 19). Porphyritic rapakivi granite xenoliths have been

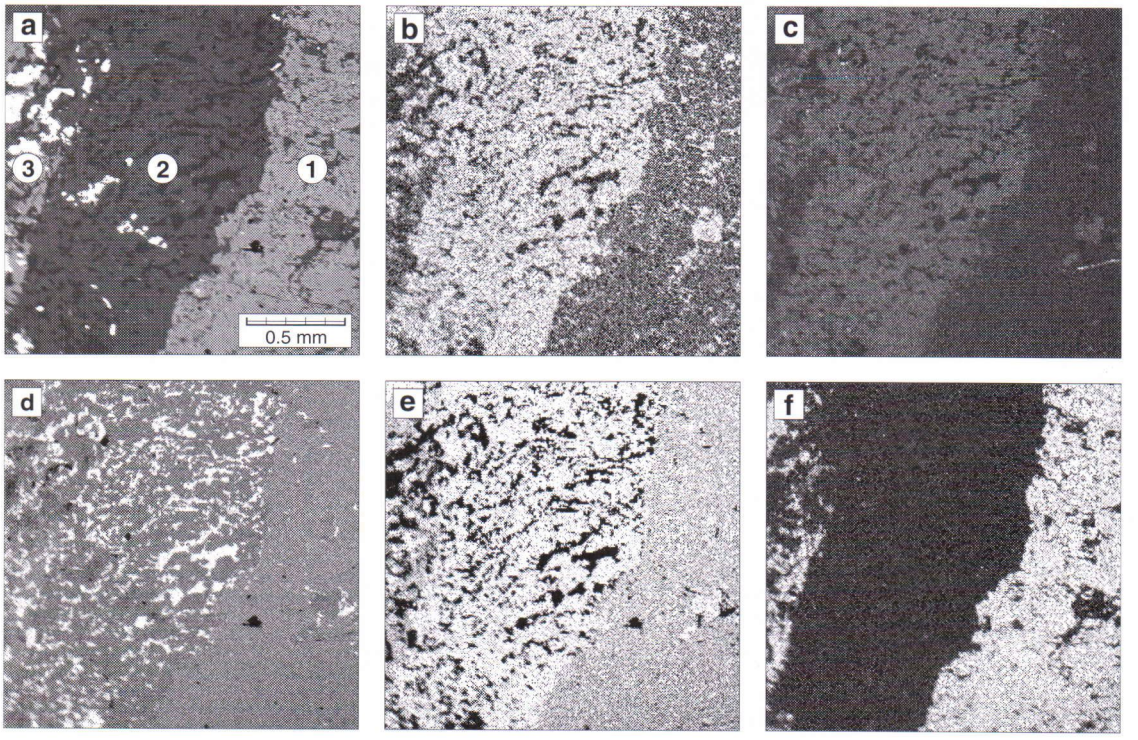

Fig. 18. (a) Scanning electron microscope images of an alkali feldspar megacryst in hybrid rock of the Jaala-Iitti complex (1) surrounded by a micrographic rim (2) in hybrid rock matrix (3). Figures show distribution of (b) Na, (c) Ca, (d) Si, (e) Al, and (f) K.

Fig. 19. Disaggregation of a porphyritic rapakivi granite xenolith (left) producing alkali feldspar and quartz xenocrysts in the hybrid rock of the Jaala-Iitti complex. Width of the picture corresponds to 19 cm.

found mostly in the eastern part of the Jaala-Iitti complex, but also less commonly in the western part, where the xenoliths can be up to several meters in diameter. The country rocks in the western part of the complex are Svecofennian (Fig. 2), and the occurrence of porphyritic rapakivi granite xenoliths in that area suggests that they were entrapped at deeper levels.

Melting of the rapakivi granite xenoliths starts along the grain boundaries resulting in quartz grains rimmed and partially replaced by amphibole, and in partially separated alkali feldspar megacrysts. Alkali feldspar megacrysts are abundant near large xenoliths, and they are usually mantled by micrographic rims. Micrographic texture is also more common in the matrix of the hybrid rock near the xenolith where it occurs either as cellular mass or as a granophyric intergrowth surrounding and replacing alkali feldspar.

Granophyric intergrowths generally have bulk compositions close to the minimum melt composition in the Or–Ab–Qz–H_2O system (Smith 1974). Within the xenolith, the incipient melting results in granophyric intergrowth of quartz in alkali feldspar megacrysts (Fig. 17). The thickness of the granophyric zone is usually less than 0.3 mm against quartz grains, but it can reach thicknesses of 2 mm when the alkali feldspar megacryst is in contact with hybrid rocks. In the latter case there is also more plagioclase in the micrographic rim. Quartz in the granophyric zone is elongated towards the enclosing quartz (Fig. 17). The boundary between alkali feldspars in a disaggregated granitoid xenolith is often crenulate and host to swapped albite rims (Fig. 17). Granophyric texture is occasionally visible as fringed quartz in plagioclase when the latter is in contact with quartz or another plagioclase.

On the margins of alkali feldspar xenocrysts enclosed in the hybrid rocks there is also a zone of granophyric intergrowth of quartz, plagioclase, and amphibole similar to the micrographic texture common in the hybrid rock.

Fenn (1986) suggests that quartz-feldspar intergrowths are produced by "the simultaneous growth of quartz and feldspar in a kinetically driven, disequilibrium situation". This is probably what has happened in the Jaala-Iitti complex. Granophyric intergrowth and micrographic textures are similar to those of the Tarkki granite described by Haapala (1977a), Kahma (1951), and Laitakari (1928). Micrographic texture in the Tarkki granite occurs at the contact zone between the granite and a younger diabase. Haapala proposed that the heat flow from the diabase to the granite has caused partial melting of the granite causing quartz to form different types of intergrowths with both alkali feldspar and plagioclase.

The micrographic textures in the Jaala-Iitti complex indicate a marked temperature difference between the hybrid magma and the alkali feldspar megacrysts which were formed before hybridization. Melting of the alkali feldspar megacryst at first caused quartz and albite to migrate to form a grano-

phyric intergrowth within the megacrysts. Afterwards, as dissolution of the alkali feldspar continues, a symplectic quartz-plagioclase rim crystallized. Diffusion of Na from the alkali feldspar and diffusion of Ca from the surrounding melt (inferred from the apatite inclusions on the border between the alkali feldspar and the micrographic rim) creates favourable conditions for plagioclase to crystallize together with quartz to form the micrographic rim. Finally, rims crystallize as in the rapakivi texture of the Wiborg batholith.

Mafic rims around quartz

MMEs, pillow-like MMEs, and hybrid rocks of the Jaala-Iitti complex typically contain quartz grains and quartz aggregates that have millimetre-thick rims of amphibole and sometimes also augite (Fig. 20). Occasionally mafic rims are also found surrounding plagioclase megacrysts in the MMEs and hybrid rocks. The amount of this texture varies locally, and there may be rocks rich in quartz with amphibole rims as in Figure 12. Amphibole rims also contain minor amounts of biotite, needle-like apatite, ilmenite, and hematite.

Quartz xenocrysts mantled by mafic minerals (usually amphibole and/or pyroxene) have been found in different plutonic and volcanic rocks and they are often referred to as ocelli quartz (e.g., Angus 1962, 1971, Hanuš & Palivcová 1969, Palivcová 1978, Eklund *et al.* 1989, Rämö 1991, Lindberg & Eklund 1992), or micro-xenoliths (Castro *et al.* 1990a). A common feature for all these occurrences is a relatively mafic host rock (gabbro, andesite, etc.). The source of the quartz is thought to be disintegrated (granitoid) xenoliths and/or a felsic end-member or host rock (Vernon 1983, Eberz & Nicholls 1988, Eklund & Lindberg 1992). Ocellar texture seems to occur more often in granitoids where MMEs occur. In these cases the quartz has been incorporated from a felsic magma and occurs in a host that is more or less hybrid in character. It has also been proposed that mafic magmas that intrude partially crystallized granitic bodies precipitate ocellar gabbros (Angus 1971). The origin of the amphibole coronas around quartz has been explained as metasomatic (Angus 1962, 1971) or that the quartz represents pseudomorphs after hydrothermally decomposed phenocrysts of olivine (Hanuš & Palivcová 1969). The possibility that quartz represents former miarolitic cavities has also been proposed (Vernon 1983).

Fig. 20. Photomicrograph of a quartz grain surrounded by amphibole-augite rim in the hybrid rock of the Jaala-Iitti complex (sample 90141) at Lokonmäki. Width of the picture corresponds to 8.0 mm.

The mafic rims around quartz grains are angular or gently rounded in form, depending on whether the rim encloses one grain or several grains (Fig. 20). Augite in the corona is commonly found as a remnant surrounded by amphibole. More commonly, amphibole occurs partially within the quartz grains rather than rimming them. This is more likely to have been caused by recrystallization rather than corrosion of quartz because amphibole inclusions are also found in the outer part of the quartz grains where needle-like apatite occurs as well. The am-

phibole grains form sharp contacts with the quartz (Fig. 20) and may occur as two generations: subhedral and "ragged". Fe–Ti oxide, and occasionally hematite, inclusions are also more common in the inner part of the rims.

The occurrence of some ocelli is clearly controlled by the amount of xenoliths present; some of the granite xenoliths have a thin corona similar to those of individual quartz xenocrysts. Contact between individual quartz grains in aggregates is sinuous (Fig. 21a) probably an indication of melting. Quartz forms grains up to 1 cm in diameter and appears to be formed of several small quartz grains those outline is shown by fluid and Fe–Ti oxide inclusions and by small differences in optic orientation (Fig. 21b). Quartz from the disaggregated xenoliths usually contains numerous zircon inclusions (Fig. 21c). Zircon is also found between quartz and the surrounding amphibole rim in which case it may originate from disaggregated xenoliths, having precipitated on the quartz grains before the amphibole, or from the hybrid magma. This might be of use in separating the origin of quartz, as to whether it originated from disaggregated xenoliths or originated from the felsic end-member of the bimodal system. This latter origin is visible in small ocelli where quartz is present as an individual grain without signs of recrystallization or large scale melting of the grain. Quartz may also contain feldspar inclusions (Fig. 21d). This suggests that the quartz and feldspar grains were derived either from a cooler, largely crystallized rapakivi magma or from partially melted and disaggregated xenoliths. The larger granitoid xenoliths occasionally have a mafic (diabase) rim possibly as a result of the quenching of mafic magma on a solid xenolith.

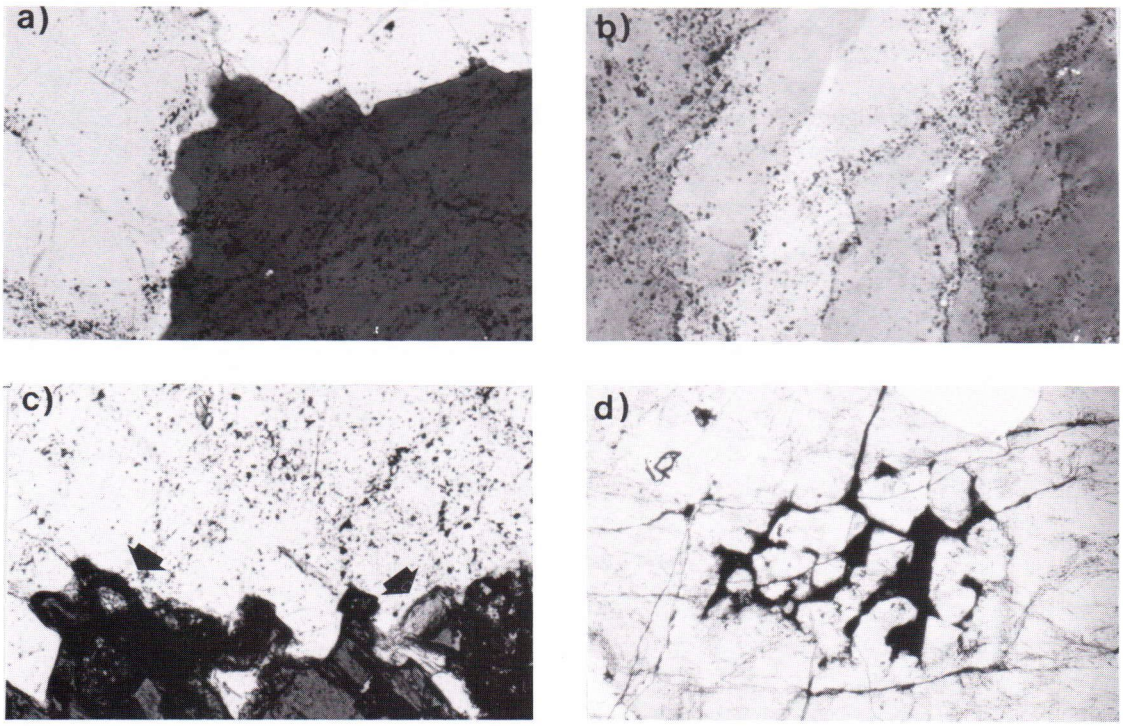

Fig. 21. Photomicrographs showing certain characteristics of ocellar texture originating by disintegration of a xenolith. a) Soft sinuous contacts between quartz grains. Sample 9014. b) Part of a large quartz grain composed of several smaller anhedral quartz grains forming a mosaic texture. The pigment probably outlines original grain boundaries. Sample 9014. c) Zircon crystals (arrows) between quartz and amphibole corona. Sample 90501. d) An altered remnant of a feldspar in a large quartz grain. Sample 90501. Width of pictures corresponds to 0.8 mm (a,b, and c) and 3.3 mm (d).

Zircon inclusions and remnants of feldspar grains in quartz obviously outline the original boundaries of the quartz grains. Usually the diameter of individual quartz grains is less than 3 mm and they do not show the characteristics of quartz aggregates derived from disaggregated xenoliths, i.e., zircon and feldspar inclusions. These quartz grains are assumed to have originated from the felsic end-member of the complex. Ocellar textures found in the MMEs, and especially in the pillow-like MMEs are typically small (under 1 cm in diameter), and they are most likely derived from the surrounding host rock.

Corona textures can be formed by reactions between the hybrid magma and partially fused quartz xenocrysts (Sato 1975). The controlling factor of generating amphibole (pyroxene) coronas around quartz is the bulk composition and the crystallization state of the host magma which provide suitable conditions for precipitating mafic rims around a quartz xenocryst. Quartz xenoliths and aggregates found in hornblende granites are commonly without coronas. Ocellar texture is not necessarily a proof of hybridization; it can also result from assimilation. It may indicate a local mingling of felsic and mafic magmas where the xenocrysts are derived from the felsic end-member of the bimodal system, and where magma mixing has created a sufficiently mafic composition within the host rock.

Habit of apatite as an indicator of hybridization

Needle-like apatite is assumed to be evidence of rapidly quenched mafic magma (e.g., Lee *et al.* 1973, Vernon 1983, Allen 1991, Hibbard 1991) a presumption based on the work by Wyllie *et al.* (1962). This feature is present in the MMEs of the Jaala-Iitti complex which carry needle-like apatite crystals more commonly than the granites. The amount of apatite in MMEs is also remarkably higher than in hornblende granites. Typically, in the hybrid rocks close to the MMEs significant amounts of needle-like apatite are found (Fig. 22) which is not indicative of rapid quenching of hybrid host but mainly intermingling of apatite crystals from the mafic magma into the hybrid magma.

The length of apatite grains varies commonly between 10 and 100 μm. In the MMEs and hybrid rocks, the length of apatite may reach 550 μm, and a length-width ratio (l/w) up to 150 has been recorded. In the hornblende granites the grain size of apatite is under 270 μm, and a l/w less than 40. Apatite is commonly stubby, and about 60 % of the apatites have a l/w between 1 and 7 (Fig. 23a). Typically, MMEs and hybrid rocks show a flat distribution of l/w between 1 and 20 (Figs. 23b and 23c, respectively). About 20 % of the apatites in the MMEs and hybrid rocks have a l/w over 20, whereas in hornblende granites the amount is under 2 %. Pillow-like MMEs contain more apatite with a high l/w (10–20) than small MMEs.

The length-width ratio of apatite (high l/w) in the MMEs is probably caused by a quenching of magma. Bulk rock F content of the MMEs is relatively high; 1100 to 8000 with an average of 2400 ppm. In the hybrid rocks and hornblende granite F content is under 2100 ppm. As a mobile element F probably diffused from the felsic end-member at an early stage of hybridization, which could have resulted in an oversaturation of F in the MMEs. High F (and H_2O) may also have stabilized amphibole over pyroxene or olivine. Zones of apatite between partially dissolved alkali feldspar xenocryst and micrographic and/or plagioclase rims are also indicative of diffusion of F into a mafic magma.

Rapid quenching of the magma is, however, not a probable explanation for occurrence of needle-like apatite in hybrid rocks of the complex. The generation of hybrid rocks took place over a relatively long time interval and the occurrence of needle-like apatite throughout the hybrid rock is probably caused by disintegration of partially crystallized mafic magma. Hybridization in the granitic rocks of the Jaala-Iitti complex is therefore typified by coexistence of stubby and needle-like apatites.

Recrystallization of magmatic mafic enclaves

Injection of a mafic magma into a magma of higher viscosity causes disintegration of the mafic magma

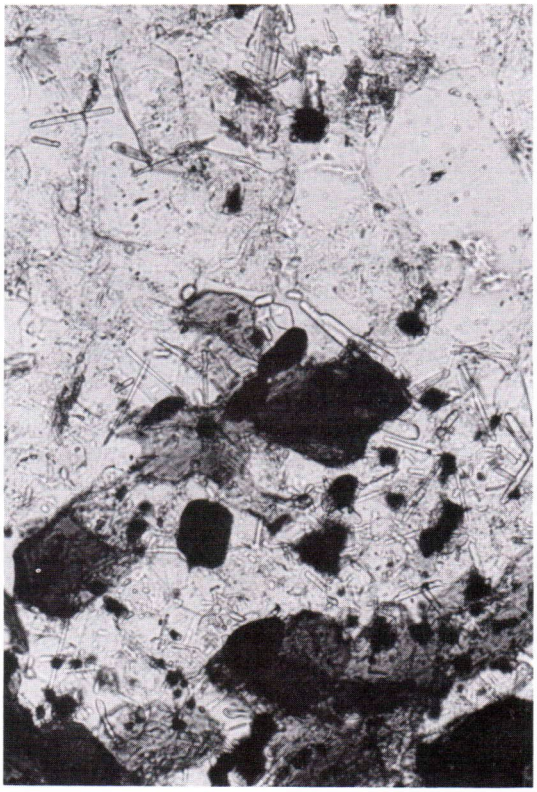

Fig. 22. Photomicrograph of the boundary zone between a small MME at the bottom of the picture and hornblende granite (sample 91381) with needle-like apatite grains. Width of the picture corresponds to 0.3 mm.

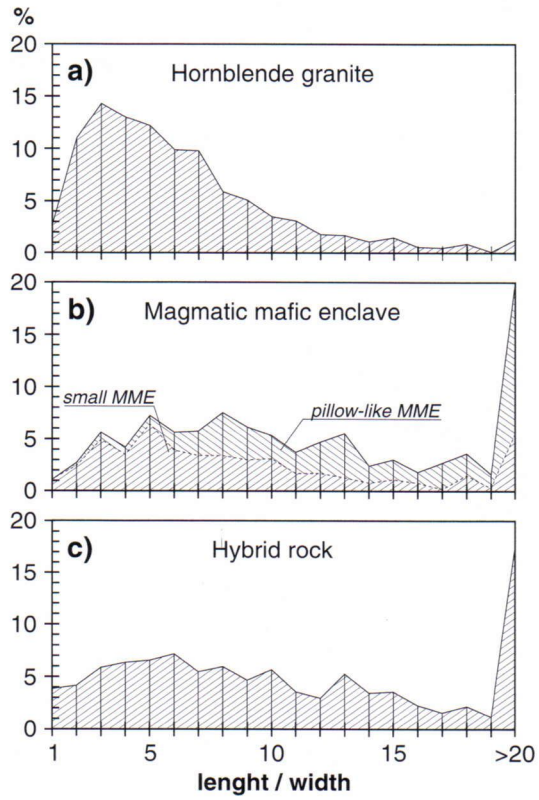

Fig. 23. Percentage distribution of apatite length-width ratios in a) hornblende granites, b) magmatic mafic enclaves, and c) hybrid rocks, based on 1000 measurements per rock type. The total distribution of apatites in magmatic mafic enclaves is based on 500 measurements from pillow-like MME and 500 measurements from small MME.

to form MMEs. The degree of disintegration of the mafic magma and the size of MMEs that form depend on the influx rate of the injected magma as well as the crystallinity of the host. In general, the degree of disintegration of the mafic magma generating smaller MMEs increases away from the fountain pipe if the influx of the mafic magma is high enough. As commingled mafic and felsic magmas equilibrate, the disintegrated MMEs may recrystallize. Recrystallization features have been described from granitic rocks by Bowen (1922), Nockolds (1932), Reid *et al.* (1983), Tindle and Pearce (1983), and Vernon (1991).

Two types of recrystallization of MMEs have been discovered in the hybrid rocks and hornblende granites of the Jaala-Iitti complex (Fig. 24): 1) recrystallized zones at the margins of MMEs, and 2) small (less than 2 cm in diameter) droplets of completely equilibrated mafic magma forming micro-enclaves. Chemical and thermal equilibrium has resulted in equilibrium zones in which the composition of minerals and the grain size is similar to those in the host rock.

In recrystallized borders of the MME, the grain size of hornblende is usually from 1 to 2 mm in diameter whereas in the central parts it is 0.2 to 0.4 mm. Individual grains of hornblende and biotite occur with inclusions of ilmenite and apatite. Ilmenite is also found as elongated mineral aggregates displaying a primary subophitic texture of MMEs. This is also comparable to some observed MMEs in rapakivi granites of the Wiborg batholith

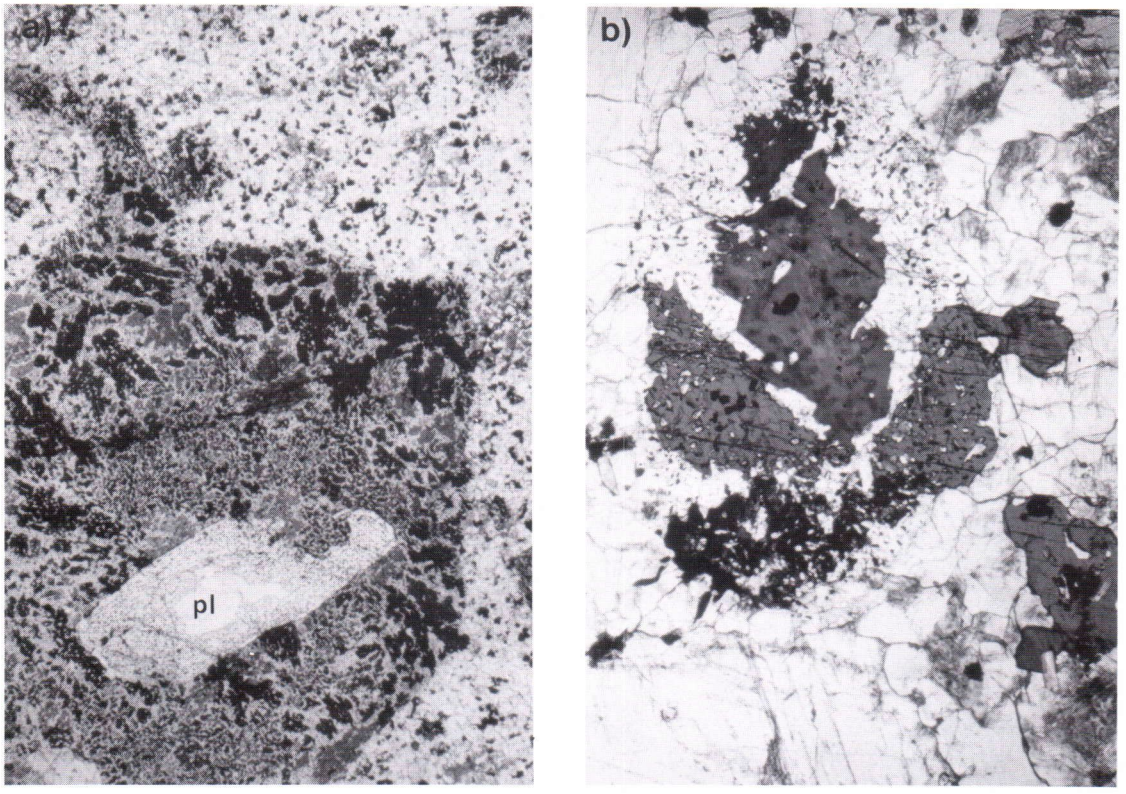

Fig. 24. Photomicrographs of recrystallized MMEs. a) Recrystallized border of MME (sample 91382) in hornblende granite (sample 91381). Note a corroded and zoned plagioclase (pl) xenocryst/phenocryst. Width of the picture corresponds to 11.5 mm. b) A micro-enclave in the hybrid rock (sample 9019) outlined by ilmenite grains. Note also a recrystallized amphibole grain across the area of the original MME at the right part of the micro-enclave. Width of the picture corresponds to 3.3 mm. See text for discussion.

where MMEs usually show a larger grain size, equalling that of their host rocks, indicating complete recrystallization under similar conditions with limited chemical exchange.

In the Jaala-Iitti complex, micro-enclaves or magmatic mafic micro-enclaves (MMMEs) occur as a small ovoidal MMEs that have the remnants of primary enclave boundaries outlined by ilmenite and apatite grains. The size of these enclaves varies from 0.5 to 2 cm and they are discernible as inclusion-rich areas within amphibole and biotite grains (Fig. 24b). The mineralogy of the micro-enclave is almost identical to that of the host rock. The matrix contains ilmenite, euhedral laths of plagioclase, needle-like apatite, and relatively large anhedral poikilitic quartz. Iddingsite pseudomorps after olivine or pyroxene also occur. Amphibole and biotite have occasional small inclusions of pyrite. The grain size of plagioclase laths (0.1 mm) is similar to those of MMEs that have not undergone recrystallization but the grain size of the amphiboles especially (from 1 to 2 mm in diameter) approaches that of the host rock, and amphibole has occasionally grown across the primary enclave border (see Fig. 24b).

Compared to micro-enclaves, amphibole aggregates in granites and hybrid rocks of the Jaala-Iitti complex show similar features: the mafic silicate is dominantly amphibole, apatite and Fe–Ti oxide inclusions are present as well as quartz but the amount of feldspars is low. The main difference between the micro-enclaves and mafic aggregates in granites and hybrid rocks is in shape; the latter are more irregular and sharp boundaries are lacking. The size

of the amphibole aggregates is up to 1 cm in diameter. Primary inclusion area is usually difficult to define, and only the greater amount of inclusions supports their different origin vis-à-vis micro-enclaves. Amphibole aggregates more commonly have both magnetite and ilmenite inclusions whereas the matrices of hybrid rocks and MMEs of the Jaala-Iitti complex are dominated by ilmenite. Apatites usually are stubby, and zoned – in contrast to apatites in the matrix. Significant amounts of apatite inclusions are concentrated in biotite and hornblende; similar inclusions have been proposed as a restite phase that was incorporated in the biotite and hornblende as a result of the primary restite pyroxene reacting with the magma (Chappell *et al.* 1987). Some apatites in the matrix also do show zoning, in which the central part may represent a restite.

Disintegration and recrystallization of MMEs are clear evidence of two magmas of different composition equilibrating and producing a commingled magma of intermediate composition, and contribute beginning of (or present) local hybridization between mafic diabase magma and felsic rapakivi granite magma. It is an effective process that adds constituents forming hornblende, biotite, and plagioclase to a felsic magma, and in extreme cases leaves little trace of the event.

COMPARATIVE MINERAL CHEMISTRY AND GEOTHERMOBAROMETRIC APPLICATIONS

Electron microprobe analyses of the main minerals from the rocks of the Jaala-Iitti complex were made to define the composition of the minerals and to study inter-mineral equilibria. Geothermometric and -barometric calibrations are used together with petrographic studies to set constraints for crystallization and hybridization events.

A total of 369 analyses of amphibole (87), apatite (45), biotite (19), alkali feldspar (40) plagioclase (72), ilmenite (51), magnetite (28), pyroxene (17), and olivine (10) were made from the rock types of the complex; average mineral analyses are given in Appendix 1.

Analytical procedures

Mineral analyses were made mainly at the Ore Mineralogical Laboratory of the Geological Survey of Finland (Espoo); some analyses were performed at the University of Oulu, Department of Electron Optics. The analyses at the Geological Survey of Finland were done by the author, those at the University of Oulu by the employees of the department.

Analyses at Geological Survey of Finland were obtained with a JEOL 733 electron microprobe with an accelerating potential of 15 kV at a beam current of 150 nA for feldspars, 200 nA for apatites, 250 nA for amphiboles, biotites, pyroxenes, and olivines, and 300 nA for Fe–Ti oxides. Mineral standards listed in Table 1 were used at the Geological Survey of Finland. Counting time was set to 30 seconds (60 seconds for F and Cl), and a spot size of 10 μm (about 1 μm for Fe–Ti oxides) was used when possible.

Amphiboles

Amphibole is the main Fe–Mg silicate in all the rock types of the Jaala-Iitti complex. Phenocrysts are rare, but occasionally amphibole forms aggregates a few centimetres in diameter. Commonly amphibole occurs as inclusions in plagioclase and alkali feldspar, and as rims surrounding fayalite and pyroxene in hybrid rocks and MMEs. In the hybrid rocks and pillow-like MMEs, amphibole is also found rimming quartz grains and quartz aggregates (ocellar texture). In hybrid rocks and MMEs (including pillow-like MMEs) amphibole has probably crystallized after thermal (and presumably chemical) equilibrium has been reached. Average amphibole analyses are presented in Appendix 1a.

Amphibole in the hybrid rocks of the Jaala-Iitti complex are mainly ferro-edenitic hornblendes, but some amphiboles of a more (magnesian) hastingsitic hornblende also occur (Fig. 25). They differ from the amphiboles in rapakivi granites of the Wiborg in having more Si and less Mg (Fig. 25 and Appendix 1a). The same is true with amphiboles of the hornblende granite and hornblende-quartz-feldspar porphyry of the complex.

Table 1. Standards used for different elements in electron microprobe analyses at the Geological Survey of Finland.

Mineral Element	**apatite**	**amphibole, biotite**	**magnetite, ilmenite**	**olivine, pyroxene**	**plagioclase, alkali feldspar**
SiO_2	n.d.	hornblende	n.d.	diopside	orthoclase
Al_2O_3	n.d.	hornblende	chromite	almandine	labradorite
TiO_2	n.d.	hornblende	rutile	rutile	garnet
FeO	almandine	hornblende	magnetite	almandine	garnet
MnO	rhodonite	garnet	willemite	rhodonite	n.d.
MgO	n.d.	hornblende	chromite	olivine	garnet
CaO	apatite	hornblende	n.d.	diopside	labradorite
Na_2O	n.d.	anorthoclase	n.d.	anorthoclase	anorthoclase
K_2O	n.d.	biotite	n.d.	biotite	orthoclase
P_2O_5	apatite	n.d.	n.d.	n.d.	n.d.
BaO	n.d.	n.d.	n.d.	n.d.	orthoclase
Cr_2O_3	n.d.	n.d.	chromite	chromite	n.d.
V_2O_3	n.d.	n.d.	synthetic V_2O_5	n.d.	n.d.
NiO	n.d.	n.d.	n.d.	olivine	n.d.
ZnO	n.d.	n.d.	n.d.	willemite	n.d.
F	fluorite	n.d.	n.d.	n.d.	n.d.
Cl	tugtupite	n.d.	n.d.	n.d.	n.d.

Note: n.d. = not determined

Amphiboles in MMEs from hybrid rocks and hornblende granites fall into three groups according to their $Mg/(Mg+Fe^{2+})$ (Fig. 25): 1) amphiboles in small "less-hybridized", and more primitive MMEs have larger $Mg/(Mg+Fe^{2+})$ (0.43–0.58) compared to 2) amphiboles in pillow-like MMEs (0.35–0.45), or 3) amphiboles in the MMEs of hornblende granites (0.24–0.46). So, amphiboles in the MMEs show a wide compositional range covering ferro-edenite, ferro-edenitic hornblende, edenitic hornblende, and magnesian hastingsitic hornblende; the composition is commonly related to the composition of the host rock and to the degree of hybridization in the MMEs. Amphiboles from the pillow-like MMEs fall into ferro-edenite and ferro-edenitic hornblende fields (Fig. 25), but since they have $(Na+K)_A$ values of 0.22–0.44 atoms per formula unit (a.f.u.), the diagram is not directly applicable because it assumes $(Na+K)_A \geq 0.50$ a.f.u. In the latter case the fields for ferro-edenite and ferro-edenitic hornblende are replaced by ferro-hornblende (Leake 1978).

The MMEs in the hornblende granite and the micro-enclaves in the hybrid rock have similar amphibole compositions as compared with amphiboles in the host rock (Appendix 1a) by utilizing elements such as Si, Al, Ti, Mn, Na, and K. A difference in Fe^{2+} (and Fe^{tot}) content with increasing degree of hybridization (in the sequence MME from the hornblende granite – MME from the hybrid rock – micro-enclave from the hybrid rock) compared to their host rock or to the composition of amphibole (sample 91053A in Appendix 1a) is apparent. A decreasing trend is visible in elements such as Ca, and Fe^{3+}. The fact that amphiboles in the MMEs are chemically similar to amphiboles in their host rocks suggests that chemical equilibrium had been reached between the two components. Amphibole aggregates in hornblende granite and wiborgite show similar Ti, Mn, $\pm Fe^{tot}$, and Ca contents (see also Fig. 25), and have, in general, they show similar compositions with matrices, but clearly differ when compared to mafic aggregates of the hybrid rock.

Compositions of amphiboles from the ocelli are, in general, similar to those in their host rock, but some small differences in composition exist. The amphibole in ocelli usually contains more Si and

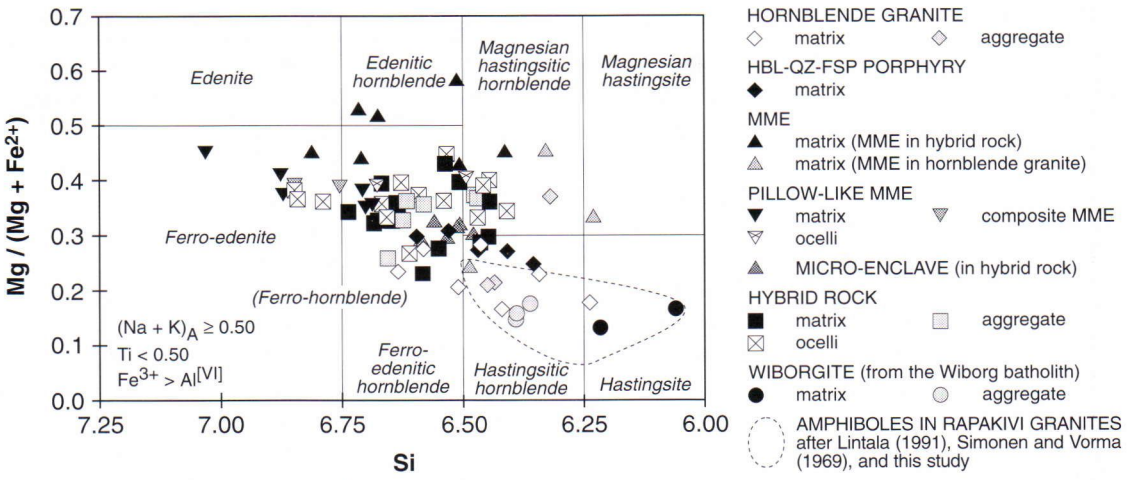

Fig. 25. Atomic Si vs. Mg/(Mg+Fe^{2+}) diagram for calcic amphiboles [$(Ca+Na)_B \geq 1.34$, $Na_B < 0.67$] after Leake (1978) showing compositions of amphiboles from the rocks of the Jaala-Iitti complex and the Wiborg batholith. Ferro-hornblende needs to be used instead of ferro-edenite and ferro-edenitic hornblende fields for amphiboles in pillow-like MMEs with $(Na+K)_A < 0.5$ after the classification scheme of Leake (1978).

Mg and less Fe, Ti, and Al compared to amphiboles in their host rock. The amounts of these elements are between those recorded from amphiboles in the host rock and amphiboles from MMEs (and pillow-like MMEs). It is probable that the ocellar amphibole that crystallized relatively early (together with or after augite) has a more primitive composition with higher Mg/(Mg+Fe). Angus (1971) has shown that ocellar hybrid rocks are enriched in Si, Na, and K and depleted in Ca, Mg, Fe, and Ti, compared with the parent mafic rocks. The enrichment of Si, Na, and K in amphiboles of the ocelli could be caused by dissolution of feldspar grains to give local enrichment in these elements.

The main compositional difference of amphiboles in the rock types of the Jaala-Iitti complex is in their Mg and Fe (Fe^{2+}+Fe^{3+}) contents. Because amphibole is the main Fe–Mg silicate its Mg and Fe contents reflect the bulk Mg and Fe composition of the rock. This feature can be used to study hybridization processes. To model hybridization features utilizing amphibole compositions, the average amphibole analyses of hornblende granites and hornblende-quartz-feldspar porphyries were used as the basis for the amphibole composition of the felsic end-member. For the mafic end-member, the average analyses of sample 91053A (see Appendix 1a) was used. These are shown in a Mg–(Fe^{2+}+Fe^{3+}) diagram in Figure 26. In Figure 26, using this scheme, the hybrid rocks show a wide range from 10 to 70 % of the mafic end-member. It is possible, however, that the crystallization of other minerals such as pyroxene and olivine has affected the bulk rock composition and the composition of amphiboles in the hybrid rocks. For pillow-like MMEs, the mafic-felsic ratios are between 40:60 and 70:30. A high degree of hybridization is apparent in the micro-enclaves and in recrystallized MME (from the hornblende granite) with mafic:felsic ratios of 20:80–40:60 and 5:95–45:55, respectively. The amphiboles of both types are extensively recrystallized and their composition is almost the same as that of the amphiboles from their host rocks (Figs. 25 and 26). It is likely that these mafic-felsic ratios are related to the degree of hybridization.

Table 2 shows modal crystallization pressures of different rock types from the Jaala-Iitti complex and the wiborgite at Summa, Hamina based on experimental calibration of total Al in amphibole as a function of pressure (Hammarstrom & Zen 1986, Hollister *et al.* 1987, Johnson & Rutherford 1989, Schmidt 1992). The calibration of Johnson and Rutherford (1989) gives about 1 kbar lower pressures than the other calibrations.

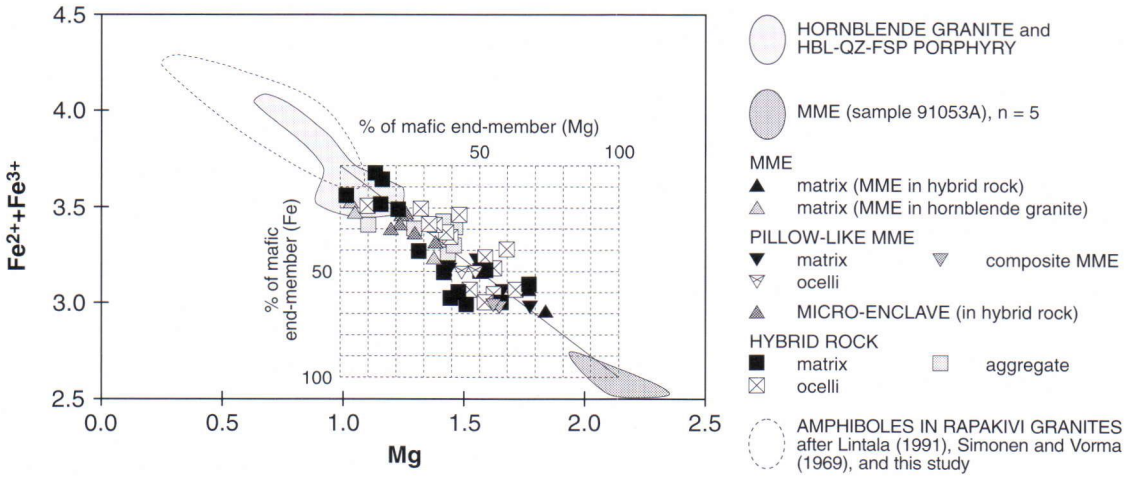

Fig. 26. Atomic Mg vs. $Fe^{2+}+Fe^{3+}$ diagram for amphiboles from the rocks of the Jaala-Iitti complex and the Wiborg batholith.

All pillow-like MMEs from north of Lake Kirkkojärvi in the western part of the complex contain quartz and feldspar megacrysts derived from the host rock, and are hybridized. Their amphibole is also less magnesian than that in the small MMEs which are less hybridized. Also the high Si contents in amphibole of pillow-like MMEs (6.69–7.03 a.f.u.) and hybrid rocks (6.44–6.74 a.f.u.) compared to those in granites (6.24–6.63 a.f.u.) of the complex are most likely connected to hybridization, either by way of a decrease in temperature (incorporation of xenolitic material) or oversaturation in Si (dissolving xenolitic material). The crystallization pressure (2.5–3.7 kbar) of the pillow-like MME is 0.6–0.7 kbar lower than that of the small MMEs or micro-enclaves. Compared to the MME host rock, pillow-like MMEs seem to have crystallized in the upper crust rather than their host (P = 3.7–4.6 kbar). This leads to the assumption that Si (and Al) content in amphiboles from the MMEs is controlled not only by pressure, but that some subsolidus chemical exchange must also have taken place. The larger MMEs solidified over a long period of time and had more time for chemical exchange. Pillow-like MMEs may represent that part of the magma chamber where the influx and hybridization rate of the mafic magma have been highest.

According to Vorma (1975, 1976), the intrusion level of rapakivi granites represents a depth of about 3 km (about 1 kbar). This is notably lower than the model crystallization pressures given by amphibole geobarometers which are calibrated for 2 to 30 kbars.

Apatite

Apatite analyses were made to detect possible chemical differences between apatites in the MMEs, hybrid rocks, and granites of the complex. Apatites in amphibole aggregates were also analysed for tracing possible changes in crystallization before and after any hybridization event. Average apatite analyses are presented in Appendix 1b.

Apatites of the Jaala-Iitti complex are fluor-apatite and hydroxylapatite and contain only trace amounts of Mn (< 0.1 wt%). Apatites in the hybrid rocks usually contain a wide range of F with 0.56–0.91 a.f.u. This distribution consists of analyses from two samples: 90141 and 90191 with F contents of 0.56–0.80 (mean 0.66) a.f.u. and 0.73–0.91 (mean 0.82) a.f.u., respectively. The highest contents of F are generally in the more

Table 2. Average model pressure estimates after amphibole geobarometers for the rocks of the Jaala-Iitti complex and wiborgite from Summa, Hamina Wiborg batholith (Fig. 1).

			Pressure (kbar)			
Rock/type	**Sample**	**N**	**P1**	**P2**	**P3**	**P4**
Hornblende granite						
matrix	90381	1	4.0	4.1	3.2	4.5
matrix	90561	3	4.0	4.2	3.2	4.5
matrix	90161	3	4.4	4.5	3.5	4.8
amph aggregate	90561	3	3.7	3.8	3.0	4.2
Hornblende-quartz-feldspar porphyry						
matrix	90542	3	3.8	3.9	3.1	4.3
inclusions in af	90542	2	3.8	3.9	3.1	4.3
MME						
matrix	91053A	5	3.0	3.0	2.4	3.5
matrix	91053C	2	3.7	3.8	3.0	4.2
matrix	91382	3	4.0	4.0	3.1	4.4
inclusions in pl	91382	4	4.6	4.8	3.7	5.0
Pillow-like MME						
matrix	90042A	2	1.7	1.5	1.2	2.3
matrix	9102A	4	2.8	2.8	2.2	3.4
composite MME	91021	2	2.8	2.8	2.2	3.4
ocelli	90042A	2	3.5	3.6	2.8	4.1
Micro-enclave						
matrix	90191	6	4.0	4.1	3.2	4.5
Hybrid rock						
matrix	90141	6	3.4	3.4	2.7	3.9
matrix	90501	3	4.0	4.1	3.2	4.5
matrix	90191	5	3.9	4.0	3.1	4.4
ocelli	90141	4	3.7	3.8	2.9	4.2
ocelli	90501	7	3.1	3.1	2.4	3.6
ocelli	90191	3	3.2	3.2	2.5	3.7
amph aggregate	90191	6	3.5	3.6	2.8	4.0
inclusions in pl	90141	3	3.5	3.6	2.8	4.1
Wiborgite						
matrix	Summa	2	4.9	5.1	3.9	5.3
amph aggregate	Summa	3	4.5	4.6	3.6	4.9

P1 = -3.92 + 5.03Al^{tot} (Hammarstrom & Zen 1986)
P2 = -4.76 + 5.64Al^{tot} (Hollister *et al.* 1987)
P3 = -3.46 + 4.23Al^{tot} (Johnson & Rutherford 1989)
P4 = -3.01 + 4.76Al^{tot} (Schmidt 1992)
N = number of analyses
amph = amphibole, pl = plagioclase, af = alkali feldspar

prismatic apatites. This possibly reflects the different degree of hybridization of the rocks when compared to mean a.f.u. values from MME (0.61), hornblende granite (0.85), and a wiborgite (0.72) from the Wiborg batholith. Also, apatites in the microenclave from the hybrid rock (sample 90191) have similar F contents (0.74–0.94 a.f.u. F) compared to apatites in the hybrid rock itself indicating equilibrium crystallization.

A survey of the literature shows that F/(F+OH) in apatites is related to the crystallization temperature of the magma. Apatites having more OH crystallized from higher temperature magmas than relatively F-rich apatites. Stormer and Carmichael's (1971) and Ludington's (1978) geothermometers are based on F–OH exchange between coexisting biotite and apatite, with increasing F/(F+OH) in apatite resulting in a decrease of the equilibrium crystallization temperature assuming a constant F/(F+OH) in biotite. Diffusion of F from the felsic to the more mafic magma probably caused rapid crystallization of F-rich apatites. In the hybrid rocks represented by samples 90141 and 90191, the relatively wide and bimodal distribution of F contents in apatites suggests that the apatites originated from two sources. Mingling of needle-like apatite from the partially crystallized mafic magma into a more felsic hybrid magma caused increasing of the content of needle-like apatite (Fig. 22) whereas most of the prismatic apatites either crystallized from the host magma or were entrained from the felsic end-member.

Apatite in amphibole aggregates is usually zoned (optically as well as compositionally), and the central part of the apatite is commonly F-rich (about 0.9 a.f.u. F) compared to the outer parts (0.7 to 0.9 a.f.u. F). Fe content in the central parts is usually about 0.2 a.f.u. whereas in the outer parts it is between 0.2 and 0.6 a.f.u.; this is possibly caused by diffusion of Fe from the amphibole to the apatite inclusion. Low F content in the outer parts of the apatite could also be a result of diffusion or a change of composition in the magma composition as crystallization proceeded. In general, apatite in the amphibole aggregates shows a similar composition to apatites from their host rock.

Biotite

Average biotite analyses of the rock types of the complex are presented in Appendix 1c. Because these are microprobe data, indirect methods for estimating ferric and ferrous iron contents were used (c.f., de Bruiyn *et al.* 1983); see Appendix 1c. As biotite occurs only in minor amounts and crystallized after amphibole in the rocks of the Jaala-Iitti complex, it is not presumed that Fe^{2+}/Fe^{3+} ratios from whole rock analyses represent the values in biotites. To evaluate the credibility of this method, a comparison of biotite analyses in wiborgite from Summa, Hamina to other biotites of the Wiborg batholith (Simonen & Vorma 1969) was made. The $Fe^{2+}/(Fe^{2+}+Fe^{3+})$ of 0.86 for biotite in wiborgite from Summa is similar to wet chemical data (0.84 to 0.90; average 0.88) published by Simonen and Vorma (1969). For the rocks of the Jaala-Iitti complex, $Fe^{2+}/(Fe^{2+}+Fe^{3+})$ ranges from 0.84 to 0.89.

All biotites from the rocks of the Jaala-Iitti complex are annite-rich with Al^{VI} under 0.16 (Fig. 27). Hybrid rock types (hybrid rock, pillow-like MME, and micro-enclave) of the complex show compositions with $Mg/(Mg+Fe^{2+})$ over 0.2 whereas the granites of the complex and the wiborgite (Summa, Hamina) show values under 0.2.

Biotite from the micro-enclave (sample 90191) has a $Fe^{tot}/(Fe^{tot}+Mg)$ value of 0.75 that is similar to that of the host rock (0.72) and differs from those of pillow-like MMEs and composite MMEs with $Fe^{tot}/(Fe^{tot}+Mg)$ from 0.64 to 0.70 and from 0.66 to 0.69, respectively. In hybrid rocks (samples 90141, 90191, and 90501) the $Fe^{tot}/(Fe^{tot}+Mg)$ values range from 0.69 to 0.79 and are lower than in the hornblende granites of the complex with (0.85–0.91; compare to Fig. 25). The non-hybrid origin of hornblende granites is also more apparent when the values for biotites are compared with biotites from biotite-hornblende-fayalite granites (dark wiborgite, wiborgite, and tirilite) of the Wiborg batholith that show $Fe^{tot}/(Fe^{tot}+Mg)$ values from 0.80 to 0.88 (Haapala *et al.* 1991).

Wones and Eugster (1965) calibrated the stability of biotite coexisting with sanidine and magnetite as a function of temperature and oxygen fugasity by

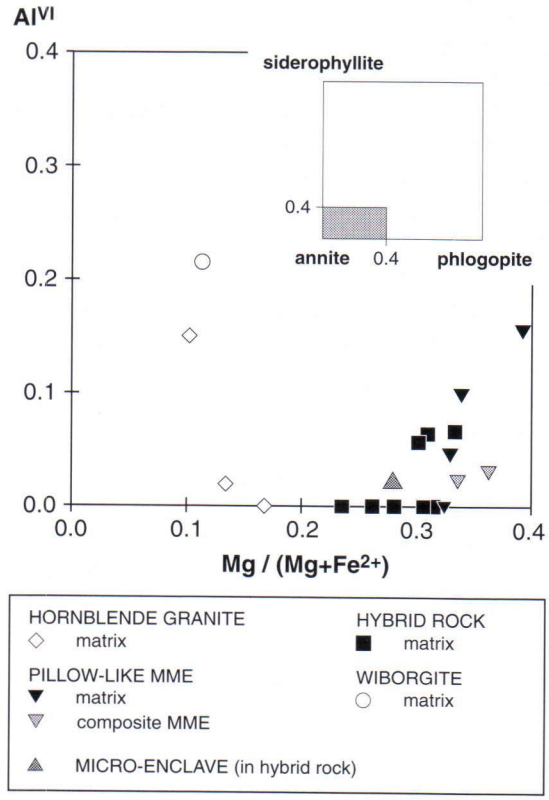

Fig. 27. Analyses of biotites from hornblende granites, MMEs, hybrid rocks from the Jaala-Iitti complex, and wiborgite in Summa, Hamina plotted in Al^{VI} vs. $Mg/(Mg+Fe^{2+})$ diagram.

using the $Fe^{tot}/(Fe^{tot}+Mg)$ ratio (see Fig. 28). Biotite with a certain $Fe^{tot}/(Fe^{tot}+Mg)$ is stable at oxygen fugacity values below the corresponding contour; above it the biotite will decompose by the reaction biotite → more magnesian biotite + alkali feldspar + magnetite (Speer 1984). The assemblage alkali feldspar+quartz+fayalite+magnetite(±biotite) is found in granites of the Jaala-Iitti complex. This assemblage has been suggested as evidence for rapakivi granite biotites having crystallized near (or more likely under) the QFM buffer (Anderson 1980, Emslie & Stirling 1993).

In Figure 28, the 100Fe/(Fe+Mg) = 90 contour represents crystallization estimates for biotites in the hornblende granite whereas the 100Fe/(Fe+Mg) = 64 contour is the lowest value pertaining to biotites from the pillow-like MMEs. The minimum

crystallization temperature and maximum $\log fO_2$ for biotites in granites of the complex are 660°C and about -17 at the conditions of the NNO buffer. Close to QFM, where more suitable conditions for the mineral assemblages present in granites of the complex are to be found, the minimum crystallization temperature is about 760°C with $\log fO_2$ of about -17. It is possible that the fayalite-bearing rapakivi granites with Fe/(Fe+Mg) > 0.90 have crystallized near the stability field of annite + quartz close to the QFM buffer at a temperature of about 700°C with $\log fO_2$ = -18 (Fig. 28).

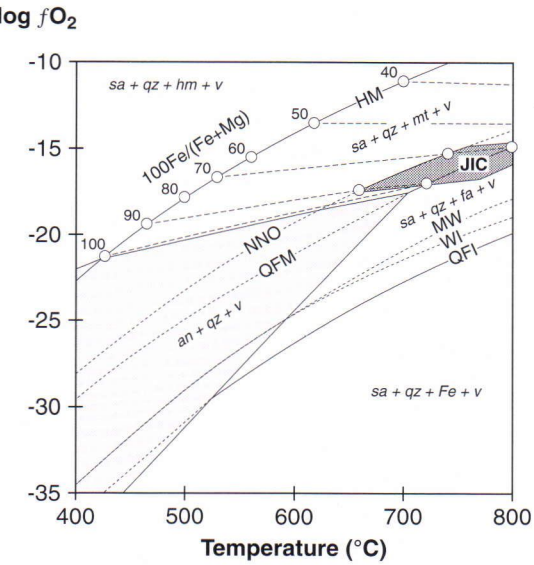

Fig. 28. LogfO_2 versus temperature diagram representing stability of biotite in the assemblage biotite+sanidine+quartz at a total pressure of 2070 bars after Wones and Eugster (1965) indicated by contours of constant 100Fe/(Fe+Mg) (numbers); Fe represents total Fe. The lightly shaded area represents the stability of annite and quartz in the oxygen fugacity–temperature space at 2000 bars (Eugster & Wones 1962) compared to hematite–magnetite (HM), nickel–nickel oxide (NNO), quartz–fayalite–magnetite (QFM), magnetite–wüstite (MW), wüstite–iron (WI), and quartz–fayalite–iron (QFI) buffers. The heavily shaded area marked with JIC represents the approximate crystallization conditions of biotites from the Jaala-Iitti complex. See text for discussion. Abbreviations: sa – sanidine, qz – quartz, hm – hematite, mt – magnetite, fa – fayalite, and v – vapour.

At the NNO buffer biotites with Fe/(Fe+Mg) > 0.64 from the pillow-like MMEs show a temperature of 760°C and a 100°C higher at -1 $\log fO_2$ ΔQFM. Conditions above QFM are unreliable as pillow-like MMEs and hybrid rocks contain predominantly ilmenite instead of magnetite (c.f., Ishihara 1977). For the hybrid rocks and granites of the Jaala-Iitti complex, realistic conditions are probably found between QFM and NNO [T(min) ≈ 740°C, $\log fO_2$(max) ≈ -15].

The composition of biotite and amphibole correlates with the degree of hybridization of the rocks (Fig. 29). The compositionally similar trend of biotite and amphibole is visible in pillow-like MMEs, micro-enclaves, hornblende granites, and wiborgites (Fig. 29). The biotite from hybrid rocks shows disequilibrium features especially in the MgO and FeO^{tot} content and has a composition between the mafic and felsic end-members. Disequilibrium is apparent in the distribution of Mg and Fe [K_D = $(Mg/Fe)_{biot}/(Mg/Fe)_{amph}$] between biotite and amphibole from the hybrid rock with a range of average K_D values from 0.66 (sample 90141) to 1.17 (sample 90501). This range is larger than the range for the K_D values for pillow-like MMEs and composite MMEs (0.93 to 0.98) and granites from the Jaala-Iitti complex and Wiborg batholith (0.72 to 0.82). Equilibrium reached between the micro-enclaves and the host is suggested by their relatively similar K_D values (0.91 and 0.84, respectively).

Feldspars

Plagioclase in the MMEs and micro-enclaves and their host rocks were analysed to assess possible compositional changes that may occur during crystallization of two coexisting melt phases before and after chemical exchange due to hybridization. Coexisting plagioclase and alkali feldspar were used as a geothermometer to estimate crystallization temperature and to study equilibria between feldspars in the rock types of the Jaala-Iitti complex. Analyses of plagioclases and alkali feldspars from the Jaala-Iitti complex are presented in Appendices 1d and 1e, respectively.

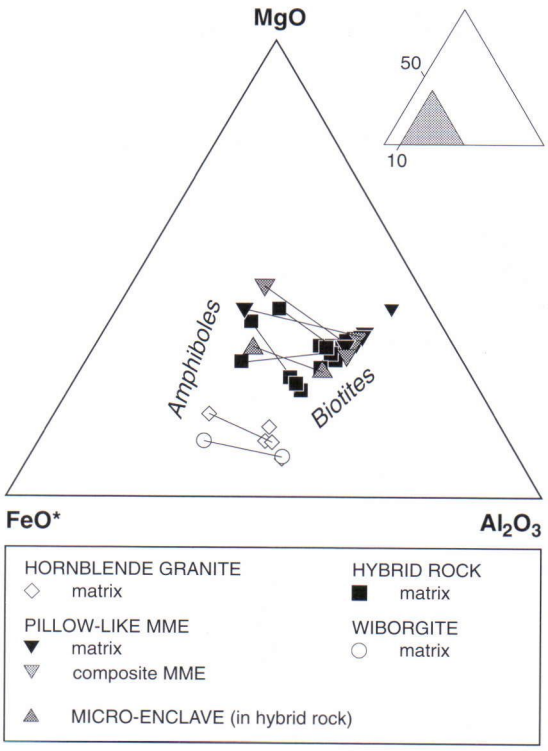

Fig. 29. Biotites and amphiboles from different rock types of the Jaala-Iitti complex plotted in a FeO(total Fe) – Al_2O_3 – MgO diagram. The lines join the average composition of biotite and amphibole in different samples.*

Plagioclase

Plagioclases from small MMEs in the hybrid rocks show a relatively wide compositional range from An_{38} to An_{54}, most of them between An_{48} and An_{51} (Fig. 30a). Large pillow-like MMEs have lower An contents ($An_{30–45}$), and these compositions are similar to those of micro-enclaves and their hybrid rock matrices (Figs. 30b, 30c, and 30d, respectively). A gradational change of plagioclase composition from small MMEs (Fig. 30a) in hornblende granite (Fig. 30e) and hornblende-quartz-feldspar porphyry (Fig. 30f) is apparent. Anorthite contents of plagioclase from the micrographic rim $An_{30–34}$ (Fig. 30g) and from the plagioclase mantling alkali feldspar $An_{28–37}$ (Fig. 30h) are similar to those in their hybrid rock matrices. One analysis from the central part of the plagioclase mantle (Fig. 30h) has a composition of An_{52}.

Or contents of plagioclases in all rock types are relatively low, usually under 2 mol%. In plagioclase xenocrysts of MMEs (Fig. 30a) and pillow-like MMEs (Fig. 30b) Or contents reach 4 mol% and 2 mol%, respectively. The low Or content is probably caused by exsolution; antiperthitic plagioclase grains occur especially in hybrid rocks and hornblende granites. That is apparent when comparing Or contents in plagioclase xenocrysts from MMEs (Fig. 30a) to plagioclase from the MME's host hornblende granite (Fig. 30e). The zoned plagioclase xenocryst (see Fig. 24a) in the MME also is an example of crystallization of a plagioclase in the MME magma before equilibrium was established between the mafic and the felsic magmas and of subsequent crystallization of plagioclase in the matrix of the MME after equilibration. The core of the plagioclase is inclusion-free, and has a composition of $An_{34–36}$, similar to those of the MME host granitoid matrix indicating a xenocrystic origin. This xenocryst has been a nucleus for crystallization of plagioclase from the mafic magma; the composition changes gradually from An_{43} to An_{54}, and amphibole inclusions appear in the outermost rim (An_{46}). In the MME matrix, the composition is $An_{39–41}$. This feature shows two things. First, these plagioclase phenocrysts in the MME magmas are xenocrystic and derived from the host granitoid rock. Second, MME magmas and their host magmas can crystallize independently, but after a certain time interval the mafic magma is influenced by chemical exchange with the enclosing felsic magma. Plagioclase that occurs as inclusions in alkali feldspar megacrysts (Figs. 30i and 30j) shows a similar composition ($An_{26–34}$) to those in their host and in the hornblende granite.

According to the restite hypothesis, corroded calcic plagioclase phenocrysts with more sodic rims (compositionally similar to the matrix) have been described as residual minerals from the source rock of the felsic melt (Presnall & Bateman 1973, White & Chappell 1977, Chappell 1978, Chen et al. 1990). Similar plagioclases were also found in the Jaala-Iitti complex. These consist of altered, calcic

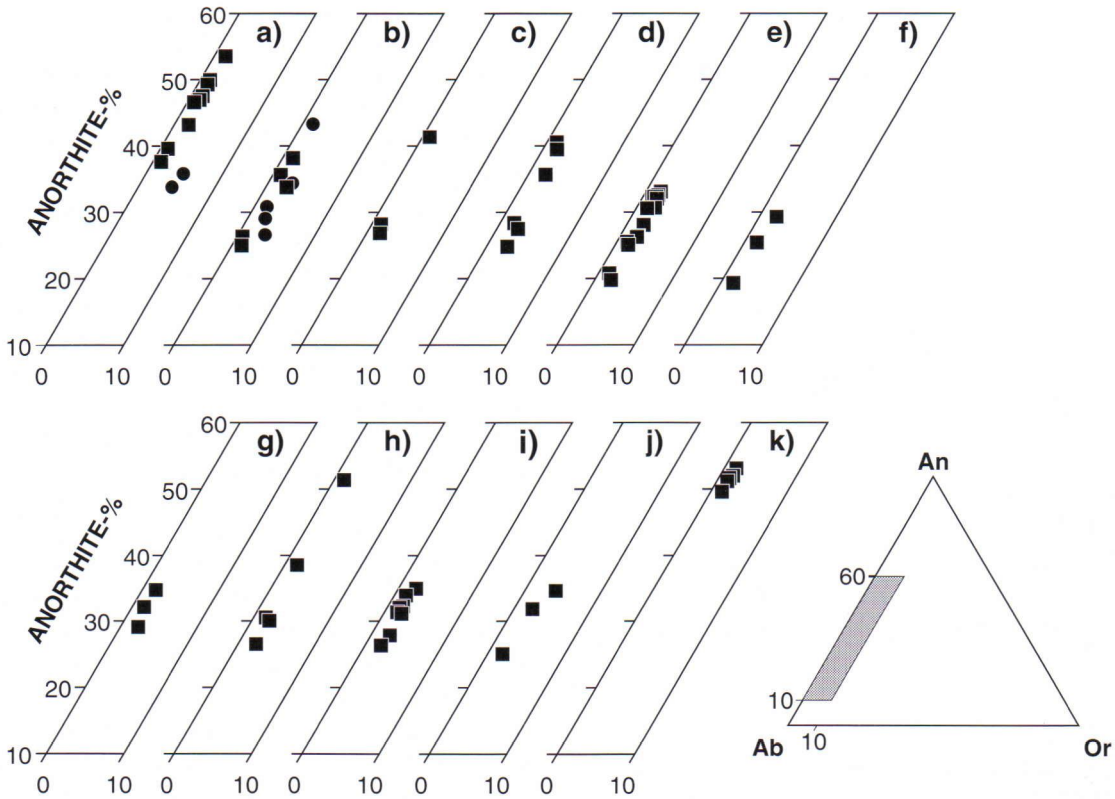

Fig. 30. An–Ab–Or plot of plagioclase compositions in (a) small MME in a hybrid rock, (b) pillow-like MME in a hybrid rock, (c) micro-enclave, (d) hybrid rock, (e) hornblende granite, (f) hornblende-quartz-feldspar porphyry, (g) micrographic rim, (h) plagioclase mantling alkali feldspar, (i) inclusions in alkali feldspar megacrysts, (j) porphyritic rapakivi granite xenolith in hybrid rock, and (k) xenocryst with a rim composition of An_{27-34} in the hornblende granite. Filled circles in (a) and (b) represent xenocryst compositions.

(An_{50-53}) cores (Fig. 30k) surrounded by a oligoclase (An_{20-35}) rim with a composition similar to the matrix plagioclase (Fig. 30e). Corroded grains are usually altered to sericite and saussurite and their diameter is less than 2 mm. If not restite material they could also represent xenocrysts derived from gabbroic or anorthositic magmas.

Alkali feldspar

Alkali feldspars in hornblende-quartz-feldspar porphyry usually lack albite lamellae; alteration to sericite and saussurite as well as large amounts of inclusions are rare. In contrast to alkali feldspar from the hornblende granite and the hybrid rocks they show less subsolidus reactions and are more Ab-rich. Alkali feldspar from the matrix of the hybrid rock (Fig. 31a) and hornblende granite (Fig. 31b) occurs generally in two compositions: ~Or_{80} and ~Or_{90}. In the hornblende-quartz-feldspar porphyry the Or content of the alkali feldspar is commonly under 80, clustering around Or_{65} and Or_{75} (Fig. 31c). Compositionally, then, alkali feldspars can be divided into three groups ($Or_{>85}$, Or_{85-70}, and $Or_{<70}$) (Fig. 31). Exsolution of albite increases in alkali feldspar megacrysts and crystals in the matrix along with an increase in the degree of hybridization. Petrographically this results in vermicular albite and exsolved plagioclase often with quartz rims on alkali feldspars of the hybrid rocks and hornblende granites.

Mantled alkali feldspar megacrysts show a wide compositional range (Figs. 31d and 31e), especially

in Or and Ab content. Alkali feldspar mantled by plagioclase and amphibole shows a relatively high celcian-component (up to 6.1 mol%) compared to alkali feldspar megacrysts with micrographic texture (less than 1 mol% of Cn). Or and Cn contents (0.9–1.7 mol% and 0.0–0.4 mol%, respectively) are also higher in the plagioclase of the mantles than in plagioclases in the enclosing rock. This may, for example, indicate a small-scale element exchange between the alkali feldspar megacryst and plagioclase mantles or more probably different crystallization temperature and/or pressure. Compositions measured from the outer parts of the megacrysts immediately in contact with micrographic texture and plagioclase mantling alkali feldspar show some similarities (see Figs. 31d, 31e, and 31f). Compositions of the outer part of the megacrysts trend towards the "intermediate" composition (with one exception in Fig. 31d of composition $Or_{91}Ab_6An_3$) that possibly represents the attainment of equilibrium between the matrix and the plagioclase rim. Composition change is apparent in the alkali feldspar megacryst rimmed by plagioclase where the composition changes from Or_{64} to Or_{82}, and at the same time Cn content decreases from 6.1 to 2.5 mol% (Fig. 31e). Variation of the outer part of the alkali feldspar megacrysts near to plagioclase mantles is $Or_{75-82}Ab_{15-25}An_{0-2}Cn_{0-3}$. This compositional variation is similar to that of the alkali feldspar in the hornblende-quartz-feldspar porphyry (Fig. 31c) and mantled alkali feldspar megacrysts in wiborgite from the Wiborg batholith (Lintala *et al.* 1991). This could be due to similar crystallizing conditions (temperature and pressure) of the micrographic intergrowth in the Jaala-Iitti complex and the rapakivi texture in the wiborgite from the Wiborg batholith.

Feldspar geothermometry

Fuhrman and Lindsley (1988) calibrated a ternary feldspar geothermometer that yields three temperatures, utilizing the An–An, Ab–Ab, and Or–Or equilibria between alkali feldspar (af) and plagioclase (pl). Model temperatures for the feldspar data on the Jaala-Iitti complex are shown in Table 3. Table 3 shows at the column initial results of temperature estimates between 1 and 2 kbars based on this method without reconstituting compositions. Commonly the difference between temperatures at 1 kbar and 2 kbar is from 0° to 20°C, depending on the equilibrium used and so the two-feldspar geothermometer is not sensitive to pressure. Temperatures calculated without reconstructing compositions are commonly unequal and identical temperatures are reached only at low temperatures. Such low temperatures probably represent sub-solidus equilibria rather crystallization temperatures of coexisting feldspars. Model 1 temperatures are calculated with the program MTHERM3 (Fuhrman & Lindsley 1988) that allows the compositions to vary by up to 2 mol%.

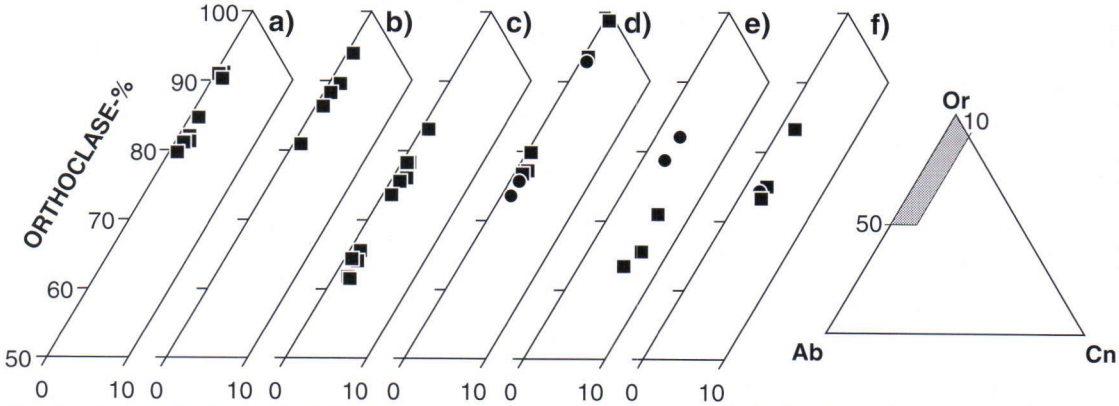

Fig. 31. Or–Ab–Cn plot of alkali feldspar compositions in the matrix of (a) hybrid rock, (b) hornblende granite, (c) hornblende-quartz-feldspar porphyry, and in megacryst mantled by (d) micrographic rim and (e) plagioclase rim and alkali feldspar megacrysts from (f) rapakivi granite xenolith. Filled circles in (d), (e), and (f) represent compositions in the outer part of the megacryst.

Table 3. Temperature estimates after the two-feldspar geothermometer of Fuhrman and Lindsley (1988) at the pressure range of 1 to 2 kbars for the rocks of the Jaala-Iitti complex. See text for discussion.

			Initial					Model 1					Model 2 or 3			
Rock	**#**		**N**	**Ab**	**Or**	**An**	**Cn**	**N**	**Ab**	**Or**	**An**		**N**	**Ab**	**Or**	**An**
Hornblende granite																
matrix	90161	T		340(15)	481(32)	438(17)			387(12)	403(12)	396(13)			503(35)	503(35)	-
		X(af)	1	0.055(0)	0.940(0)	0.001(0)	0.003(0)	1	0.074(4)	0.921(4)	0.001(0)		1	0.130(11)	0.866(11)	0.001(0)
		X(pl)	5	0.695(37)	0.015(3)	0.290(37)	0.001(1)	5	0.694(31)	0.007(1)	0.299(39)		4	0.694(39)	0.016(2)	0.290(37)
matrix	90591	T		509(94)	402(15)	560(154)			519(97)	518(73)	521(102)			559(120)	559(120)	-
		X(af)	2	0.147(37)	0.845(40)	0.005(3)	0.004(1)	2	0.148(52)	0.846(61)	0.004(4)		2	0.171(67)	0.821(71)	0.005(3)
		X(pl)	3	0.726(57)	0.008(1)	0.266(58)	0.000(0)	3	0.718(72)	0.020(9)	0.262(70)		3	0.705(67)	0.029(21)	0.266(58)
Hornblende-quartz-feldspar porphyry																
matrix	90301	T		490(7)	439(1)	1036(6)			532(4)	528(12)	529(4)			733(1)	733(1)	733(1)
		X(af)	1	0.160(0)	0.819(0)	0.018(0)	0.004(0)	1	0.175(0)	0.819(0)	0.003(0)		1	0.313(5)	0.666(5)	0.018(0)
		X(pl)	1	0.779(0)	0.013(0)	0.208(0)	0.000(0)	1	0.774(5)	0.026(3)	0.200(8)		1	0.717(0)	0.075(0)	0.208(0)
af pheno-	90542	T		699(87)	467(3)	656(189)			665(108)	644(94)	658(112)			649(31)	649(31)	-
cryst vs.		X(af)	8	0.300(75)	0.677(91)	0.017(13)	0.009(6)	5	0.269(92)	0.712(111)	0.014(15)		3	0.223(12)	0.767(13)	0.004(1)
pl matrix		X(pl)	1	0.733(0)	0.013(0)	0.254(0)	0.000(0)	1	0.727(40)	0.049(34)	0.221(44)		1	0.702(7)	0.044(7)	0.254(0)
af pheno-	90301	T		691(8)	523(0)	584(6)			no	no	no			743(12)	743(12)	-
cryst vs.		X(af)	1	0.254(0)	0.732(0)	0.009(0)	0.006(0)		result	result	result		1	0.254(0)	0.732(0)	0.009(0)
pl incl.		X(pl)	1	0.699(0)	0.017(0)	0.283(0)	0.001(0)						1	0.652(4)	0.065(4)	0.283(0)
Hybrid rock																
matrix	90141	T		580(28)	501(2)	556(18)			570(7)	569(3)	560(8)			592(28)	592(28)	-
		X(af)	2	0.183(11)	0.804(8)	0.006(0)	0.009(3)	2	0.173(3)	0.813(5)	0.005(1)		2	0.184(11)	0.803(8)	0.006(0)
		X(pl)	1	0.703(0)	0.016(0)	0.281(0)	0.000(0)	1	0.698(5)	0.026(0)	0.276(5)		1	0.689(5)	0.029(5)	0.281(0)
matrix	90501	T		502(82)	541(8)	620(38)			587(17)	568(39)	593(33)			580(38)	580(38)	575(45)
		X(af)	3	0.144(45)	0.846(50)	0.006(2)	0.005(4)	2	0.191(6)	0.796(7)	0.007(1)		3	0.188(29)	0.802(33)	0.006(2)
		X(pl)	1	0.725(0)	0.024(0)	0.251(0)	0.000(0)	1	0.717(7)	0.032(7)	0.251(0)		1	0.718(6)	0.030(6)	0.251(0)
matrix	90191	T		424(26)	498(44)	607(37)			405(13)	388(31)	394(14)			556(11)	556(11)	556(11)
		X(af)	2	0.084(2)	0.905(4)	0.006(0)	0.005(2)	2	0.083(4)	0.913(7)	0.001(0)		2	0.144(26)	0.846(28)	0.006(0)
		X(pl)	4	0.625(57)	0.014(7)	0.360(64)	0.000(0)	2	0.691(59)	0.006(1)	0.303(59)		4	0.620(60)	0.020(5)	0.360(64)
af mega-	90141	T		689(28)	540(12)	415(15)			671(10)	658(3)	664(6)			760(10)	760(10)	-
cryst vs.		X(af)	2	0.220(4)	0.771(2)	0.003(0)	0.007(2)	2	0.215(3)	0.767(3)	0.013(0)		2	0.229(8)	0.762(9)	0.003(0)
pl incl.		X(pl)	2	0.651(12)	0.017(1)	0.331(11)	0.001(0)	2	0.640(3)	0.038(1)	0.321(6)		2	0.606(13)	0.063(3)	0.331(11)
af mega-	90141	T		730(91)	501(2)	526(34)			655(12)	643(9)	655(19)			851(31)	851(31)	
cryst vs.		X(af)	3	0.276(40)	0.670(39)	0.014(3)	0.056(5)	1	0.230(5)	0.709(5)	0.019(4)		2	0.278(13)	0.667(17)	0.013(3)
pl incl.		X(pl)	2	0.662(9)	0.013(0)	0.324(10)	0.003(0)	2	0.647(20)	0.033(1)	0.319(24)		2	0.586(25)	0.090(12)	0.323(10)
af mega-	90141	T		491(150)	514(28)	542(49)			606(44)	607(48)	606(44)			698(76)	698(76)	-
cryst vs.		X(af)	2	0.129(68)	0.867(69)	0.004(1)	0.001(0)	1	0.190(10)	0.806(15)	0.008(2)		2	0.219(24)	0.776(24)	0.004(1)
pl incl.		X(pl)	4	0.683(20)	0.018(3)	0.299(22)	0.000(1)	3	0.696(50)	0.025(12)	0.309(46)		4	0.649(36)	0.052(19)	0.299(22)
micro-	90141	T		694(31)	496(14)	707(35)			686(3)	652(2)	682(1)			747(43)	744(37)	-
graphic		X(af)	2	0.238(10)	0.740(12)	0.017(2)	0.006(0)	1	0.214(5)	0.766(5)	0.015(0)		2	0.238(10)	0.740(12)	0.017(2)
texture		X(pl)	2	0.653(10)	0.013(1)	0.334(10)	0.000(0)	1	0.622(0)	0.034(0)	0.344(0)		2	0.609(18)	0.057(9)	0.334(10)
micro-	90141	T		336(6)	504(1)	1180(4)			no	no	no			809(0)	809(0)	808(0)
graphic		X(af)	1	0.062(0)	0.906(0)	0.031(0)	0.001(0)		result	result	result		1	0.288(4)	0.679(4)	0.031(0)
texture		X(pl)	1	0.682(0)	0.017(0)	0.301(0)	0.001(0)						1	0.616(0)	0.083(0)	0.301(0)
pl	90141	T		572(70)	507(13)	345(82)			577(41)	581(40)	582(43)			716(84)	716(84)	-
mantle		X(af)	2	0.168(18)	0.809(16)	0.002(1)	0.025(1)	2	0.168(20)	0.802(21)	0.008(3)		2	0.225(18)	0.752(17)	0.002(1)
		X(pl)	4	0.664(42)	0.015(3)	0.320(45)	0.001(2)	3	0.647(50)	0.025(8)	0.327(50)		4	0.628(62)	0.052(17)	0.320(45)
Rapakivi granite xenolith																
af mega-	9014X	T		619(103)	541(30)	499(93)			618(73)	620(61)	622(65)			653(101)	653(101)	-
cryst vs.		X(af)	3	0.205(46)	0.774(49)	0.005(1)	0.020(5)	3	0.205(51)	0.769(59)	0.010(6)		3	0.212(43)	0.767(46)	0.005(1)
pl incl.		X(pl)	2	0.689(28)	0.020(2)	0.290(25)	0.002(2)	2	0.682(41)	0.350(13)	0.283(38)		2	0.667(45)	0.042(21)	0.290(25)
micro-	9014X	T		741(8)	651(0)	408(4)			708(1)	711(2)	714(2)			790(16)	790(16)	-
graphic		X(af)	1	0.238(0)	0.746(0)	0.004(0)	0.016(0)	1	0.231(8)	0.739(8)	0.019(0)		1	0.238(0)	0.746(0)	0.004(0)
texture		X(pl)	1	0.629(0)	0.034(0)	0.337(0)	0.000(0)	1	0.622(8)	0.049(0)	0.329(8)		1	0.592(6)	0.070(6)	0.337(0)

X(af) and X(pl) are albite (Ab), orthoclase (Or), anorthite (An), and celsian (Cn) contents in alkali feldspar and plagioclase, respectively. Parenthesized numbers indicate one standard deviation of measurement in terms of least digits cited.
N = number of alkali feldspar or plagioclase analyses used in temperature calculations.
T = temperature (°C) calculated after model of Fuhrman and Lindsley (1988) for ternary feldspars.

Initial: Temperatures calculated by the program MTHERM3 (Fuhrman & Lindsley 1988) without reconstructing compositions.

Model 1: Temperatures and composition calculated by the program MTHERM3 allowing compositions to vary up to 2 mol%. The difference of accepted temperatures is less than 80.

Model 2: Temperatures and compositions calculated by shifting X_{ab} and X_{or} contents of both alkali feldspar and plagioclase at constant X_{an} until $T_{ab\text{-}ab} = T_{or\text{-}or} = T_{an\text{-}an}$. Method adopted from Kroll *et al.* (1993).

Model 3: Temperatures and compositions calculated by shifting X_{ab} and X_{or} contents of both alkali feldspar and plagioclase at a constant X_{an} until $T_{ab\text{-}ab} = T_{or\text{-}or}$ (rows without $T_{an\text{-}an}$). Used if Model 2 gave no result.

Kroll *et al.* (1993) modified Fuhrman & Lindsley's (1988) programme to evaluate retrograde intercrystalline K–Na exchange. This procedure is adopted here as Model 2; it increases the X_{ab} and decreases the X_{or} content of alkali feldspar and decreases the X_{ab} and increases the X_{or} content of plagioclase at a constant X_{an} until a common (minimum) isotherm with $T_{ab\text{-}ab} = T_{or\text{-}or} = T_{an\text{-}an}$ is found. Temperatures from Model 2 in Table 3 are only accepted if the standard deviation (s.d.) is less than one. This method of assuming a constant X_{an} content is reliable only in cases without exsolution of X_{an}. Temperatures of Model 2 are often equal to those of Model 1 because of low X_{an} (and high X_{or}) in alkali feldspar and low X_{or} in plagioclase. Alkali feldspar phenocrysts and grains in the matrix of the hornblende-quartz-feldspar porphyry are less perthitic compared to other alkali feldspar -bearing rocks of the complex, and the Model 2 temperatures for the hornblende-quartz-feldspar porphyry is 733°C. A ternary feldspar model temperature of an alkali feldspar megacryst with a micrographic rim is 809°C with $X_{or} = 0.031$ in plagioclase.

Some ternary temperature estimates by using Model 2 have a s.d. close to one or no solution has been found (s.d. > 1). In these cases (Model 3) the calculation procedure was executed only for $T_{ab\text{-}ab} = T_{or\text{-}or}$ at a constant X_{an}. This model is more applicable for temperature estimates for the matrix of the hybrid rocks, which have low X_{an} (< 0.01; see Appendix 1e and Table 3) and relatively high X_{or} contents (0.80–0.90) in the alkali feldspar. By assuming a constant X_{an} Models 2 and 3 give temperatures below 600°C which are obviously not probable crystallization temperatures for feldspars in the hybrid rocks. Linear shifting of X_{ab} and X_{or} in the alkali feldspar and plagioclase would increase the model temperature but also lead to several possible temperature estimates. Also, if X_{an} is allowed to vary (even by only 2 mol%) several possible results may be found.

Using Model 3, temperature estimates for the hornblende-quartz-feldspar porphyry are between 650° and 750°C corresponding to the results of Model 2. Temperatures from 750° to 800°C for the micrographic rim surrounding alkali feldspar megacrysts and the micrographic texture in the rapakivi granite xenolith are acceptable because of their origin by melting of the alkali feldspar mega(xeno)crysts. This temperature range is reached with X_{or} = 0.679–0.740 and X_{ab} = 0.238–0.288 in alkali feldspar. X_{or} of 0.679–0.740 in alkali feldspar is lower than the assumed equilibrium composition for alkali feldspars (X_{or} = 0.75–0.82) as discussed above. This composition of alkali feldspars in the matrix of the hybrid rocks and hornblende granites give Model 1 temperatures usually under 600°C.

Systematically lower temperatures of the matrices of the hybrid rocks compared to the model temperatures of the micrographic rims can be ascribed to thermal disequilibrium between minerals of the hybrid rock. Also, the existence of MMEs in hybrid rocks of the complex is simple proof that thermal equilibrium has not been reached completely during the evolution of the magmas of the complex, because MMEs have occurred as globules of a hotter magma within the hybrid magma whereas the rapakivi granite magma has occurred as a cooler magma near the hybrid magma that probably had an intermediate temperature. The temperature estimates of the micrographic rims suggest that this equilibrium may have been reached on a local scale.

Recent seismic soundings (Luosto *et al.* 1990) indicate that the Wiborg batholith is about 8 km thick at the present erosion level which corresponds to a depth of about 2 kbar. Two kilobars was thus probably the pressure for the formation of the micrographic texture in the hybrid rocks of the Jaala-Iitti complex. Inasmuch as the Jaala-Iitti complex represents a subvolcanic complex, a pressure of 2 kbar may be regarded as the maximum pressure that prevailed during the disintegration of the rapakivi granite xenoliths that supplied alkali feldspar xenocrysts into the hybrid magma.

Amphibole-plagioclase geothermometry

Blundy and Holland (1990) calibrated a geothermometer for coexisting amphibole and plagioclase. Even though the suitability of this geothermometer

was criticized by Hammarstrom and Zen (1992), Rutherford and Johnson (1992), and Poli and Schmidt (1992), the method was used for temperature calculations in the Jaala-Iitti complex; a comparison to other geothermometres is also given. Blundy and Holland (1990) also (see also Blundy & Holland 1992a, 1992b) made the case that the Al content in amphibole is not suitable for use as a barometer. Model temperatures based on the geothermometer of Blundy and Holland (1990) for the rocks of the Jaala-Iitti complex are listed in Table 4. Temperatures were calculated at 1 and 5 kbar by using amphibole compositions (Appendix 1a) and plagioclase compositions (Appendix 1d) based on micro-probe analyses. In general, temperatures at 1 kbar are 50° to 80°C higher than those at 5 kbar. Choosing a maximum pressure as high as 5 kbar is reasonable for the possible early crystallization of the MMEs. The emplacement level of the Jaala-Iitti complex may be less than 2 kbar and it is probable that a pressure estimate of 1 kbar represents the emplacement level, at least for the major crystallization event(s) of the complex.

Problems with the geothermometer results correlate directly with the degree of hybridization and subsolidus re-equilibration of the rocks suggestive of thermal disequilibrium between alkali feldspars and plagioclases. In the hybrid rocks this is possibly caused by the coexistence of the hotter mafic magma in the hybrid rock and the cooler granite magma of the complex throughout the hybridization event and the possible remixing of the different magmas.

Hornblende granites and hornblende-quartz-feldspar porphyries show relatively similar model temperatures at 1 kbar for plagioclase and amphibole: 820–840°C. For MME, model temperature estimates vary from 890° to 950°C being higher in the MME from the hybrid rock (sample 91053C) rather than in the MME from the hornblende granite (sample 91382). Plagioclase xenocrysts that have been the nuclei for crystallizing plagioclase with compositions from An_{43} to An_{54} show slightly higher temperatures of 880–940°C more than in the host MME matrix that shows recrystallization features.

Table 4. Model crystallization temperature estimates after Blundy and Holland's (1990) plagioclase–amphibole geothermometer for the rocks of the Jaala-Iitti complex.

		Amph		Plag		T (°C)	
Rock	**#**	**N**	**Si**	**N**	**Ab**	**1 kbar**	**5 kbar**
Hornblende granite							
matrix	90381	1	6.46(0)	2	0.672(9)	837(3)	775(3)
matrix	90161	3	6.43(20)	5	0.695(37)	838(56)	776(52)
Hornblende-quartz-feldspar porphyry							
matrix	90542	3	6.45(10)	1	0.733(0)	821(21)	760(20)
MME							
matrix	91053C	2	6.46(5)	4	0.506(23)	920(41)	854(40)
matrix	91382	3	6.35(14)	2	0.596(7)	891(36)	825(34)
amph incl	91382	4	6.44(7)	3	0.514(63)	906(45)	840(43)
Pillow-like MME							
matrix	90041A	2	6.96(8)	3	0.660(68)	732(34)	675(32)
matrix	9102A	4	6.74(13)	1	0.639(0)	785(29)	726(27)
comp. MME	9102A	2	6.80(5)	1	0.730(0)	747(10)	689(9)
Micro-enclave							
matrix	90191	6	6.53(6)	3	0.668(88)	824(41)	763(38)
Hybrid rock							
matrix	90141	6	6.60(7)	1	0.703(0)	797(14)	737(14)
matrix	90501	3	6.45(1)	1	0.725(0)	824(3)	762(3)
matrix	90191	5	6.65(14)	4	0.625(76)	811(45)	750(43)
pl mantle	90141	6	6.60(7)	3	0.663(20)	808(21)	748(20)
pl mantle	90141	3	6.45(18)	4	0.664(50)	843(60)	780(56)
pl mantle	90141	3	6.45(18)	1	0.474(0)	945(48)	878(46)

Si = Si in amphibole (a.f.u.), Ab = albite content of plagiclase

Parenthesized numbers indicate standard deviation of measurement in terms of least digits cited.

N = number of analyses in average composition

$T(°C) = [(0.677P-48.98+Y)/(-0.0429-0.008314\ln K)]-273.15$,
where $K = [(Si-4)/(8-Si)]X_{ab}$, $Y = 0$ for $X_{ab} > 0.5$, and
$Y = -8.06 + 25.5(1-X_{ab})^2$ for $X_{ab} < 0.5$

plm = plagioclase mantling alkali feldspar

Hybrid rock temperatures of 797° to 945°C (1 kbar) are lower as are the temperatures of pillow-like MMEs (732–785°C at 1 kbar). These low temperatures correlate with high Si contents in the amphiboles of the hybrid rocks (6.60–6.65 a.f.u., samples 90141 and 90191) and pillow-like MME (6.74–6.96 a.f.u.); X_{ab} of plagioclases vary from 0.59 to 0.70 and from 0.62 to 0.73, respectively. Amphiboles from the micro-enclaves contain slightly more Si (6.53 a.f.u.) than those in the other

rock types (Si = 6.35–6.46 a.f.u.) of the complex including the MMEs.

The temperature estimation for the formation of the micrographic intergrowth rimming alkali feldspar is based on the plagioclase in the intergrowth and amphibole from the surrounding matrix. Temperature estimates from 800 to 820°C are equal to those of the hybrid rock matrix. The two-feldspar geothermometer gives a Model 2 temperature of 809°C (Table 3) that corresponds to the temperatures of the amphibole–plagioclase geothermometer implying that the crystallizing temperature for the micrographic rim was between 800° and 820°C. Plagioclase mantles surrounding alkali feldspar in the rocks of the Jaala-Iitti complex show amphibole inclusions; these have reached temperatures in the range of 831° to 944°C, with a mean at 860°C. The highest temperature (944°C) is based on an analysis of the core of a plagioclase of An_{52}. The Si content of the amphibole inclusions in plagioclase is lower than in amphiboles of the hybrid rocks. For comparison, when Si = 6.45 is adopted, from plagioclase mantling alkali feldspar, for amphibole composition (samples 90141 and 90191), the model temperature varies between 830° and 870°C at 1 kbar. With Si = 6.44 (amphibole inclusions in plagioclase, sample 90382) for an amphibole in the pillow-like MME, the temperature ranges from 825° to 860°C. This is lower than those of the small MME and supports the idea that pillow-like MMEs have remained liquid longer than the small MMEs which usually show less features of hybridization. It is worth mentioning that these modal calculations do not take into account the possibility that the composition of the plagioclase may have changed. Changes in X_{ab} content affect less the model temperatures than do changes in the Si content of the amphibole.

Fe–Ti oxides

Ilmenite and magnetite analyses from the granites and hybrid rocks are presented in Appendices 1f and 1g, respectively. Fe^{3+} contents were calculated from charge balance and stoichiometry. Mole fractions of ilmenite and hematite in ilmenite–hematite solid solution and magnetite and ulvöspinel in magnetite–ulvöspine solid solution are calculated after the method of Stormer (1983).

In the granites of the Jaala-Iitti complex magnetite and ilmenite commonly form lamellar intergrowths. In the hybrid rocks and especially in the MMEs and pillow-like MMEs ilmenite is the dominant Fe–Ti oxide. If magnetite is far more abundant than ilmenite, the interoxide cooling trend will closely follow the magnetite isopleths with ilmenite changing its composition (Frost *et al.* 1988). On the other hand, if ilmenite is the dominant oxide, as it is in the hybrid rocks and the MMEs, the composition of ilmenite will be largely unaltered during cooling, while the composition of magnetite changes according to the reaction $Fe_2TiO_4 + Fe_2O_3 = FeTiO_3 + Fe_3O_4$.

Ilmenite in the rocks of the complex is relatively low in hematite; from 0.6 to 5.9 mol% in granites and 0.8 to 7.9 mol% in hybrid rocks. It is also almost Mg-free (under 0.06 wt% MgO). MnO contents vary between 0.86 and 1.42 wt% in the ilmenites of the granites and the contents are slightly higher in hybrid rocks with 0.74–2.21 wt% MnO.

Magnetites from the granites show a relatively wide variation in terms of the ulvöspinel component fraction; 5.2 to 17.1 mol%. In the hybrid rocks the variation is even larger; in sample 91501 it is 21.8–26.0 mol% whereas in sample 90191 it varies from 8.5 to 9.4 mol%. There is not much variation in magnetites occurring as inclusions in amphiboles (7.1–8.0 mol% ulvöspinel). Magnetites have less than 0.03 wt% MgO.

Two magnetite–ilmenite lamellar intergrowth pairs from the hybrid rocks (samples 90141 and 90491E) and from the hornblende-quartz-feldspar porphyry (sample 90402) were used to approximate the initial spinel composition. The area-weighted compositions are presented in Table 5 and calculated X_{USP} contents vary from 0.48 to 0.55 and 0.67 to 0.87, respectively. In the hornblende-quartz-feldspar porphyry the variation of the X_{USP} is smaller than in the hybrid rocks and suggests that the spinel composition (or the compositions of magnetite and ilmenite in the lamellar texture) have changed less compared to the composition of the ilmenite that

Table 5. Model spinel compositions and formulas for the hornblende-quartz-feldspar porphyry (sample 91402) and hybrid rocks (samples 90141 and 90491E) calculated from area ratios and compositions of the individual lamellae.

	Hbl-qz-fsp porphyry		Hybrid rock			
Sample	91402	91402	90141	90141	90491E	90491E
No.	1	2	1	2	1	2
FeO^{tot}	79.72	75.42	70.29	67.18	72.82	67.78
TiO_2	16.91	18.93	25.36	29.31	22.66	27.69
MnO	0.51	0.67	0.71	0.65	0.51	0.67
MgO	0.00	0.02	0.01	0.00	0.00	0.04
Cr_2O_3	0.02	0.02	0.19	0.03	0.03	0.05
V_2O_3	0.44	0.46	2.20	0.97	0.83	1.02
Al_2O_3	0.09	0.21	0.19	0.21	0.31	0.21
Total	97.69	95.73	98.95	98.35	97.16	97.46
FeO*	46.68	47.70	54.16	57.51	51.49	55.74
Fe_2O_3*	36.72	30.81	17.93	10.75	23.70	13.38
Total	101.37	98.82	100.75	99.43	99.53	98.80
Formula based on 4 oxygen atoms						
Fe^{2+}	1.47	1.53	1.68	1.81	1.63	1.77
Fe^{3+}	1.03	0.89	0.50	0.30	0.67	0.38
Ti	0.47	0.54	0.71	0.83	0.64	0.79
Mn	0.02	0.02	0.02	0.02	0.02	0.02
Mg	0.00	0.00	0.00	0.00	0.00	0.00
Cr	0.00	0.00	0.01	0.00	0.00	0.00
V	0.01	0.01	0.07	0.03	0.03	0.03
Al	0.00	0.01	0.01	0.01	0.01	0.01
Total	3.00	3.00	3.00	3.00	3.00	3.00
X_{USP}	0.48	0.55	0.76	0.86	0.67	0.82
X_{MAG}	0.52	0.45	0.24	0.14	0.33	0.18

Note: FeO^{tot} represents total iron.
Fe^{2+} and Fe^{3+} are calculated from charge balance and stoichiometry.
* recalculated after Fe^{2+} and Fe^{3+} in formula.
See Appendix 1g for X_{USP} and X_{MAG} calculations.

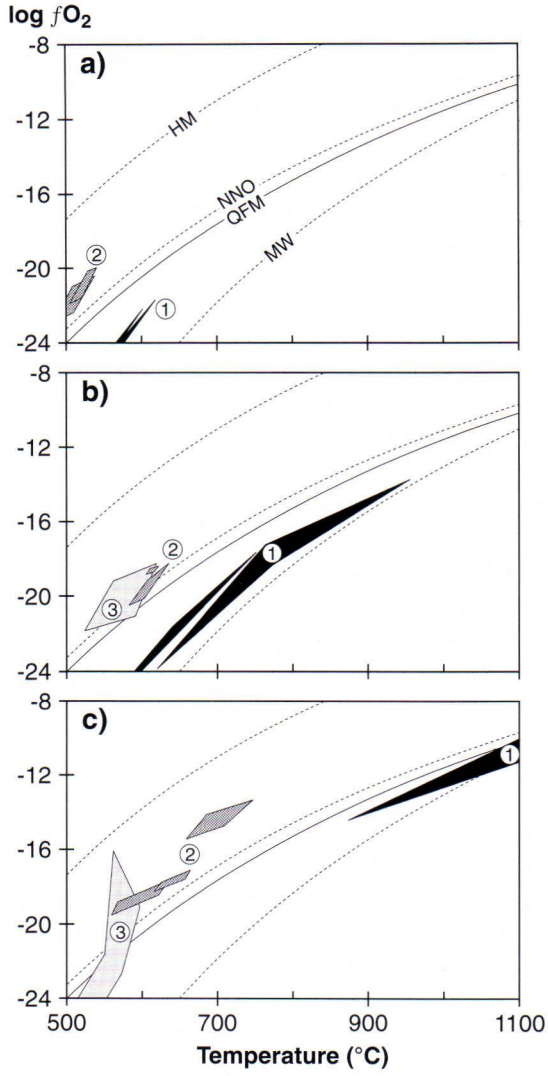

Fig. 32. Temperature and oxygen fugacity calculated for magnetite–ilmenite pairs from a) the hornblende-quartz-feldspar porphyry (sample 91402) and b) and c) hybrid rocks (samples 90491E and 90141, respectively) using the program QUILF (Andersen et al. 1993). Areas represent fO_2–T space calculated from: 1) model spinel and matrix ilmenite, 2) ilmenomagnetite, and 3) individual magnetite and ilmenite grains in the matrix. Curved lines are solid state oxygen buffers HM (hematite–magnetite, Myers & Eugster 1983), NNO (nickel–nickel oxide, Huebner & Sato 1970), QFM (quartz–fayalite–magnetite, Berman 1988), and MW (magnetite–wüstite, Myers & Eugster 1983). See text for discussion.

occurs in minor amounts in granites of the complex. In the hybrid rocks with ilmenite as a major Fe–Ti oxide the calculated spinel compositions are less reliable with a greater variation in the X_{USP} composition.

The temperature–oxygen fugacity space calculated by using the program QUILF (Andersen *et al.* 1993) to model spinel composition and ilmenite from the matrix (number 1 in Fig. 32a) and lamellae compositions (number 2 in Fig. 32a) of the hornblende-quartz-feldspar porphyry show temperatures below 650°C and logfO_2 below -20. For the

hybrid rocks (Figs. 32b and 32c) the T–fO_2 space calculated from spinel-ilmenite pairs gives a wide temperature range from 600°C to over 1100°C and the logfO_2 values are commonly 1–4 log units below the QFM buffer. Spinel #2 and spinel #1 in Table 5 combined with matrix ilmenite give temperatures under 800°C and over 1100°C.

As in the case of the hornblende-quartz-feldspar porphyry, the temperatures calculated for the hybrid rocks by using the lamellae pairs give variable temperatures of less than 750°C and logfO_2 values varying below and above the QFM. Compared to temperature estimates from the amphibole–plagioclase geothermometer for crystallization temperatures of the plagioclase mantling alkali feldspar with a plagioclase (rim) composition of An_{52} giving temperatures of 945°C (see Table 4) the initial spinel (X_{USP} = 0.76–0.82) – ilmenite temperatures of over 900°C are believed realistic estimates of the equilibrium temperature for the hybrid magma. At these temperatures the logfO_2 values (-10 – -16) are 1–2 log units below the QFM buffer.

Pyroxenes

Analyses of pyroxenes from the MMEs and hybrid rocks are presented in Appendix 1h. Pyroxene end-members ($Mg_2Si_2O_6$, $Fe_2Si_2O_6$, and $CaSi_2O_6$) are calculated after Morimoto (1988); by normalizing Ca + Mg + SFe to 100 ($\Sigma Fe = Fe^{2+} + Fe^{3+} + Mn^{2+}$). In Figure 33, pyroxene compositions are plotted in the Wo–En–Fs diagram for Ca–Mg–Fe pyroxenes.

Pyroxenes in the MMEs are commonly calcian (iron-rich) pigeonite ($En_{32-37}Fs_{48-57}Wo_{11-16}$) or subcalcic (iron-rich) augite ($En_{22-23}Fs_{50}Wo_{22-23}$), but iron-rich augite also occurs ($En_{25}Fs_{32}Wo_{43}$) (see Fig. 33 and Appendix 1h). An enstatite phenocryst ($En_{63-64}Fs_{31-32}Wo_5$, number 1 in Fig. 33) is not stable with the MME host as indicated by a biotite rim around it. Augite or pigeonite in equilibrium with the enstatite is assumed to have an Mg content higher than the Fe content (i.e. less Fs component). It is probable that the crystallization of the enstatite took place before injection of the mafic magma into the felsic magma. The composition of the inner parts of pigeonite in one of the MMEs (number 2 in Fig. 33) probably reflects the composition of pigeonite before hybridization. Pigeonite phenocrysts with more Fe-rich rims probably represent crystallization close to the point at which thermal equilibrium between the mafic and felsic magmas was reached. As the hybrid magma was formed, more Mg and Ca relative to Fe was diffused from the mafic magma into the hybrid magma changing the T–fO_2–X conditions so that magnesium-rich pyroxenes were no longer stable but amphibole and iron-rich augite were (number 3 in Fig. 33).

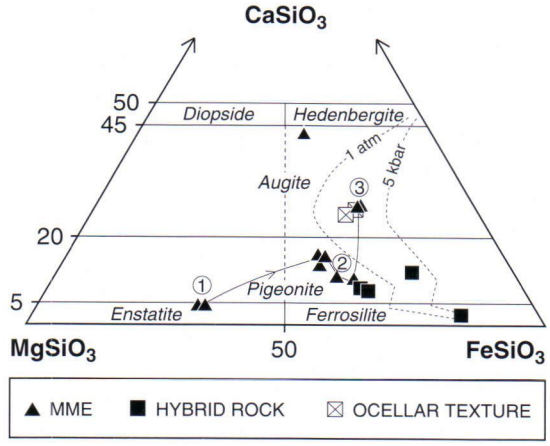

Fig. 33. Classification diagram for Ca–Mg–Fe pyroxenes after Rock (1990) adopted to pyroxenes from the MMEs and hybrid rocks of the Jaala-Iitti complex. Solid line joins assumed pyroxene compositions in MME before hybridization (1), during hybridization (2), and after hybridization (3) in thermal equilibrium with host hybrid magma. Dotted lines represent a polythermal boundary of the "forbidden zone" after Lindsley (1983) at the pressure of 1 atm and 5 kbar. See text for discussion.

In the hybrid rocks of the Jaala-Iitti complex all the pyroxenes are rimmed by amphibole, and usually occur as small grains with Fe–Ti oxide pigment. Augite ($En_{24-26}Fs_{49-50}Wo_{27-28}$) in the ocellar texture is more fresh than augite in the matrix. Pigeonite occurs in two compositions: $En_{30-31}Fs_{60-61}Wo_{8-9}$ and $En_{20}Fs_{68}Wo_{12}$, with the main difference in Mg and Fe. Note also that augite and pigeonite from the hybrid rock and MMEs have a similar composition as shown by Figure 33 indicative of similar crystallization conditions. A ferrosilite ($En_{15}Fs_{82}Wo_3$) and a pigeonite from the

hybrid rocks plot in the "forbidden zone" of the Wo–En–Fs diagram (Fig. 33). To the right of the 1 atm and 5 kbar curves pyroxene relations are metastable with respect to the system augite + olivine + silica indicating that ferrosilite and quartz can not be stable with fayalite at low pressures. Ferrosilite was obviously the earliest pyroxene in the hybrid rocks at higher pressures (≥ 5 kbar?), and it is possible that fayalite was not stable during crystallization of the hybrid magma but is xenocrystic and derived from the felsic end-member of the complex.

The MgO content in the pyroxenes from the MMEs and hybrid rocks ranges from 0.25 to 1.34 wt%. Cr_2O_3 contents are less than 0.01 wt% except in the orthopyroxene phenocrysts from MME sample 91053E that has 0.07–0.08 wt% Cr_2O_3. NiO, Na_2O, and K_2O contents are less than 0.07, 0.76, and 0.20 wt%, respectively.

Although pyroxenes were found in the MMEs and hybrid rocks of the complex they were rimmed by amphibole and not in equilibrium with each other. The crystallization of pyroxenes apparently took place at different stages of hybridization as the mafic and felsic magmas interacted with each other. This and subsolidus reactions with the host and perhaps continuous hybridization during changes of the T–X (and possibly P) conditions during crystallization limit the use of any two-pyroxene geothermobarometers for the pyroxenes of the Jaala-Iitti complex. The approximate temperature of minimum stability for Ca–Mg–Fe pigeonite with Fe/(Fe+Mg) from 0.55 to 0.64 in MME (sample 91053A) varies from 930° to 880°C based on Lindsley (1983) and Davidson and Lindsley (1985) under low pressure conditions. The minimum temperature for pigeonite coexisting with augite and orthopyroxene at low pressures varies from 825° to 880°C with Fe/(Fe+Mg) = 0.65–0.77. Lowest temperature at which Fe-rich and Mn-poor pigeonite is stable is 825°C (Lindsley 1983). These temperatures are compatible with those of the amphibole–plagioclase and Fe–Ti oxide geothermometers.

Olivine

Fe-rich olivine, commonly surrounded by amphibole, is found in the granites, hybrid rocks, and occasionally also in the pillow-like MMEs of the complex. In the hornblende-quartz-feldspar porphyry fayalite is found as remnants in almost all amphibole phenocrysts. Average olivine analyses from the hornblende-quartz-feldspar porphyry and the hybrid rocks are presented in Appendix 1i.

Forsterite contents of olivine in the hornblende-quartz-feldspar porphyry vary from 3.2 to 5.4 mol% with an average of $Fo_{4.3}$ and are similar to olivines analyzed from the hybrid rock ($Fo_{3.8–4.9}$). Olivines of the complex are low in both Cr_2O_3 and NiO, under 0.02 wt% and 0.08 wt%, respectively. Olivine from the hybrid rock is slightly higher in MnO (mean 2.01 wt%) than that from the hornblende-quartz-feldspar porphyry with (mean 1.49 wt% MnO). The forsterite content of the olivines in the rapakivi granite of the Wiborg batholith (Simonen 1961) is about 6 mol%.

When olivine becomes richer in Mg it can no longer coexist with quartz, and orthopyroxene becomes stable; orthopyroxene can coexist with oxides and with either olivine or quartz (Lindsley & Frost 1992, Andersen *et al.* 1993). This feature is apparent in the hybrid rocks and hornblende-quartz-feldspar porphyry of the complex, where olivine is mainly found surrounded by amphibole, and also in the hornblende granite in which olivine is found as inclusions in plagioclase (An_{30}). Ferrosilite is rare and is surrounded by amphibole so that equilibrium between the Fe–Mg silicates was not reached. Fayalitic olivine may have been stable in the early stages of crystallization, followed by ferrosilite (not found in the granites of the complex), pigeonite, and augite. It is more probable that fayalite crystallized in the felsic end-member and was incorporated into the hybrid magma. This means that the use of fayalite to evaluate crystallization or equilibrium conditions in the hybrid rocks is meaningless. In the pillow-like MMEs crystallization of fayalite did not occur because of the relatively low Fe (and high Si) content and therefore olivine was probably derived from the felsic magma.

In Fe-rich metamorphic and highly evolved igneous rocks, quartz can coexist with Fe_2SiO_4-rich olivine (Frost *et al.* 1988). One pertinent reaction is given by QUIIF (Frost *et al.* 1988, Frost & Lindsley 1992, Lindsley & Frost 1992):

$$SiO_2 + 2Fe_2TiO_4 = 2FeTiO_3 + Fe_2SiO_4$$
$$\text{Quartz} + \text{Ulvöspinel} = \text{Ilmenite} + \text{Fayalite}$$

Above the QUIIF, fayalite and ilmenite are both not stable with ulvöspinel and quartz and below the QUIIF quartz and ulvöspinel are both not stable with fayalite and ilmenite (Frost *et al.* 1988). This is apparent in the hybrid rocks which have predominantly ilmenite and magnetite and grains with magnetite–ilmenite lamellar intergrowths are rare. In the hornblende-quartz-feldspar porphyries magnetite–ilmenite lamellae are more common than ilmenite, and in this case the stability is above the QUIIF. The approximate stability of fayalite (sample 90301 in Appendix 1i), spinel (sample 91402, spinel #1 in Table 5), and ilmenite (sample 91402) with quartz was calculated by using the program QUILF (Andersen *et al.* 1993). It is probable that in hornblende-quartz-feldspar porphyry, the ilmenite composition has changed more than the approximate spinel composition, so in the calculations the mole fraction of X_{HEM} (and X_{ILM}) were allowed to change to achieve QUIIF stability. The results, calculated for 1 to 5 kbars, show a temperature range from 800° to 840°C and $\log fO_2$ from -15.1 to -13.9 (0.5 to 0.6 log units below QFM) when X_{ILM} = 0.920–0.906 (initial X_{ILM} = 0.985). The calculated X_{ILM} values have been lowered up to 8 mol% but are correlated with X_{ILM} contents of the hybrid rocks (X_{ILM} = 0.932 in sample 90141 in Appendix 1f).

GEOCHEMICAL CHARACTERISTICS OF THE ROCK TYPES OF THE JAALA-IITTI COMPLEX

In this chapter the geochemical characteristics of the granites, MMEs, and hybrid rocks are given as well as their tectonomagmatic affinities. Compositional data with major and minor elements and normative compositions are given in Appendices 2a, 2b, and 2c, and in Figure 34 to Figure 46. In Figure 34 the rocks of the Jaala-Iitti complex are plotted in the R_1R_2-diagram of de la Roche *et al.* (1980). The composition of the rocks varies almost linearly from granites (hornblende granite and hornblende-quartz-feldspar porphyry) to gabbros (MMEs) with the hybrid rocks of granodiorite composition having more Mg and Ca (i.e., tonalite affinities) compared to granites of the complex. Pillow-like MMEs are inclined toward the hybrid rocks and the least evolved small MMEs approach the gabbro field.

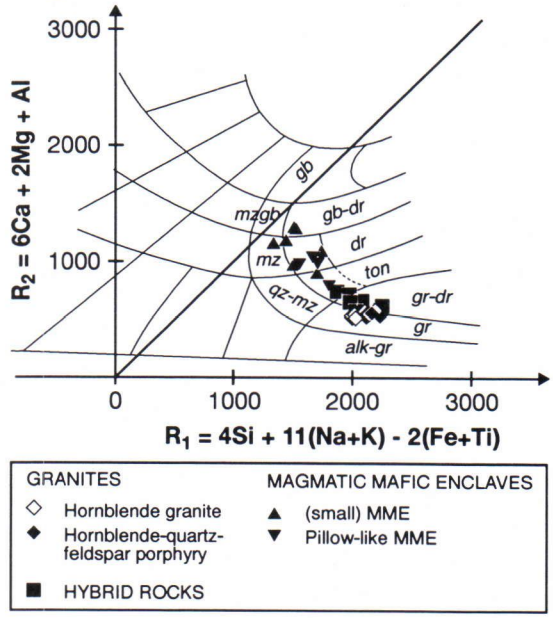

Fig. 34. Geochemical classification of the granites, MMEs, and the hybrid rocks of the Jaala-Iitti complex according to the multication R_1R_2-diagram of de la Roche et al. (1980). Abbreviations: alk-gr – alkali-feldspar (or alkali) granite, gr – granite, grdr – granodiorite, ton – tonalite, mz – monzonite, mzdr – monzodiorite, dr – diorite, mzgb – monzogabbro, gb – gabbro, qz – quartz.

Analytical procedures

All whole-rock samples were analysed at the X-Ray Assay Laboratories Ltd (XRAL), Canada. Since all samples were agate-milled, the maximum amount of extra SiO_2 that can occur is of interest, this is 0.3

wt% according to XRAL. The weight of the felsic samples was usually about 2 kilograms. MME samples were obviously smaller, and before being analyzed they were sawn into thin slabs in order to avoid parts with xenocrysts. Felsic samples were treated in a similar fashion to avoid contamination by MMEs. However, pillow-like MMEs were analysed as such using samples weighing about two kilograms. Analytical methods are shown in Figure 35.

For two samples (MME 91053B and quartz-feldspar porphyry 91402) Sm–Nd isotope analysis were performed at the Unit for Isotope Geology, Department of Petrology, Geological Survey of Finland by O. Tapani Rämö (see O'Brien *et al.* 1993, pp. 151–152, for analytical procedures).

Granites

The diagnostic chemistry of rapakivi granites compared to other granite suites of southeastern Fennoscandia include high Si, K, F, Rb, Ga, Zr, Hf, Th, U, Zn, total alkalies, and REE (except Eu) abundances as well as high K/Na, Fe/Mg, Ga/Al, and low Ca, Mg, Al, P, and Sr (Sahama 1945, Vorma 1976, Haapala 1977b, Nurmi & Haapala 1986, Rämö 1991, Haapala & Rämö 1992, Rämö & Haapala 1995). Rapakivi granites in general show the characteristics of A-type and within plate granites (see also Haapala & Rämö 1992, Rämö & Haapala 1995, and references therein).

The chemical composition of the hornblende granites and hornblende-quartz-feldspar porphyries of the Jaala-Iitti complex are presented in Appendix 2a, Table 6, and Figures 36 through 38. The granites of the Jaala-Iitti complex show only relatively small variation in the SiO_2 contents: 66.40–67.90 wt% SiO_2 in hornblende granites and 67.60–69.30 wt% SiO_2 in hornblende-quartz-feldspar porphyries. FeO*/(FeO*+MgO) ratios range from 0.89 to 0.93. Total alkali (Na_2O+K_2O) contents of the rocks vary from 7.41 to 8.11 wt% reflecting subalkaline characteristics (c.f., Irvine & Baragar 1971) which is also seen in the relatively low NK/A (molecular $(Na_2O+K_2O)/Al_2O_3$)) ratios of 0.75 to 0.81. The granites are clearly metaluminous with A/CNK (molecular $Al_2O_3/(CaO+Na_2O+K_2O)$) ratios in range of 0.87 to 0.93.

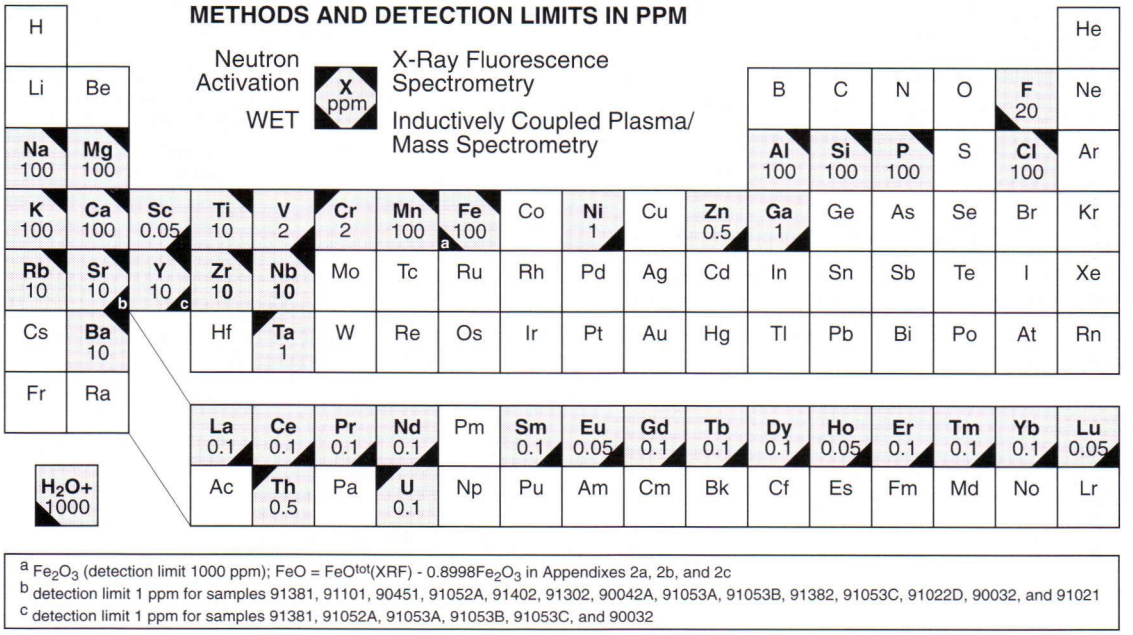

[a] Fe_2O_3 (detection limit 1000 ppm); FeO = FeO^{tot}(XRF) - 0.8998Fe_2O_3 in Appendixes 2a, 2b, and 2c
[b] detection limit 1 ppm for samples 91381, 91101, 90451, 91052A, 91402, 91302, 90042A, 91053A, 91053B, 91382, 91053C, 91022D, 90032, and 91021
[c] detection limit 1 ppm for samples 91381, 91052A, 91053A, 91053B, 91053C, and 90032

Fig. 35. Analytical methods and detection limits (in ppm). Analysed elements are shaded.

The variation of trace element contents in hornblende granites and hornblende-quartz-feldspar porphyries are (in ppm): F 1190 to 2100, Cl 303 to 499, Ba 785 to 1230, Zr 371 to 534, Rb 182 to 250, Sr 102 to 182, Zn 75 to 177, Y 39 to 86, Nb 21 to 34, Ga 22.5 to 28, U 5 to 7.4, and Th 16 to 29. The H_2O+ contents are low, 0.30 to 0.90 wt%.

REE abundances (Fig. 36) of the granites show typically negative Eu anomalies with $(Sm/Eu)_N$ ratios in the range from 2.12 to 2.80 (Eu/Eu* = 0.42–0.55) and enrichment of LREE relative to HREE ($(La/Yb)_N$ = 8.57–10.65). No major differences occur between hornblende granites (Fig. 36a) and hornblende-quartz-feldspar porphyries (Fig. 36b). Large scale fractional crystallization effecting the composition of granites of the complex is not obvious. The most evolved hornblende granite sample (91381) shows an enrichment of REE, Rb, and F and a depletion of Ba compared to other samples (see Appendix 2a). This sample also contains more Ti, Ca, and Mg compared to the other analysed samples which may reflect interaction with a mafic magma.

Sm–Nd isotopic data for the hornblende-quartz-feldspar porphyry sample 90402 are given in Table 6 compared with the average of three hornblende granite analyses from the Suomenniemi complex (Rämö 1991). The hornblende-quartz-feldspar porphyry sample was chosen as a representative of the felsic end-member because of the lack of MMEs in it and because petrographic studies suggest that it is the least hybridized rock type of the complex. The Sm (13.93 ppm) and Nd (78.03 ppm) contents of sample 91402 are lower than those of the hornblende granites from the Suomenniemi complex with an average Sm = 19.92 ppm and Nd = 108.07 ppm. The $^{147}Sm/^{144}Nd$ and $^{143}Nd/^{144}Nd$ values for sample 90402 are 0.1080 and 0.511586, respectively, being slightly lower than those of the average hornblende granite from the Suomenniemi complex with $^{147}Sm/^{144}Nd$ = 0.1094–0.1128 and $^{143}Nd/^{144}Nd$ = 0.511629–0.511638. The ε_{Nd}(1630 Ma) = -2.0 is lower than in the hornblende granite average of the Suomenniemi complex but it lies within the evolution path of the Finnish rapakivi granites in the ε_{Nd} versus age diagram (see Rämö 1991, Fig. 32) with T_{CHUR} = 1807 Ma and T_{DM} = 2098 Ma. The $\varepsilon_{Nd}(T)$ of the hornblende-quartz-feldspar porphyry calculated at 1640 Ma is similar to that value $\varepsilon_{Nd}(T)$ = -1.7 of the mean for the hornblende granite from the Suomenniemi complex.

In the discrimination diagram of Whalen *et al.* (1987) the granites of the complex plot into the A-type field (Fig. 37) simply because of their high

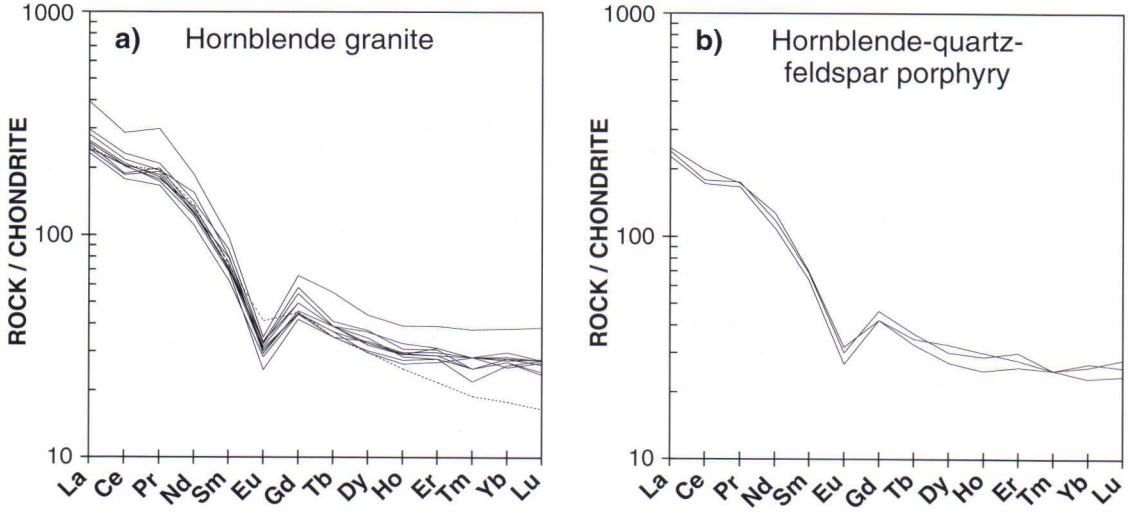

Fig. 36. Chondrite-normalized rare earth element analyses of (a) hornblende granites and (b) hornblende-quartz-feldspar porphyries of the Jaala-Iitti complex.

Table 6. Sm–Nd isotopic data for the hornblende-quartz-feldspar porphyry sample 91402 of the Jaala-Iitti complex and average Sm–Nd isotopic data (n=3) of the hornblende granites from the Suomenniemi complex (data from Rämö 1991).

	Age (Ma)	Sm (ppm)	Nd (ppm)	$^{147}Sm/^{144}Nd$	$^{143}Nd/^{144}Nd$	$\varepsilon_{Nd}(T)$	T_{CHUR} (Ma)	T_{DM} (Ma)
Jaala-Iitti complex	1630* (±5)	13.93	78.03	0.1080	0.511586 (±15)	-2.0 (±0.5)	1807 (±35)	2098
Suomenniemi complex	1640	19.92	108.07	0.1114	0.511634	-1.7		2093

* Vaasjoki *et al.* (1991).

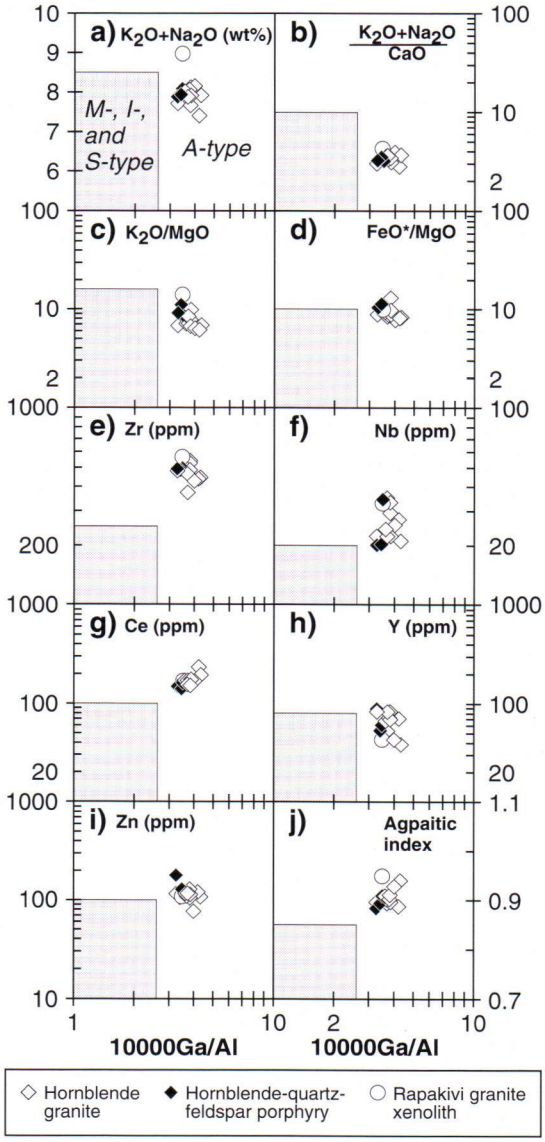

Ga/Al (10000Ga/Al = 3.27–4.31). Besides the high Ga/Al, A-type characteristics of the rocks are clearly visible in the high contents of Zr, Nb, Ce, and Zn and in the high agpaitic index. In Figure 37 an analysis of the rapakivi granite xenolith (sample 9014X, Appendix 2a) in the hybrid rock (sample 90141) is also plotted. It is similar to the granites of the complex, except in having a higher K_2O+Na_2O. This is due to the higher alkali feldspar content in the xenolith.

Figure 38 shows the granites of the Jaala-Iitti complex plotted in the tectonomagmatic discrimination diagrams of Pearce *et al.* (1984). The hornblende granites and hornblende-quartz-feldspar porphyries of the complex show within plate granite characteristics but plot in two diagrams (Figs. 38a and 38b) also in the ocean ridge granite field separated by a dotted line representing the upper compositional boundary for ORG. The granites of the complex plot, in Figures 38b and 38d, in the "triple point" of syn-COLG, WPG, and VAG fields but show WPG characteristics again in Figure 38e when separating WBG and ORG fields and in Figure 38f when separating WPG and VAG+COLG fields.

Fig. 37. Geochemical discrimination diagrams after Whalen et al. (1987) adopted to the analyses of the hornblende granites and quartz-feldspar porphyries of the Jaala-Iitti complex. a) K_2O+Na_2O vs. Ga/Al, b) $(K_2O+Na_2O)/CaO$ vs. Ga/Al, c) K_2O/MgO vs. Ga/Al, d) FeO/MgO vs. Ga/Al, e) Zr vs. Ga/Al, f) Nb vs. Ga/Al, g) Ce vs. Ga/Al, h) Y vs. Ga/Al, i) Zn vs. Ga/Al, and j) agpaitic index vs. Ga/Al. Shaded areas represent the joint compositional space of the M-, I-, and S-type granites. Open circles represent the composition of a porphyritic rapakivi granite xenolith (sample 9014X in Appendix 2a) in hybrid rock.*

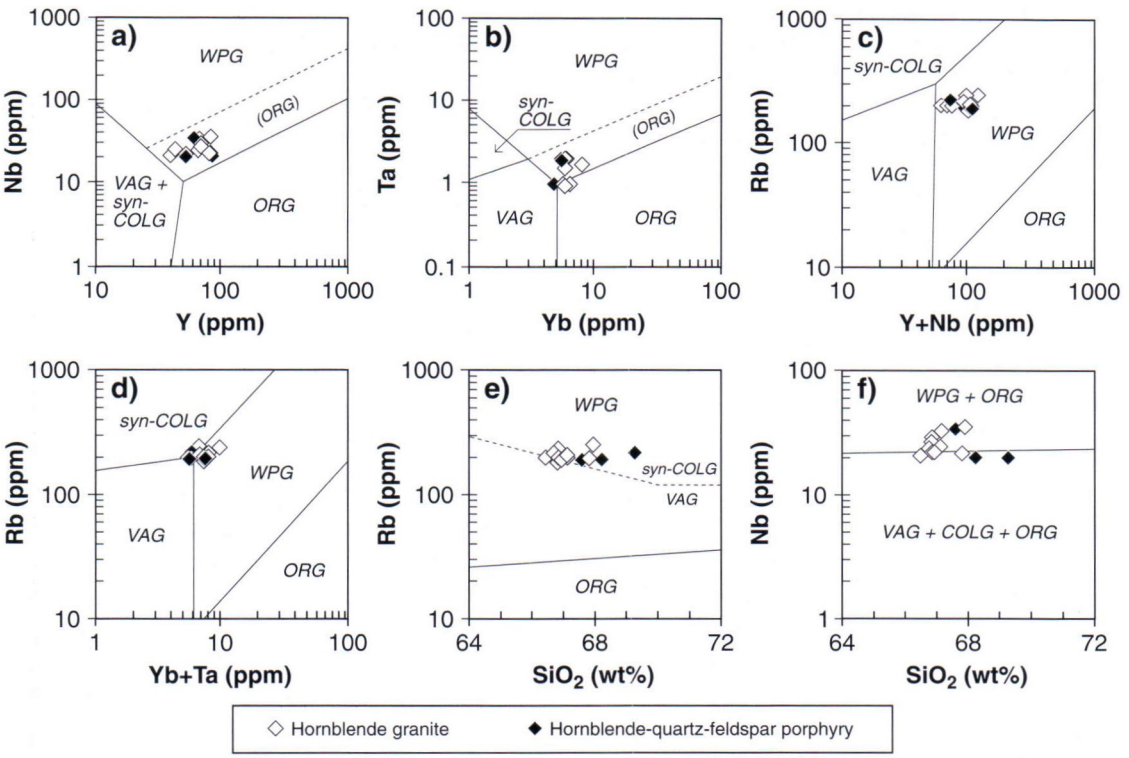

Fig. 38. Tectonomagmatic discrimination diagrams after Pearce et al. (1984) adopted to analyses of the hornblende granites and hornblende-quartz-feldspar porphyries of the Jaala-Iitti complex. a) Nb vs. Y, b) Ta vs. Yb, c) Rb vs. Y+Nb, d) Rb vs. Yb+Ta, e) Rb vs. SiO_2, and f) Nb vs. SiO_2. Abbreviations: WPG – within plate granites; VAG – volcanic arc granites, ORG – ocean ridge granites, and COLG – collision granites.

Small MMEs and pillow-like MMEs

Magmatic mafic enclaves of the Jaala-Iitti complex are assumed to represent pieces of the Subjotnian mafic magmas that were emplaced between 1665 to 1635 Ma in southeastern Finland (Vaasjoki *et al.* 1991). This mafic magmatism temporally and spatially associated with the rapakivi granite magmatism comprises diabase dykes and minor gabbroic and anorthositic bodies. The Subjotnian diabase dykes in southeastern Finland range in composition from quartz tholeiite to olivine tholeiite with SiO_2 from 47 to 53 wt%, and they are hypersthene-normative, alkaline or subalkaline in composition (Rämö 1990, 1991).

The chemical composition of the MMEs and pillow-like MMEs from the Jaala-Iitti complex are presented in Appendix 2b, Table 7, and Figures 39 through 43. As discussed earlier, MMEs and pillow-like MMEs show signs of interaction between the mafic and felsic magmas; recrystallized MMEs, for example, contain variations in mineral compositions and variable amounts of xenocrysts. All these have affected the composition of the MMEs. MME specimen (9004A), a composite enclave in a pillow-like MME, has 50.30 wt% SiO_2, 5.07 wt% total alkalies (Na_2O+K_2O), and Mg number of 36.50. These values are similar to those from the least hybrid MMEs (i.e., samples 91053A, 91053B, and 91053E) with SiO_2 from 50.80 to 51.80 wt%, total alkalies from 4.62 to 5.34 wt%, and Mg numbers from 35.84 to 37.54. The Mg numbers are lower than those of the diabase dykes of the Suomenniemi (26 to 49) and Häme (38 to 61) swarms (Laitakari 1969, Boyd 1972, Rämö 1990, 1991). In the pillow-like MMEs, the Mg numbers

vary from 28.5 to 34.3 possibly reflecting a decrease in the Mg/Fe due to hybridization with the felsic magma. All MMEs show subalkaline characteristics (Fig. 39), with a composition range from (high-K) basalt to (high-K) trachyte in the chemical classification of Le Bas (1986). K_2O contents of the MMEs range from 1.83 to 3.85 wt%. K_2O/Na_2O for the least hybrid MMEs vary from 0.66 to 0.70, for hybrid MMEs from 0.89 to 1.58, and for pillow-like MMEs from 0.90 to 1.21. In general, MMEs show high FeO (6.70–11.40 wt%) and fall in the tholeiitic field in Na_2O+K_2O–MgO–FeO* space (Fig. 40) and show an alkali-enriched trend. All MMEs and pillow-like MMEs are quartz-normative with 4.01–4.54 wt% normative quartz in the least hybrid MMEs and 9.60–15.78 wt% in hybrid MMEs and pillow-like MMEs (see Appendix 2b).

In the tectonomagmatic K_2O–P_2O_5–TiO_2 diagram after Pearce *et al.* (1975) (Fig. 41a) the MMEs and pillow-like MMEs plot in the non-oceanic field with increasing K_2O content controlled by the degree of hybridization. In Figure 41b, most of the MME analyses fall into spreading island center field despite the clear continental trend shown in Figure 41a. This may be due to hybridization having increased the Al_2O_3 content of the rocks. It should be noted, however, that the MgO–Al_2O_3–FeO* diagram applies only to subalkaline rocks of basaltic andesite composition with 51–56 wt% SiO_2 (Pearce *et al.* 1977) thus excluding some of the MME compositions but those with 51–56 wt% SiO_2 fall in the CFB space. In the Zr–3Y–Ti/100 diagram (Fig. 41c) three analyses fall into the field of within plate basalts, and in the Zr/4–Y–2Nb diagram (Fig. 41d) most of the samples show within plate characteristics. It is possible that those MMEs showing CFB characteristics have retained their initial Ti, Nb, Y, and Zr, whereas other MMEs and pillow-like MMEs in Figure 41 show increasing K_2O, Al_2O_3, and Zr and a loss of Ti. Three MME analyses in Figures 41a through 41d may closely approach the unmixed initial composition of the injected mafic magma.

The mean composition (MME^p, Appendix 2b) of the three most primitive MMEs (samples 9004A, 91053A, and 91053B, Appendix 2b) is assumed to

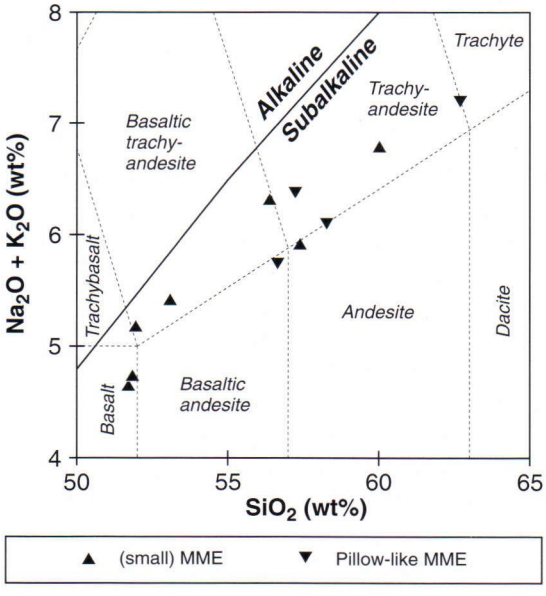

Fig. 39. Na_2O+K_2O vs. SiO_2 diagram of the MMEs and pillow-like MMEs of the Jaala-Iitti complex. Chemical classification and nomenclature after Le Bas et al. (1986). The solid line divides the fields of alkaline and subalkaline rocks after Irvine and Baragar (1971).

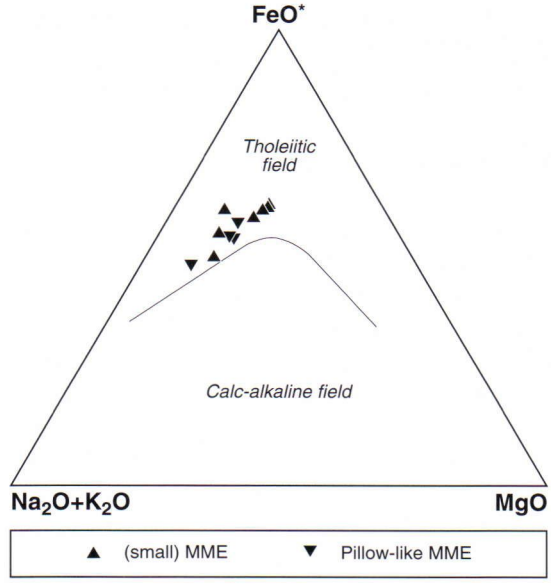

Fig. 40. Chemical composition of the MMEs and pillow-like MMEs of the Jaala-Iitti complex plotted in an AFM (Na_2O+K_2O–MgO–FeO) diagram. Tholeiitic and calc-alkaline field after Irvine and Baragar (1971).*

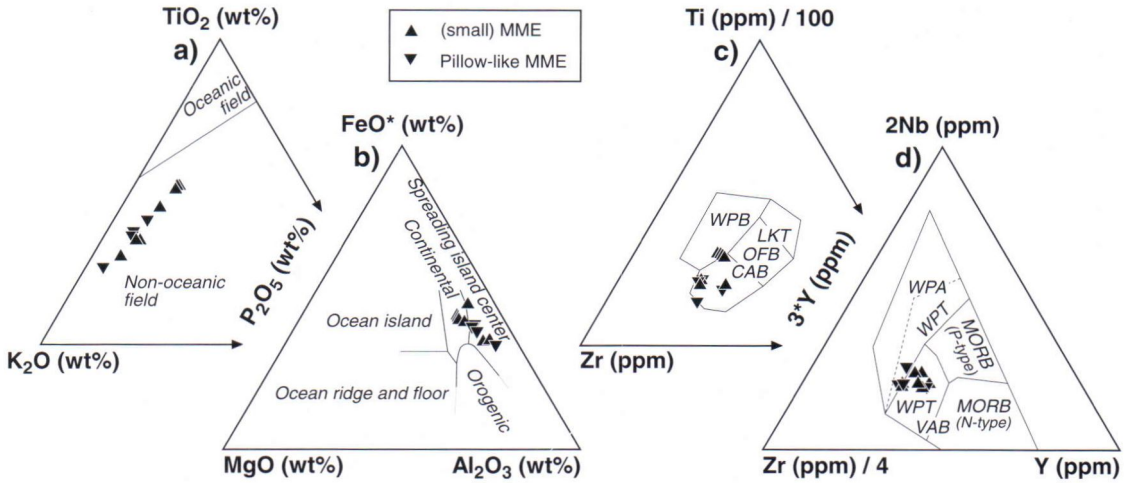

Fig. 41. Chemical composition of the MMEs and pillow-like MMEs of the Jaala-Iitti complex plotted in (a) the K_2O–P_2O_5–TiO_2 diagram of Pearce et al. (1975), (b) the MgO–Al_2O_3–FeO diagram of Pearce et al. (1977), (c) the Zr–3Y–Ti diagram of Pearce and Cann (1973), and (d) the Zr–Y–Nb diagram of Meschede (1986). FeO* represents total Fe. Abbreviations in (c) and (d): WPB – within plate basalts (ocean island + continental basalts), LKT – low potassium tholeiites, OFB – ocean floor basalts, CAB – calc-alkali basalts, WPA – within plate alkali basalts, WPT – within plate tholeiites, MORB – mid-ocean ridge basalts, and VAB – volcanic arc basalts.*

be the initial composition of the mafic magma of the complex. In Figure 42, this has been used to normalize other MME and pillow-like MME analyses of the complex (Fig. 42a) as well as the diabases and the assumed initial liquid composition (Rämö 1991, Table 13) from the Suomenniemi complex (Fig. 42b).

Hybrid MMEs and pillow-like MMEs show less Ti, Fe^{tot}, Mn, Mg, and Na compared to MME^p. The remarkably high K (up to two times that in MME^p) in MMEs reflects assimilation of alkali feldspar xenocrysts or diffusion of K from the felsic magma.

The MME^p composition corresponds to the initial liquid composition of the Suomenniemi complex as regards Si, Fe^{tot}, Mn, and Na which differ less than 10 % from the MME^p composition; the difference of Al (1.3*MME^p) and K (0.7*MME^p) content can not be directly correlated with the possible small amounts of alkali feldspar contamination of the MME^p. In Figure 42b two groups of diabases from the Suomenniemi complex with different Ti_N contents are apparent. Those diabases having Ti_N less than one seem to have an excess of Al when compared to the Ti and Al composition of the MME^p. Rämö (1991) suggested that the high Al contents may be due to enrichment of plagioclase as a cumulate. Initial composition of the diabases of the Suomenniemi complex also contain 1.2*Mg# by comparison with MME^p, and it is possible that the mafic magma of the Jaala-Iitti complex is slightly more evolved than the average diabase magma of the Suomenniemi complex.

Similarly, the more evolved composition of the MMEs as compared to the mean composition of the Subjotnian diabases from the Suomenniemi complex is also apparent in the Sm-Nd isotopic data of Table 7. The Sm and Nd contents of sample 91053B (9.96 ppm and 48.88 ppm, respectively) are only slightly lower than those of the Suomenniemi complex with Sm = 10.21 ppm and Nd = 49.91 ppm (average of 9 analyses). The $^{147}Sm/^{144}Nd$ as well as $^{143}Nd/^{144}Nd$ are also lower compared to average diabase composition of the Suomenniemi complex, but in general the $\varepsilon_{Nd}(1630\ Ma) = -0.5$ and $T_{DM} = 2045$ Ma (Suomenniemi complex 2030 Ma) shows a close relationship to the general evolution of the Subjotnian diabases (see Rämö 1991) and for the primary, not hybrid composition of the mafic magma of the Jaala-Iitti complex. To summarize, the least evolved MMEs represent Subjotnian mafic

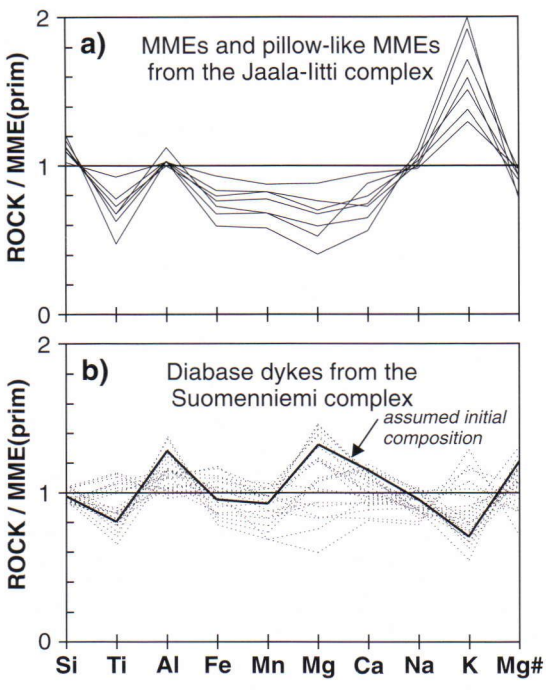

Fig. 42. Elements of (a) MMEs and pillow-like MMEs from the Jaala-Iitti complex and (b) diabase dykes from the Suomenniemi complex (data from Rämö 1991) normalized against the MME^p of the Jaala-Iitti complex. Fe represents total Fe.

magmas, and they most probably are globules of that mafic magma without significant chemical exchange with the felsic magmas they intruded.

The REE-patterns of the MMEs ($[Gd/Yb]_N$ = 1.9) and pillow-like MMEs ($[Gd/Yb]_N$ = 1.9 to 2.0) are similar to those of the evolved diabases of the Suomenniemi complex (Fig. 43). One sample (91382) shows a REE pattern dissimilar to the others. It is a MME ($[La/Yb]_N$ = 9.93, $[Sm/Eu]_N$ = 2.54, and Eu/Eu* = 0.47) enclosed in the hornblende granite with $(La/Yb)_N$ = 10.41, $[Sm/Eu]_N$ = 2.80, and Eu/Eu* = 0.42. This MME is recrystallized (Fig. 24a) and its amphibole and plagioclase are compositionally similar to those in the host hornblende granite. This points to a local equilibrium between the mafic and felsic magmas which is also manifested by a slight increase of the Ti, Ca, and Mg contents of the hornblende granite compared to the bulk of the granites of the complex.

The pillow-like MMEs show slightly negative Eu anomalies with a $(Sm/Eu)_N$ ratio from 1.54 to 2.02 (MME^p = 1.44). Alkali feldspar and plagioclase usually contain more Ba, Sr, and Eu than other minerals (Arth 1976) and therefore a positive Eu anomaly in the pillow-like MMEs is expected due to assimilation of feldspar xenocrysts. Otherwise the Eu content in pillow-like MMEs varies from 1.92 to 2.59 ppm; these values lie between the Eu contents of the MME^p (2.69 ppm) and granites (1.78–2.51 ppm, average 2.20 ppm) of the complex. Thus the negative Eu anomaly in the pillow-like MMEs probably reflects chemical exchange between the mafic magma and felsic magma instead of xenocryst assimilation. The hybrid character of the composition of the pillow-like MMEs is also reflected in their LREE-enriched character relative to the MME^p composition. Hybridization of the mafic magma is also denoted by the higher LREE/HREE of the pillow-like MMEs (6.92–9.18) and hybrid MMEs (6.61–8.61) compared to MME^p (6.52). For comparison, LREE/HREE in hornblende granites and hornblende-quartz-feldspar porphyries ranges from 8.10 to 9.34.

Xenocryst assimilation is shown by an increase of Ba content in the pillow-like MMEs (759–1020

Table 7. Sm–Nd isotopic data for the MME sample 91053B of the Jaala-Iitti complex and average Sm–Nd isotopic data (n=9) of the diabases from the Suomenniemi complex (data from Rämö 1991).

	Age (Ma)	Sm (ppm)	Nd (ppm)	$^{147}Sm/^{144}Nd$	$^{143}Nd/^{144}Nd$	$\varepsilon_{Nd}(T)$	T_{CHUR} (Ma)	T_{DM} (Ma)
Jaala-Iitti complex	1630* (±5)	9.96	48.88	0.1232	0.511826 (±7)	-0.5 (±0.5)	1686 (±26)	2045
Suomenniemi complex	1639	10.21	49.91	0.1254	0.511862	-0.2		2030

* Vaasjoki *et al.* (1991).

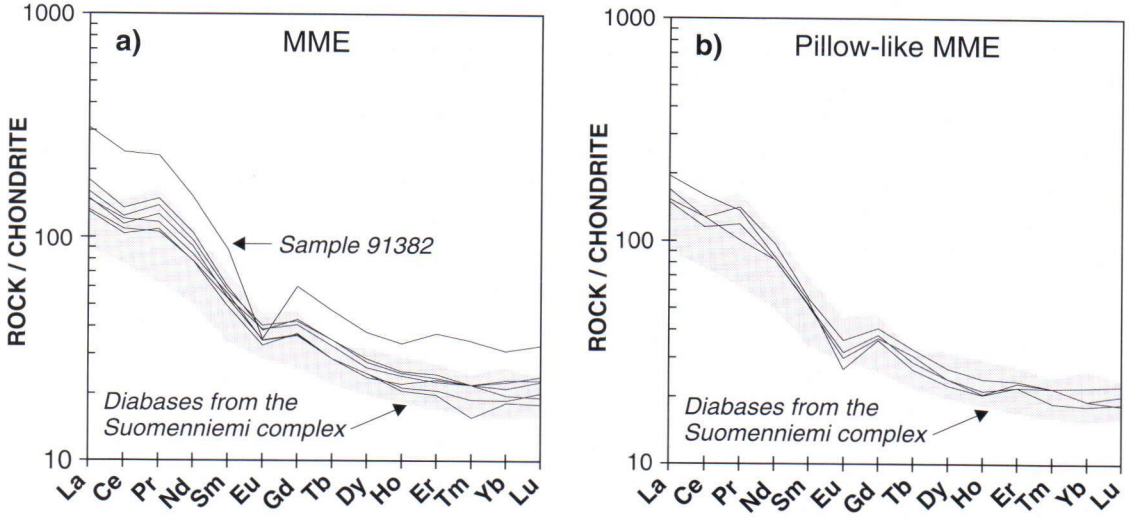

Fig. 43. Chondrite-normalized rare earth element compositions of (a) MMEs from hybrid rocks and hornblende granite and (b) pillow-like MMEs in hybrid rocks from north of lake Kirkkojärvi. Shaded areas represent REE-analyses of the diabases from the Suomenniemi complex (data from Rämö 1991).

ppm) compared to MME^P (594 ppm). The highest Rb and lowest Sr contents occur in a recrystallized MME (sample 91382) and the lowest Rb and the highest Sr contents in the least hybridized MMEs. Cr and Ni contents of the MMEs and pillow-like MMEs are low, varying from 9 to 49 ppm and 3 to 20 ppm, respectively.

The F content in the MMEs varies usually from 1100 to 1800 ppm (pillow-like MMEs) and from 1100 to 3000 ppm (small MMEs), and an exceptionally high F content, 8000 ppm, was found in MME (sample 91382) from the hornblende granite. These values are higher than for example those in the diabases of the Suomenniemi complex where F contents vary from 800 to 2200 ppm (O.T. Rämö 1994, personal communication). It is probable that the high F content of MMEs compared to pillow-like MMEs is connected to the degree of hybridization; extra fluorine was added to the mafic magma as in MME sample 91382 that contains almost four times more F than its host, hornblende granite (sample 91381). A similar feature, but on a smaller scale, is apparent in the H_2O+ contents of the MMEs that vary from 0.60 to 1.60 wt% in the pillow-like MMEs and from 0.30 to 0.90 wt% in the granites of the complex. Diffusion of fluorine from felsic to mafic magma had the probable effect of crystallizing needle-like apatite in the mafic magma, and together with the increase of the H_2O+ content it decreased the crystallization temperature.

Hybrid rocks

The criteria used to distinguish hybrid rocks and granites in the Jaala-Iitti complex is based on the occurrence of ocellar and micrographic textures. Megacrysts were in part derived from the partially crystallized rapakivi granite magma and denote thermal disequilibrium with the host hybrid magma. Mantling of quartz xenocrysts by amphibole and augite coronas is lacking in the granites of the complex. MMEs are also more prevalent in the hybrid rocks than in the granites of the complex.

The chemical composition of the hybrid rocks of the Jaala-Iitti complex is presented in Appendix 2c, and Figures 44 through 46. In Figure 44, SiO_2, TiO_2, Al_2O_3, Fe_2O_3, FeO, MnO, CaO, Na_2O, K_2O, P_2O_5, F, Ba, Zr, Rb, and Sr contents of the hornblende granites, hornblende-quartz-feldspar porphyries, MMEs, pillow-like MMEs, and hybrid rocks are plotted against their MgO contents. The hybrid rocks plot clearly between the MMEs and granites

in Figures 44a, 44b, 44e, 44f, 44g, 44i, 44j, 44l, 44m, 44n, and 44o. Sample 90491E (see Appendix 2c) shows a composition similar to that of the hornblende granites but is included in the hybrid rocks because ocellar texture is common in the rock. This sample is assumed to be the least hybridized granite of the complex and supports the idea that there is a gradual change in composition between the hybrid rocks and granites.

The granites of the complex are compositionally homogeneous except in terms of their Fe_2O_3 (Fig. 44d), Na_2O (Fig. 44h), and Ba (Fig. 44l) contents. In the hybrid rocks and some of the MMEs the variation of Na_2O content may be related to local heterogeneity in the amount of MMEs in the hybrid magmas and mixing of the hybrid magmas with granite magmas or mafic magmas. In such circumstances, Na (and K) behave as extremely mobile elements (Watson & Jurewicz 1984). Most of the elements in the hybrid rocks have concentrations between those in the MMEs and granites, but the hybrid rocks are closer in composition to the granites than MMEs indicating that the proportion of mafic end-member is relatively low compared with the proportion of the felsic end-member.

Geochemically, the hybrid rocks differ from the granites in their contents of SiO_2 (63.10–68.10 wt%) MgO (0.80–1.42 wt%), TiO_2 (0.87–1.17 wt%) FeO (4.40–6.00 wt%), MnO (0.08–0.12 wt%), CaO (2.54–3.78 wt%), K_2O (4.14–4.81 wt%), Zr (373–513 ppm), Rb (158–219 ppm), and Sr (126–219 ppm). Al_2O_3 (Fig. 44c) does not show much variation in the rock types of the complex. A relatively good correlation of K_2O and MgO contents (Fig. 44i) is the result of chemical exchange of K between the mafic magma and the felsic magma, rather than assimilation of alkali feldspar xenocrysts by hybrid rocks and MMEs. The fluorine content in hybrid rocks (830 to 2100 ppm) is similar to that of the granites (1190 to 2100 ppm). The H_2O+ content (0.50–1.10 wt%) in the hybrid rocks is, on the average, slightly higher than in the granites (0.30–0.90 wt%).

REE patterns of the hybrid rocks from are similar to those of the other rock types of the complex (Fig. 45). In detail, however, the hybrid rocks show slightly lower HREE contents (35.13 to 42.16 ppm, average 37.56 ppm) compared to the granites (34.95–55.35 ppm, average 41.10 ppm). LREE/HREE ratios for hybrid rocks vary from 7.36 to 10.41 and for hornblende granites and hornblende-quartz-feldspar porphyries from 8.10 to 9.34.

In Figure 46a, normative An/(An+Or) ratios are plotted against Mg number. The An/(An+Or) ratios of the granites vary from 19.89 to 24.63 whereas in hybrid rocks the range is 24.90–32.97. A similar but negative trend appears in the normative quartz (Q) versus Mg number diagram of Figure 46b in which the normative Q values decrease in hybrid rocks with increasing Mg number and normative Q increases in MMEs along with decreasing Mg number. Both Figures 46a and 46b show that, in the granites, the normative An/(An+Or) and normative Q values (13.98–21.14) remain relatively constant with increasing Mg number. The normative An/(An+Or) to normative Q (ANOR/Q) for the granites varies from 0.81 to 0.96. For the hybrid rocks ANOR/Q values are from 0.98 to 1.78 and clearly correlate with the degree of hybridization. For comparison, the ANOR/Q values for the silicic rocks of the Suomenniemi complex, which are non-hybrid in origin, range from 0.18 to 1.01, so that ANOR/Q = 1 seems to be the maximum value for separating hybrid rocks and granites. ANOR/Q values for MMEs and pillow-like MMEs range from 2.93 to 16.03 and from 2.27 to 4.79, respectively.

MAGMATIC EVOLUTION OF THE JAALA-IITTI COMPLEX

On the origin of the end-member magmas

The granites and non-hybridized MMEs of the Jaala-Iitti complex show little chemical variation. Local chemical heterogeneity in the granites is caused mainly by small amounts of MMEs and xenoliths. As regards heterogeneity in the mafic rocks of the complex, it is related mainly to chemical exchange between the mafic magma and the felsic magma resulting in hybrid MMEs. Magma

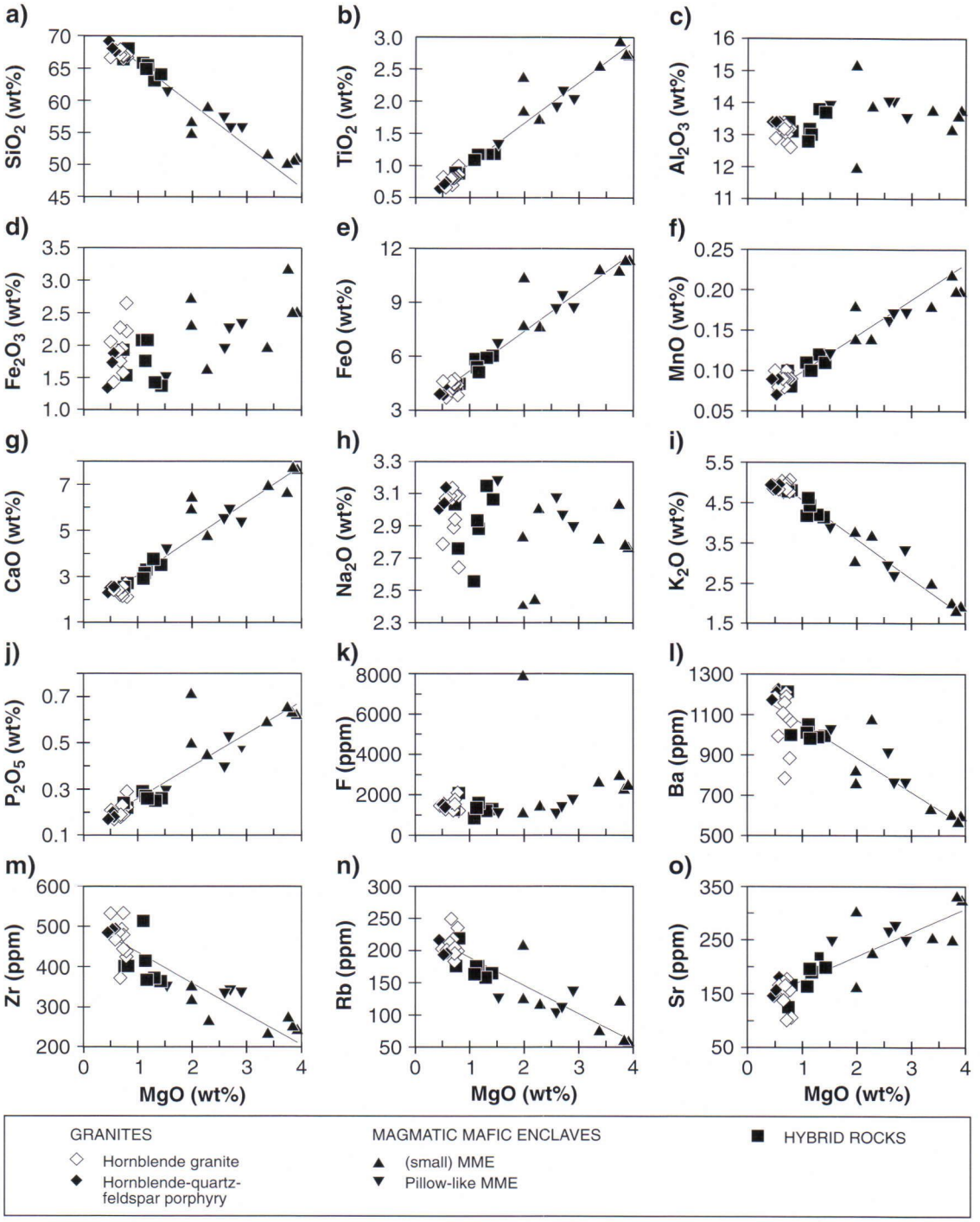

Fig. 44. The analyses of granites, MMEs, and hybrid rocks of the Jaala-Iitti complex plotted as a) SiO_2 vs. MgO, b) TiO_2 vs. MgO, c) Al_2O_3 vs. MgO, d) Fe_2O_3 vs. MgO, e) FeO vs. MgO, f) MnO vs. MgO, g) CaO vs. MgO, h) Na_2O vs. MgO, i) K_2O vs. MgO, j) P_2O_5 vs. MgO, k) F vs. MgO, l) Ba vs. MgO, m) Zr vs. MgO, n) Rb vs. MgO, and o) Sr vs. MgO. The lines are least square fits through the data.

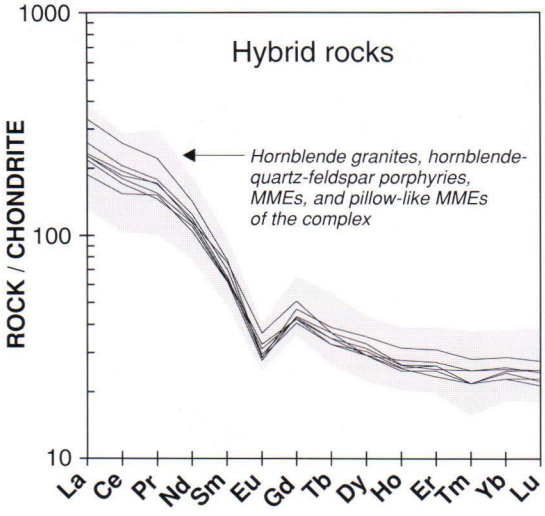

Fig. 45. Chondrite-normalized rare earth element analyses of the hybrid rocks of the Jaala-Iitti complex. The shaded area covers the whole range of REE compositions of the complex.

mixing has probably been a major mechanism in the generation of the hybrid rocks of the complex.

Felsic end-member

Mafic underplating has been proposed as the cause of partial melting in the crust producing rapakivi granite magmas (Huppert & Sparks 1988, Rämö & Haapala 1991). These, in turn, are intruded at high crustal levels (Vorma 1975, 1976) forming rapakivi granite batholiths, stocks, and silicic dykes. The granites of the Jaala-Iitti complex plot, in the Ab–Or–Q diagram of Figure 47a, in an area corresponding to pressures of 7 to 10 kbars. This is what has been found from the rapakivi granites of the Wolf River Granite, U.S.A. (Anderson & Cullers 1978) and the Suomenniemi complex (Rämö 1991). In Figure 47b, the minimum melt compositions in the system Q–Ab–Or at pressures of 2, 5, and 10 kbars at water activities of 0.1, 0.5, and 1.0 are shown (data from Ebadi & Johannes 1991). For comparison, Figure 47b also contains a data set for the Finnish rapakivi granites, area-weighted compositions of the Laitila and Wiborg batholith, and the initial magma of the Suomenniemi complex (data from Rämö & Haapala 1995). In this diagram,

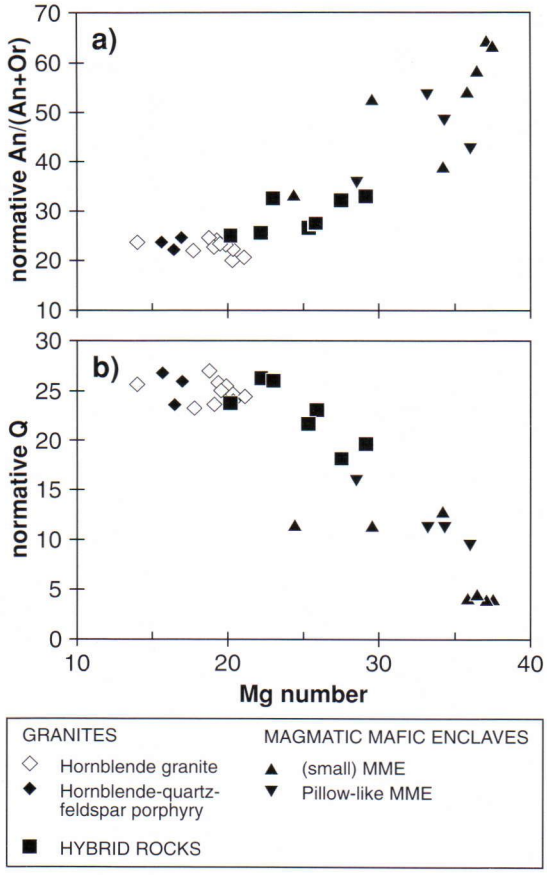

Fig. 46. Chemical composition of the granites, MMEs, and hybrid rocks from the Jaala-Iitti complex shown in (a) normative An/(An+Or) vs. Mg number and (b) normative quartz vs. Mg number diagrams.

the granites of the Jaala-Iitti complex plot at low a(H_2O) activity (< 0.1) and moderate total pressure which is consistent with the fact that these granites are relatively water-poor.

The Jaala-Iitti complex cuts sharply topaz-bearing granite in the east (see Fig. 5) and has occasional xenoliths of it near the contact. The topaz-bearing granite also shows metasomatic reactions caused by the Jaala-Iitti complex, these show up as a change in the colour of the rock from grey to pale red. Non-altered topaz-bearing granite has a minimum melt composition corresponding to about 2 kbar (equal to about 7 km), and this may be regarded as an approximate depth of the emplacement of the Jaala-Iitti complex.

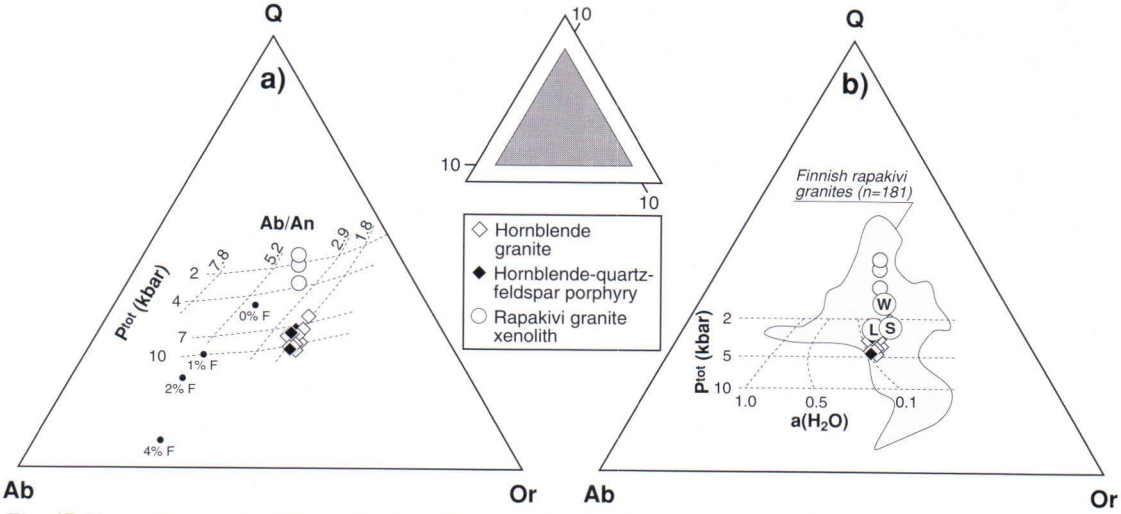

Fig. 47. Normative quartz–albite–orthoclase diagrams showing the composition of the hornblende granites and the hornblende-quartz-feldspar porphyries of the Jaala-Iitti complex. Open circles represent the composition of the topaz-bearing granite (data from Salonsaari & Haapala 1994) cut by the complex. (a) An/Ab ratios of 1.8, 2.9, 5.2, and 7.8, and P(H_2O) of 2, 4, 7, and 10 kbars are adopted from Anderson and Cullers (1978). Dots represent the position of the minimum melting (or solidus/eutectic crystallization) composition at 1, 2, and 4 wt% F (with excess H_2O at 1 kbar) after Manning (1981); the fluorine-free (0% F) point is from Tuttle and Bowen (1958). b) Minimum melt compositions as a function of total pressure and activity of water in the melt (data from Ebadi & Johannes 1991). Data for the Finnish rapakivi granites, the area-weighted mean compositions of the Wiborg (W) and Laitila (L) batholiths, and the initial magma of the Suomenniemi complex (S) are from Rämö and Haapala (1995).

Mafic end-member

As the most mafic MMEs in the hybrid rocks from the Jaala-Iitti complex show a limited compositional range they been interpreted as the mafic end-member of the complex (MME^p in Appendix 2b). Mafic magma of this composition was probably injected into a felsic magma chamber and interacted with the felsic end-member. Although some compositional differences in pillow-like MMEs and one MME in the hornblende granite host indicate chemical equilibrium was reached by MMEs with their host it is possible that magma mixing has effected the composition of MMEs. This shows up in samples 91053C and 91053F that are from the same host rock (samples 90141A and 90141B) as the most primitive samples.

It has been shown that the Subjotnian diabase dykes in southeastern Fennoscandia are products of extensive fractionation in intra-crustal magma chambers (Boyd 1972, Rämö 1991) and this probably is true of the mafic end-member of the Jaala-Iitti complex. This is suggested by the relatively low Mg numbers (37), as well as Ni (19 ppm) and Cr (44 ppm) contents.

One of the problems related to the evolution of the complex is whether the mafic magma has intruded a felsic one as a single pulse or as multiple pulses. If the mafic magma was intruded into a partly crystallized granite magma at an early stage, the mafic magma has more time to equilibrate and mingle with the felsic magma. Capturing of feldspar and quartz xenocrysts could therefore occur to a greater extent than in mafic magmas injected later. Multiple injection is suggested by the composite enclaves; these MMEs are usually primitive in composition; they usually do not contain xenocrysts. Pillow-like MMEs that always contain xenocrysts probably result from the first injections of the mafic magma into the felsic magma chamber. It is possible that both magma pulses are from the same parental magma because the composition of the composite enclave (sample 90042A) is similar to primitive MMEs (e.g., samples 91053A and 91053B). The compositional shift probably regis-

ters magma evolution prior to hybridization. When this mafic magma was intruded into a felsic magma chamber in the crust a stratified magma chamber was formed. The pillow-like MMEs were probably formed closest to an injection pipe where conditions for the interaction of the mafic and felsic magma were most favourable. Injection of mafic magma as a fountain will result in disintegrated globules of mafic magma in the felsic magma. It is also presumable that disintegration of the mafic magma increases away from the mafic magma pipe if the mafic magma remains liquid long enough. Flow structures (see Fig. 10) and the presence of xenocrysts in the pillow-like MMEs suggest extensive movement and mechanical interaction of mafic and felsic magmas.

Origin of mafic enclaves

Mafic enclaves in this study are considered to be of magmatic origin. Several possibilities for the origin of more mafic fragments in granites have been proposed. These are briefly discussed below. In this chapter, the term mafic enclave is used for a fragment of a mafic rock in a felsic rock without petrogenetic implications.

The importance of the study of rock fragments, especially MMEs, in granite petrology is essential to an understanding of the origin and evolution of granites. A controversy exists as to whether (mafic) enclaves in granitoid rocks represent restites, xenoliths, or originate by magma mingling. Numerous models and theories (see e.g., Didier 1973, Chen *et al.* 1990, Didier & Barbarin 1991a, for detailed summaries and comparison) have been proposed to explain the petrogenesis of mafic enclaves in felsic rocks. The two favoured hypotheses in dealing with I- and S-type granites propose that mafic enclaves represent globules of mafic magma incorporated into a more felsic host by mingling (e.g., Didier 1973, Vernon 1983) or that they represent unmelted residual source rock material (restite, e.g., White & Chappell 1977, Chappell *et al.* 1987).

Restite (Chappell *et al.* 1987) or surmicaceous (Didier 1987) inclusions or residues from pre-existing rocks are usually rich in micas, Al-rich minerals, apatite, zircon, and opaque minerals. Vernon (1983) lists evidence favouring the origin of mafic enclaves as globules of mafic magma instead of restites. This evidence is based on the occurrence, shape and size, microstructure, and composition of mafic enclaves. The abundance of MMEs in the Jaala-Iitti complex is not related to proximity of contacts with the country rock, and the distribution of MMEs is irregular throughout the complex. Some flow structures in the MMEs (Fig. 10) and the occurrence of xenocrysts support the hypothesis that these MMEs and their host rock matrices must have been in a partially liquid stage penecontemporaneously. This contrasts with the restite hypothesis of unmelted residual (mafic) rock material. Chappell and White (1991) suggest that most of the restites in granites are carried up from the source as single crystals or small aggregates, and not as large fragments or enclaves. The restite hypothesis is, therefore, not adopted to explain the large amounts of mafic enclaves in the rocks of the Jaala-Iitti complex even though Chen *et al.* (1990) reported numerous mafic enclaves of possible restite origin with similar characteristics to mafic enclaves in the Jaala-Iitti complex. The best possibility for the inclusions of large amounts of restites is if a pluton were situated near the site where the granitic melt was formed; this is unlikely in the case of the Jaala-Iitti complex.

MMEs, especially the pillow-like MMEs, in the Jaala-Iitti complex contain variable amounts of feldspar and quartz xenocrysts derived from the more felsic host rock indicating that both MME and the host magma have been at partially liquid stage simultaneously. Some MMEs also contain composite MMEs indicating that there were at least two magma pulses were injected. Country rocks similar to the MMEs near the complex are lacking. These, and the shape of the MMEs indicate that mafic enclaves in the Jaala-Iitti complex have formed by magma mingling and mixing of a mafic magma with a felsic one. This observation also rejects the possibility that mafic enclaves in the Jaala-Iitti complex are accidental xenoliths such as was proposed for the origin of mafic enclaves by Hurlbut (1935) and Grout (1937). The bimodal association

of rapakivi granites and mafic tholeiitic diabase dykes and gabbroic and anorthositic bodies in southeastern Fennoscandia suggests the possibility that mafic enclaves in the rapakivi granites are fragments of the Subjotnian mafic rocks. This is also supported by the geochemical relationship between mafic rocks of the Jaala-Iitti complex and diabases of the Suomenniemi complex as shown by Salonsaari and Haapala (1994). If mafic enclaves in the Jaala-Iitti complex represent xenoliths of more mafic rocks, a more angular shape of the xenoliths as well as a lack of feldspar and quartz xenocrysts would be expected.

Mafic enclaves have also been proposed as cumulates of earlier minerals crystallized in a magma parental to the host rock and enclaves (e.g., Wall *et al.* 1987). If gravitational settling of crystals (pyroxene, amphibole, and plagioclase) formed mafic enclaves in the Jaala-Iitti complex, this obviously took place in a deep-seated magma chamber before emplacement of the complex. Minerals of mafic enclaves and their host rocks are similar but the relatively small amount of pyroxene and relatively high content of feldspar and quartz megacrysts in mafic enclaves with rare phenocrysts of plagioclase and pyroxenes are not consistent with a cumulate theory. Lack of cumulus texture also rejects a cumulate origin for the mafic enclaves in the Jaala-Iitti complex. The evidence given for rejecting the cumulus origin of mafic enclaves in the complex can also be adopted to reject a theory that mafic enclaves represent fragments of an earlier parental magma common to mafic enclaves and their host rocks as suggested by Bailey (1984).

Geringer *et al.* (1987) proposed that mafic enclaves are products of partial melting of a common source for mafic enclaves and their host rock under relatively high $X(CO_2)$ conditions. This theory proposes intrusion and consolidation of a first mafic melt that is later incorporated by a second-stage granitic melt. Vernon and Flood (1982) had also previously described mafic enclaves as representing small batches of an early, more mafic magma, but they assumed that the earlier mafic magma formed a conduit through which the later granitic melt rose. This two-stage partial melting process cannot form mafic enclaves because the first melts generated by partial melting of the crust are granitic in composition as noted by Chen *et al.* (1990). More mafic melts may, however, be generated by partial melting of the mantle.

Mafic enclaves have also been assumed to be fragments reflecting multiple injections of contrasting magmas but with unmixing due to liquid immiscibility (Bender *et al.* 1982, Metzger *et al.* 1985). Metzger *et al.* (1985) gives evidence in favour of liquid immiscibility, including similar compositions of those minerals present in both mafic and felsic parts, enrichment of HFS elements (i.e., P, middle and heavy REE, Zr, HF, Nb, and Ta) in the mafic rocks, and similar Sr isotope initial ratios. Even though liquid immiscibility is an important factor in magma mixing systems, the evidence listed above more likely points to chemical interaction (mixing) than unmixing. Liquid immiscibility involves the evolution and interaction of two melts in the first stage of hybridization by injection of a mafic magma into felsic one forming MMEs and by favouring magma mingling instead of mixing. After sufficient time for thermal equilibrium, interaction between the MME and the host rocks magma by mixing will take place (Poli & Tommasini 1991).

One possible explanation for the mafic enclaves in rapakivi granites is that they represent fragments of disrupted chilled margins of a granite body (Grout 1937, Vernon & Flood 1982, Vorma 1976). Vorma (1976) describes disrupted chilled margins (autoliths) from the Ytö and Suutila rapakivi granites (Laitila batholith). These mafic enclaves resemble those in the Jaala-Iitti complex in having sizes from a few centimetres to a few tens of centimetres, being ovoidal in shape, having orientations parallel to the contact of the batholith, containing alkali feldspar megacrysts similar to those of the host rock, and similar mineral compositions. But there is a difference when the composition of mafic enclaves from the Laitila batholith and the Jaala-Iitti complex are compared to their host rocks. Autoliths from the Ytö granite have a similar bulk rock composition compared to the host granite whereas mafic enclaves in the Jaala-Iitti complex are more mafic in composition, representative of a diabase. This

suggests that mafic enclaves in the Jaala-Iitti complex do not represent disrupted chilled margins even though smaller grain size suggests the relatively rapid crystallization of the mafic enclaves.

Fractional crystallization versus magma mixing

When assessing the magmatic evolution of the complex it is also necessary to consider such processes as partial melting of mixed sources, differentiation, contamination, and alteration (Langmuir *et al.* 1978). Possible factors that have an influence on the chemical composition of MMEs after emplacement in their felsic host are chemical exchange by diffusion (magma mixing) and closed system crystal/liquid fractionation (Eberz & Nicholls 1990).

As remarked, the granites of the complex show only a small geochemical and mineral chemical variation (see Figs. 25–27, 29–31, 34, 36–38, 44, 46, and 47). However, the possibility exists that the rock series hybrid rock – hornblende granite – hornblende-quartz-feldspar porphyry could represent a fractionation series of an initial intermediate magma. Figure 48 shows that this is not possible, however. Magmas that evolved from the hybrid magmas should contain less Zr and more SiO_2 and Al_2O_3 (Fig. 48). In-situ fractionation of the rapakivi granite magmas (and hybrid magmas) must also have been negligible assuming that the magmas of the complex have been intruded together as a dyke-like body. When compared to the evolutionary trend of the rapakivi granites of the Suomenniemi complex (SNC), the granites of the Jaala-Iitti complex show higher overall (4[Ca+Na]+0.5[Fe+Mg])/Zr. This may indicate that a small amount of mafic end-member is present in almost all the granites, especially in the hornblende granites of the complex if the evolution of granites is similar to those of the Suomenniemi complex. In Figure 48, the hybrid rocks of the complex fall, together with pillow-like MMEs, between the Subjotnian mafic rocks and rapakivi granites of the southeastern Fennoscandia and follow the "zircon critical" (ZCRIT) contour (Bradshaw 1992) that separates the fractional crystallization trends of mafic and felsic magmas of the Suomenniemi complex (SNC).

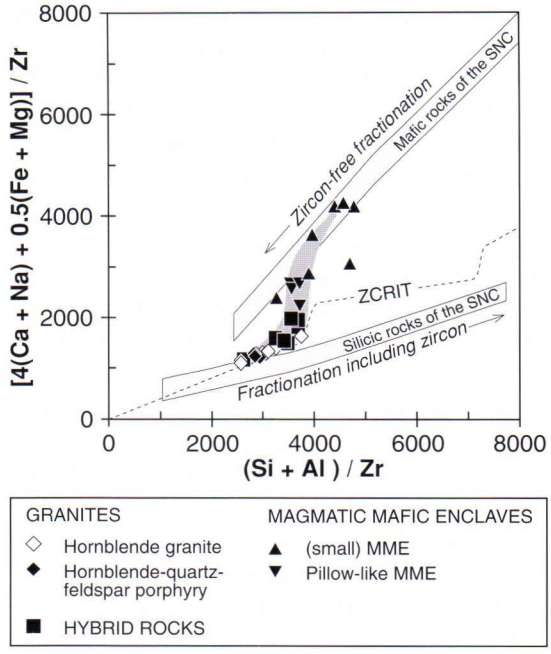

Fig. 48. (Si+Al)/Zr vs. (4[Ca+Na]+0.5[Fe+Mg])/Zr diagram after Bradshaw (1992) for the MMEs, pillow-like MMEs, hybrid rocks, hornblende granites, and hornblende-quartz-feldspar porphyries of the Jaala-Iitti complex compared to the silicic and mafic rocks of the Suomenniemi complex (SNC, data from Rämö 1991). ZCRIT separates rocks that plot above and below the critical SiO_2 value of 68 wt%; in those rocks that fall below ZCRIT Zr may combine with the SiO_2 to produce zircon (Bradshaw 1992).

The non-hybridized MMEs plot in Figure 48 on the evolutionary trend of the mafic rocks of the Suomenniemi complex (SNC) which indicates a similar source for them. A few of the MMEs plot below the SNC trend which is due to local differences in the amounts of xenocrysts and the degree of hybridization. Compositional change engendered by fractional crystallization of a mafic magma is not a viable option. MMEs have to be interpreted as closed-system magma globules, and the only possible factor that may change their composition is magma mixing with the host felsic magma. In-situ fractional crystallization of the mafic globules

(MME) has, however, been proposed to be operative; K, Rb, Ba, Nb, Y, and REE are found to be enriched in the margins of the MMEs, and Si and Zr depleted relative to the centre of the MME (Eberz & Nicholls 1990). Recrystallized borders of MMEs and micro-enclaves with modal compositions near to that of their host rocks favour magma mixing over other processes in changing the compositions of the MMEs.

Geochemical modelling of hybridization

Mineral chemical data and petrographic features indicate a chemical and thermal disequilibrium between megacrysts and the host magma in hybrid rocks and MMEs. Corroded and mantled feldspars as well as quartz megacrysts suggest the interaction of felsic and mafic magmas. The intermediate hybrid rocks appear to have formed mainly by mixing and mingling of the two compositionally contrasted melts, with a relatively low mass-fraction of the mafic magma (X_m) present in the newly formed hybrid magma. The alkali feldspar and quartz, and probably also many of the plagioclase megacrysts, nucleated and grew in the felsic magma, and subsequently were trapped in the hybrid magma during the interaction of the magmas. Furthermore, some megacrysts in the hybrid rocks of the complex are clearly xenocrysts derived from partially melted and disintegrated Svecofennian granitoid or rapakivi granite xenoliths, and dissolution of xenocrysts has also effected the bulk composition of the hybrid rocks.

All of the above features as well as proportions of mafic and felsic end-members in the mixture have affected the bulk composition of the hybrid rocks. The weight proportion (or mass-fraction) of the mafic magma (X_m) in an ideal mixture (X^i_H) can be evaluated if the concentration of element i is known (or can be approximated) in the mafic end-member (X^i_M) and the felsic end-member (X^i_F) (Fourcade & Allegre 1981):

$$X^i_H - X^i_F = X_m(X^i_M - X^i_F)$$

In a mixing test (Fig. 49) $X_H - X_F$ versus $X_M - X_F$ for i = Si, K, Mn, Ti, Mg, Ca, and Fe^{2+} are used to evaluate X_m in the hybrid MMEs, pillow-like MMEs and hybrid rocks of the complex, utilizing the least sum of squares method. The acronyms HQFP and MME^p denote the felsic and mafic end-member, respectively (see Appendices 2a and 2b). The average composition of the hornblende-quartz-feldspar porphyries (Appendix 2a), HQFP, is used for the felsic end-member because it is the most felsic rock type in the complex. The composition of MME^p is thought to represent the initial non-hybrid composition of the mafic magma that was injected into the magma chamber.

Elements selected for the mixing test were those displaying a relatively good linear correlation (Fig. 44) and high enough concentrations so that analytical errors play a minor role. Al_2O_3 and Na_2O are excluded from the mixing test because of their heterogeneous content in the rocks of the complex (see Figs. 44c and 44h) and also to avoid the problem of feldspar contamination. CaO and K_2O are, however, included on the basis of a linear trend against MgO as shown in Figures 44g and 44i, especially in the hybrid rocks.

The results of the mixing test (Fig. 49) show a large variation without any remarkable break in the X_m values. The hybrid MMEs show a variation of X_m from 0.51 to 0.94 (Fig. 49a). The higher proportion of felsic end-member in the pillow-like MMEs (Fig. 49b) compared to small MMEs is also reflected by their lower X_m values (0.39–0.72). The elements show a relatively good correlation between different i values, and usually the given X_m values for separate elements are less than 0.10 units when compared to each other, so that the highest observed X_m value for the hybrid rocks is 0.29 decreasing systematically to the value of 0.08 (Fig. 49c). It is worth mentioning that the X_m values for Mg and Fe^{2+} are similar (±0.01) to those after the mixing test (Fig. 49) with multiple elements. Other elements that show similar X_m values to the elements chosen above are Ba, Rb, Zn, Ni, and Th, but individual X_m values for the REE are not comparable, giving X_m values from -196 to 114 for the hybrid rocks and the ΔX_m for individual samples

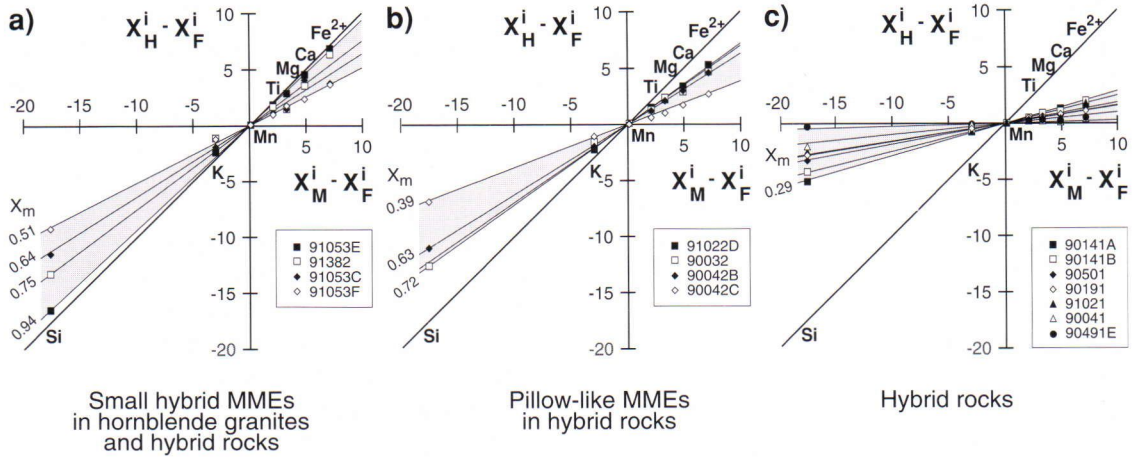

Fig. 49. Mixing test to evaluate the mass proportion of mafic magma (X_m) in (a) small hybrid MME in the hybrid rock and hornblende granite, (b) pillow-like MME in the hybrid rock, and (c) a hybrid rock with i = SiO_2, K_2O, MnO, TiO_2, MgO, CaO, and FeO. X^i_M, X^i_F, and X^i_H represent the content of element i in the MME, HQFP, and hybrid rock, respectively.

may be as much as 200 units. The lack of fit for these elements may be a result of being redistributed by residual granitic melts, exsolved volatiles, or that the MMEs were not closed systems with respect to these elements (see Bédard 1990). The large variation of individual X_m values are also apparent when using Al, Na, Cl, Y, Nb, and Ta which may give both negative and positive X_m values for the hybrid rocks probably caused by local heterogeneities of the rock or relatively high analytical detection limits especially when the concentration of the element is low. It is also probable that the content of some element in the end-members may have changed from their initial composition.

Rheological properties of contrasting magmas

The interaction of the coeval felsic (granitic) and mafic magmas is constrained mainly by their initial temperatures, relative volumes, compositions, water contents, and crystallinities all of which affect the rheological properties of the resulting melt (Fernandez & Barbarin 1991). In Figure 50, the role of mixing and mingling in forming hybrid rocks is expressed as a function of the crystallization state of the felsic magma. Whether mixing or mingling is the dominate process is controlled by the compositional and temperature contrasts of the interacting magmas. If both magmas have a low crystallinity together with high temperature the viscosity contrast is low and a homogeneous hybrid magma can be formed. As the crystallinity of the felsic magma increases, a proportion of mafic magma may still interact with the felsic magma, forming local hybrid magmas but mingling dominates the system. The injected mafic magma may then disintegrate to form mafic globules (MME) which are scattered in the felsic magma by convection. Disintegration of the mafic magma encourages the mixing of the mafic and the felsic magmas if the proportion of the mafic component is large. This is because the heat contrast of the two magmas is balanced as the diffusion of heat between the two magmas is now faster than the compositional exchange (Turner & Campbell 1986). When the composition and temperature contrast of the two magmas is large, the injected mafic magma fills the fractures (as in composite dykes) or form separate dykes in the felsic host. In this event mixing of the magmas occurs in low proportions or the mafic magma crystallizes rapidly forming chilled margins against the felsic magma/rock restraining further chemical or mechanical exchange.

In the Jaala-Iitti complex alkali feldspar, plagioclase, and quartz xenocrysts have mainly crystal-

lized from the felsic magma before the mafic magma was injected. It is therefore probable that mingling of megacrysts has occurred mainly at higher crustal levels where the granitic melt was originally formed but before magmas of the complex were intruded. The small amount of intermediate hybrid rocks in the Jaala-Iitti complex indicates that the amount of the mafic magma was relatively small compared to the amount of felsic magma or that there was not enough time for complete thermal equilibration of the magmas. This is also suggested by the relatively small amounts of mafic rocks compared to granites and that the MMEs are scattered throughout the complex but usually without extensive mixing with the granites of the complex.

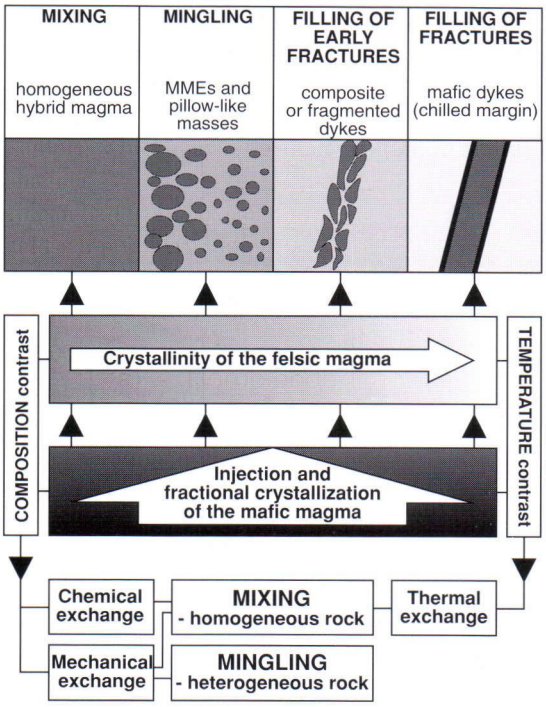

Fig. 50. Dependence of the different types of hybridization between mafic and felsic magmas on the crystallinity of the felsic magma. Crystallization of the felsic magma raises the compositional and temperature contrasts of the two magmas, and the role of mingling becomes more important. Modified after Fernandez and Barbarin (1991) and Barbarin and Didier (1992).

Magma mixing is favoured by the following factors (Vernon *et al.* 1988): (1) decrease in the viscosity of the injected magma, which increases both its velocity and turbulence, (2) decrease in the viscosity of the host magma, which decreases its resistance to deformation at the boundary of the turbulent fountain, and (3) increase in the diffusion rate. The viscosity contrast of coexisting magmas therefore plays an important role in defining if magmas can mix or mingle with each other.

Shaw (1972) and Bottinga and Weill (1972) created empirical equations for evaluating viscosities at different temperatures. It has been shown that these equations conform to laboratory measurements, at least for low pressures, low water contents, and temperatures above the liquidus of magmas (McBirney & Murase 1984). Model viscosities at different temperatures calculated according to the method of Shaw (1972) for the mean hornblende-quartz-feldspar porphyry (HQFP) and assumed initial mafic magma (MME^p) are shown in Figure 51a. The model viscosity change for HQFP at temperatures from 700° to 1000°C varies from 11 to 6.5 log poise whereas for the MME^p viscosity is less than 4 log poise at temperatures over 900°C, i.e., the crystallization temperature based on the amphibole–plagioclase geothermometer. The difference of hypothetical viscosities between the liquid HQFP and liquid MME^p varies from 4 to 5 log poise over a temperature range from 600° to 1200°C.

Increase of fluorine in melts (Fig. 51b) has been proposed as an important factor in lowering the viscosity in a similar way as an increase in H_2O will lower the viscosity of the magma (Dingwell *et al.* 1985, Dingwell & Webb 1992). As one weight percent increase of water lowers the viscosity (at a constant temperature) of silica-rich liquids by nearly an order of magnitude, by assuming a similar effect of F on the viscosity, the viscosities in Figure 51a may be slightly higher (about 0.5–1 poise) than the actual values at least for the hornblende-quartz-feldspar porphyry magma with 0.30–0.40 wt% H_2O and 0.14–0.16 wt% F. The effect of H_2O (and probably also F) on the viscosity of the liquids with lower silica contents is less pronounced because the polymerization of mafic melts is already low and

cannot be substantially reduced by the addition of water (McBirney & Murase 1984). The addition of F, however, cannot be disregarded in MMEs as they contain on the order of 2 to 8 times more fluorine than diabases in general, so that the increase of fluorine must have affected the viscosity as well as the solidus temperature of the mafic magma. The relatively high fluorine contents of the MMEs would have changed the rheological properties of the mafic magma only after it came in contact with the felsic magma; the initial low fluorine content will not change the viscosity values shown in Figure 51a dramatically.

Incorporation of feldspar and quartz xenocrysts from the felsic magma into the MMEs would have happened before the crystallization of amphibole and plagioclase in the MMEs. This is suggested by their corroded shape, crystallization of amphibole on quartz, simultaneous crystallization of amphibole and plagioclase mantling alkali feldspar megacrysts, and the occurrence of micrographic texture in the MMEs. The approximate crystallinity of the mafic magma before hybridization, but after thermal equilibrium had been reached, was less than 0.05 based on the amount of pyroxene and plagioclase phenocrysts so that the mafic magma was near its liquidus at the beginning of the hybridization event.

For the felsic magma the crystallinity is more difficult to approximate, but hybridization has obviously occurred after crystallization of some alkali feldspar, plagioclase, quartz, olivine, and amphibole phenocrysts. The maximum crystallinity, 0.40, for the felsic magma is based on the measured amount of phenocrysts in hornblende-quartz-feldspar porphyry. If fluorine is included in the evaluation, the solidus temperature is reduced compared to the fluorine-free systems (Manning 1981) and thus the crystallinity at a higher temperature is lower. The problems that arise in this example are that the crystallization of the felsic magma will increase the SiO_2 content of the liquid phase and that mingling predominates instead of mixing if the compositional difference between the host and injected magmas is more than 10 wt% SiO_2 (Frost & Mahood 1987; see also Fig. 50). Temperatures much over 900°C for a felsic magma with 40 vol% of crystals may need the felsic magma to be reheated by the mafic magma, assuming a large volume of mafic magma, before any interaction with the felsic magma can occur. A large volume of mafic magma is also needed to keep the mafic magma at its liquidus during the interaction.

As emphasized by Sparks and Marshall (1986) and Frost and Mahood (1987), the ability of two contrasting magmas to mix depends on their physical properties, especially viscosities, after they have come to thermal equilibrium. Turbulent flow contributes effectively to the mixing (Turner & Champbell 1986) and basaltic and dacitic magmas can easily be mixed by forced convection as shown by experimental work (Kouchi & Sunagawa 1983).

Complete mixing occurs only when the two magmas behave as liquids at the same temperature. The equilibrium temperature (Θ) of the mixture of magmas depends on the initial temperature, heat

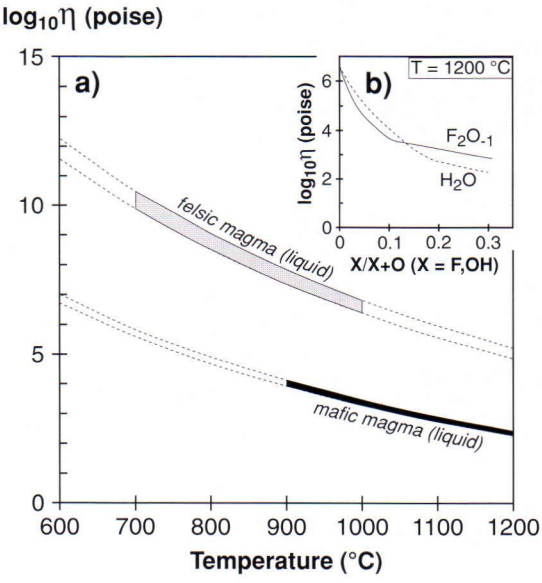

Fig. 51. a) Viscosities of the liquid felsic magma (hornblende-quartz-feldspar porphyry; 68.20–69.30 wt% SiO_2, 0.30–0.40 wt% H_2O) and the mafic magma (MME; 50.30–51.20 wt% SiO_2, 0.90–1.30 wt% H_2O) as a function of temperature calculated using equations of Shaw (1972). b) Comparison of the effect of H_2O and F on the viscosity of rhyolite at 1200°C after Dingwell and Webb (1992). See text for discussion.

capacity, heat of fusion, change of crystallinity, and mass fraction of each magma (Sparks & Marshall 1986). One important requirement for hybridization is that the mafic magma brings enough heat into the system and that there is sufficient time for chemical diffusion. If the proportion of the mafic magma is too low, the cooling effect of the felsic magma is sufficient to convert entrained portions of the mafic magma into solid enclaves (Sparks & Marshall 1986). The principles of Sparks and Marshall (1986) were adopted by Frost and Mahood (1987) and were used in the program MAGMIX (Frost & Lindsay 1988) for calculating viscosities at thermal equilibrium of interacting magmas at high crustal levels ($P \leq 2$ kbar). The mass-fraction of the mafic magma (X_m, i.e., the proportion of the mafic magma in thermal equilibrium with the felsic magma at Θ) is discernible in a viscosity versus X_m diagram at the point where the viscosity curves of felsic and mafic magmas intersect.

In Figures 52a and 52b, the temperatures were calculated using the program MAGMIX with respect to SiO_2 and water contents at 2 kbar giving an initial liquidus temperature for the MME^p to be 1190°C and a solidus temperature to be 760°C. Calculated liquidus and solidus temperatures for the HQFP are 1167°C and 676°C, respectively, and calculations for the interacting magmas were performed over a temperature range from 1100° to 700°C. The results shown in Figure 52 are not necessary accepted as being true values for the magmas of the Jaala-Iitti complex because the hybridization may have taken place deeper in the crust (Salonsaari & Haapala 1994). They do, however, give an approximate idea about the relative temperature and viscosity changes and, more importantly, to what extent magma mixing could have taken place at higher crustal levels, and whether it is possible to generate large amounts of hybrid magmas near the emplacement level (about 2 kbars) of the complex. Load pressure has been found to reduce the viscosity of magmas at a constant temperature above the liquidus (Kushiro 1980), as well as has an effect on the liquidus temperature (McBirney & Murase 1984). The increase of pressure may therefore facilitate the interaction of mafic and felsic magmas in the upper crust.

Hybridization by the interaction of an anhydrous

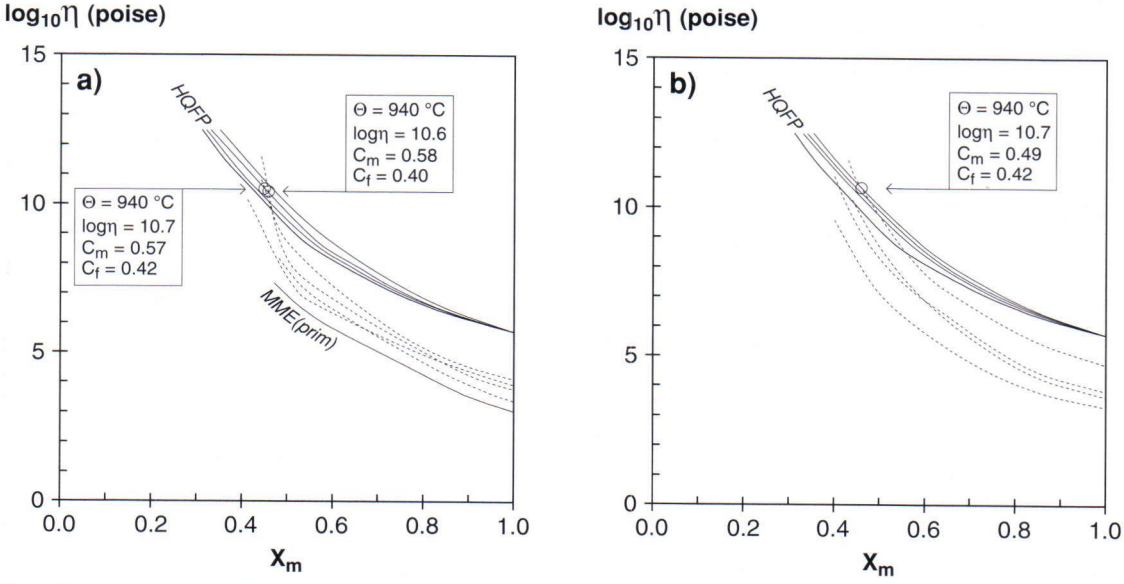

Fig. 52. Mass-fraction (X_m)–viscosity diagrams for (a) MMEs and the average hornblende-quartz-feldspar porphyry (HQFP; see appendix 2a) and (b) pillow-like MMEs and HQFP at P less than 2 kbar calculated for fluorine-free compositions from their initial liquidus temperature to the temperature where the crystallinity is 0.60. C_m and C_f are crystallinities of mafic and felsic magmas, respectively, at the equilibrium temperature (Θ) marked by a circle. See text for discussion.

mafic magma with ~50 wt% SiO_2 and an anhydrous felsic magma with ~70 wt% SiO_2 (MME^p and HQFP in Fig. 52a, respectively) seems unlikely at the emplacement level of the complex because of their high compositional contrast (Fig. 52a). MMEs (Fig. 52a) and pillow-like MMEs (Fig. 52b) with a hybrid composition (55–61 wt% SiO_2) and higher viscosity (Fig. 52b) may theoretically form hybrid magmas in some proportion with the assumed felsic end-member of the complex but as the difference of SiO_2 content is higher than 10 wt% and the given X_m is lower than 0.5, homogenization is unlikely at least in the schemata as postulated by Frost and Mahood (1987). The equilibrium temperature for the hybridization is 940°C at $\log\eta = 10.6$, but the crystallinity of the mafic magma, $C_m = 0.5–0.6$, suggests that little mixing would occur. The main mixing event probably took place before emplacement of the complex magmas, but Figure 52 implies that mixing of evolved Subjotnian mafic magmas and a relatively mafic rapakivi granite magma could have occurred to some (small) extent in the upper crust in a closed system.

In Figure 53 the MMEs and pillow-like MMEs and their hosts are plotted to estimate if a mafic magma has subsequently mixed with the host (hybrid) magma. Sample 91382 (dashed thick curve in Fig. 53a) representing a recrystallized MME in the hornblende granite shows that recrystallization must have happened at high crustal levels. Note that the curves define the viscosity only for magmas with a crystallinity less than 0.60 so that mixing and especially a late stage mixing between the hybrid mafic magma and the hybrid host magma most probably generates recrystallized MMEs with numerous hybrid features.

Other MMEs and the pillow-like MMEs indicate that mixing of the mafic magma and the host hybrid magma has occurred at the emplacement levels but only between the already hybridized MMEs and pillow-like MMEs whereas the most primitive MMEs of the complex have probably already been crystallized and have not taken part in the magma mixing. Hybridization in a conduit during the ascent of the magmas is also suggested by the relatively high Θ temperatures (between 950° and 1050°C)

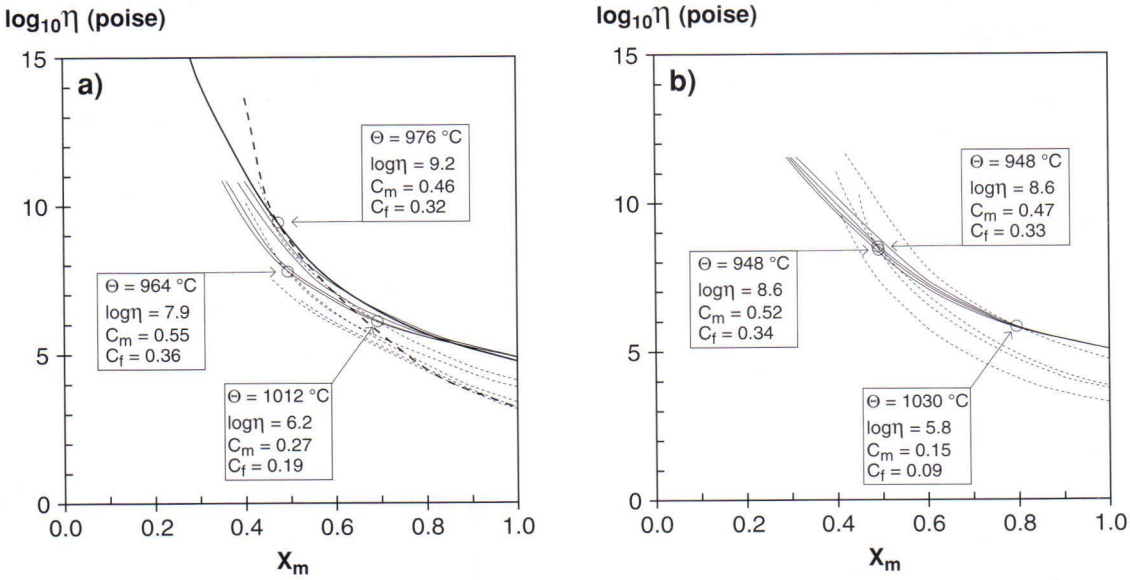

Fig. 53. Mass-fraction (X_m)–viscosity diagrams for: a) MMEs (dotted lines) and their host rock (solid lines); heavy lines represent a MME – hornblende granite pair (samples 91382 and 91381, respectively), host for the other samples is #90141A (see Appendix 2c) and b) pillow-like MMEs and their host (sample 90042) at P less than 2 kbar calculated for fluorine-free compositions from their initial liquidus temperature to the temperature where the crystallinity is 0.60. C_m and C_f are crystallinities of mafic and felsic magmas, respectively, at the equilibrium temperature (Θ) marked by a circle. See text for discussion.

and by the fact that the calculated viscosity of the hybrid host magmas lies between 6 and 10 $\log_{10}$ poises.

Some concluding remarks as to the rheological properties of the interacting magmas in the Jaala-Iitti complex in terms of the viscosity contrast between the interacting magmas and their temperatures can be made: 1) the proportion of the interacting mafic magma must have been relatively high with a low degree of crystallinity, 2) the felsic magma must have been reheated by the mafic magma before intensive mixing took place as is also shown by the petrographical studies; evidence of thermal disequilibrium being visible as mantled feldspars and corroded quartz, and 3) the high fluorine content in the mafic magma may have increased the time the magmas were able to interact by lowering the solidus temperature of the mafic magma, and 4) the hybrid mafic magma could have subsequently mixed with its felsic host at the level of emplacement whereas the most primitive globules of mafic magma most probably behaved as solids and did not interact with the host felsic or hybrid magma.

A model for hybridization

Direct methods for estimating the depth of hybridization are lacking in the rocks of the Jaala-Iitti complex. Several facts, however, suggest that hybridization took place at a deeper level before the magmas were finally emplaced at $\leq$ 2 kbar. The following observations and relations between the granites, MMEs, pillow-like MMEs, and hybrid rocks suggest that the hybridization occurred in the conduit.

1) Hybrid rocks are widespread in the complex even though they occur in minor quantities as compared to the granites of the complex. If hybridization occurred near the emplacement level or in the conduit that led the complex hybrid rock would be assumed to occur only at certain places related to the relative proportions of the interacting magmas.

2) MMEs without chilled margins occur throughout the complex. This implies that the hybridization took place in the conduit as large mafic dykes and masses are lacking. The pillow-like MMEs in the southwestern part of the complex are not necessarily directly related to the MMEs in the other parts of the complex. The pillow-like MMEs are the most hybrid MMEs of the complex so they are not a likely source for other MMEs found in the complex.

3) Non-hybridized MMEs with compositions similar to the Subjotnian diabase dykes of the region (Rämö 1990, 1991) are lacking in the Jaala-Iitti complex.

4) The relatively wide compositional range of the MMEs suggests that the mafic magma has interacted with the felsic magma in different proportions and under different conditions. If the hybridization had occurred at high crustal levels near the emplacement level a more homogeneous MME composition would be expected and MMEs with chilled margins would occur in greater amounts. The same source for the MMEs and pillow-like MMEs is also suggested by a similar bulk composition for the composite MME (sample 9004A) in a pillow-like MME and other non-hybridized MMEs (samples 91053A and 91053B).

5) As has been shown (Fig. 52), at temperatures of 940°C about 40–60 vol% of the mafic magma has already crystallized so that temperatures of approximately 1100°C are needed so that the crystallinity of the mafic magma is less than 0.10. This requires that the mafic magma stays near its liquidus temperature (1100°C) and heats the felsic magma so that extensive mixing may occur. If the proportion of the mafic magma to the felsic magma is too low, the cooling effect of the felsic magma is sufficient to convert entrained portions of the mafic magma into solid enclaves (Sparks & Marshall 1986). The petrographical observations also indicate that hybridization did not happen deep in the crust because the interacting felsic magma must have contained some crystals such as quartz and feldspar that now occur as xenocrysts especially in the pillow-like MMEs. A middle crust depth is therefore favoured.

A model of the generation of the bimodal rapakivi magmatism and hybridization, based in part (Figs. 54a and 54b) to Huppert and Sparks (1988),

Haapala (1989), and Rämö and Haapala (1991), is presented in Figure 54.

Interaction of mafic and rapakivi granite magmas may occur at several places (Fig. 54b). The most obvious place for hybridization is deep in the crust at a level where the rapakivi magmas were formed. Other favourable places for hybridization are magma chambers in the middle and upper crust where injections of a more evolved mafic magma may hybridize with the partially crystallized rapakivi granite magma (see Fig. 54b). Hybridization at the emplacement level of the rapakivi granite

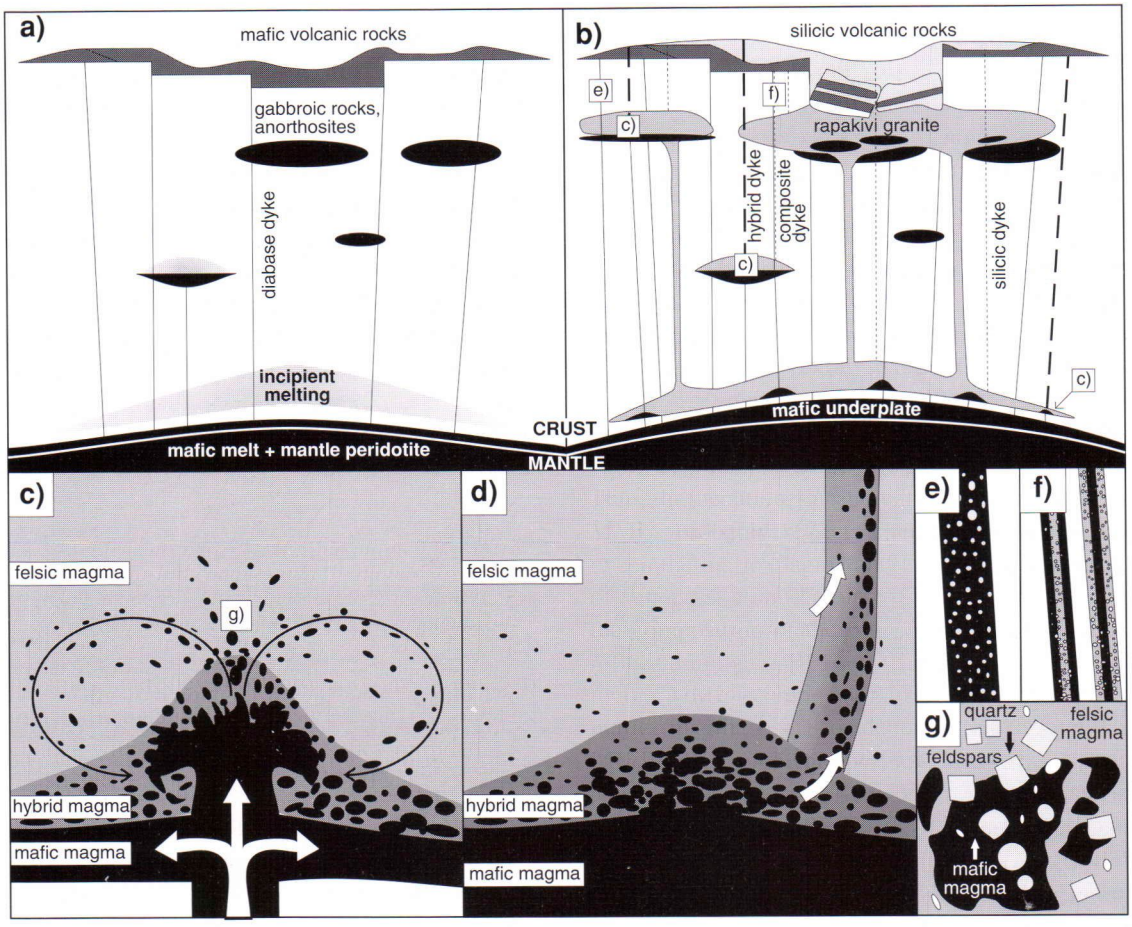

Fig. 54. Schematic model of the generation of rapakivi granites and hybridization with a coeval mafic magma. a) Upwelling mantle-derived mafic magma forms a mafic underplate below the crust and is injected into higher levels producing gabbroic and anorthositic rocks, diabase dykes, and mafic volcanics (Haapala 1989, Rämö & Haapala 1991). b) The mafic underplating causes partial melting of the lower crust (Rämö 1991) producing silicic magmas which are injected episodically upward within the crust forming rapakivi granite complexes (accompanied by cauldron subsidence), silicic (quartz-feldspar porphyry) dykes and volcanic rocks. c) Repeated injections of mafic magma in felsic magma chambers (see Fig. 54b for possible locations) causes convection in the felsic part of the magma chamber and spreads mafic magma into globules. d) As thermal equilibrium is reached chemical exchange produces a layered hybrid series of intermediate magmas which are injected upward through fracture zones. e) Injection of mafic magma through partially crystallized rapakivi granite magma causes formation of composite dykes with intermingled megacrysts that are also visible when the coeval rapakivi granite magma and diabase magma are injected into higher crustal levels forming composite dykes (f). g) A enlargement from Figure 54c, to show capturing of alkali feldspar megacrysts from the felsic magma into mafic magma, and subsequent rounding of the megacrysts. Figures a) and b) are modified after Huppert and Sparks (1988) and Rämö and Haapala (1991). See text for discussion.

plutons would require a major input of mafic magma.

Repeated injections of mafic magma into the magma chamber can produce zones of mingling and mixing and result in hybrid magmas with composite MMEs. Turbulent flow (Fig. 54c) contributes effectively to the mixing (Blake 1981, Campbell & Turner 1985, Turner & Champbell 1986, Zorpi *et al.* 1989) by spreading the mafic magma throughout the magma chamber and disrupting it.

Crystallization of mafic magma continues until the temperature and density of the residual magma is equal to that of the felsic magma (Huppert *et al.* 1982, Turner & Campbell 1986). At this time, the two liquids will be intimately mixed; complete mixing can occur only when the two magmas behave as liquids at the same temperature. This requires a substantial proportion of the mafic magma to bring enough heat into the system. In the case of a denser, hot magma injected into a cooler, less dense magma, the former will quench and crystallize due to rapid heat loss with contemporaneous superheating of felsic magma. The final injection of the hybrid magmas into the upper crust took place after the emplacement and crystallization of the main rapakivi magmas of the Wiborg batholith and opening of the required channelways. The injection of magmas from the stratified magma chambers (Fig. 54d) may result in further mixing of the magmas as they are assumed to be in thermal equilibrium at about 950°C.

Injections of a mafic magma into a felsic magma conduit (or vice versa) or into partially crystallized rapakivi granite magma in the upper part of the crust results in alkali feldspar diabase dykes (Rämö 1990, 1991) and composite dykes with structures as shown in Figures 54e and 54f. The interaction in these cases is limited but with the inclusion of quartz and feldspar megacrysts from the felsic magma to the mafic magma. In the Suomenniemi complex, the capture of megacrysts is related to movement in the mafic magma. It is possible that the pillow-like MMEs of the Jaala-Iitti complex represent that part of a combined mafic–felsic magma chamber where the injection rate of the mafic magma has been highest (see Figs. 54c and 54g). This is also suggested by the greater abundance of xenocrysts, larger size, and higher degree of hybridization of the pillow-like MMEs as compared to other MMEs of the complex. According to Grasset and Albaréde (1994) large melt globules become hybridized faster than smaller ones because their larger fall velocity makes stirring more vigorous. Also, large melt globules crystallize slower than small ones.

HYBRIDIZATION IN THE RAPAKIVI GRANITES OF SOUTHEASTERN FENNOSCANDIA

Major problems as regards the petrogenesis of the rapakivi granites are: 1) the source of the rapakivi granite magma, 2) the genetic relations between the rapakivi granites and the penecontemporaneous mafic rocks, 3) the geotectonic framework in which these rocks were emplaced, 4) the overall relation of the rapakivi granites to the evolution of the continental crust, and 5) the origin of the rapakivi texture (Rämö 1991). In the following pages, problems 2) and 5) are discussed in the light of the results from the Jaala-Iitti complex.

Rapakivi granites and associated diabase dykes, and gabbroic and anorthositic intrusions are cogenetic. As discussed in previous chapters, mafic and felsic magmas are found together in many localities and have, locally, been hybridized. Magma mixing and mingling has recently been proposed as playing an important role in generating large volumes of rapakivi granite magmas, especially wiborgites (Eklund 1993, Eklund *et al.* 1991, 1994). Such features as rapakivi magmatism caused by mafic mantle magmatism, contemporaneous or closely contemporaneous intrusion of mafic and felsic magmas sometimes generating hybrid dikes and complexes, and the multiple nature of most of the larger rapakivi batholiths favour a hybrid origin for rapakivi granites. Eklund *et al.* (1994) proposed that wiborgites are the result of magma mixing at deep crustal levels with a long homogenization time, and therefore they do not have any signs of the mixing event; pyterlites represent a possible fractionated result of the hybrid wiborgite. Such ideas have an

old currency: von Wolff (1932) proposed that tirilites represent chemically a mixture of 62 % andesite and 38 % pyterlite.

The role of MMEs in the petrogenesis of the rapakivi granites

The MMEs found in rapakivi granites from the Wiborg batholith area (Fig. 1b) have been described as "Subjotnian inclusions" by Hackman (1934), Vorma (1975), and Simonen (1987), and they include diabases, gabbros, norites, and anorthosites (Simonen 1987). In the Simola district, south of Lappeenranta (see Fig. 1b), enclaves of gabbroic composition occur over large areas (Hackman 1934). Their host rocks are mainly even-grained and pyterlitic rapakivi granites (see Simonen 1979a), but occasionally also wiborgite. In other parts of the Wiborg rapakivi batholith the host rocks of MMEs are mainly wiborgites and dark wiborgites (see Simonen 1979b), and the MMEs show petrographical similarities to MMEs from the Jaala-Iitti complex. Micro-enclaves and recrystallized MMEs are found also within the Wiborg batholith (Salonsaari 1993). Anorthosites related to an earlier mafic magmatism are also found as larger fragments in southeastern Finland. The age of the large anorthositic bodies (Mäntyharju and Ylämaa) within the Wiborg batholith varies from 1645 to 1633 Ma (Vaasjoki *et al.* 1991, Suominen 1991). The Wiborg batholith is dated at 1650 and 1625 Ma (Vaasjoki *et al.* 1991).

MMEs can be found in several rapakivi granite types, but only locally can the host rapakivi granite be identified as a hybrid rock generated by mixing and mingling of mafic and felsic magmas, as it is in parts of the Jaala-Iitti complex.

Rapakivi texture – a mixing texture?

Rapakivi texture (*sensu stricto*), as described by Vorma (1976, p. 5) is characterized by: 1) the ovoidal shape of alkali feldspar megacrysts, 2) mantling of ovoids by oligoclase-andesine shells, some ovoids, however, remaining unmantled, and 3) the ubiquitous occurrence of two generations of alkali feldspar and quartz, and in the latter, the idiomorphic older generation having crystallized as high quartz.

Magma mixing has been proposed as one possible mechanism controlling the generation of various types of mantled feldspars and also rapakivi texture (Elders 1967, Hibbard 1981, Barbarin 1988, Bussy 1990, Stimac & Wark 1992, Haapala & Rämö 1992, Salonsaari & Haapala 1994; see also Barbarin & Didier 1992, Hibbard 1991, Vernon 1990, 1991). Rapakivi texture is also found in MMEs as oligoclase-mantled alkali feldspar mega(xeno)crysts (Phillips 1880, Thomas & Smith 1932, Pesquera & Pons 1989, Castro *et al.* 1990a, Bussy 1991), and from diabases and hybrids associated with rapakivi granites (Volborth 1963, 1973, Rämö 1991, Salonsaari & Haapala 1994). Experimental work that simulates mantling of alkali feldspar by plagioclase has been published by Wark and Stimac (1992). The micrographic texture and alkali feldspar mantled by plagioclase found in the Jaala-Iitti complex show that magma mixing can generate mantled feldspar ovoids under suitable conditions.

Hibbard (1981) suggested that rapakivi texture forms as a result of magma mixing; here magma mixing leads to quenching of a hotter, mafic magma and superheating of a cooler, more felsic magma. Also needed is an effective cooling mechanism related to the sudden loss of volatile components. This rapid cooling and also the loss of volatiles is facilitated in two ways: 1) heat is transferred to the wallrock or 2) magma ascent to higher levels. The physical changes (rapid decrease of pressure and slow cooling) in the granitic magma during ascension is also proposed to be a principal factor in generating rapakivi textures (Nekvasil 1991).

The relatively heterogeneous rapakivi plutons can be generated as shown in Figure 54, where rapakivi granite magma with alkali feldspar megacrysts is injected by varying amounts of mafic magma. Decompression of the ascending mixed magma leaves it unequilibrated with the alkali feldspar megacrysts, yet saturated with components from the mafic magma (e.g., Na, Ca, Mg, Fe) until it reaches the crystallization field of plagioclase

which crystallizes around the alkali feldspar megacrysts (within the new hybrid magma).

Rounded shape of alkali feldspar megacrysts and mantling of some of the ovoids by oligoclase-andesine shells are present locally in the hybrid rocks and in the mafic rocks where alkali feldspar megacrysts have been entrained in the mafic magma. Such mantled feldspar ovoids as well as amphibole-mantled quartz xenocrysts are indicative of a local disequilibrium. Hybrid complexes also occasionally contain two generations of quartz (and alkali feldspar) but their idiomorphic shape is questionable.

If hybridization between rapakivi granite magma and a mafic (diabase) magma took place after quartz phenocrysts were crystallized, amphibole will crystallize almost immediately around the quartz xenocrysts to form ocellar texture as is shown in most hybrid complexes (see references above). Adding a mafic component to the system may leave plagioclase as the main liquidus phase in the magma, but amphibole will also crystallize simultaneously with plagioclase and mantles around alkali feldspars will be composed of plagioclase with amphibole inclusions, as in the Jaala-Iitti complex (see Fig. 15). Simultaneous crystallization of plagioclase and amphibole is also seen in some MMEs of the Jaala-Iitti complex (Fig. 24).

In the Wiborg batholith which covers an area of over 18 000 km^2, about 80 % is composed of wiborgite (Vorma 1976), in which ocellar quartz is rare. Mantled feldspar ovoids are also more common in rapakivi granites than in hybrid rocks in which the origin of the texture is obviously related to magma mixing and mingling. If magma mixing was the cause for the mantled ovoids wiborgites would have to represent highly hybridized rocks, and they should therefore contain more evidence of magma mixing. Therefore *rapakivi texture*, in general, is not a hybrid texture and the majority of rapakivi granites do not represent hybrid rocks. Locally, however, hybridization is present, and it can produce *alkali feldspar ovoids with plagioclase*, quartz (micrographic texture) and/or amphibole. The high Fe/Fe+Mg (Simonen & Vorma 1969, Rämö & Haapala 1995) of the mafic minerals of the rapakivi granites relative to those in the hybrid rocks of the Jaala-Iitti complex (see Figs. 25, 27, and 29) is compatible with a non-hybrid origin or highly limited mixing origin of the rapakivi granites.

In spite of the fact that most rapakivi granites do not seem have formed by mechanical or chemical exchange between mafic and felsic magmas, interaction of these contrasting magmas may have had some effect in rapakivi texture. Rapakivi granites do not show any visible large-scale signs of mechanical or chemical magma mixing such as large amounts of mafic rock within the rapakivi granites, or large amounts of xenoliths that could be the source of alkali feldspar megacrysts in the partially crystallized rapakivi granite magma.

In the Jaala-Iitti complex, the occurrence of micrographic texture in alkali feldspar megacrysts is related to thermal disequilibrium between the mega(xeno)crysts and the host melt. Micrographic texture is more common in the matrix of wiborgites, especially dark wiborgite, than in the rapakivi varieties without rapakivi texture (Vorma 1971). A correlation between the occurrence of micrographic texture in the rock matrix and rapakivi texture is noticeable. In some cases plagioclase mantles surround (granitoid)xenoliths (e.g., Vorma 1971, p. 26), and in this case it is likely that mantling has been formed at high crustal levels. Vorma (1971, p. 25) describes concave quartz that occurs only as inclusions in alkali feldspar ovoids and on the interface between the megacryst and plagioclase mantle. That feature is similar to the graphic texture that results from partial melting of alkali feldspar xenocryst in the hybrid rocks of the Jaala-Iitti complex.

Haapala (1977a) suggested that the occurrence of micrographic texture in rapakivi granites of the Eurajoki stock may have been produced by subhorizontal diabase dikes located just over or below the present erosion level. A three km thick high velocity layer (Fig. 55a) has been located under the Wiborg batholith at a depth of 10 to 13 km by deep seismic soundings (e.g., Luosto *et al.* 1990) (Fig. 55b). This layer, interpreted as being a Subjotnian mafic (gabbro–anorthosite) body (Korja 1995) could represent

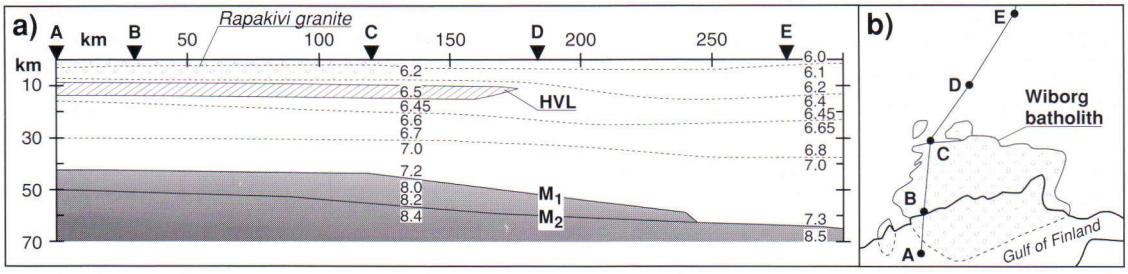

Fig. 55. a) Cross section of the crust in the Wiborg batholith area (b). HVL is a high velocity layer under the rapakivi granite, M_1 and M_2 represent the Moho discontinuities, and dotted lines represent P-wave velocity boundaries (km/s) within the crust. Modified after Luosto et al. (1990) and Haapala and Rämö (1992).

a heat source underlying the partially crystallized rapakivi granite and causing partial melting of alkali feldspar phenocrysts. Bussy (1990) suggests a similar mechanism on a smaller scale for alkali feldspar xenocrysts occurring in a MME magma; disequilibrium between alkali feldspar megacrysts and the host mafic melt (MME) causes dissolution of alkali feldspar megacrysts and formation of a plagioclase rim by recrystallization. Recrystallization in partially solidified rapakivi granite magmas after heating may have produced some textures occasionally visible such as rhythmic zoning of quartz and plagioclase inclusions within alkali feldspar megacrysts, concave quartz orientated towards the micrographic rims, and, more significantly, the rapakivi texture. This postulate assumes rapakivi texture to be an indicator of thermal disequilibrium between alkali feldspar megacrysts and the host melt. This results in dissolution of crystals and the formation of mantling textures in the hybrid rocks of the Jaala-Iitti complex.

One critical point of this hypothesis is whether all rapakivi granite stocks and batholiths have a high velocity layer (mafic body) underlying the granite or not and, if so, does it explain why some rocks of batholiths contain rapakivi texture and some do not. More commonly stocks do not contain rapakivi texture, but some exceptions exist as the Rödö rapakivi granite of central Sweden (Andersson 1992). The relatively small (2.5 km^2) Rödö rapakivi granite complex consists of a porphyritic rapakivi granite where about 50 % of alkali feldspars have a plagioclase mantle. Moreover, there are associated mafic dykes and possibly an associated mafic intrusion below the Rödö granite as suggested by Andersson (1992). This also supports the theory outlined above also favoured by Emslie and Stirling (1993) for the origin of the rapakivi texture in the Nain complex of Labrador.

One example of possible small-scale (thermal) interaction of mafic magma and rapakivi granite magma to form rapakivi texture is shown in Figure 56. Alkali feldspar phenocrysts in a porphyritic rapakivi granite of the Simola district that occurs in contact with a MME has plagioclase rim only in the vicinity of the MME.

DISCUSSION

Rapakivi granite and associated mafic (tholeiitic) magmatism in southeastern Finland are visible as large rapakivi batholiths, diabase dykes and dyke swarms, and minor gabbroic and anorthositic bodies. The dyke swarms together with minor quartz-feldspar porphyry dykes, reflect the extensional tectonic regime of the magmatism. Three episodes of diabase dyke emplacement, at 1665, 1645, and 1635 Ma, have been recognized in the area (Vaasjoki *et al.* 1991). They typically trend in a WNW direction but most of the dykes related to the younger rapakivi granites of southwestern Finland (Åland rapakivi granite area; see Fig. 1a) trend to the NNE direction. Locally diabase magmas form composite dykes with quartz-feldspar porphyries (e.g., Rämö 1991, Eklund 1993). This occurs at high crustal levels where magma mingling predominates. More pronounced hybridization is visible in

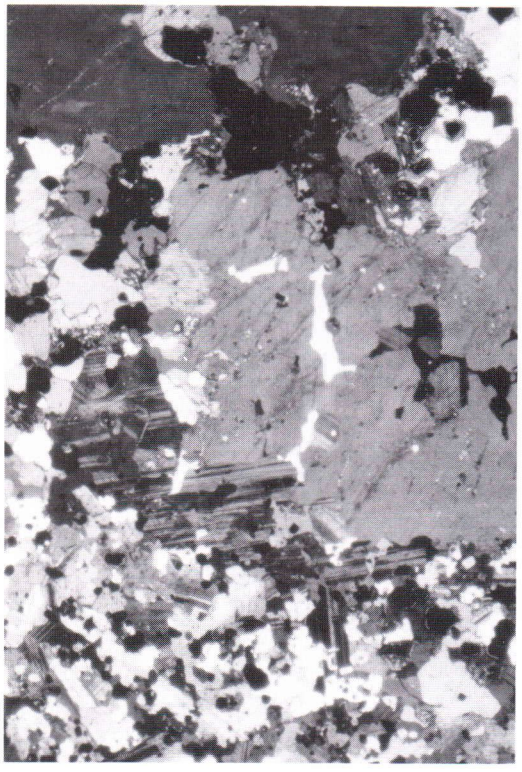

Fig. 56. Photomicrograph of the rapakivi texture at a contact with a MME (bottom). Porphyritic rapakivi granite from Simola. Alkali feldspar is strongly corroded and both alkali feldspar and plagioclase mantle show a similar optical orientation. Width of the picture corresponds to 6.1 mm.

the dyke-like Jaala-Iitti complex where the interaction of (rapakivi) granite and diabase magmas has occurred at moderate crustal levels generating a small amount of intermediate hybrid magma. The products of the interaction were injected through the Svecofennian metamorphic and igneous rocks and rapakivi granites of the Wiborg batholith.

The mafic end-member in the bimodal plutonic associations when mixed with felsic magmas usually occurs as globules that form MMEs. In the Jaala-Iitti complex, both MMEs and large pillow-like MMEs have various amounts of feldspar and quartz (commonly rimmed by amphibole) xenocrysts. The alkali feldspar and quartz, and probably also many of the plagioclase megacrysts nucleated and grew in the felsic magma and were incorporated into the hybrid rock either by mixing of the two melts or by mechanical entrainment from the felsic magma into the mafic magma. Similar features have also been described from some of the composite diabase–quartz-feldspar porphyry dykes in the Suomenniemi complex (Rämö 1990, 1991) and the Åland rapakivi granite area (cf. Eklund 1993). Some megacrysts in the rocks of the Jaala-Iitti complex are clearly xenocrysts derived from partially melted Svecofennian granitoid or rapakivi granite xenoliths (Fig. 20).

Convection caused by injection of the mafic magma (Bacon & Metz 1984) contributes to the mixing event (Kouchi & Sunagawa 1983) by spreading the mafic magma globules throughout the felsic magma and reducing the thermal contrast between the magmas. The injection of the mafic magma into a felsic magma chamber results in a rapid superheating of the felsic magma (Sparks *et al.* 1977), which then becomes physically mixed after thermal equilibrium is reached. Convection in a magma chamber may be driven by heating the magma from below as well as by cooling from above (Koyaguchi *et al.* 1993). This may lead to two convection systems in a stratified magma chamber. These features contribute to the mixing event by balancing the heat difference between felsic and mafic magmas. Multiple injection of a mafic magma is best seen in pillow-like MMEs with composite MMEs. The composition of the composite MMEs is similar to the non-hybridized MMEs indicating a similar source for all MMEs.

Several factors, both physical and chemical, have an effect on the chemical diffusion (mixing) between felsic and the injected mafic magma. These are:

1) The time interval between the emplacement of mafic magma and crystallization of the host magma. Thermal equilibrium is reached relatively fast and certainly before intensive chemical diffusion can occur.

2) Compositional difference between the mafic and felsic magmas. Homogenization is likely only if the compositional difference between host and injected magma is less than 10 wt% SiO_2 or if the mass fraction of the mafic magma is greater than 0.5 (Frost & Mahood 1987).

3) The proportion of the mafic magma to the felsic magma. Hybridization is effective if the proportion of mafic magma is high (Frost & Mahood 1987).

4) The size of MMEs; only small enclaves show complete recrystallization and composition of hornblende and plagioclase similar to those in the host rock. According to Castro *et al.* (1991a), the size of the MMEs is controlled by the viscosity contrast between the two magmas. The size of the enclaves also depends much on the proportion of mafic magma injected into the felsic magma. The pillow-like MMEs do not have chilled margins which suggests relatively slow crystallization and an ambient temperature close to that of the mafic magma itself. The occurrence of quartz and alkali feldspar in the matrix is to be expected if magma mixing has influenced the composition of the mafic magma. The occurrence of quartz and feldspar xenocrysts in the MMEs seems to be controlled by the size of the MME; larger enclaves usually have more xenocrysts than the small ones. This could be caused by the greater heat capacity of the large globules of mafic magma; they have spent more time in the felsic or hybrid magma. Complete mixing of mafic and felsic magmas is relatively rare because the mafic magma reaches its solidus at a higher temperature than the felsic magma.

A single factor alone cannot produce equilibrium, several, maybe all, of those listed above are needed to attain the required conditions.

An increase of temperature favours mixing by decreasing the viscosities and the viscosity difference between the magmas, increasing the velocity and turbulence, and increasing the diffusion rate (Vernon *et al.* 1988). Superheating of the felsic (hybrid) magma results in granophyric texture that indicates the beginning of melting in the alkali feldspar. Also ocellar texture indicates thermal disequilibrium between the megacrysts and the host magma. The micrographic texture commonly visible in hybrid rocks of the Jaala-Iitti complex may have been formed at a stage during a balanced thermal regime that followed one producing corroded alkali feldspar megacrysts rimmed by plagioclase and quartz in hybrid rocks, pillow-like MMEs, and MMEs.

Theoretically, complete hybridization between two different magmas is expected to leave no sign of either end-member. In such cases, the occurrence of hybridization may be difficult to prove. One key for the identification of hybridization between mafic and felsic magmas is to compare the composition of the minerals crystallized after the magma mixing event, in this case, amphibole and biotite. Distribution of Mg and Fe in these phases may form a continuum with those in the end-members. That such spread is not recognized in Fe–Mg silicates of the typical Finnish rapakivi granites (Simonen & Vorma 1969, Emslie 1991, Rämö & Haapala 1995) suggests that these rocks are not of hybrid origin. Instead, rapakivi texture of the common rapakivi granites may be formed by superheating the rapakivi granite magma without chemical exchange between the felsic and mafic magmas. Relative calcic-rich granite magmas are needed for crystallizing plagioclase to the extent that is present in wiborgites as compared to rapakivi granite varieties without mantled ovoids. That superheating of the rapakivi granite magma generates the rapakivi texture without magma mixing is also suggested by the relatively low abundance of MMEs in wiborgites. The high velocity layer beneath the Wiborg batholith (Elo & Korja 1993, Korja 1995) may have contributed a heat source for the superheating.

The composition of amphibole and plagioclase in the hybrid MMEs is similar those in their host rock, indicative of local equilibrium at least between the smaller globules of mafic magma and the felsic magma. Several studies indicate that the mineral compositions of apatite, biotite, hornblende, and plagioclase tend to equilibrate with their host rock (e.g., Barbarin 1986, Dorais *et al.* 1990, Debon 1991, Allen 1991). Relatively large variations of mineral composition and whole rock composition in hybrid rocks and pillow-like MMEs, occurrence of micro-enclaves in hybrid rocks, and the rheological modelling indicate, however, that hybridization in the Jaala-Iitti complex did not reach equilibrium before the magmas solidified. Hybridization, including mixing and mingling, was an ongoing pro-

gressive episode the intensity of which decreased with time.

Bateman *et al.* (1963) suggest that one of the possible explanations for the occurrence of mafic inclusions in the central part of the Sierra Nevada Batholith is that they represent "refractory material that was not melted when the magma was formed". Chappell and White (1991, p. 376) define restite as "any solid material in a plutonic or volcanic rock that is residual from partial melting of the source"; most of the restites in granites are carried up from the source as single crystals or small aggregates, and not as large fragments or enclaves. Thus, mafic clots composed of anhedral hornblende and biotite with magnetite, apatite, and sphene according to this hypothesis represent residual, largely crystallized material that was carried in and equilibrated with the magma from its place of origin (e.g., Presnall & Bateman 1973, Bateman & Chappell 1979). Zoned plagioclase xenocrysts in MMEs and granitoid rocks have been shown to be formed by magma mixing (Barbarin 1990). The restite hypothesis does not explain the occurrence of those micro-enclaves similar to amphibole aggregates common in rapakivi granites. Even though the amount of restite in A-type granites is assumed to be low (Collins *et al.* 1982), one possible restite component in the rapakivi granites might be the amphibole aggregates with noticeable amounts of prismatic apatite and both magnetite and ilmenite inclusions. Compared to the micro-enclaves, these aggregates are irregular in shape. Some zoned apatite crystals found in rapakivi granites may also represent original restite minerals.

The habit of apatite is different in MMEs and their host rock: in MMEs, apatite commonly occurs as needles but in the granites of the complex apatite is stubby and prismatic. In the hybrid rocks needle-like apatite is not necessarily a product of rapid quenching of the host magma, but may be a product of mingling of apatites from mafic magma undergoing disaggregation.

Studies of the crystallization conditions of the rapakivi granites dealing with the mineral assemblage amphibole–biotite–fayalite indicate crystallization temperatures of 640–800°C at an oxygen fugacity parallel to and slightly below the QFM buffer (Anderson & Cullers 1978, Emslie & Stirling 1993). These values correspond to those calculated for the hornblende granite and hornblende-quartz-feldspar porphyry of the Jaala-Iitti complex. For the hybrid rocks of the complex, crystallization temperature is calculated to be higher based on observations of the mineral chemistry of apatite, amphibole, feldspars, Fe–Ti oxides, and pyroxenes. The composition of the hybrid magma and geothermometric calculations, indicate an equilibrium temperature of about 950°C. A high temperature of equilibration in comparison to the crystallization temperature of the rapakivi granites is also suggested by plagioclase cores with compositions of An_{52} found within plagioclase mantling alkali feldspar in the hybrid rock. The main phase of crystallization probably occurred under 850°C with oxygen fugacity 1–2 log units below the QFM buffer.

The level of emplacement of the Jaala-Iitti complex cannot be determined directly but contact relations with the rapakivi granites and topaz-bearing granites of the Wiborg batholith indicate that the magmas of the complex were intruded at high crustal levels, most likely at a pressure less than 2 kbar. Amphibole geobarometers after Hammarstrom and Zen (1986), Hollister *et al.* (1987), Johnson and Rutherford (1989), and Schmidt (1990) give a relatively wide pressure range from 1 to 5 kbar. An error limit of 0.6–3 kbar, depending on the calibration, should be taken into account when calculating the pressures. The thermal heterogeneity and the sporadic cooling or reheating during the evolution of the magmas may also have effected the composition of the amphibole and thus, the calculated pressures.

Volcanic rocks related to rapakivi granite magmatism in southeastern Fennoscandia have been recognized, with both mafic and felsic members on the island of Suursaari in the Gulf of Finland (Wahl 1925, 1947). This and the roof pendants and breccias in the northeastern part of the Wiborg batholith (Vorma 1975) indicate a relatively high emplacement level of the rapakivi granite magmas. It is also possible that the magmas of the Jaala-Iitti complex extruded to the surface forming a volcanic complex as proposed by Vorma (1971).

CONCLUSIONS

Petrographical, mineral chemical, geochemical characteristics, and the petrogenetical implications for the rocks of the Jaala-Iitti complex lead to the following conclusions:

1) The felsic end-member of the complex consists of hornblende granites and minor hornblende-quartz-feldspar porphyries. The mafic end-member is represented by non-hybridized MMEs which compositionally are analogous to some of the evolved Subjotnian diabases in southeastern Fennoscandia; the majority of the MMEs and large pillow-like MMEs have interacted with their felsic host. The magma mixing and mingling of mafic and felsic magmas forming hybrid magmas has taken place at moderate crustal levels probably in a stratified magma chamber before final emplacement as a subvolcanic dyke-like complex.

2) Geochemical modelling indicates that the hybrid rocks and hybrid MMEs including pillow-like MMEs are formed by a mass-fraction of the mafic magma from 0.1 to 0.3 and from 0.4 to 0.9, respectively, at an equilibrium temperature of about 950°C.

3) Mixing of magmas was assisted by the low crystallinity of the mafic magma, an intermediate crustal depth of hybridization, convection regime, superheating of the felsic magma, and an increase of fluorine in the mafic magma by diffusion that reduced both the viscosity and the solidus temperature of the mafic magma. Magma mixing continued during the emplacement of the magmas.

4) The hybrid rocks, hybrid MMEs, and pillow-like MMEs are characterized by: a) quartz mantled by amphibole±augite (ocellar texture), b) alkali feldspar megacrysts mantled by a micrographic plagioclase–quartz intergrowths, and c) alkali feldspar megacrysts mantled by a plagioclase with occasional amphibole inclusions. A characteristic of the hybrid rocks is also that they contain more needle-like apatite than the granites of the complex.

5) Alkali feldspar and quartz megacrysts in the hybrid rocks are derived from the felsic end-member of the complex and from disaggregated rapakivi granite and Svecofennian granitoid xenoliths. The MMEs and pillow-like MMEs contain feldspar and quartz xenocrysts that were captured from the partially crystallized rapakivi granite magma.

6) Geochemistry and mineral chemistry of the MMEs shows that local equilibrium between the mafic and felsic end-members was reached. Recrystallization is apparent in the recrystallized borders of the MMEs and as micro-enclaves which represent recrystallized small droplets of mafic magma.

7) The crystallization of the granites of the complex has occurred between 850–650°C at a pressure less than 2 kbar. After thermal equilibration of the mafic and felsic magmas at about 950°C, the crystallization of the hybrid magmas took place in a temperature range from 900° to 750°C parallel or slightly below the QFM buffer.

8) The hybrid rocks, MMEs, and pillow-like MMEs contain feldspar megacrysts with micrographic rims or plagioclase rims; the latter suggest crystallization temperatures of 750–850°C at a pressure of less than 2 kbar.

9) The mineral chemistry of amphiboles and biotites as well as field observations suggest that the classic wiborgite rapakivi granite of southeastern Fennoscandia was not formed by chemical interaction between felsic and mafic magmas.

10) Petrographical similarity of rapakivi texture and mantled textures in the hybrid rock types of the Jaala-Iitti complex suggests that the rapakivi texture may form if alkali feldspar megacrysts become thermally unstable in a reheated rapakivi granite magma. In the case of the Wiborg batholith this may have been caused by a mafic body (high-velocity layer) beneath the batholith.

ACKNOWLEDGEMENTS: *Continuous support and encouragement was received from Professor Ilmari Haapala, supervisor of this work, who critically reviewed the manuscript. Dr Tapani Rämö and Dr Walter Boyd shared their experience in various problems considering on rapakivi granites and mafic rocks not only as the official reviewers but throughout the work.*

Professor Jouko Talvitie from the Geological Survey of Finland is gratefully acknowledged for permission to use the micro-probe at the Ore Min-

eralogical Laboratory of the Geological Survey of Finland where Bo Johanson and Lassi Pakkanen worked overtime to guide me to operate the micro-probe. Jyrki Juhanaho operated the SEM equipment at the Department of Electron Optics, University of Helsinki and Jussi Liipo the micro-probe at the University of Oulu.

Dr Juha Pekka Lunkka, Editor of the Bulletin of the Geological Society of Finland, is gratefully acknowledged for approving publication of this paper as Bulletin of the Geological Society of Finland.

I finally acknowledge financial support from the University of Helsinki, the Academy of Finland, and the Wilhelm Ramsay and Th.G. Sahama's Foundation.

REFERENCES

Allen, C.M., 1991. Local equilibrium of mafic enclaves and granitoids of the Turtle pluton, southeast California: mineral, chemical and isotopic evidence. American Mineralogist 76, 574–588.

Andersen, D.J., Lindsley, D.H. & Davidson, P.M., 1993. QUILF: a Pascal program to assess equilibria among Fe–Mg–Mn–Ti oxides, pyroxenes, olivine, and quartz. Computers & Geosciences 19, 1333–1350.

Anderson, J.L., 1980. Mineral equilibria and crystallization conditions in the late Precambrian Wolf River rapakivi massif, Wisconsin. American Journal of Science 280, 289–332.

Anderson, J.L. & Cullers, R.L., 1978. Geochemistry and evolution of the Wolf River Batholith, a Late Precambrian rapakivi massif in North Wisconsin, U.S.A. Precambrian Research 7, 287–324.

Andersson, U.B., 1992. The Rödö rapakivi granite complex, central Sweden. 29th International Geological Congress, Abstracts, Volume 2 of 3, 564.

Andersson, U.B. & Eklund, O., 1991. Compositions and textures of feldspars in mingled quartz-feldspar porphyry and doleritic magmas of the Hammarudda complex, Åland rapakivi batholith, SW Finland. In: I. Haapala & O.T. Rämö (Editors), Symposium on Rapakivi Granites and Related Rocks, Abstract Volume. Geological Survey of Finland, Guide 34, 5.

Angus, N.S., 1962. Ocellar hybrids from the Tyrone igneous series, Ireland. Geological Magazine 99, 9–26.

Angus, N.S., 1971. Comments on the origin of ocellar quartz-gabbros. Lithos 4, 381–388.

Bacon, C.R., 1986. Magmatic inclusions in silicic and intermediate volcanic rocks. Journal of Geophysical Research 91, 6091–6112.

Bacon, C.R. & Metz, J., 1984. Magmatic inclusions in rhyolites, contaminated basalts, and compositional zonation beneath the Coso volcanic field, California. Contributions to Mineralogy and Petrology 85, 346–365.

Bailey, J.C., 1984. Geochemistry and origin of hornblende-bearing xenoliths in the I-type Petford Granite, north-east Queensland. Australian Journal of Earth Sciences 31, 7–23.

Barbarin, B., 1986. Comparison of mineralogy of mafic magmatic enclaves and host granitoids, Central Sierra Nevada, California. Geological Society of America, Abstracts with Programs 18(2), 83.

Barbarin, B., 1988. Field evidence for successive mixing and mingling between the Piolard Diorite and the Saint-Julien-la-Vêtre Monzogranite (Nord–Forez, Massif Central, France). Canadian Journal of Earth Science 25, 49–59.

Barbarin, B., 1990. Plagioclase xenocrysts and mafic magmatic enclaves in some granitoids of the Sierra Nevada Batholith, California. Journal of Geophysical Research 95, 17747–17756.

Barbarin, B., 1991. Enclaves of the Mesozoic calc-alkaline granitoids of the Sierra Nevada Batholith, California. In: J. Didier & B. Barbarin (Editors), Enclaves and granite petrology. Elsevier, Amsterdam, 135–153.

Barbarin, B. & Didier, J., 1992. Genesis and evolution of mafic microgranular enclaves through various types of interaction between coexisting felsic and mafic magmas. Transactions of the Royal Society of Edinburgh: Earth Sciences 83, 145–153.

Bateman, P.C. & Chappell, B.W., 1979. Crystallization, fractionation, and solidification of the Tuolumne Intrusive Series, Yosemite National Park, California. Geological Society of America, Bulletin 90, 465–482.

Bateman, P.C., Clark, L.D., Huber, N.K., Moore, J.G. & Rinehart, C.D., 1963. The Sierra Nevada batholith–a synthesis of recent work across the central part. U.S. Geological Survey Professional Paper 414-D, 19 p.

Bateman, R., Martín, M.P. & Castro, A., 1992. Mixing of cordierite granitoid and pyroxene gabbro, and fractionation, in the Santa Olalla tonalite (Andalucia). Lithos 28, 111–131.

Bédard, J., 1990. Enclaves from the A-type granite of the Mégantic complex, White Mountain magma series: clues to granite magmagenesis. Journal of Geophysical Research 95, 17797–17819.

Bender, J.F., Hanson, G.N. & Bence, A.E., 1982. The Cortlandt complex: evidence for large-scale liquid immiscibility involving granodiorite and diorite magmas. Earth and Planetary Science Letters 58, 330–344.

Bergman, L., 1979. Geological map of Finland, 1:100 000, pre-Quaternary rocks, Sheet 1012 Mariehamn. Geological Survey of Finland.

Berman, R.G., 1988. Internally-consistent thermodynamic data for minerals in the system Na_2O–K_2O–CaO–MgO–FeO–Fe_2O_3–Al_2O_3–SiO_2–TiO_2–H_2O–CO_2. Journal of Petrology 29, 445–522.

Blake, S., 1981. Eruptions from zoned magma chambers. Journal of the Geological Society of London 138, 281–287.

Blake, S. & Campbell, I.H., 1986. The dynamics of magma-mixing during flow in volcanic conduits. Contributions to Mineralogy and Petrology 94, 72–81.

Blake, S. & Koyaguchi, T., 1991. Insights on the magma mixing model from volcanic rocks. In: J. Didier & B. Barbarin (Editors), Enclaves and granite petrology. Elsevier, Amsterdam, 403–413.

Bloomfield, A.L. & Arculus, R.J., 1989. Magma mixing in the San Francisco Volcanic Field, AZ. Petrogenesis of the O'Leary Peak and Strawberry Crater Volcanics. Contributions to Mineralogy and Petrology 102, 429–453.

Blundy, J.D. & Holland, T.J.B., 1990. Calcic amphibole equilibria and a new amphibole-plagioclase geothermometer. Contributions to Mineralogy and Petrology 104, 208–224.

Blundy, J.D. & Holland, T.J.B., 1992a. "Calcic amphibole equilibria and a new amphibole-plagioclase geothermometer": Reply to the comments of Hammarstrom and Zen, and Rutherford and Johnson. Contributions to Mineralogy and Petrology 111, 269–272.

Blundy, J.D. & Holland, T.J.B., 1992b. "Calcic amphibole equilibria and a new amphibole-plagioclase geothermometer"–reply to the comment of Poli and Schmidt. Contributions to Mineralogy and Petrology 111, 278–282.

Bottinga, Y. & Weill, D.F., 1972. The viscosity of magmatic silicate liquids: a model for calculation. American Journal of Science 272, 438–475.

Boyd, W.W., Jr., 1972. Diabase variation and genesis. Bulletin of the Geological Society of Finland 44, 21–34.

Boyd, W.W., Jr. & Rämö, O.T., 1991. Miscegenation in the Proterozoic. In: I. Haapala & O.T. Rämö (Editors), Symposium on Rapakivi Granites and Related Rocks, Abstract Volume. Geological Survey of Finland, Guide 34, 9.

Bowen, N.L., 1922. The behavior of inclusions in igneous magmas. Journal of Geology 30, 513–570.

Bradshaw, T.K., 1992. The adaptation of Pearce element ratio diagrams to complex high silica systems. Contributions to Mineralogy and Petrology 109, 450–458.

Briot, D., 1990. Magma mixing versus xenocryst assimilation: the genesis of trachyandesites in Sancy volcano, Massif Central, France. Lithos 25, 227–241.

Bunsen, R., 1851. Über die Prozesse der vulkanischen Gesteinbildungen Islands. Annalen der Physik und Chemie 83, 197–272.

Bussy, F., 1990. The rapakivi texture of feldspars in a plutonic mixing environment: a dissolution- recrystallization process? Geological Journal 25, 319–324.

Bussy, F., 1991. Enclaves of the Late Miocene Monte Capanne granite, Elba Island, Italy. In: J. Didier & B. Barbarin (Editors), Enclaves and granite petrology. Elsevier, Amsterdam, 167–178.

Campbell, I.H. & Turner, J.S., 1985. Turbulent mixing between fluids with different viscosities. Nature 313, 39–42.

Campbell, I.H. & Turner, J.S., 1986. The influence of viscosity on fountains in magma chambers. Journal of Petrology 27, 1–30.

Carrigan, C.R. & Eichelberger, J.C., 1990. Zoning of magmas by viscosity in volcanic conduits. Nature 343, 248–254.

Castro, A., de la Rosa, J.D. & Stephens W.E., 1990a. Magma mixing in the subvolcanic environment: petrology of the Gerena interaction zone near Seville, Spain. Contributions to Mineralogy and Petrology 105, 9–26.

Castro, A., Moreno-Ventas, I. & de la Rosa, J.D., 1990b. Microgranular enclaves as indicators of hybridization processes in granitoid rocks, Hercynian belt, Spain. Geological Journal 25, 391–404.

Castro, A., Moreno-Ventas, I. & de la Rosa, J.D., 1991a. Multistage crystallization of tonalitic enclaves in granitoid rocks (Hercynian belt, Spain): implications for magma mixing. Geologische Rundschau 80, 109–120.

Castro, A., Moreno-Ventas, I. & de la Rosa, J.D., 1991b. H-type (hybrid) granitoids: a proposed revision of the granite-type classification and nomenclature. Earth-Science Reviews 31, 237–253.

Chapman, C.A., 1962. Diabase-granite composite dikes, with pillow-like structure, Mount Desert Island, Maine. Journal of Geology 70, 539–564.

Chappell, B.W., 1978. Granitoids from the Moonbi district, New England Batholith, eastern Australia. Journal of the Geological Society of Australia 25, 267–283.

Chappell, B.W. & White, A.J.R., 1991. Restite enclaves and the restite model. In: J. Didier & B. Barbarin (Editors), Enclaves and granite petrology. Elsevier, Amsterdam, 375–381.

Chappell, B.W., White, A.J.R. & Wyborn, D., 1987. The importance of residual source material (restite) in granite petrogenesis. Journal of Petrology 28, 1111–1138.

Chen, Y.D., Price, R.C., White, A.J.R. & Chappell, B.W., 1990. Mafic inclusions from the Glenborg and Blue Gum Granite suites, southeastern Australia. Journal of Geophysical Research 95, 17757–17785.

Collins, W.J., Beams, S.D., White, A.J.R. & Chappell, B.W., 1982. Nature and origin of A-type granites with particular reference to southeastern Australia. Contributions to Mineralogy and Petrology 80, 189–200.

Cook, N.D.J., 1988. Diorites and associated rocks in the Anglem Complex at the Neck, northeastern Stewart Island, New Zealand: an example of magma mingling. Lithos 21, 247–262.

Davidson, P.M. & Lindsley, D.H., 1985. Thermodynamic analysis of quadrilateral pyroxenes. Part II: model calibration from experiments and applications to geothermometry. Contributions to Mineralogy and Petrology 91, 390–404.

Debon, F., 1991. Comparative major element chemistry in various "microgranular enclave–plutonic host" pairs. In: J. Didier & B. Barbarin (Editors), Enclaves and granite petrology. Elsevier, Amsterdam, 293–312.

De Bruiyn, H., van der Westhuized, W.A. & Schoch, A.E., 1983. The estimation of FeO, F and H_2O+ by regression in microprobe analyses of natural biotite. Journal of Trace and Microprobe Techniques 1(4), 399–413.

De la Roche, H., Leterrier, J., Grandclaude, P. & Marchal, M., 1980. A classification of volcanic and plutonic rocks using R_1R_2-diagram and major-element analyses – its relationships with current nomenclature. Chemical Geology 29, 183–210.

Didier, J., 1973. Granites and their enclaves. Elsevier Scientific Publishing Company, Amsterdam, London, New York, 393 p.

Didier, J., 1987. Contribution of enclave studies to the understanding of origin and evolution of granitic magmas. Geologische Rundschau 76, 41–50.

Didier, J. & Barbarin, B. (Editors), 1991a. Enclaves and granite petrology. Elsevier, Amsterdam, 625 p.

Didier, J. & Barbarin, B., 1991b. The different types of enclaves – Nomenclature. In: J. Didier & B. Barbarin (Editors), Enclaves and granite petrology. Elsevier, Amsterdam, 19–23.

Dingwell, D.B. & Webb, S.L., 1992. The fluxing effect of fluorine at magmatic temperatures (600-800 °C): a scanning calorimetric study. American Mineralogist 77, 30–33.

Dingwell, D.B., Scarfe, C.M. & Cronin, D.J., 1985. The effect of fluorine on the viscosities in the system Na_2O–Al_2O_3–SiO_2: implications for phonolites, trachytes and rhyolites. American Mineralogist 70, 80–87.

Dorais, M.J. & Floss, C., 1992. An ion and electron microprobe study of the mineralogy of enclaves and host syenites of the Red Hill complex, New Hampshire, USA. Journal of Petrology 33, 1193–1218.

Dorais, M.J., Whitney, J.A. & Roden, M.F., 1990. Origin of mafic enclaves in the Dinkey Creek pluton, central Sierra Nevada batholith, California. Journal of Petrology 31, 853–881.

Ebadi, A. & Johannes, W., 1991. Beginning of melting and composition of first melts in the system Qz–Ab–Or–H_2O–CO_2. Contributions to Mineralogy and Petrology 106, 286–295.

Eberz, G.W. & Nicholls, I.A., 1988. Microgranitoid enclaves from the Swifts Creek Pluton SE-Australia: textural and physical constraints on the nature of magma mingling processes in the plutonic environment. Geologische Rundschau 77, 713–736.

Eberz, G.W. & Nicholls, I.A., 1990. Chemical modification of enclave magma by post-emplacement crystal fractionation, diffusion and metasomatism. Contributions to Mineralogy and Petrology 104, 47–55.

Edén, P., 1991. A specialized topaz-bearing rapakivi granite and associated mineralized greisen in the Ahvenisto complex, SE Finland. Bulletin of the Geological Society of Finland 63, 25–40.

Ehlers, C. & Ehlers, M., 1978. Geological map of Finland, 1:100 000, pre-Quaternary rocks, Sheet 1023 Kumlinge. Geological Survey of Finland.

Eklund, O., 1993. Coeval contrasting magmatism and magma mixing in Proterozoic post- and anorogenic granites, Åland, SW Finland. Department of Geology and Mineralogy, Åbo Akademi University, Åbo, Finland, 57 p.

Eklund, O. & Lindberg, B., 1992. Interaction between basaltic melts and their wallrock in dykes and sills in Åland, southwestern Finland. Geologiska Föreningens i Stockholm Förhandlingar 114, 93–102.

Eklund, O., Lindberg, B. & Johanson, B., 1989. Origin of ocellar textures in postorogenic granitoids and related mafic dykes, Åland, southwestern Finland. In: I. Haapala & Y. Kähkönen (Editors), Precambrian granitoids abstracts. Geological Survey of Finland, Special Paper 8, 40.

Eklund, O., Fröjdö, S., Lindberg, B. & Andersson, U.B., 1991. The link between anorthositic suites and rapakivi granites. In: I. Haapala & O.T. Rämö (Editors), Symposium on Rapakivi Granites and Related Rocks, Abstract Volume. Geological Survey of Finland, Guide 34, 14.

Eklund, O., Fröjdö, S. & Lindberg, B., 1994. Magma mixing, the petrogenetic link between anorthositic suites and rapakivi granites, Åland, SW Finland. Mineralogy and Petrology 50, 3–19.

Elders, W.A., 1967. Experimental hybridization and rapakivi texture. Geological Society of America, Special Paper 115, 56.

Elo, S. & Korja, A., 1993. Geophysical interpretation of the crustal and upper mantle structure in the Wiborg rapakivi granite area, southeastern Finland. Precambrian Research 64, 273–288.

Emslie, R.F., 1991. Granitoids of rapakivi granite–anorthosite and related associations. Precambrian Research 51, 173–192.

Emslie, R.F. & Stirling, J.A.R., 1993. Rapakivi and related granitoids of the Nain plutonic suite: geochemistry, mineral assemblages and fluid equilibria. Canadian Mineralogist 31, 821–847.

Eskola, P., 1928. On rapakivi rocks from the bottom of the Gulf of Bothnia. Fennia 50(27), 29 p.

Eskola, P., 1930. On the disintegration of rapakivi. Bulletin de la Commission Géologique de Finlande 92, 96–105.

Eskola, P., 1949. The mica of the moro. Bulletin de la Commission Géologique de Finlande 144, 113–116.

Eugster, H.P. & Wones, D.R., 1962. Stability relations of the ferruginous biotite, annite. Journal of Petrology 3, 82–125.

Fenn, P.M., 1986. On the origin of graphic granite. American Mineralogist 71, 325–330.

Fernandez, A.N. & Barbarin, B., 1991. Relative rheology of coeval mafic and felsic magmas: nature of resulting interaction processes and shape and mineral fabrics of mafic microgranular enclaves. In: J. Didier & B. Barbarin (Editors), Enclaves and granite petrology. Elsevier, Amsterdam, 263–275.

Fernandez, A.N. & Gasquet, D.R., 1994. Relative rheological evolution of chemically contrasted coeval magmas: example of the Tichka plutonic complex (Morocco). Contributions to Mineralogy and Petrology 116, 316–326.

Fourcade, S. & Allegre, C.J., 1981. Trace elements behavior in granite genesis: a case study the calc-alkaline plutonic association from the Querigut complex (Pyrénées, France). Contributions to Mineralogy and Petrology 76, 177–195.

Frost, B.R. & Lindsley, D.H., 1992. Equilibria among Fe-Ti oxides, pyroxenes, olivine, and quartz: Part II. Application. American Mineralogist 77, 1004–1020.

Frost, B.R., Lindsley, D.H. & Andersen, D.J., 1988. Fe-Ti oxide – silicate equilibria: assemblages with fayalitic olivine. American Mineralogist 73, 727–740.

Frost, T.P. & Mahood, G.A., 1987. Field, chemical, and physical constraints on mafic-felsic magma interaction in the Lamarck Granodiorite, Sierra Nevada, California. Geological Society of America, Bulletin 99, 272–291.

Frost, T.P. & Lindsay, J.R., 1988. MAGMIX: a basic program to calculate viscosities of interacting magmas of differing composition, temperature, and water content. Computers & Geosciences 14, 213–228.

Fuhrman, M.L. & Lindsley, D.H., 1988. Ternary-feldspar modeling and thermometry. American Mineralogist 73, 201–215.

Geringer, G.J., de Bruiyn, H., Schoch, A.E., Botha, B.J.V. & van der Westhuizen, W.A., 1987. The geochemistry and petrogenetic relationships of two granites and their inclusions in the Keimoes Suite of the Namaqua mobile belt, South Africa. Precambrian Research 36, 143–162.

Gerlach, D.C. & Grove, T.L., 1982. Petrology of Medicine Lake Highland volcanics: characterization of endmembers of magma mixing. Contributions to Mineralogy and Petrology 80, 147–159.

Gourgaud, A., 1991. Comagmatic enclaves in lavas from the Mont-Dore composite volcano, Massif Central, France. In: J. Didier & B. Barbarin (Editors), Enclaves and granite petrology. Elsevier, Amsterdam, 221–233.

Grasset, O. & Albarède, F., 1994. Hybridization of mingling magmas with different densities. Earth and Planetary Science Letters 121, 327–332.

Gray, C.M., 1984. An isotopic mixing model for the origin of granitic rocks in southeastern Australia. Earth and Planetary Science Letters 70, 47–60.

Grout, F.F., 1937. Criteria of origin of inclusions in plutonic rocks. Geological Society of America, Bulletin 48, 1521–1572.

Haapala, I., 1977a. Petrography and geochemistry of the Eurajoki stock, a rapakivi-granite complex with greisen-type mineralization in southwestern Finland. Geological Survey of Finland, Bulletin 286, 128 p.

Haapala, I., 1977b. The controls of tin and related mineralizations in the rapakivi granite areas of southeastern Fennoscandia. Geologiska Föreningens i Stockholm Förhandlingar 99, 130–142.

Haapala, I., 1988. Metallogeny of the Proterozoic rapakivi granites of Finland. In: R.P. Taylor & D.F. Strong (Editors), Recent advances in the geology of granite-related mineral deposits. Canadian Institute of Mining and Metallurgy, Special Volume 39, 124–132.

Haapala, I., 1989. Suomen rapakivigraniiteista – Rapakivi granites of Finland. Academica Fennica, Vuosikirja – Year Book 1988–1989, 135–140.

Haapala, I., 1993. Graniittien geokemia ja petrografia tinamalmien etsinnässä (in Finnish). In: I. Haapala, L. Hyvärinen & P. Salonsaari (Editors), Malminetsinnän menetelmät. Yliopistopaino, Helsinki, 138–146.

Haapala, I., 1995. Metallogeny of the rapakivi granites. Mineralogy and Petrology (in press).

Haapala, I. & Ojanperä, P., 1969. Triplite and wolframite from a greisen-bordered veinlet in Eurajoki, SW Finland. Bulletin of the Geological Society of Finland 41, 99–105.

Haapala, I. & Ojanperä, P., 1972a. Magnetite and ilmenite from some Finnish rocks. Bulletin of the Geological Society of Finland 44, 13–20.

Haapala, I. & Ojanperä, P., 1972b. Genthelvite-bearing greisens in southern Finland. Geological Survey of Finland, Bulletin 259, 22 p.

Haapala, I. & Rämö, O.T., 1990. Petrogenesis of the Proterozoic rapakivi granites of Finland. In: H.J. Stein & J.L. Hannah (Editors), Ore-bearing granite systems; petrogenesis and mineralizing processes. Geological Society of America, Special Paper 246, 275–286.

Haapala, I. & Rämö, O.T., 1992. Tectonic setting and origin of the Proterozoic rapakivi granites of southeastern Fennoscandia. Transactions of the Royal Society of Edinburgh: Earth Sciences 83, 165–171.

Haapala, I., Rieder, M. & Povondra, P., 1991. Mineralogy of dark micas from the Wiborg rapakivi batholith. In: I. Haapala & O.T. Rämö (Editors), Symposium on Rapakivi Granites and Related Rocks, Abstract Volume. Geological Survey of Finland, Guide 34, 23.

Hackman, V., 1934. Das rapakiwirandgebiet der gegend von Lappeenranta (Willmanstrand). Bulletin de la Commission Géologique de Finlande 106, 87 p.

Hammarstrom, J.M., & Zen, E-an, 1986. Aluminium in hornblende: an empirical igneous geobarometer. American Mineralogist 71, 1297–1313.

Hammarstrom, J.M. & Zen, E-an, 1992. Discussion of Blundy and Holland's (1990) "Calcic amphibole equilibria and a new amphibole-plagioclase geothermometer". Contributions to Mineralogy and Petrology 111, 264–268.

Halliday, A.N., Stephens, W.E. & Harmon, R.S., 1980. Rb-Sr and O isotopic relationships in 3 zoned Caledonian granitic plutons, Southern Uplands, Scotland: evidence for varied sources and hybridization of magmas. Journal of the Geological Society of London 137, 329–348.

Hanuš, V. & Palivcová, M., 1969. Quartz-gabbros recrystallized from olivine-bearing volcanics. Lithos 2, 147–166.

Härme, M., 1980. General geological map of Finland, 1:400 000, pre-Quaternary rocks, Sheets C1-D1 Helsinki. Geological Survey of Finland.

Hibbard, M.J., 1981. The magma mixing origin of mantled feldspars. Contributions to Mineralogy and Petrology 76, 158–170.

Hibbard, M.J., 1991. Textural anatomy of twelve magma-mixed granitoid systems. In: J. Didier & B. Barbarin (Editors), Enclaves and granite petrology. Elsevier, Amsterdam, 431–444.

Hollister, L.S., Grissom, G.C., Peters, E.K., Stowell, H.H. & Sisson, V.B., 1987. Confirmation of the empirical correlation of Al in hornblende with pressure of solidification of calc-alkaline plutons. American Mineralogist 72, 231–239.

Huebner, J.S. & Sato, M., 1970. The oxygen fugacity-temperature relationships to manganese oxide and nickel oxide buffers. American Mineralogist 55, 934–952.

Huppert, H.E. & Sparks, R.S.J., 1988. The generation of granitic magmas by intrusion of basalt into continental crust. Journal of Petrology 29, 599–624.

Huppert, H.E., Turner, J.S. & Sparks, R.S.J., 1982. Replenished magma chambers: effects of compositional zonation and input rates. Earth and Planetary Science Letters 57, 345–357.

Hurlbut, C.S., Jr., 1935. Dark inclusions in a tonalite of southern California. American Mineralogist 20, 609–630.

Irvine, T.N. & Baragar, W.R.A., 1971. A guide to the chemical classification of the common volcanic rocks. Canadian Journal of Earth Sciences 8, 523–548.

Ishihara, S., 1977. The magnetite-series and ilmenite-series granitic rocks. Mining Geology 27, 293–305.

Johanson, B.S., 1984. Ahvenisto gabbro-anortositkomplex – en petrografisk och mineralogisk undersökning. Unpublished M.Sc. thesis. University of Helsinki, Department of Geology, 85 p.

Johanson, B.S., 1989. Monzodioritic rocks of the gabbro-anorthosite complex associated with the Ahvenisto rapakivi granite batholith, southern Finland. In: I. Haapala & Y. Kähkönen (Editors), Symposium Precambrian Granitoids, Abstracts. Geological Survey of Finland, Special Paper 8, 74.

Johnson, M.C. & Rutherford, M.J., 1989. Experimental calibration of the aluminum-in-hornblende geobarometer with application to Long Valley caldera (California) volcanic rocks. Geology 17, 837–841.

Kahma, A., 1951. On the contact phenomena of the Satakunta diabase. Bulletin de la Commission Géologique de Finlande 152, 84 p.

Korja, A., 1995. Upper crust of the Baltic Profile, Finland. University of Oulu, Department of Geophysics, Report 19, 19 p.

Kouchi, A. & Sunagawa, I., 1983. Mixing of basaltic and dacitic magmas by forced convection. Nature 304, 527–528.

Kouchi, A. & Sunagawa, I., 1985. A model for mixing basaltic and dacitic magmas as deduced from experimental data. Contributions to Mineralogy and Petrology 89, 17–23.

Koyaguchi, T., 1985. Magma mixing in a conduit. Journal of Volcanology and Geothermal Research 25, 365–369.

Koyaguchi, T. & Blake, S., 1991. Origin of mafic enclaves: constraints on the magma mixing model from fluid dynamic experiments. In: J. Didier & B. Barbarin (Editors), Enclaves and granite petrology. Elsevier, Amsterdam, 415–429.

Koyaguchi, T., Hallworth, M.A. & Huppert, H.E., 1993. An experimental study on the effects of phenocrysts on convection in magmas. Journal of Volcanology and Geothermal Research 55, 15–32.

Kroll, H., Evangelakakis, C. & Voll, G., 1993. Two-feldspar geothermometry: a review and revision for slowly cooled rocks. Contributions to Mineralogy and Petrology 114, 510–518.

Kushiro, I., 1980. Viscosity, density, and structure of silicate melts at high pressures, and their petrological applications. In: R.B. Hargraves (Editor), Physics of magmatic processes. Princeton University Press, 93–120.

Laitakari, A., 1928. Palingenese am kontakt des Postjotnischen olivindiabases. Fennia 50(35), 25 p.

Laitakari, I., 1969. On the set of olivine diabase dikes in Häme, Finland. Bulletin de la Commission Géologique de Finlande 241, 65 p.

Laitakari, I., 1987. Hämeen subjotuninen diabaasijuoniparvi. English abstract: The Subjotnian diabase dyke swarm of Häme. In: K. Aro & I. Laitakari (Editors), Suomen diabaasit ja muut mafiset juonikivilajit (Diabases and other mafic dyke rocks in Finland). Geological Survey of Finland, Report of Investigation 76, 99–116.

Laitakari, I. & Simonen, A., 1962. Geological map of Finland, 1:100 000, pre-Quaternary rocks, Sheet 3022 Lapinjärvi. Geological Survey of Finland.

Laitakari, I. & Leino, H., 1989. A new model for the emplacement of the Häme diabase dyke swarm, central Finland, In: S. Autio (Editor), Geological Survey of Finland current research 1988. Geological Survey of Finland, Special Paper 10, 7–8.

Langmuir, C.H., Vocke, R.D., Jr., Hanson, G.N. & Hart, S.R., 1978. A general mixing equation with applications to Icelandic basalts. Earth and Planetary Science Letters 37, 380–392.

Leake, B.E., 1978. Nomenclature of amphiboles. Canadian Mineralogist 16, 501–520.

Le Bas, M.J., Le Maitre, R.W., Streckeisen, A. & Zanettin, B., 1986. A chemical classification of volcanic rocks based on the total alkali–silica diagram. Journal of Petrology 27, 745–750.

Lee, D.E., van Loenen, R.E. & Mays, R.E., 1973. Accessory apatite from hybrid granitoid rocks of the southern Snake Range, Nevada. Journal of Research of the U.S. Geological Survey 1, 89–98.

Lehijärvi, M. & Lonka, A., 1964. The hornblende rapakivi dike of Jaala-Iitti. Bulletin de la Commission Géologique de Finlande 215, 127–141.

Lehijärvi, M. & Tyrväinen, A., 1969. Geological map of Finland, 1:100 000, pre-Quaternary rocks, Sheet 3114 Vuohijärvi. Geological Survey of Finland.

Lesher, C.E., 1990. Decoupling of chemical and isotopic exchange during magma mixing. Nature 344, 235–237.

Lindberg, B. & Eklund, O., 1989. The rapakivi granite - diabase association in southwestern Finland. In: I. Haapala & Y. Kähkönen (Editors), Symposium Precambrian Granitoids, Abstracts. Geological Survey of Finland, Special Paper 8, 82.

Lindberg, B. & Eklund, O., 1992. Mixing between basaltic and granitic magmas in a rapakivi related quartz-feldspar porphyry, Åland, SW Finland. Geologiska Föreningens i Stockholm Förhandlingar 114, 103–112.

Lindberg, B., Eklund, O. & Suominen, V., 1991. Middle Proterozoic, Subjotnian diabases and related mafic rocks in the archipelago of southwestern Finland. In: I. Laitakari (Editor), IGCP-257 Fennoscandian Meeting and Excursion on Precambrian Dyke Swarms. IGCP-257 Technical Report 4, 18–30.

Lindsley, D.H., 1983. Pyroxene thermometry. American Mineralogist 68, 477–493.

Lindsley, D.H. & Frost, B.R., 1992. Equilibria among Fe-Ti oxides, pyroxenes, olivine, and quartz: Part I. Theory. American Mineralogist 77, 987–1003.

Lintala, J., 1991. Viipurin batoliitin rapakivigraniiteista sekä havaintoja niiden syntyolosuhteista kahden maasälvän termometrin valossa. Unpublished M.Sc. thesis. University of Helsinki, Department of Geology, 88 p.

Lintala, J., Haapala, I. & Boyd, W.W., Jr., 1991. Rapakivi textures from the Wiborg batholith. In: I. Haapala & O.T. Rämö (Editors), Symposium on Rapakivi Granites and Related Rocks, Abstract Volume. Geological Survey of Finland, Guide 34, 33.

Lonka, A., 1957. Jaala-Iitin sarvivälkerapakivi ja ympäröivät kivilajit. Unpublished M.Sc. thesis, University of Helsinki, Department of Geology, 65 p.

Lonka, A., 1960. Jaalan-Iitin sarvivälkerapakivijuoni. Unpublished Ph.Lic. thesis, University of Turku, Department of Geology, 78 p.

Lorenc, M.W., 1990. Magmatic mafic enclaves in granitoids of northern Sierra de Paimán, Argentina. Geological Journal 25, 405–412.

Lowell, G.R. & Young, G.J., 1993. Coexisting mafic-felsic magmas in the St. Francois Terrane of southeastern Missouri: field and chemical evidence from the Silvermine Granite. Geological Society of America, Abstracts with Programs 25(3), 63–64.

Ludington, S., 1978. The biotite–apatite geothermometer revisited. American Mineralogist 63, 551–553.

Luosto, U., 1990. Seismic data from the northern segment of the EGT and from the nearby profiles. In: R. Freeman & St. Mueller (Editors), Proceedings of the sixth workshop of the geotraverse (EGT) project. European Science Foundation, Strasbourg, 53–61.

Luosto, U., Tiira, T., Korhonen, H., Azbel, I., Burmin, V., Buyanov, A., Kosminskaya, I., Ionkis, V. & Sharov, N., 1990. Crust and upper mantle structure along the DSS Baltic profile in SE Finland. Geophysical Journal International 101, 89–110.

Manning, D.A.C., 1981. The effect of fluorine on liquidus phase relationships in the system Qz–Ab–Or with excess water at 1 kb. Contributions to Mineralogy and Petrology 76, 206–215.

Marsh, B.D., 1981. On the crystallinity, probability of occurrence, and rheology of lava and magma. Contributions to Mineralogy and Petrology 78, 85–98.

McBirney, A.R. & Murase, T., 1984. Rheological properties of magmas. Annual Review of Earth and Planetary Sciences 12, 337–357.

Mcsween, H.Y., Jr., Coish, R.A. & Norman, M.D., 1979. Coexisting acidic and basic melts: geochemistry of a composite dike–a discussion. Journal of Geology 87, 209–214.

Meriläinen, K., 1966. Geological map of Finland, 1:100 000, pre-Quaternary rocks, Sheet 4112+4111 Imatra. Geological Survey of Finland.

Meschede, M., 1986. A method of discriminating between different types of mid-ocean ridge basalts and continental tholeiites with the Nb-Zr-Y diagram. Chemical Geology 56, 207–218.

Metzger, K., Altherr, R., Okrusch, M., Henjes-Kunst, F. & Kreuzer, H., 1985. Genesis of acid/basic rock associations: a case study the Kallithea intrusive complex, Samos, Greece. Contributions to Mineralogy and Petrology 90, 353–366.

Moberg, K.AD., 1885. Beskifning till kartbladet No 8. Finlands Geologiska Undersökning, 77 p.

Morimoto, N., 1988. Nomenclature of pyroxenes. American Mineralogist 73, 1123–1133.

Myers, J. & Eugster, H.P., 1983. The system Fe–S–O: oxygen buffer calibrations to 1,500K. Contributions to Mineralogy and Petrology 82, 75–90.

Nekvasil, H., 1991. Ascent of felsic magmas and formation of rapakivi. American Mineralogist 76, 1279–1290.

Nockolds, S.R., 1932. The contaminated granite of Bibette Head, Alderney. Geological Magazine 69, 433–452.

Nurmi, P.A. & Haapala, I., 1986. The Proterozoic granitoids of Finland: granite types, metallogeny and relation to crustal evolution. Bulletin of the Geological Society of Finland 58, 203–233.

O'Brien, H., Huhma, H. & Sorjonen-Ward, P., 1993. Petrogenesis of the late Archean Hattu schist belt, Ilomantsi, eastern Finland: Geochemistry and Sr, Nd isotopic composition. In: P.A. Nurmi & P. Sorjonen-Ward (Editors), Geological development, gold mineralizations and exploration methods in the late Archean Hattu schist belt, Ilomantsi, eastern Finland. Geological Survey of Finland, Special Paper 17, 147–184.

Palivcová, M., 1978. Ocellar quartz leucogabbro (Central Bohemian pluton) and genetic problems of ocellar rocks. Geologický Zborník – Geologica Carpathica 29, 19–41.

Pearce, J.A. & Cann, J.R., 1973. Tectonic setting of basic volcanic rocks determined using trace element analyses. Earth and Planetary Science Letters 19, 290–300.

Pearce, T.H., Gorman, B.E. & Birkett, T.C., 1975. The TiO_2–K_2O–P_2O_5 diagram: a method of discriminating between oceanic and non-oceanic basalts. Earth and Planetary Science Letters 24, 419–426.

Pearce, T.H., Gorman, B.E. & Birkett, T.C., 1977. The relatioship between major element chemistry and tectonic environment of basic and intermediate volcanic rocks. Earth and Planetary Science Letters 36, 121–132.

Pearce, J.A., Harris, N.B.W. & Tindle, A.G., 1984. Trace element discrimination diagrams for the tectonic interpretation of granitic rocks. Journal of Petrology 25, 956–983.

Pesquera, A. & Pons, J., 1989. Field evidence of magma mixing in the Aya granitic massif (Basque Pyrenees, Spain). Neues Jahrbuch für Mineralogie, Monatshäfte 10, 441–454.

Phillips, J.A., 1880. On concretionary patches and fragments of other rocks contained in granite. Quarterly Journal of the Geological Society of London 36, 1–21.

Poli, G.E. & Tommasini, S., 1991. Model for the origin and significance of microgranular enclaves in calc-alkaline granitoids. Journal of Petrology 32, 657–666.

Poli, S. & Schmidt, M.W., 1992. A comment on "Calcic amphibole equilibria and a new amphibole- plagioclase geothermometer" by J.D. Bludy and T.J.B. Holland (Contrib Mineral Petrol (1990) 104: 208–224). Contributions to Mineralogy and Petrology 111, 273–282.

Presnall, D.C. & Bateman, P.C., 1973. Fusion relations in the system $NaAlSi_3O_8$-$CaAl_2Si_2O_8$-$KAlSi_3O_8$-SiO_2-H_2O and generation of granitic magmas in the Sierra Nevada batholith. Geological Society of America, Bulletin 84, 3181–3202.

Rämö, O.T., 1989. Silicic-basic magmatism associated with rapakivi granites: petrography and petrology of composite diabase - quartz porphyry dykes and K-feldspar diabases in the Suomenniemi complex, southeastern Finland. In: I. Haapala & Y. Kähkönen (Editors), Symposium Precambrian Granitoids, Abstracts. Geological Survey of Finland, Special Paper 8, 105–106.

Rämö, O.T., 1990. Diabase dyke swarms and silicic magmatism – evidence from the Proterozoic of Finland. In: A.J. Parker, P.C. Rickwood & D.H. Tucker (Edi-

tors), Mafic dykes and emplacement mechanisms. Rotterdam, A.A. Balkema, 185–199.

Rämö, O.T., 1991. Petrogenesis of the Proterozoic rapakivi granites and related basic rocks of southeastern Fennoscandia: Nd and Pb isotopic and general geochemical constraints. Geological Survey of Finland, Bulletin 355, 161 p.

Rämö, O.T. & Haapala, I., 1991. The rapakivi granites of eastern Fennoscandia: a review with insights into their origin in the light of new Sm-Nd isotopic data. In: C.F. Gower, T. Rivers & B. Ryan (Editors), Mid-Proterozoic Laurentia-Baltica. Geological Association of Canada, Special Paper 38, 401–415.

Rämö, O.T. & Haapala, I., 1995. One hundred years of rapakivi granite. Mineralogy and Petrology 52, 129–185.

Rämö, T., Haapala, I. & Salonsaari, P., 1994. Rapakivi granite magmatism: implications for lithospheric evolution. In: M. Pajunen (Editor), High temperature-low pressure metamorphism and deep crustal structures. Meeting of IGCP project 304 'Deep Crustal Processess in Finland, September 16–20, 1994. Geological Survey of Finland, Guide 37, 61–68.

Reid, J.B., Jr., Evans, O.C. & Fates, D.G., 1983. Magma mixing in granitic rocks of the central Sierra Nevada, California. Earth and Planetary Science Letters 66, 243–261.

Robinson, P., Spear, F.S., Schumacher, J.C., Laird, J., Klein, C., Evans, B.W. & Doolan, B.L., 1982. Phase relations of metamorphic amphiboles: natural occurrence and theory. In: D.R. Veblen & P.H. Ribbe (Editors), Amphiboles: petrology and experimental phase relations. Reviews in Mineralogy, Volume 9B, 1–227.

Rock, N.M.S., 1990. The international mineralogical association (IMA/CNMMN) pyroxene nomenclature scheme: computerization and its consequences. Mineralogy and Petrology 43, 99–119.

Russell, J.K., 1990. Magma mixing processes: insights and constraints from thermodynamic calculations. In: J. Nicholls & J.K. Russell (Editors), Modern methods of igneous petrology: understanding magmatic processes. Reviews in Mineralogy 24, 153–190.

Rutherford, M.J. & Johnson, M.C., 1992. Comment on Blundy and Holland's (1990) "Calcic amphibole equilibria and a new amphibole-plagioclase geothermometer". Contributions to Mineralogy and Petrology 111, 266–268.

Sahama, Th.G., 1945. On the chemistry of the east Fennoscandian rapakivi granites. Bulletin de la Commission Géologique de Finlande 136, 15–67.

Sahama, Th.G., 1947. Rapakivi amphibole from Uuksunjoki, Salmi area. Bulletin de la Commission Géologique de Finlande 140, 159–162.

Sakuyama, M., 1981. Petrological study of the Myoko and Kurohime volcanoes, Japan: crystallization sequence and evidence for magma mixing. Journal of Petrology 22, 553–583.

Salonsaari, P.T., 1993. Disintegration and recrystallization of magmatic mafic enclaves in rapakivi granites of southeastern Finland. Geological Society of America, Abstracts with Programs 25(3), 77.

Salonsaari, P.T. & Haapala, I., 1991. The Jaala-Iitti rapakivi complex: an example of bimodal magmatism and hybridization in the Wiborg rapakivi batholith, Finland. In: I. Haapala & O.T. Rämö (Editors), Symposium on Rapakivi Granites and Related Rocks, Abstract Volume. Geological Survey of Finland, Guide 34, 45.

Salonsaari, P.T. & Haapala, I., 1994. The Jaala-Iitti rapakivi complex: an example of bimodal magmatism and hybridization in the Wiborg rapakivi batholith, southeastern Finland. Mineralogy and Petrology 50, 21–34.

Salonsaari, P.T. & Lintala, J.M., 1994. Ocellar, micrographic, and rapakivi textures in rapakivi granites of southeastern Finland. International Mineralogical Association, 16th General Meeting, Pisa, 4–9 September 1994, Abstracts, p. 363.

Sato, H., 1975. Diffusion coronas around quartz xenocrysts in andesite and basalt from tertiary volcanic region in northeastern Shikoku, Japan. Contributions to Mineralogy and Petrology 50, 49–64.

Savolahti, A., 1956. The Ahvenisto massif in Finland. Bulletin de la Commission Géologique de Finlande 174, 96 p.

Savolahti, A., 1962. The rapakivi problem and the rules of idiomorphism in minerals. Bulletin de la Commission Géologique de Finlande 204, 33–112.

Schmidt, M.W., 1992. Amphibole composition in tonalite as a function of pressure: an experimental calibration of the Al-in-hornblende barometer. Contributions to Mineralogy and Petrology 110, 304–310.

Sederholm, J.J., 1891. Ueber die finnländischen Rapakiwigesteine. Tschermak's Mineralogische und Petrographische Mittheilungen 12, 1–31.

Shaw, H.R., 1972. Viscosities of magmatic silicate liquids: an empirical method of prediction. American Journal of Science 272, 870–893.

Siivola, J., 1987. Lovasjärven mafinen intruusio. English summary: The mafic intrusion of Lovasjärvi. In: K. Aro & I. Laitakari (Editors), Suomen diabaasit ja muut mafiset juonikivilajit (Diabases and other mafic dyke rocks in Finland). Geological Survey of Finland, Report of Investigation 76, 121–128.

Simonen, A., 1961. Olivine from rapakivi. Bulletin de la Commission Géologique de Finlande 196, 371–376.

Simonen, A., 1965. Geological map of Finland, 1:100 000, pre-Quaternary rocks, Sheet 3024 Karhula. Geological Survey of Finland.

Simonen, A., 1973. Geological map of Finland, 1:100 000, pre-Quaternary rocks, Sheet 3042 Hamina. Geological Survey of Finland.

Simonen, A., 1975. Geological map of Finland, 1:100 000, pre-Quaternary rocks, Sheet 3131 Luumäki. Geological Survey of Finland.

Simonen, A., 1979a. Geological map of Finland, 1:100 000, pre-Quaternary rocks, Sheet 3133 Ylämaa. Geological Survey of Finland.

Simonen, A., 1979b. Geological map of Finland, 1:100 000, pre-Quaternary rocks, Sheet 3044 Vaalimaa. Geological Survey of Finland.

Simonen, A., 1987. Kaakkois-Suomen rapakivimassiivin kartta-alueiden kallioperä. English summary: Pre-Quaternary rocks of the map-sheet areas of the rapakivi massif in SE Finland, Geological map of Finland, 1:100 000, Explanation to the maps of Pre-Quaternary rocks, Sheets 3023+3014, 3024, 3041, 3042, 3044, 3113, 3131, and 3133. Geological Survey of Finland, 49 p.

Simonen, A. & Laitala, M., 1970. Geological map of Finland, 1:100 000, pre-Quaternary rocks, Sheet 3023+3014 Kotka. Geological Survey of Finland.

Simonen, A. & Laitala, M., 1972. Geological map of Finland, 1:100 000, pre-Quaternary rocks, Sheet 3041 Haapasaari. Geological Survey of Finland.

Simonen, A. & Lehijärvi, M., 1963. Geological map of Finland, 1:100 000, pre-Quaternary rocks, Sheet 3113 Kouvola. Geological Survey of Finland.

Simonen, A. & Tyrväinen A., 1965. Geological map of Finland, 1:100 000, pre-Quaternary rocks, Sheet 3132 Savitaipale. Geological Survey of Finland.

Simonen, A. & Vorma, A., 1969. Amphibole and biotite from rapakivi. Bulletin de la Commission Géologique de Finlande 238, 28 p.

Smith, J.V., 1974. Feldspar minerals 2. Chemical and textural properties. Springer-Verlag, Berlin, Heidelberg, New York, 690 p.

Sparks, R.S.J. & Marshall, L.A., 1986. Thermal and mechanical constraints of mixing between mafic and silicic magmas. Journal of Volcanology and Geothermal Research 29, 99–124.

Sparks, R.S.J., Sigurdsson, H. & Wilson, L., 1977. Magma mixing: a mechanism for triggering acid explosive eruptions. Nature 267, 315–318.

Speer, J.A., 1984. Micas in igneous rocks. In: S.W. Bailey (Editor), Micas. Reviews in Mineralogy 13, 299–356.

Stimac, J.A. & Wark, D.A., 1992. Plagioclase mantles on sanidine in silicic lavas, Clear Lake, California: implications for the origin of rapakivi texture. Geological Society of America, Bulletin 104, 728–744.

Stimac, J.A., Pearce, T.H., Donnelly-Nolan, J.M. & Hearn, B.C., Jr., 1990. The origin and implications of undercooled andesitic inclusions in rhyolites, Clear Lake Volcanics, California. Journal of Geophysical Research 95, 17729–17746.

Stormer, J.C., Jr., 1983. The effects of recalculation on estimates of temperatures and oxygen fugacity from analyses of multicomponent iron–titanium oxides. American Mineralogist 68, 586–594.

Stormer, J.C. & Carmichael, I.S.E., 1971. Fluorine–hydroxyl exchange in apatite and biotite: a potential igneous geothermometer. Contributions to Mineralogy and Petrology 31, 121–131.

Streckeisen, A.L., 1973. Plutonic rocks: classification and nomenclature recommended by the IUGS Subcommission of the systematics of igneous rocks. Geotimes 18, 26–30.

Streckeisen, A.L., 1976. To each plutonic rock its proper name. Earth Science Reviews. International Magazine for Geo-Scientists Amsterdam 12, 1–33.

Suominen, V., 1987. Lounais-Suomen mafiset juonikivet. English abstract: mafic dyke rocks in southwestern Finland. In: K. Aro & I. Laitakari (Editors), Suomen diabaasit ja muut mafiset juonikivilajit (Diabases and other mafic dyke rocks in Finland). Geological Survey of Finland, Report of Investigation 76, 151–172.

Suominen, V., 1991. The chronostratigraphy of southwestern Finland with special reference to Postjotnian and Subjotnian diabases. Geological Survey of Finland, Bulletin 356, 100 p.

Taylor, T.R., Vogel, T.A. & Wilband, J.T., 1980. The composite dikes at Mount Desert Island, Maine: an example of coexisting acidic and basic magmas. Journal of Geology 88, 433–444.

Thomas, H.H. & Smith, W.C., 1932. Xenoliths of igneous origin in the Trégastel-Ploumanac'h granite, Gôtes du Nord, France. Quarterly Journal of the Geological Society of London 88, 274–296.

Tindle, A.G. & Pearce, J.A., 1983. Assimilation and partial melting of continental crust: evidence from the mineralogy and geochemistry of autoliths and xenoliths. Lithos 16, 185–202.

Turner, J.S. & Campbell, I.H., 1986. Convection and mixing in magma chambers. Earth-Science Reviews 23, 255–352.

Tuttle, O.F. & Bowen, N.L., 1958. Origin of granite in the light of experimental studies in the system $NaAlSi_3O_8$–$KAlSi_3O_8$–SiO_2-H_2 O. Geological Society of America, Memoir 74, 153 p.

Vaasjoki, M., 1977. Rapakivi granites and other postorogenic rocks in Finland; their age and lead isotopic composition of certain associated galena mineralizations. Geological Survey of Finland, Bulletin 294, 64 p.

Vaasjoki, M. & Rämö, O.T., 1989. The Wiborg rapakivi batholith and associated rocks in southeastern Finland. Precambrian granitoids, petrogenesis, geochemistry and metallogeny, Excursion A2. Geological Survey of Finland, Guide 30, 32 p.

Vaasjoki, M. & Sakko, M., 1989. The radiometric age of the Virmaila diabase dyke: evidence for 20 Ma of continental rifting in Padasjoki, southern Finland. In: S. Autio (Editor), Geological Survey of Finland current research 1988. Geological Survey of Finland, Special Paper 10, 43–44.

Vaasjoki, M., Rämö, O.T. & Sakko, M., 1991. New U–Pb ages from the Wiborg rapakivi area: constraints on the temporal evolution of the rapakivi granite–anorthosite–diabase dyke association of southeastern Finland. In: I. Haapala & K.C. Condie (Editors), Precambrian granitoids–petrogenesis, geochemistry and metallogeny. Precambrian Research 51, 227–243.

Vaasjoki, M., Rämö, O.T., Alviola, R. & Johanson, B.S., 1993. Petrography and new U–Pb age data on the Ahvenisto rapakivi granite complex, southeastern Finland. Geological Society of America, Abstracts with Programs 25(3), 86.

Van der Laan, S.R. & Wyllie, P.J., 1993. Experimental interaction of granitic and basaltic magmas and implications for mafic enclaves. Journal of Petrology 34, 491–517.

Vernon, R.H., 1983. Restite, xenoliths and microgranitoid enclaves in granites. Journal and Proceedings of the Royal Society of New South Wales 116, 77–103.

Vernon, R.H., 1990. Crystallization and hybridism in microgranitoid enclave magmas: microstructural evidence. Journal of Geophysical Research 95, 17849–17859.

Vernon, R.H., 1991. Interpretation of microstructures of microgranitoid enclaves. In: J. Didier & B. Barbarin (Editors), Enclaves and granite petrology. Elsevier, Amsterdam, 277–291.

Vernon, R.H. & Flood, R.H., 1982. Some problems in the interpretation of microstructures in granitoid rocks. In: B. Runnegar & P. Flood (Editors), New England geology. University of New England and AHV Club, Armidale, New South Wales, Australia, 201–210.

Vernon, R.H., Etheridge, M.A. & Wall, V.J., 1988. Shape and microstructure of microgranitoid enclaves: indicators of magma mingling and flow. Lithos 22, 1–11.

Vogel, T.A. & Wilband, J.T., 1978. Coexisting acidic and basic melts: geochemistry of a composite dike. Journal of Geology 86, 353–371.

Volborth, A., 1963. Rapakivi texture in roof portion and included dikes, and breccias of a granitic batholith in Newberry and Eldorado Mountains, Clark County, Nevada. Geological Society of America, Special Paper 76, 173–174.

Volborth, A., 1973. Geology of the granite complex of the Eldorado, Newberry, and northern Dead Mountains, Clark County, Nevada. Nevada Bureau of Mines and Geology 80, 40 p.

Vorma, A., 1964. Geological map of Finland, 1:100 000, pre-Quaternary rocks, Sheet 3134 Lappeenranta. Geological Survey of Finland.

Vorma, A., 1971. Alkali feldspars of the Wiborg rapakivi massif in southeastern Finland. Bulletin de la Commission Géologique de Finlande 246, 72 p.

Vorma, A., 1972. On the contact aureole of the Wiborg rapakivi massif in southeastern Finland. Geological Survey of Finland, Bulletin 255, 28 p.

Vorma, A., 1975. On two roof pendants in the Wiborg rapakivi massif, southeastern Finland. Geological Survey of Finland, Bulletin 272, 86 p.

Vorma, A., 1976. On the petrochemistry of rapakivi granites with special reference to the Laitila massif, southwestern Finland. Geological Survey of Finland, Bulletin 285, 98 p.

Vorma, A. & Paasivirta, T., 1979. Contribution to the mineralogy of rapakivi granites: I. Zircon of the Laitila rapakivi, southwestern Finland. Geological Survey of Finland, Bulletin 303, 40 p.

Wahl, W., 1925. Die Gesteine des wiborger Rapakiwigebietes. Fennia 45(20), 127 p.

Wahl, W., 1938. Några iakttagelser från Wiborgs-rapakiviområdets södra gränsgebiet. Geologiska Föreningens i Stockholm Förhandlingar 60, 88–96.

Wahl, W., 1947. A composite lava flow from Lounatkorkia, Hogland. Bulletin de la Commission Géologique de Finlande 140, 287–302.

Wall, V.J., Clemens, J.D. & Clarke, D.B., 1987. Models for granitoid evolution and source compositions. Journal of Geology 95, 731–749.

Wark, D.A. & Stimac, J.A., 1992. Origin of mantled (rapakivi) feldspars: experimental evidence of a dissolution- and diffusion-controlled mechanism. Contributions to Mineralogy and Petrology 111, 345–361.

Watson, E.B. & Jurewicz, S.R., 1984. Behavior of alkalies during diffusive interaction of granitic xenoliths with basaltic magma. Journal of Geology 92, 121–131.

Whalen, J.B., Currie, K.L. & Chappell, B.W., 1987. A-type granites: geochemical characteristics, discrimination and petrogenesis. Contributions to Mineralogy and Petrology 95, 407–419.

White, A.J.R. & Chappell, B.W., 1977. Ultrametamorphism and granitoid genesis. Tectonophysics 43, 7–22.

Wiebe, R.A., 1979. Fractionation and liquid immiscibility in an anorthositic pluton of the Nain complex, Labrador. Journal of Petrology 20, 239–269.

Wiebe, R.A., 1991. Commingling of contrasted magmas and generation of mafic enclaves in granitic rocks. In:

J. Didier & B. Barbarin (Editors), Enclaves and granite petrology. Elsevier, Amsterdam, 393–402.

Von Wolff, F., 1932. Das präkambrium Finnlands. Geologische Rundschau 23, 89–122.

Wones, D.R. & Eugster, H.P., 1965. Stability of biotite: experiment, theory, and application. American Mineralogist 50, 1228–1272.

Wyllie, P.J., Cox, K.G. & Biggar, G.M., 1962. The habit of apatite in synthetic systems and igneous rocks. Journal of Petrology 3, 238–243.

Zorpi, M.J., Coulon, C., Orsini, J.B. & Cocirta, C., 1989. Magma mingling, zoning and emplacement in calc-alkaline granitoid plutons. Tectonophysics 157, 315–329.

Appendix 1a. Electron microprobe analyses of amphiboles of the Jaala-Iitti complex.

	Hornblende granite				Hbl-qz-fsp porphyry		MME				Pillow-like MME	
Sample	91381	90561	90161	90561	90542	90542	91053A	91053C	91382	91381	90041A	9102A
	matrix	matrix	matrix	aggr.	matrix	incl. af	matrix	matrix	matrix	incl. pl	matrix	matrix
Number of analyses	1	3	3	3	3	2	5	2	3	4	2	4
SiO_2 (wt%)	40.84	40.85	40.99	41.06	40.99	41.28	45.02	41.68	41.18	41.17	46.46	43.80
Al_2O_3	8.45	8.46	8.90	8.29	8.32	8.30	7.87	8.31	8.56	9.14	6.31	7.37
TiO_2	1.73	1.64	1.36	1.84	1.57	1.32	1.46	1.51	1.68	1.52	1.19	1.53
FeO^{tot}	26.18	27.83	30.13	28.18	27.96	27.51	20.98	23.28	26.47	26.37	24.17	24.79
MnO	0.46	0.30	0.46	0.33	0.36	0.38	0.20	0.19	0.36	0.40	0.46	0.41
MgO	5.20	4.28	3.19	3.95	4.66	4.80	9.68	7.81	5.02	5.08	7.68	6.53
CaO	11.28	11.36	10.37	11.82	10.29	10.17	11.78	11.38	12.11	11.21	10.78	10.95
Na_2O	1.99	1.86	1.89	1.92	1.95	2.06	1.56	1.62	1.83	1.87	1.24	1.52
K_2O	1.51	1.11	1.35	1.51	1.44	1.39	1.25	1.02	1.46	1.53	0.69	0.83
Total	97.64	97.69	98.64	98.90	97.54	97.21	99.80	96.80	98.67	98.29	98.98	97.73
FeO*	23.57	24.68	23.76	21.48	21.62	21.42	16.99	17.55	17.86	23.05	18.09	20.15
Fe_2O_3*	2.90	3.50	7.08	7.44	7.04	6.78	4.43	6.36	9.57	3.69	6.75	5.16
Total	97.93	98.04	99.35	99.64	98.24	97.90	100.24	97.43	99.63	98.66	99.65	98.25
Formula based on 23 oxygen atoms												
Si	6.46	6.48	6.43	6.40	6.45	6.50	6.68	6.46	6.35	6.44	6.96	6.74
Al^{IV}	1.54	1.49	1.57	1.37	1.52	1.47	1.30	1.49	1.35	1.56	1.04	1.26
Fe^{3+}	0.00	0.03	0.00	0.23	0.03	0.03	0.02	0.05	0.30	0.00	0.00	0.00
T-site	8.00	8.00	8.00	8.00	8.00	8.00	8.00	8.00	8.00	8.00	8.00	8.00
Al^{VI}	0.04	0.09	0.08	0.15	0.03	0.07	0.08	0.03	0.20	0.13	0.07	0.08
Ti	0.21	0.20	0.16	0.22	0.19	0.16	0.16	0.18	0.19	0.18	0.13	0.18
Fe^{2+}	3.12	3.27	3.12	2.81	2.85	2.82	2.11	2.28	2.31	3.02	2.26	2.59
Fe^{3+}	0.35	0.42	0.84	0.86	0.83	0.80	0.49	0.74	1.10	0.43	0.76	0.60
Mn	0.06	0.04	0.06	0.04	0.05	0.05	0.02	0.02	0.05	0.05	0.06	0.05
Mg	1.23	1.01	0.74	0.92	1.09	1.13	2.14	1.80	1.15	1.19	1.72	1.50
M,1,2,3-sites	5.01	5.03	5.00	5.00	5.04	5.03	5.00	5.05	5.00	5.00	5.00	5.00
Ca	1.91	1.93	1.74	1.97	1.73	1.72	1.88	1.89	2.00	1.88	1.73	1.80
Na	0.09	0.07	0.26	0.03	0.27	0.28	0.12	0.11	0.00	0.12	0.27	0.20
M4-site	2.00	2.00	2.00	2.00	2.00	2.00	2.00	2.00	2.00	2.00	2.00	2.00
K	0.30	0.22	0.27	0.30	0.29	0.28	0.24	0.20	0.29	0.31	0.13	0.16
Na	0.52	0.50	0.32	0.55	0.33	0.35	0.32	0.38	0.55	0.45	0.09	0.26
A-site	0.82	0.72	0.59	0.85	0.62	0.63	0.56	0.58	0.84	0.76	0.22	0.42
Total	15.83	15.75	15.59	15.85	15.66	15.66	15.56	15.63	15.84	15.76	15.22	15.42
$Fe^{3+}/(Fe^{2+}+Fe^{3+})$	0.10	0.11	0.21	0.23	0.23	0.22	0.19	0.25	0.32	0.12	0.25	0.19
$Mg/(Mg+Fe^{2+})$	0.28	0.24	0.19	0.25	0.28	0.29	0.50	0.44	0.33	0.28	0.43	0.37
Al^{tot}	1.58	1.58	1.65	1.52	1.55	1.54	1.38	1.52	1.55	1.69	1.11	1.34

Appendix 1a (Continued).

	Pillow-like MME		ME	Hybrid rock								Wiborgite	
Sample	9102A	90041A	90191	90141	90501	90191	90141	90501	90191	90191	90141	Summa	Summa
	c-MME	ocelli	matrix	matrix	matrix	matrix	ocelli	ocelli	ocelli	aggr.	incl. pl	matrix	aggr.
Number of analyses	2	2	6	6	3	5	4	7	3	6	3	2	3
SiO_2 (wt%)	44.03	43.66	42.41	42.67	41.60	43.26	42.12	43.23	43.56	43.58	41.63	39.14	40.55
Al_2O_3	7.38	8.34	8.63	7.96	8.61	8.53	8.32	7.67	7.77	8.33	8.11	9.45	8.97
TiO_2	1.56	1.67	1.62	1.64	1.69	1.75	1.84	1.24	1.00	1.70	1.55	1.91	1.83
FeO^{tot}	23.14	25.07	26.43	25.32	27.36	24.16	24.67	26.51	24.14	26.64	26.18	31.62	30.26
MnO	0.40	0.47	0.35	0.34	0.35	0.29	0.33	0.39	0.28	0.28	0.37	0.40	0.33
MgO	7.09	6.75	5.52	6.20	5.11	6.39	6.92	6.07	6.94	6.07	6.26	2.36	2.84
CaO	10.87	10.75	10.68	11.32	10.05	10.73	11.51	10.59	10.62	10.77	11.53	11.87	11.39
Na_2O	1.56	1.44	2.08	1.72	1.92	1.91	1.79	1.84	1.81	1.78	1.78	1.88	1.99
K_2O	0.89	1.04	1.41	1.21	1.29	1.45	1.50	1.15	1.26	1.41	1.12	1.64	1.62
Total	96.92	99.19	99.13	98.38	97.98	98.47	99.00	98.69	97.38	100.56	98.53	100.27	99.78
FeO*	19.62	18.18	21.92	21.85	20.00	21.26	20.84	20.17	19.41	20.89	20.99	24.67	26.72
Fe_2O_3*	3.92	7.66	5.01	3.86	8.18	3.21	4.25	7.05	5.27	6.40	5.77	7.73	3.93
Total	97.32	99.96	99.63	98.77	98.80	98.78	99.42	99.40	97.92	101.21	99.11	101.05	100.17
Formula based on 23 oxygen atoms													
Si	6.80	6.59	6.53	6.60	6.45	6.65	6.48	6.63	6.72	6.57	6.45	6.14	6.38
Al^{IV}	1.20	1.41	1.47	1.37	1.51	1.35	1.47	1.34	1.25	1.39	1.45	1.54	1.62
Fe^{3+}	0.00	0.00	0.00	0.03	0.03	0.00	0.05	0.03	0.03	0.04	0.10	0.33	0.00
T-site	8.00	8.00	8.00	8.00	7.99	8.00	8.00	8.00	8.00	8.00	8.00	8.01	8.00
Al^{VI}	0.14	0.07	0.10	0.08	0.06	0.19	0.04	0.05	0.17	0.09	0.03	0.21	0.04
Ti	0.18	0.19	0.19	0.19	0.20	0.20	0.21	0.14	0.12	0.19	0.18	0.23	0.22
Fe^{2+}	2.53	2.29	2.82	2.83	2.60	2.74	2.68	2.59	2.51	2.64	2.72	3.24	3.52
Fe^{3+}	0.46	0.87	0.58	0.45	0.95	0.37	0.49	0.81	0.61	0.72	0.67	0.91	0.47
Mn	0.05	0.06	0.05	0.05	0.05	0.04	0.04	0.05	0.04	0.04	0.05	0.05	0.04
Mg	1.63	1.52	1.27	1.43	1.18	1.46	1.59	1.39	1.60	1.36	1.45	0.55	0.67
M1,2,3-sites	4.99	5.00	5.01	5.03	5.04	5.00	5.05	5.03	5.05	5.04	5.10	5.19	4.96
Ca	1.80	1.74	1.76	1.88	1.67	1.77	1.90	1.74	1.76	1.74	1.91	1.99	1.92
Na	0.20	0.26	0.24	0.12	0.33	0.23	0.10	0.26	0.24	0.26	0.09	0.01	0.08
M4-site	2.00	2.00	2.00	2.00	2.00	2.00	2.00	2.00	2.00	2.00	2.00	2.00	2.00
K	0.18	0.20	0.28	0.24	0.26	0.28	0.29	0.22	0.25	0.27	0.22	0.33	0.33
Na	0.26	0.16	0.38	0.39	0.25	0.34	0.43	0.29	0.30	0.26	0.45	0.57	0.53
A-site	0.44	0.36	0.66	0.63	0.51	0.62	0.72	0.51	0.55	0.53	0.67	0.90	0.86
Total	15.43	15.36	15.67	15.66	15.54	15.62	15.77	15.54	15.60	15.57	15.77	16.10	15.82
$Fe^{3+}/(Fe^{2+}+Fe^{3+})$	0.15	0.28	0.17	0.14	0.27	0.12	0.15	0.24	0.20	0.21	0.20	0.22	0.12
$Mg/(Mg+Fe^{2+})$	0.39	0.40	0.31	0.34	0.31	0.35	0.37	0.35	0.39	0.34	0.35	0.15	0.16
Al^{tot}	1.34	1.48	1.57	1.45	1.57	1.54	1.51	1.39	1.42	1.48	1.48	1.75	1.66

Note: ME = micro-enclave, c-MME = composite MME.

aggr. = amphibole aggregate, incl. af = amphibole inclusion in alkali feldspar, incl. pl = amphibole inclusion in plagioclase.

FeO^{tot} represents total iron.

Stoichiometric formulae were calculated based on utilization of the $Fe^{3+}/(Fe^{3+}+Fe^{2+})$ ratio iterations and assuming total cations in T, M1, M2, and M3-sites to be 13 (excluding Ca, Na, and K). Crystal-chemical limits (Robinson *et al.* 1982) are: 1) T-site (sum = 8) is filled by Si, Al^{IV}, and Fe^{3+} (if needed).
2) M4-site (sum = 2) is filled by Ca and Na. 3) M1-, M2-, and M3-sites (sum = 5) are filled by Al^{VI}, Ti, Fe^{2+}, Fe^{3+}, Mn, and Mg. 4) A-site (sum = 0–1) is filled by K and remaining Na.

* recalculated after Fe^{2+} and Fe^{3+} in formula.

Al^{tot} represent total Al.

Appendix 1b. Electron microprobe analyses of apatites of the Jaala-Iitti complex.

	Hornblende granite		MME	ME	Hybrid rock			Wiborgite	
Sample	90561	90561	91053C	90191	90141	90191	90191	Summa	Summa
	matrix	amph aggr.	matrix	matrix	matrix	matrix	amph aggr.	matrix	amph aggr.
Number of analyses	1	2	10	3	10	4	7	3	5
P_2O_5 (wt%)	41.11	42.48	41.62	40.52	41.63	42.77	41.44	41.27	40.64
CaO	55.23	54.21	57.56	54.37	53.94	54.37	55.09	54.60	53.39
FeO^{tot}	0.06	0.35	0.14	0.13	0.09	0.09	0.49	0.05	0.50
MnO	0.06	0.06	0.02	0.03	0.02	0.04	0.02	0.01	0.01
F	3.11	3.12	2.27	3.20	2.39	3.05	3.14	2.62	2.69
Cl	0.01	0.01	0.01	0.01	0.01	0.01	0.01	0.01	0.01
-O≡F,Cl	1.31	1.31	0.96	1.35	1.01	1.29	1.32	1.10	1.13
Total	98.27	98.92	100.66	96.91	97.07	99.04	98.87	97.46	96.11
Formula based on 13 oxygen atoms									
P	2.99	3.05	2.98	2.99	3.06	3.06	3.00	3.03	3.02
Ca	5.09	4.93	5.22	5.08	5.02	4.93	5.04	5.07	5.03
Fe^{tot}	0.00	0.03	0.01	0.01	0.01	0.01	0.04	0.00	0.04
Mn	0.00	0.00	0.00	0.00	0.00	0.00	0.00	0.00	0.00
F	0.85	0.83	0.61	0.88	0.66	0.82	0.85	0.72	0.75
Cl	0.00	0.00	0.00	0.00	0.00	0.00	0.00	0.00	0.00
OH*	0.15	0.16	0.39	0.12	0.34	0.18	0.15	0.28	0.25
Total	9.08	9.00	9.21	9.08	9.09	9.00	9.08	9.10	9.09

Note: ME = micro-enclave

amph aggr. = apatite in amphibole aggregate.

FeO^{tot} and Fe^{tot} represent total iron.

* calculated by assuming F + Cl + OH = 1.00.

Appendix 1c. Electron microprobe analyses of biotites of the Jaala-Iitti complex.

	Hbl-granite	Pillow-like MME		ME	Hybrid rock			Wiborgite
Sample	90161	9102A	9102A	90191	90141	90191	90501	Summa
	matrix	matrix	c-MME	matrix	matrix	matrix	matrix	matrix
Number of analyses	3	4	2	1	2	2	4	1
SiO_2 (wt%)	34.36	35.97	35.61	36.00	35.55	36.14	36.32	34.20
Al_2O_3	13.16	13.73	13.53	12.55	13.23	12.86	13.25	14.06
TiO_2	3.32	4.22	4.33	4.03	3.66	3.63	4.04	2.79
FeO^{tot}	33.12	26.59	26.37	27.82	32.01	27.96	28.64	33.59
MnO	0.31	0.17	0.18	0.22	0.21	0.13	0.15	0.14
MgO	2.51	6.98	7.04	5.27	5.13	6.14	6.29	2.06
CaO	0.02	0.04	0.01	0.00	0.02	0.02	0.02	0.03
Na_2O	0.11	0.08	0.09	0.31	0.09	0.11	0.11	0.04
K_2O	8.64	8.48	8.73	9.25	8.30	9.65	9.03	8.14
Total	95.55	96.26	95.89	95.45	98.20	96.64	97.85	95.05
FeO*	28.61	23.47	23.33	24.24	27.63	24.60	25.23	28.87
Fe_2O_3*	5.02	3.47	3.38	3.99	4.87	3.74	3.79	5.25
Total	96.06	96.61	96.23	95.86	98.69	97.02	98.23	95.58
Formula based on 22 oxygen atoms								
Si	5.55	5.56	5.54	5.69	5.51	5.65	5.59	5.53
Al^{IV}	2.45	2.43	2.46	2.31	2.42	2.34	2.37	2.47
Fe^{3+}	0.00	0.01	0.00	0.00	0.07	0.01	0.04	0.00
T-site	8.00	8.00	8.00	8.00	8.00	8.00	8.00	8.00
Al^{VI}	0.06	0.08	0.03	0.02	0.00	0.03	0.03	0.21
Ti	0.40	0.49	0.51	0.48	0.43	0.43	0.47	0.34
Fe^{2+}	3.86	3.04	3.04	3.20	3.58	3.21	3.25	3.91
Fe^{3+}	0.61	0.40	0.40	0.47	0.50	0.42	0.40	0.64
Mn	0.04	0.02	0.02	0.03	0.03	0.02	0.02	0.02
Mg	0.61	1.61	1.63	1.24	1.19	1.43	1.44	0.50
O-site	5.58	5.64	5.63	5.44	5.73	5.54	5.61	5.62
Ca	0.00	0.01	0.00	0.00	0.00	0.00	0.00	0.01
Na	0.04	0.02	0.03	0.10	0.03	0.03	0.03	0.01
K	1.78	1.68	1.73	1.86	1.64	1.92	1.77	1.68
A-site	1.82	1.71	1.76	1.96	1.67	1.95	1.80	1.70
Total	15.40	15.35	15.39	15.40	15.40	15.49	15.41	15.32
$Fe^{2+}/(Fe^{2+}+Fe^{3+})$	0.86	0.88	0.88	0.87	0.86	0.88	0.88	0.86
$Mg/(Mg+Fe^{2+})$	0.14	0.35	0.35	0.28	0.25	0.31	0.31	0.11
Fe/(Fe+Mg)	0.88	0.68	0.68	0.75	0.78	0.72	0.72	0.90
Al^{tot}	2.51	2.51	2.49	2.33	2.42	2.37	2.40	2.68

Note: Hbl-granite = hornblende granite, ME = micro-enclave, c-MME = composite MME.

FeO^{tot} represents total iron.

* FeO (and Fe_2O_3) content was recalculated by using the following empirical equation (Bruiyn *et al.* 1983):
$FeO = -10.7325 + 0.0705 \cdot SiO_2 + 0.4598 \cdot TiO_2 + 0.3067 \cdot Al_2O_3 + 0.8433 \cdot FeO^{tot} + 0.288 \cdot MnO - 0.0581 \cdot MgO - 0.0765 \cdot CaO - 1.1294 \cdot Na_2O + 0.4172 \cdot K_2O$.

Fe represents total Fe.

Al^{tot} represents total Al.

Appendix 1d. Electron microprobe analyses of plagioclases of the Jaala-Iitti complex.

	Hornblende granite					Hbl-qz-fsp porphyry		
Sample	91381	90161	90591	90591	90591	90542	90302	90302
	matrix	matrix	matrix	xcr. (core)	xcr. (rim)	matrix	matrix	phenocryst
Number of analyses	2	5	3	5	4	1	1	1
SiO_2 (wt%)	60.18	59.31	62.39	55.29	61.79	60.69	62.93	60.04
Al_2O_3	26.31	25.14	24.54	29.41	25.01	23.74	23.53	25.18
TiO_2	0.02	0.02	0.02	0.06	0.02	0.00	0.00	0.00
FeO^{tot}	0.11	0.09	0.08	0.07	0.12	0.07	0.11	0.11
MgO	0.00	0.01	0.01	0.00	0.01	0.01	0.00	0.00
CaO	6.57	5.72	5.68	10.36	5.77	5.51	4.40	5.85
Na_2O	7.66	7.57	8.56	5.25	8.01	8.80	9.12	7.98
K_2O	0.17	0.25	0.14	0.14	0.24	0.23	0.22	0.30
BaO	0.01	0.04	0.00	0.03	0.02	0.00	0.00	0.08
Total	101.03	98.15	101.42	100.61	100.99	99.05	100.31	99.54
Formula based on 8 oxygen atoms								
Si	2.65	2.68	2.73	2.47	2.72	2.73	2.78	2.68
Al	1.37	1.34	1.27	1.55	1.30	1.26	1.22	1.33
Ti	0.00	0.00	0.00	0.00	0.00	0.00	0.00	0.00
Fe^{tot}	0.00	0.00	0.00	0.00	0.00	0.00	0.00	0.00
Mg	0.00	0.00	0.00	0.00	0.00	0.00	0.00	0.00
Ca	0.31	0.28	0.27	0.50	0.27	0.27	0.21	0.28
Na	0.65	0.66	0.73	0.45	0.68	0.77	0.78	0.69
K	0.01	0.01	0.01	0.01	0.01	0.01	0.01	0.02
Ba	0.00	0.00	0.00	0.00	0.00	0.00	0.00	0.00
Total	4.99	4.97	5.01	4.98	4.98	5.04	5.00	5.00
X_{An}	0.319(8)	0.290(40)	0.266(62)	0.518(15)	0.282(80)	0.254	0.208	0.283
X_{Ab}	0.672(9)	0.695(37)	0.726(60)	0.474(15)	0.703(80)	0.733	0.779	0.699
X_{Or}	0.010(1)	0.015(3)	0.008(2)	0.008(2)	0.014(1)	0.013	0.013	0.017
X_{Cn}	0.000(0)	0.001(1)	0.000(0)	0.001(1)	0.000(0)	0.000	0.000	0.001

Appendix 1d (Continued).

	MME				Pillow-like MME				ME
Sample	91053C	91382	91382	91382	9102A	90041A	9102A	90041A	90191
	matrix	matrix	xcr. (core)	xcr. (rim)	matrix	matrix	c-MME	megacryst	matrix
Number of analyses	4	2	2	3	1	3	1	5	3
SiO_2 (wt%)	56.39	57.81	59.94	55.99	56.83	56.69	59.76	60.36	60.09
Al_2O_3	28.44	26.22	26.71	28.37	24.97	25.69	23.34	25.59	24.99
TiO_2	0.09	0.00	0.00	0.03	0.01	0.03	0.06	0.03	0.06
FeO^{tot}	0.47	0.19	0.23	0.11	0.53	0.30	0.43	0.20	0.20
MgO	0.02	0.02	0.01	0.01	0.06	0.03	0.01	0.01	0.00
CaO	9.81	8.27	6.76	9.55	7.21	6.86	5.49	6.81	6.81
Na_2O	5.67	6.83	6.46	5.70	7.46	7.57	8.71	7.21	7.77
K_2O	0.15	0.10	0.66	0.15	0.36	0.16	0.21	0.27	0.13
BaO	0.11	0.00	0.01	0.03	0.09	0.04	0.10	0.04	0.02
Total	101.15	99.44	100.78	99.94	97.52	97.37	98.11	100.52	100.07
Formula based on 8 oxygen atoms									
Si	2.51	2.60	2.65	2.51	2.62	2.61	2.72	2.67	2.68
Al	1.49	1.39	1.39	1.50	1.36	1.39	1.25	1.34	1.31
Ti	0.00	0.00	0.00	0.00	0.00	0.00	0.00	0.00	0.00
Fe^{tot}	0.02	0.01	0.01	0.00	0.02	0.01	0.02	0.01	0.01
Mg	0.00	0.00	0.00	0.00	0.00	0.00	0.00	0.00	0.00
Ca	0.47	0.40	0.32	0.46	0.36	0.34	0.27	0.32	0.33
Na	0.49	0.60	0.55	0.50	0.67	0.67	0.77	0.62	0.67
K	0.01	0.01	0.04	0.01	0.02	0.01	0.01	0.02	0.01
Ba	0.00	0.00	0.00	0.00	0.00	0.00	0.00	0.00	0.00
Total	4.99	5.01	4.96	4.98	5.05	5.03	5.04	4.98	5.01
X_{An}	0.484(23)	0.398(8)	0.351(10)	0.477(62)	0.340	0.331(66)	0.255	0.337(102)	0.324(92)
X_{Ab}	0.506(23)	0.596(7)	0.608(12)	0.514(63)	0.639	0.66(68)	0.733	0.647(92)	0.668(88)
X_{Or}	0.009(1)	0.006(0)	0.041(3)	0.009(4)	0.020	0.009(2)	0.012	0.016(10)	0.007(4)
X_{Cn}	0.002(3)	0.000(0)	0.000(0)	0.001(1)	0.002	0.001(0)	0.002	0.001(1)	0.000(0)

Appendix 1d (Continued).

	Hybrid rock									Rpk gr
Sample	90141	90501	90191	90191	90141	90141	90141	90141	90141	9014X
	matrix	matrix	matrix	phenocryst	incl. af	incl. af	incl. af	mct	plm	incl. af
Number of analyses	1	1	1	3	4	2	2	3	5	3
SiO_2 (wt%)	62.50	61.16	56.62	58.42	59.11	59.68	60.68	59.31	58.31	60.75
Al_2O_3	24.29	23.43	26.38	26.15	24.11	23.83	25.59	24.87	25.75	24.83
TiO_2	0.04	0.01	0.00	0.04	0.01	0.02	0.02	0.02	0.02	0.01
FeO^{tot}	0.09	0.09	0.07	0.27	0.17	0.24	0.20	0.11	0.11	0.39
MgO	0.00	0.01	0.00	0.02	0.00	0.00	0.01	0.01	0.00	0.01
CaO	5.51	5.50	8.52	6.90	6.40	6.60	6.54	6.71	7.37	6.22
Na_2O	7.62	8.76	6.78	7.06	8.08	7.17	7.36	7.62	7.06	7.51
K_2O	0.26	0.44	0.13	0.28	0.31	0.29	0.23	0.25	0.23	0.42
BaO	0.00	0.01	0.00	0.01	0.03	0.07	0.17	0.03	0.09	0.08
Total	100.31	99.50	98.50	99.15	98.22	97.90	100.80	98.93	98.94	100.22
Formula based on 8 oxygen atoms										
Si	2.75	2.74	2.58	2.63	2.69	2.71	2.68	2.67	2.63	2.70
Al	1.26	1.24	1.42	1.39	1.29	1.28	1.33	1.32	1.37	1.30
Ti	0.00	0.00	0.00	0.00	0.00	0.00	0.00	0.00	0.00	0.00
Fe^{tot}	0.00	0.00	0.00	0.01	0.01	0.01	0.01	0.00	0.00	0.01
Mg	0.00	0.00	0.00	0.00	0.00	0.00	0.00	0.00	0.00	0.00
Ca	0.26	0.26	0.42	0.33	0.31	0.32	0.31	0.32	0.36	0.30
Na	0.65	0.76	0.60	0.62	0.71	0.63	0.63	0.67	0.62	0.65
K	0.01	0.03	0.01	0.02	0.02	0.02	0.01	0.01	0.01	0.02
Ba	0.00	0.00	0.00	0.00	0.00	0.00	0.00	0.00	0.00	0.00
Total	4.93	5.03	5.03	5.00	5.03	4.97	4.97	4.99	4.99	4.98
X_{An}	0.281	0.251	0.407	0.345(66)	0.299(22)	0.331(11)	0.324(10)	0.323(22)	0.359(156)	0.306(41)
X_{Ab}	0.703	0.725	0.586	0.638(62)	0.683(23)	0.651(12)	0662(9)	0.663(20)	0.626(152)	0.669(48)
X_{Or}	0.016	0.024	0.008	0.017(4)	0.018(3)	0.017(1)	0.013(0)	0.014(3)	0.014(5)	0.025(9)
X_{Cn}	0.000	0.000	0.000	0.000(0)	0.000(0)	0.001(0)	0.003(0)	0.000(0)	0.002(2)	0.001(1)

Note: ME = micro-enclave, c-MME = composite MME, Rpk gr = rapakivi granite xenolith in hybrid rock.

xcr. = xenocryst, mgt= micrographic texture, plm = plagioclase mantling alkali feldspar, incl. af = inclusion in alkali feldspar.

FeO^{tot} and Fe^{tot} represent total iron.

Parenthesized numbers indicate one standard deviation of measurement in terms of least digits cited (e.g., 0.319(8) should be read 0.319±0.008).

Appendix 1e. Electron microprobe analyses of alkali feldspars of the Jaala-Iitti complex.

	Hornblende granite		Hbl-qz-fsp porphyry			Pillow-like MME
Sample	90161	90591	90302	90542	90542	9102A
	matrix	matrix	matrix	megacryst	megacryst	matrix
Number of analyses	2	3	2	3	5	1
SiO_2 (wt%)	64.56	66.21	61.94	63.83	63.94	63.04
Al_2O_3	18.65	18.74	18.77	18.31	18.81	17.94
TiO_2	0.00	0.04	0.02	0.01	0.02	0.01
FeO^{tot}	0.03	0.05	0.07	0.09	0.13	0.26
MgO	0.01	0.01	0.00	0.00	0.01	0.00
CaO	0.01	0.06	0.26	0.08	0.50	0.00
Na_2O	1.01	1.35	2.17	2.47	3.82	1.20
K_2O	15.04	13.70	12.41	12.99	10.57	14.40
BaO	0.18	0.28	0.25	0.40	0.58	0.02
Total	99.49	100.44	95.89	98.18	98.38	96.87
Formula based on 8 oxygen atoms						
Si	2.99	3.01	2.96	2.99	2.97	3.00
Al	1.02	1.00	1.06	1.01	1.03	1.00
Ti	0.00	0.00	0.00	0.00	0.00	0.00
Fe^{tot}	0.00	0.00	0.00	0.00	0.01	0.01
Mg	0.00	0.00	0.00	0.00	0.00	0.00
Ca	0.00	0.00	0.01	0.00	0.02	0.00
Na	0.09	0.12	0.20	0.22	0.34	0.11
K	0.89	0.80	0.76	0.78	0.63	0.87
Ba	0.00	0.00	0.00	0.01	0.01	0.00
Total	4.99	4.93	4.99	5.01	5.01	4.99
X_{An}	0.001(1)	0.003(5)	0.013(4)	0.004(1)	0.025(5)	0.000
X_{Ab}	0.093(37)	0.129(54)	0.207(47)	0.223(12)	0.346(18)	0.112
X_{Or}	0.904(37)	0.863(58)	0.776(43)	0.767(16)	0.622(24)	0.887
X_{Cn}	0.003(0)	0.005(3)	0.005(1)	0.007(5)	0.011(7)	0.000

Appendix 1e (Continued).

	Hybrid rock						Rpk. gr
Sample	90141	90501	90191	90141	90141	90141	9014X
	matrix	matrix	matrix	megacryst	megacryst	megacryst	megacryst
Number of analyses	2	3	2	4	4	5	4
SiO_2 (wt%)	65.20	65.15	63.39	63.92	62.73	64.82	65.37
Al_2O_3	18.02	18.81	19.24	19.10	17.88	19.12	18.54
TiO_2	0.01	0.03	0.02	0.02	0.02	0.02	0.01
FeO^{tot}	0.01	0.12	0.17	0.07	0.02	0.02	0.08
MgO	0.00	0.01	0.02	0.01	0.00	0.01	0.00
CaO	0.10	0.11	0.11	0.20	0.20	0.17	0.10
Na_2O	1.85	1.53	0.88	2.43	0.90	2.36	2.24
K_2O	12.49	13.81	14.55	12.25	15.01	11.70	12.48
BaO	0.46	0.26	0.27	0.35	0.03	2.29	1.00
Total	98.14	99.83	98.65	98.35	96.79	100.51	99.82
Formula based on 8 oxygen atoms							
Si	3.03	2.99	2.96	2.97	2.99	2.97	3.00
Al	0.99	1.02	1.06	1.05	1.00	1.03	1.00
Ti	0.00	0.00	0.00	0.00	0.00	0.00	0.00
Fe^{tot}	0.00	0.00	0.01	0.00	0.00	0.00	0.00
Mg	0.00	0.00	0.00	0.00	0.00	0.00	0.00
Ca	0.01	0.01	0.01	0.01	0.01	0.01	0.00
Na	0.17	0.14	0.08	0.22	0.08	0.21	0.20
K	0.74	0.81	0.87	0.73	0.91	0.69	0.73
Ba	0.01	0.00	0.00	0.01	0.00	0.04	0.02
Total	4.95	4.97	4.99	4.99	4.99	4.95	4.95
X_{An}	0.006(0)	0.006(2)	0.006(0)	0.010(9)	0.010(21)	0.009(8)	0.005(1)
X_{Ab}	0.183(11)	0.144(57)	0.084(2)	0.229(19)	0.082(115)	0.233(83)	0.213(65)
X_{Or}	0.804(8)	0.846(63)	0.905(4)	0.755(28)	0.908(110)	0.726(100)	0.767(66)
X_{Cn}	0.009(3)	0.005(4)	0.005(2)	0.007(3)	0.001(0)	0.044(19)	0.019(5)

Note: Rpk gr = rapakivi granite xenolith in hybrid rock.

FeO^{tot} and Fe^{tot} represent total iron.

Parenthesized numbers indicate one standard deviationof measurement in terms of least digits cited (e.g., 0.001(1) should be read 0.001±0.001).

Appendix 1f. Electron microprobe analyses of ilmenites of the Jaala-Iitti complex.

	Hbl-gr.	HQF porphyry		Micro-enclave			Hybrid rock							
Sample	90561	91402	91402	90191	90191	90191	90141	91501	90191	90491E	90191	90141	90141	90491E
	amph	matrix	matrix	matrix	amph	biot	matrix	matrix	matrix	matrix	aggr.	ocelli	matrix	matrix
	grain	lamell	grain	grain	grain	grain	grain	grain	grain	grain	grain	grain	lamell	lamell
Number of analyses	5	4	3	3	2	1	4	2	5	6	2	3	6	5
FeO^{tot} (wt%)	48.30	47.21	45.01	45.70	47.23	46.98	48.29	47.49	46.99	45.23	45.85	48.24	49.04	48.27
TiO_2	49.98	49.81	49.53	50.46	51.10	51.56	49.00	51.90	50.25	48.99	51.78	49.45	48.75	49.82
MnO	1.23	1.64	0.90	1.31	1.29	1.50	2.04	1.10	1.17	1.16	2.20	1.74	1.21	1.15
MgO	0.01	0.02	0.00	0.01	0.00	0.02	0.01	0.03	0.02	0.00	0.01	0.02	0.01	0.00
Cr_2O_3	0.01	0.00	0.01	0.00	0.02	0.00	0.00	0.00	0.01	0.03	0.01	0.00	0.03	0.01
V_2O_3	1.39	1.04	0.18	1.40	1.53	1.66	1.40	0.00	1.50	0.19	1.58	1.35	1.34	1.10
Al_2O_3	0.01	0.01	0.05	0.01	0.01	0.01	0.00	0.01	0.01	0.02	0.01	0.00	0.02	0.02
Total	100.93	99.73	95.68	98.89	101.18	101.74	100.75	100.53	99.95	95.62	101.44	100.80	100.40	100.37
FeO*	43.68	43.09	43.63	44.02	44.63	44.80	41.98	45.50	43.95	42.87	44.32	42.67	42.59	43.63
Fe_2O_3*	5.13	4.57	1.54	1.87	2.88	2.42	7.02	2.21	3.38	2.63	1.71	6.20	7.16	5.16
Total	101.44	100.20	95.84	99.08	101.47	101.97	101.45	100.75	100.30	95.88	101.61	101.43	101.11	100.89
Formula based on 3 oxygen atoms														
Fe^{2+}	0.91	0.91	0.97	0.94	0.93	0.93	0.88	0.96	0.94	0.95	0.92	0.89	0.89	0.92
Fe^{3+}	0.10	0.08	0.03	0.03	0.05	0.05	0.13	0.04	0.06	0.05	0.03	0.11	0.13	0.10
Ti	0.94	0.95	0.98	0.97	0.96	0.96	0.92	0.98	0.95	0.97	0.97	0.93	0.92	0.94
Mn	0.03	0.04	0.02	0.03	0.03	0.03	0.04	0.02	0.02	0.03	0.05	0.04	0.03	0.02
Mg	0.00	0.00	0.00	0.00	0.00	0.00	0.00	0.00	0.00	0.00	0.00	0.00	0.00	0.00
Cr	0.00	0.00	0.00	0.00	0.00	0.00	0.00	0.00	0.00	0.00	0.00	0.00	0.00	0.00
V	0.03	0.02	0.00	0.03	0.03	0.03	0.03	0.00	0.03	0.00	0.03	0.03	0.03	0.02
Al	0.00	0.00	0.00	0.00	0.00	0.00	0.00	0.00	0.00	0.00	0.00	0.00	0.00	0.00
Total	2.00	2.00	2.00	2.00	2.00	2.00	2.00	2.00	2.00	2.00	2.00	2.00	2.00	2.00
X_{ILM}	0.950	0.955	0.985	0.982	0.972	0.977	0.932	0.979	0.967	0.974	0.983	0.940	0.930	0.950
X_{HEM}	0.050	0.045	0.015	0.018	0.028	0.023	0.068	0.021	0.033	0.026	0.017	0.060	0.070	0.050

Note: Hbl-gr. = hornblende granite; HQF porphyry = hornblende quartz-feldspar porphyry

amph = ilmenite inclusion in amphibole; biot = ilmenite inclusion in biotite; aggr. = ilmenite inclusion in amphibole aggregate.

FeO^{tot} represent total iron.

Fe^{2+} and Fe^{3+} in formula were calculated from stoichiometry and charge balance.

* recalculated after Fe^{2+} and Fe^{3+} in formula.

$X_{ILM} = (\sqrt{Fe^{2+} \cdot Ti}) / [(0.5 \cdot Fe^{3+}) + \sqrt{Fe^{2+} \cdot Ti}]$; $X_{HEM} = 1 - X_{ILM}$ (Stormer 1983).

Appendix 1g. Electron microprobe analyses of magnetites of the Jaala-Iitti complex.

	Hbl-granite	HQF porphyry	Hybrid rock					
Sample	90561	91402	91501	90191	90491E	90191	90141	90491E
	amph aggr.	matrix	matrix	matrix	matrix	amph aggr.	matrix	matrix
	grain	lamell	grain	grain	grain	grain	lamell	lamell
Number of analyses	3	6	2	3	1	3	6	4
FeO^{tot} (wt%)	93.20	92.84	84.70	92.13	84.02	93.09	90.38	89.11
TiO_2	2.87	1.43	8.02	3.00	5.48	2.80	3.23	4.19
MnO	0.11	0.04	0.29	0.11	0.28	0.09	0.08	0.10
MgO	0.00	0.01	0.00	0.00	0.03	0.01	0.01	0.04
Cr_2O_3	0.05	0.03	0.00	0.20	0.02	0.09	0.21	0.07
V_2O_3	0.56	0.14	0.00	1.38	0.91	0.77	1.89	0.77
Al_2O_3	0.38	0.26	0.75	0.35	0.74	0.35	0.32	0.45
Total	97.17	94.75	93.76	97.17	91.48	97.20	96.12	94.73
FeO*	34.80	32.80	38.01	34.90	35.00	34.75	34.76	35.09
Fe_2O_3*	64.90	66.72	51.88	63.60	54.48	64.83	61.81	60.04
Total	103.67	101.43	98.95	103.54	96.94	103.69	102.31	100.75
Formula based on 4 oxygen atoms								
Fe^{2+}	1.08	1.04	1.22	1.08	1.15	1.08	1.09	1.12
Fe^{3+}	1.80	1.91	1.51	1.77	1.62	1.80	1.74	1.72
Ti	0.08	0.04	0.23	0.08	0.16	0.08	0.09	0.12
Mn	0.00	0.00	0.01	0.00	0.01	0.00	0.00	0.00
Mg	0.00	0.00	0.00	0.00	0.00	0.00	0.00	0.00
Cr	0.00	0.00	0.00	0.01	0.00	0.00	0.01	0.00
V	0.02	0.00	0.00	0.04	0.03	0.02	0.06	0.02
Al	0.02	0.01	0.03	0.02	0.03	0.02	0.01	0.02
Total	3.00	3.00	3.00	3.00	3.00	3.00	3.00	3.00
X_{USP}	0.082	0.041	0.239	0.089	0.171	0.081	0.098	0.125
X_{MAG}	0.918	0.959	0.761	0.911	0.829	0.919	0.902	0.875

Note: Hbl-granite = hornblende granite; HQF porphyry = hornblende quartz-feldspar porphyry

amph aggr. = magnetite inclusion in amphibole aggregate.

FeO^{tot} represents total iron.

Fe^{2+} and Fe^{3+} in formula were calculated from stoichiometry and charge balance.

* recalculated after Fe^{2+} and Fe^{3+} in formula.

$X_{USP} = \{Ti[Fe^{2+}/(Fe^{2+}+Mn+Mg)]\}/\{\{Ti[Fe^{2+}/(Fe^{2+}+Mn+Mg)]\}+\{0.5\cdot Fe^{3+}[Fe^{3+}/(Fe^{3+}+Cr+V+Al)]\}\}$, $X_{MAG} = 1 - X_{USP}$ (Stormer 1983).

Appendix 1h. Electron microprobe analyses of pyroxenes of the Jaala-Iitti complex.

	MME					Hybrid rock			
Sample	91053E enstatite phcr.	91053A pigeonite phcr. (core)	91053A pigeonite phcr. (rim)	91053C augite matrix	91053A augite matrix	90141 ferrosilite matrix	90141 pigeonite matrix	90141 pigeonite matrix	90141 augite ocelli
Number of analyses	2	3	2	2	1	1	2	1	2
SiO_2 (wt%)	51.31	50.02	50.01	48.38	50.72	49.11	51.74	48.57	51.58
Al_2O_3	2.41	0.77	0.33	3.31	0.74	0.12	0.79	0.49	0.71
TiO_2	0.48	0.24	0.16	0.24	0.20	0.03	0.22	0.31	0.10
FeO^{tot}	19.24	28.60	32.24	26.57	18.15	40.61	31.41	35.64	26.18
MnO	0.29	0.60	0.64	0.37	0.40	1.34	0.70	0.86	0.47
MgO	22.46	12.01	11.09	6.85	8.34	4.31	9.18	5.96	7.50
CaO	2.26	7.16	5.11	11.50	19.91	1.13	3.57	5.25	11.06
Na_2O	0.10	0.17	0.00	0.63	0.13	0.08	0.19	0.14	0.25
K_2O	0.00	0.01	0.01	0.19	0.07	0.00	0.08	0.02	0.13
Cr_2O_3	0.08	0.00	0.00	0.01	0.00	0.00	0.01	0.00	0.00
NiO	0.02	0.04	0.03	0.01	0.00	0.03	0.00	0.02	0.02
ZnO	0.02	0.05	0.08	0.05	0.05	0.14	0.11	0.18	0.07
Total	98.67	99.67	99.70	98.11	98.71	96.90	98.00	97.44	98.07
FeO*	18.01	27.86	32.24	26.54	18.15	40.61	31.41	35.64	26.18
Fe_2O_3*	1.37	0.82	0.00	0.03	0.00	0.00	0.00	0.00	0.00
Total	98.81	99.75	99.70	98.11	98.71	96.90	98.00	97.44	98.07
Formula based on 6 oxygen atoms									
Si	1.92	1.97	1.99	1.95	1.99	2.08	2.07	2.03	2.06
Al	0.11	0.04	0.02	0.16	0.03	0.01	0.04	0.02	0.03
Ti	0.01	0.01	0.00	0.01	0.01	0.00	0.01	0.01	0.00
Fe^{2+}	0.56	0.92	1.08	0.89	0.60	1.44	1.05	1.24	0.87
Fe^{3+}	0.04	0.02	0.00	0.00	0.00	0.00	0.00	0.00	0.00
Mn	0.01	0.02	0.02	0.01	0.01	0.05	0.02	0.03	0.02
Mg	1.25	0.71	0.66	0.41	0.49	0.27	0.55	0.37	0.45
Ca	0.09	0.30	0.22	0.50	0.84	0.05	0.15	0.23	0.47
Na	0.01	0.01	0.00	0.05	0.01	0.01	0.01	0.01	0.02
K	0.00	0.00	0.00	0.01	0.00	0.00	0.00	0.00	0.01
Cr	0.00	0.00	0.00	0.00	0.00	0.00	0.00	0.00	0.00
Ni	0.00	0.00	0.00	0.00	0.00	0.00	0.00	0.00	0.00
Zn	0.00	0.00	0.00	0.00	0.00	0.00	0.00	0.01	0.00
Total	4.00	4.00	3.99	3.99	3.98	3.91	3.90	3.95	3.93
Fe/(Fe+Mg)	0.31	0.57	0.62	0.69	0.55	0.84	0.66	0.77	0.66
X_{Wo}	0.046	0.153	0.110	0.273	0.433	0.028	0.086	0.125	0.262
X_{En}	0.641	0.358	0.334	0.227	0.252	0.150	0.309	0.197	0.247
X_{Fs}	0.313	0.489	0.555	0.500	0.315	0.821	0.605	0.678	0.492

Note: phcr. = phenocryst.

FeO^{tot} represents total iron.

Fe^{2+} and Fe^{3+} in formula werecalculatedfrom stoichiometryand charge balance.

* recalculated after Fe^{2+} and Fe^{3+} in formula.

X_{Wo} = Ca/(Ca+Mg+ΣFe), X_{En} = Mg/(Mg+Ca+ΣFe), and X_{Fs} = ΣFe/(ΣFe+Ca+Mg); ΣFe = Fe^{2+}+Fe^{3+}+Mn (Morimoto 1988).

Appendix 1i. Electron microprobe analyses of olivines of the Jaala-Iitti complex.

	Hbl-qz-fsp porphyry		Hybrid rock
Sample	90542	90302	90141
Number of analyses	2	4	4
SiO_2	30.36	30.21	30.31
Al_2O_3	0.43	0.01	0.01
TiO_2	0.01	0.01	0.04
FeO^{tot}	64.87	66.72	65.36
MnO	1.31	1.58	2.01
MgO	1.69	1.70	1.74
CaO	0.10	0.05	0.05
Cr_2O_3	0.00	0.00	0.01
NiO	0.04	0.01	0.02
ZnO	0.10	0.11	0.11
Total	99.07	100.44	99.76
FeO*	62.09	66.24	64.86
Fe_2O_3*	3.08	0.53	0.57
Total	99.37	100.49	99.83
Formula based on 4 oxygen atoms			
Si	1.01	1.00	1.01
Al	0.02	0.00	0.00
Ti	0.00	0.00	0.00
Fe^{2+}	1.72	1.84	1.81
Fe^{3+}	0.08	0.01	0.01
Mn	0.04	0.04	0.06
Mg	0.08	0.08	0.09
Ca	0.00	0.00	0.00
Cr	0.00	0.00	0.00
Ni	0.00	0.00	0.00
Zn	0.00	0.00	0.00
Total	2.95	2.97	2.99
X_{Fo}	0.043	0.042	0.044
X_{Fa}	0.957	0.958	0.956

Note: FeO^{tot} represents total iron.

Fe^{2+} and Fe^{3+} in formula werecalculated from stoichiometryand charge balance

* recalculated after Fe^{2+} and Fe^{3+} in formula.

$X_{Fo} = Mg/(Mg+Fe^{2+}+Fe^{3+}+Mn)$, $X_{Fa} = 1 - X_{Fo}$.

Appendix 2a. Chemical composition of hornblende granites, hornblende-quartz-feldspar porphyries, and a rapakivi granite xenolith in the Jaala-Iitti complex.

	Hornblende granite										Hbl-qz-fsp porphyry				Rpk gr
Sample	90591	91381	90361	90461	90561	91101	90451	90291	91052A	90161	91402	90542	91302	HQFP	9014X
SiO_2 (wt%)	66.70	66.80	67.10	66.40	66.80	66.80	66.90	67.10	67.80	67.90	68.20	67.60	69.30	68.37	68.00
TiO_2	0.80	1.00	0.85	0.83	0.82	0.81	0.81	0.80	0.66	0.69	0.72	0.75	0.65	0.70	0.50
Al_2O_3	13.30	12.60	13.20	12.70	13.20	12.90	13.00	13.40	13.30	13.20	13.40	13.40	13.40	13.40	14.30
Fe_2O_3	2.28	2.21	2.65	1.58	1.88	2.06	1.94	1.92	1.43	1.75	1.73	1.87	1.33	1.64	1.33
FeO	4.20	4.40	3.80	4.50	4.70	4.60	4.40	4.60	3.70	4.10	3.80	4.40	3.90	4.03	3.10
MnO	0.09	0.09	0.09	0.10	0.09	0.10	0.10	0.09	0.08	0.08	0.07	0.09	0.09	0.08	0.70
MgO	0.69	0.78	0.79	0.72	0.72	0.50	0.71	0.65	0.57	0.67	0.52	0.57	0.45	0.51	0.43
CaO	2.25	2.71	2.07	2.12	2.32	2.50	2.55	2.41	2.42	2.19	2.50	2.57	2.27	2.45	2.09
Na_2O	3.07	2.64	3.08	2.94	3.09	2.79	2.89	3.08	3.07	3.13	3.04	3.14	3.00	3.06	2.89
K_2O	4.95	4.77	5.06	4.98	4.84	4.86	4.83	5.03	4.82	4.78	4.83	4.95	4.95	4.91	6.07
P_2O_5	0.19	0.29	0.22	0.21	0.19	0.21	0.23	0.19	0.17	0.18	0.20	0.18	0.17	0.18	0.12
H_2O+	0.70	0.70	0.90	0.80	0.80	0.80	0.70	0.70	0.50	0.70	0.40	0.40	0.30	0.37	0.50
L.O.I.	0.77	0.50	0.85	0.85	0.77	0.54	0.70	0.77	0.25	0.70	0.23	0.31	0.08	0.21	0.70
Total	100.00	99.40	100.40	98.70	100.20	99.40	99.80	100.80	98.80	100.00	99.90	100.60	100.20	100.23	100.30
Trace elements in ppm															
F	1200	2100	1190	1700	1500	1500	1400	1300	1300	1600	1600	1400	1500	1500	480
Cl	303	499	336	354	298	356	318	339	491	402	373	292	366	344	300
Ba	1160	885	1070	1090	1210	1190	1190	1110	993	785	1210	1230	1170	1203	1740
Zr	494	438	424	444	534	532	479	483	466	371	493	492	483	489	568
Rb	216	235	199	204	182	202	196	211	200	250	193	195	216	201	179
Sr	166	158	106	102	176	146	154	173	166	138	157	182	146	162	241
Zn	112	118	75.1	107	108	130	117	102	114	108	177	125	103	135	110
V	37	31	23	22	36	14	16	32	18	20	12	39	13	21	22
Y	67	71	43	39	70	82	82	69	53	83	86	60	53	66	43
Nb	24	27	25	21	29	22	22	33	22	35	20	34	20	25	33
Ga	25.4	28	28	29	26.5	26.1	22.5	27	26	25.9	23.3	24.8	24.3	24.1	26.3
Cr	8	9	11	8	13	<2	15	6	11	9	16	14	23	18	8
Sc	10.2	12.6	9.46	8.99	10.5	12.9	12.6	9.81	9.47	9.94	10.9	9.24	9.28	9.8	7.59
Ni	3	<1	<1	<1	2	2	2	2	<1	2	4	2	<1	3	1
Th	23	29	18	19	20	20	20	16	19	25	17	17	21	18	8
U	7.1	5.4	5.2	6.2	6.9	6.5	5	3.5	6	6.6	6.5	5.4	7.4	6.4	1.5
Ta	2	1.7	<1	<1	1	2	2	1	1.5	1	2	<1	1	1.5	1
La	81.5	124.0	81.4	93.1	88.5	76.2	73.2	83.2	79.7	76.4	75.7	78.3	71.7	75.2	77.6
Ce	165	233	167	188	177	151	145	170	153	166	145	161	140	149	165
Pr	17.8	29.8	18.6	20.9	19.5	19.2	16.7	18.2	19.9	17.4	17.5	17.3	16.7	17.2	19.5
Nd	79.9	111	74.1	84.3	92.6	75.5	65.9	75.1	77.6	72.6	70.9	76.4	65.3	70.9	81.2
Sm	14.5	18.9	15.3	16.6	15.5	13.9	12.1	13.6	13.5	13.3	13.1	13.3	12.2	12.9	14.1
Eu	2.22	2.51	2.34	2.38	2.11	2.27	2.04	2.17	2.38	1.78	2.17	2.30	1.93	2.13	2.96
Gd	11.4	17	14.1	15	11.8	12.8	11.4	11.5	12.8	10.8	12	10.9	10.9	11.3	11.6
Tb	1.7	2.7	1.9	2	1.9	1.9	1.8	1.8	1.9	1.7	1.8	1.7	1.6	1.7	1.7
Dy	10.8	14.2	11.2	12.1	11.9	10.4	9.6	10.6	10.6	9.8	9.8	10.6	8.8	9.7	9.6
Ho	2.13	2.81	2.04	2.21	2.34	2.09	1.89	2.11	2.09	1.97	2.07	2.16	1.79	2.01	1.79
Er	6.3	8.3	5.9	6.5	6.6	6.6	5.7	6.1	6.1	5.9	6.4	5.9	5.5	5.9	4.6
Tm	0.9	1.2	0.7	0.8	0.9	0.9	0.9	0.8	0.9	0.8	0.8	0.8	0.8	0.8	0.6
Yb	5.8	7.9	5.4	5.8	6.2	5.9	5.3	5.6	5.7	5.6	5.4	5.6	4.8	5.3	3.7
Lu	0.84	1.24	0.88	0.88	0.88	0.88	0.86	0.78	0.89	0.76	0.90	0.83	0.76	0.83	0.53
C.I.P.W. norms															
Q	26.90	23.72	24.36	24.44	23.45	25.57	24.86	23.07	25.71	25.34	25.84	23.45	26.61	25.30	21.67
Zr	0.09	0.10	0.09	0.09	0.11	0.11	0.10	0.10	0.10	0.08	0.10	0.10	0.10	0.10	0.11
Or	28.77	29.78	30.31	30.40	29.07	29.35	29.10	30.03	29.14	28.73	28.91	29.47	29.48	29.29	36.11
Ab	21.22	25.46	25.34	24.55	25.61	22.98	23.90	25.24	25.02	25.63	24.86	25.83	24.42	25.04	23.67
An	9.40	8.53	7.89	7.55	8.48	9.08	8.91	8.51	9.26	8.61	9.37	8.38	9.14	8.96	8.71
Hl	0.08	0.05	0.06	0.06	0.05	0.06	0.05	0.06	0.08	0.07	0.06	0.05	0.06	0.06	0.05
Di	1.53	1.24	0.78	1.28	1.47	1.67	1.93	1.84	1.42	0.69	1.34	2.66	0.70	1.57	1.14
Hy	6.05	5.87	5.19	7.15	7.04	6.12	6.24	6.44	5.49	6.50	5.16	5.56	5.96	5.56	5.55
Mt	3.26	3.36	3.88	2.36	2.76	3.04	2.86	2.80	2.12	2.57	2.53	2.72	1.94	2.40	1.94
Il	1.93	1.54	1.63	1.61	1.58	1.57	1.56	1.53	1.27	1.33	1.38	1.43	1.23	1.35	0.95
Ap	0.71	0.47	0.54	0.52	0.47	0.52	0.56	0.46	0.42	0.44	0.49	0.44	0.41	0.45	0.30
Fl	0.78	0.44	0.42	0.66	0.57	0.56	0.51	0.48	0.49	0.61	0.61	0.53	0.57	0.57	0.16
Mg#[a]	18.80	20.39	21.14	20.32	19.11	13.98	19.50	17.72	19.34	19.85	16.91	16.42	15.62	16.32	17.33
NK/A[b]	0.78	0.75	0.80	0.81	0.78	0.76	0.77	0.78	0.77	0.78	0.76	0.79	0.77	0.77	0.79
A/CNK[c]	0.92	0.87	0.92	0.90	0.91	0.90	0.89	0.90	0.91	0.92	0.91	0.88	0.93	0.91	0.95
Ga/Al[d]	3.61	4.20	4.01	4.31	3.79	3.82	3.27	3.81	3.69	3.71	3.29	3.50	3.43	3.40	3.48
R_1[e]	2000	2193	1998	2028	2021	2121	2108	2002	2143	2117	2166	2041	2234	2147	1951
R_2[f]	536	576	520	512	543	545	563	553	548	526	556	566	528	550	525
ANOR/Q[g]	0.92	0.94	0.85	0.81	0.96	0.92	0.94	0.96	0.94	0.91	0.95	0.94	0.89	0.93	0.90

Appendix 2b. Chemical composition of MMEs and pillow-like MMEs in the Jaala-Iitti complex.

	MME								Pillow-like MME			
Sample	90042A	91053A	91053B	91382	91053C	91053E	91053F	MME[p]	91022D	90032	90042B	90042C
SiO_2 (wt%)	50.30	50.80	51.20	55.10	56.90	51.80	59.20	50.77	55.70	55.70	57.30	61.40
TiO_2	2.95	2.74	2.72	2.38	1.87	2.57	1.74	2.80	2.15	2.02	1.89	1.33
Al_2O_3	13.20	13.60	13.80	12.00	15.20	13.80	13.90	13.53	14.00	13.50	14.00	13.90
Fe_2O_3	3.20	2.53	2.53	2.74	2.33	1.99	1.64	2.75	2.26	2.33	1.94	1.49
FeO	10.80	11.40	11.40	10.40	7.80	10.90	7.70	11.20	9.30	8.70	8.60	6.70
MnO	0.22	0.20	0.20	0.18	0.14	0.18	0.14	0.21	0.17	0.17	0.16	0.12
MgO	3.75	3.85	3.92	1.98	1.98	3.38	2.28	3.84	2.69	2.90	2.58	1.53
CaO	6.67	7.81	7.68	5.99	6.50	6.99	4.82	7.39	5.87	5.34	5.47	4.14
Na_2O	3.04	2.79	2.77	2.41	2.84	2.82	3.01	2.87	2.96	2.89	3.07	3.18
K_2O	2.03	1.83	1.94	3.81	3.07	2.52	3.72	1.93	2.67	3.31	2.92	3.85
P_2O_5	0.66	0.64	0.63	0.72	0.50	0.60	0.45	0.64	0.52	0.47	0.39	0.29
H_2O+	1.30	0.90	0.90	0.70	0.60	0.80	1.20	1.03	1.00	1.60	1.00	0.60
L.O.I.	1.08	0.30	0.25	0.31	0.35	0.20	0.90	0.54	0.54	1.10	1.00	0.54
Total	99.20	99.90	100.40	99.30	100.50	99.10	100.60	99.83	100.00	99.50	100.50	99.40
Trace elements in ppm												
F	3000	2300	2500	8000	1100	2660	1450	2600	1400	1800	1100	1100
Cl	325	199	210	380	278	142	395	245	890	324	333	252
Ba	610	571	602	829	761	639	1080	594	759	759	910	1020
Zr	277	253	246	354	320	237	268	259	340	335	331	348
Rb	123	62	60	210	127	77	117	82	111	135	102	125
Sr	251	332	325	164	304	254	227	303	273	246	264	246
Zn	168	185	171	193	138	139	131	175	169	187	147	127
V	234	240	233	202	115	233	120	236	157	146	166	97
Y	52	46	43	73	44	39	37	47	48	44	66	49
Nb	16	19	15	23	17	17	15	17	18	17	19	25
Ga	31.1	25	25	29.5	25	26	24	27.0	25.2	24	27	25.6
Cr	41	41	49	9	19	43	27	44	30	38	32	25
Sc	30.4	30.8	29.6	27.1	20	26.8	18.9	30.3	24	21.9	18.6	14.4
Ni	17	20	19	3	4	16	9	19	15	12	13	7
Th	4.8	4.3	4.6	14	8.3	4.7	7.3	5	8.1	9.3	8.6	12
U	3.1	1.3	1.5	4	2.7	1.4	2.3	2.0	3.1	3	2.7	3.7
Ta	1	0.6	0.6	1	1	<1	<1	0.7	1	0.9	1	1
La	41.0	50.5	47.1	97.3	56.8	41.9	46.5	46.2	46.8	53.3	48.2	61.5
Ce	84	101	93	195	110	89	98	93	94	104	104	130
Pr	10.9	13.9	12.7	23.2	14.9	10.6	11.7	12.5	11.9	14.2	10.1	13.7
Nd	46.7	57.7	54.1	90.1	62.3	46.8	50.1	52.8	49.3	58.5	49.3	51.3
Sm	9.4	11.1	10.3	17	11.5	10.2	10.7	10.3	9.9	10.6	9.8	10.3
Eu	2.37	2.91	2.80	2.53	2.77	2.50	2.49	2.69	2.29	2.59	2.16	1.92
Gd	9.6	10.9	10.5	15.6	11.1	9.5	9.4	10.3	9.8	10.5	9.5	9.3
Tb	1.4	1.7	1.6	2.3	1.7	1.4	1.4	1.6	1.4	1.6	1.5	1.3
Dy	7.7	9.3	8.5	12.2	9	8	8	8.5	7.8	8.7	7.8	7.3
Ho	1.59	1.81	1.73	2.41	1.78	1.53	1.48	1.71	1.53	1.73	1.48	1.47
Er	4.9	5.2	4.8	7.9	5	4.4	4.2	5.0	4.7	5	4.9	4.7
Tm	0.7	0.7	0.7	1.1	0.7	0.6	0.5	0.7	0.7	0.7	0.7	0.6
Yb	4.1	4.7	4.4	6.5	4.8	3.9	3.8	4.4	4	4.6	4	3.8
Lu	0.62	0.77	0.73	1.06	0.74	0.65	0.58	0.71	0.65	0.72	0.59	0.60
C.I.P.W. norms												
Q	4.54	4.01	4.06	11.34	11.33	4.15	12.83	4.20	11.24	9.60	11.23	15.78
Zr	0.06	0.05	0.05	0.07	0.06	0.05	0.05	0.05	0.07	0.07	0.07	0.07
Or	12.44	11.04	11.63	23.13	18.35	15.30	22.34	11.70	16.10	20.15	17.59	23.28
Ab	25.57	23.44	23.09	19.72	23.41	24.03	24.64	24.03	22.80	24.14	25.42	26.71
An	17.45	19.88	20.09	11.53	20.30	18.25	14.29	19.14	18.77	15.02	16.63	12.98
Hl	0.06	0.03	0.04	0.06	0.05	0.02	0.07	0.04	0.15	0.05	0.06	0.04
Di	9.59	12.50	11.56	9.26	7.65	10.64	5.86	11.22	6.21	7.36	7.12	5.17
Hy	18.01	18.46	18.99	13.88	10.77	18.11	13.13	18.49	15.88	15.07	14.52	10.56
Mt	4.79	3.74	3.71	4.07	3.41	2.95	2.42	4.08	3.33	3.47	2.86	2.21
Cm	0.01	0.01	0.01	0.00	0.00	0.01	0.01	0.01	0.01	0.01	0.01	0.01
Il	5.79	5.30	5.23	4.63	3.58	5.00	3.35	5.44	4.15	3.94	3.65	2.58
Ap	1.62	1.55	1.52	1.76	1.20	1.46	1.09	1.56	1.26	1.15	0.95	0.71
Fl	1.03	0.73	0.81	3.12	0.27	0.90	0.44	0.57	0.39	0.59	0.32	0.36
Mg#[a]	36.50	37.12	37.54	24.40	29.56	35.84	34.25	37.06	33.23	36.03	34.34	28.52
R_1[e]	1341	1515	1523	1505	1740	1441	1705	1460	1664	1558	1707	1802
R_2[f]	1159	1293	1287	975	1092	1186	901	1246	1036	980	988	792
ANOR/Q[g]	12.86	16.03	15.60	2.93	4.64	13.11	3.04	14.76	4.79	4.45	4.33	2.27

Appendix 2c. Chemical composition of hybrid rocks in the Jaala-Iitti complex.

	Hybrid rock						
Sample	90141A	90141B	90501	90191	90041	91021	90491E
SiO_2 (wt%)	63.10	64.00	65.00	65.50	66.30	65.80	68.10
TiO_2	1.17	1.17	1.17	1.17	0.88	1.08	0.87
Al_2O_3	13.80	13.70	13.20	13.00	13.40	12.80	13.10
Fe_2O_3	1.42	1.38	1.76	2.07	1.93	2.07	1.53
FeO	5.90	6.00	5.40	5.10	4.40	5.80	4.50
MnO	0.12	0.11	0.10	0.10	0.10	0.11	0.08
MgO	1.30	1.42	1.13	1.16	0.74	1.09	0.80
CaO	3.78	3.52	3.15	3.29	2.54	2.92	2.68
Na_2O	3.15	3.06	2.93	2.88	3.03	2.56	2.76
K_2O	4.19	4.14	4.63	4.42	4.78	4.17	4.81
P_2O_5	0.25	0.26	0.27	0.26	0.24	0.29	0.22
H_2O+	0.60	0.90	0.50	0.50	1.00	1.10	0.50
L.O.I.	0.62	0.77	0.70	0.85	0.80	0.77	0.07
Total	99.70	100.40	100.30	100.60	99.90	100.30	100.10
Trace elements in ppm							
F	1200	1300	1400	1600	1130	830	2100
Cl	386	393	457	275	325	510	381
Ba	990	995	1050	982	1210	1010	1000
Zr	373	362	415	365	401	513	400
Rb	158	164	176	175	176	163	219
Sr	219	199	196	190	126	163	167
Zn	118	138	103	136	109	119	106
V	89	88	88	82	29	36	51
Y	60	67	65	72	34	57	78
Nb	27	23	27	21	24	23	38
Ga	29	27.6	25.7	27	28	24.6	26.5
Cr	15	18	11	13	16	21	17
Sc	12.3	12.9	11.9	12.5	9.61	14.6	9.79
Ni	7	7	3	5	2	4	2
Th	14	14	17	17	16	15	25
U	4.2	4.3	3.5	4.7	4.2	4.7	5.2
Ta	1	1	1	2	<1	1	1
La	68.6	71.5	73.2	82.1	71.6	59.0	105.0
Ce	139	146	158	167	151	125	211
Pr	14.6	15.5	17	17.8	17.2	15.2	22.2
Nd	66	68.3	71.4	74.7	69.1	62.6	85.6
Sm	12.1	12.3	12.6	13.6	14.6	12	15
Eu	2.25	2.36	2.07	2.12	2.64	2.00	2.05
Gd	10.9	10.9	10.5	11.1	13.1	11.2	12.1
Tb	1.7	1.6	1.6	1.7	1.8	1.8	1.9
Dy	9.5	9.5	9.9	10.2	10.7	9.5	11.5
Ho	1.84	1.79	1.85	1.90	1.91	2.00	2.27
Er	5	5.3	5.6	5.4	5.6	5.8	6.6
Tm	0.7	0.7	0.7	0.8	0.7	0.8	0.9
Yb	4.8	4.8	5.1	5.4	5.2	5.3	6
Lu	0.69	0.74	0.72	0.79	0.81	0.81	0.89
C.I.P.W. norms							
Q	18.04	19.55	21.55	22.93	23.51	25.98	26.16
Zr	0.08	0.07	0.08	0.07	0.08	0.10	0.08
Or	25.29	24.84	27.78	26.47	28.80	25.04	28.67
Ab	25.98	25.04	23.74	23.80	25.09	20.42	22.35
An	11.99	12.22	10.06	10.05	9.55	12.12	9.83
Hl	0.06	0.07	0.08	0.05	0.05	0.09	0.06
Di	4.58	3.08	3.25	3.77	1.40	0.64	1.32
Hy	9.08	10.28	8.01	6.99	6.46	9.89	7.08
Mt	2.10	2.03	2.58	3.03	2.85	3.04	2.23
Il	2.26	2.25	2.25	2.25	1.71	2.08	1.66
Ap	0.61	0.63	0.66	0.63	0.59	0.71	0.53
Fl	0.42	0.45	0.49	0.58	0.39	0.24	0.80
Mg#[a)]	27.53	29.14	25.34	25.89	20.18	22.98	22.21
R_1[e)]	1875	1976	1982	2083	2029	2257	2245
R_2[f)]	740	716	652	665	571	618	583
ANOR/Q[g)]	1.78	1.69	1.23	1.20	1.06	1.26	0.98

Note: Rpk gr. = rapakivi granite xenolith in hybrid roc

HQFP = average of samples 91402, 90542, and 91302 felsic end-member

MME^p = average of samples 90042A, 91053A, and 91053B, mafic end-member

a) Mg number, molecular $100 \cdot Mg/(Mg + 0.85 \cdot Fe^{tot})$

b) molecular $(Na_2O + K_2O)/Al_2O_3$

c) molecular $Al_2O_3/(CaO + Na_2O + K_2O)$

d) $10000 \cdot Ga/Al$

e) $4 \cdot Si - 11 \cdot (Na + K) - 2 \cdot (Fe+Ti)$; oxides converted to millications

f) $6 \cdot Ca + 2 \cdot Mg + Al$; oxides converted to millications

g) normative $[100 \cdot An/(An+Or)]/Q$

Bulletin of

The Geological Society of Finland

Number 67, Part 1b,
1995

CONTENTS

The Geological Society of Finland founded in 1886, began its publishing activities in 1929. Volumes 1-39 were entitled 'Comptes Rendus de la société géologique de Finlande' and they appeared as a double edition with the 'Bulletin de la Commission géologique de Finlande'. Since 1968, from number 40 onwards, the Society's serial publication has borne the title 'Bulletin of the Geological Society of Finland'.

Non-members may subcribe to the 'Bulletin of the Geological Society of Finland' on application to the Akateeminen Kirjakauppa (Academic Bookstore), Keskuskatu 1, FIN-00100 Helsinki Finland.

ISSN 0367-5211

University Printing House, Helsinki, 1995